Spring 2015

Design and synthesis of pyrimido[4,5-b]indoles and furo[2,3-d]pyrimidines as single agents with combination chemotherapy potential or as inhibitors of tubulin or thymidylate synthase

Ravi Kumar Vyas Devambatla

DESIGN AND SYNTHESIS OF PYRIMIDO[4,5-*b*]INDOLES AND FURO[2,3-*d*]PYRIMIDINES AS SINGLE AGENTS WITH COMBINATION CHEMOTHERAPY POTENTIAL OR AS INHIBITORS OF TUBULIN OR THYMIDYLATE SYNTHASE

A Dissertation

Submitted to The Graduate School of Pharmaceutical Sciences

Duquesne University

In partial fulfillment of the requirements for the degree of

Doctor of Philosophy in Medicinal Chemistry

By

Ravi Kumar Vyas Devambatla

May 2015

Name:	Ravi Kumar Vyas Devambatla
Dissertation:	DESIGN AND SYNTHESIS OF PYRIMIDO[4,5-*b*]INDOLES AND FURO[2,3-*d*]PYRIMIDINES AS SINGLE AGENTS WITH COMBINATION CHEMOTHERAPY POTENTIAL OR AS INHIBITORS OF TUBULIN OR THYMIDYLATE SYNTHASE
Degree:	Doctor of Philosophy
Date:	March 17, 2015

APPROVED & ACCEPTED

Aleem Gangjee, Ph.D. (Committee Chair)
Professor of Medicinal Chemistry
Graduate School of Pharmaceutical Sciences
Duquesne University, Pittsburgh, PA

APPROVED

Marc W. Harrold, Ph.D. (Committee member)
Professor of Medicinal Chemistry
Graduate School of Pharmaceutical Sciences
Duquesne University, Pittsburgh, PA

APPROVED

Patrick T. Flaherty, Ph.D. (Committee member)
Associate Professor of Medicinal Chemistry
Graduate School of Pharmaceutical Sciences
Duquesne University, Pittsburgh, PA

APPROVED

David J. Lapinsky, Ph.D. (Committee member)
Associate Professor of Medicinal Chemistry
Graduate School of Pharmaceutical Sciences
Duquesne University, Pittsburgh, PA

APPROVED

Lawrence H. Block, Ph.D. (Committee member)
Professor of Pharmaceutics, Emeritus
Graduate School of Pharmaceutical Sciences
Duquesne University, Pittsburgh, PA

APPROVED

James K. Drennen, Ph.D.
Associate Dean, Research and Graduate Programs
Graduate School of Pharmaceutical Sciences
Duquesne University, Pittsburgh, PA

APPROVED

J. Douglas Bricker, Ph.D.
Dean of Mylan School of Pharmacy and the Graduate School of Pharmaceutical Sciences, Duquesne University, Pittsburgh, PA

ABSTRACT

DESIGN AND SYNTHESIS OF PYRIMIDO[4,5-*b*]INDOLES AND FURO[2,3-*d*]PYRIMIDINES AS SINGLE AGENTS WITH COMBINATION CHEMOTHERAPY POTENTIAL OR AS INHIBITORS OF TUBULIN OR THYMIDYLATE SYNTHASE

By

Ravi Kumar Vyas Devambatla

May 2015

Dissertation supervised by Professor Aleem Gangjee

This dissertation describes an introduction, background and research progress in the areas of multitargeted single agents and tubulin inhibitors in cancer chemotherapy and selective *Toxoplasma gondii* TS inhibitors for the treatment of toxoplasmosis.

Tubulin inhibitors are important antitumor agents that disrupt microtubule dynamics. Thymidylate synthase (TS) inhibitors prevent cell division by interfering with *de novo* thymidylate synthesis. Antiangiogenic agents target tumor angiogenesis crucial for tumor growth and metastasis. Under normal circumstances, angiogenesis is typically limited to tumor cells and is mediated by receptor tyrosine kinases (RTKs). Combination chemotherapies of RTK inhibitors with cytotoxic agents that target either TS or tubulin have shown significant promise and several preclinical and clinical studies with such combinations are in progress. Multitargeted single agents with dual antiangiogenic and

cytotoxic mechanisms could avoid the major limitations associated with cancer chemotherapy: multidrug resistance and dose limiting toxicities. This dissertation focuses on the design and synthesis of pyrimido[4,5-*b*]indoles and furo[2,3-*d*]pyrimidines as potential single agents with dual antiangiogenic and cytotoxic activities. These efforts led to the identification of structural features that are necessary for inhibition of RTKs and/or tubulin polymerization. Novel synthetic strategies were developed for efficient synthesis of 2,4-diamino-5-thioaryl-pyrimido[4,5-*b*]indoles and 4-anilino-5-methyl-furo[2,3-*d*]pyrimidines.

Taxanes and vinca alkaloids are widely used tubulin inhibitors in cancer chemotherapy. However, their clinical use is compromised by two major mechanisms of drug resistance: the overexpression of Pgp and βIII-tubulin. This dissertation describes the design and synthesis of pyrimido[4,5-*b*]indoles as tubulin inhibitors that circumvent Pgp and βIII-tubulin mediated resistance. This work identified the structural features crucial for tubulin inhibition for the pyrimido[4,5-*b*]indole scaffold.

Infection by *Toxoplasma gondii* can lead to toxoplasmosis in immune compromised patients such as organ transplant, cancer and AIDS patients. Current therapy involving combination of sulfadiazine and pyrimethamine is limited by drug resistance and treatment failures. The thymidylate synthase–dihydrofolate reductase enzyme is important for thymidylate synthesis in *T. gondii*, and hence can be targeted to treat *T. gondii* infection. TS is highly conserved across species and selectivity for tgTS over human TS is significantly more challenging. The present work provides an efficient synthesis of 2-diamino-4-oxo-5-thioaryl-pyrimido[4,5-*b*]indoles as selective tgTS inhibitors.

Dedicated to My Mom and Dad

ACKNOWLEDGEMENTS

I would never have been able to finish my dissertation without the guidance of my committee members, help from colleagues, and support from my parents and wife.

I would like to express my deepest gratitude to my advisor, Professor Dr. Aleem Gangjee, for his guidance and support which made the research presented in this dissertation possible. I am indebted to him for his scientific guidance and training and also for providing me with an excellent atmosphere for doing research.

I sincerely thank the members of my dissertation committee: Drs. Marc W. Harrold, David J. Lapinsky, Patrick T. Flaherty, Lawrence H. Block and Aleem Gangjee for their valuable insights and guidance. I would like to thank Drs. Bruce Beaver and Fraser Fleming for their valuable courses in Organic Chemistry.

I wish to express my sincere appreciation to Ms. Nancy Hosni, Ms. Jackie Farrer, Ms. Mary Caruso, and Ms. Deborah Willson for their unconditional assistance in administrative issues. I would like to thank the Graduate School of Pharmaceutical Sciences for financial support.

I am extremely grateful to Drs. Roheeth K Pavana, Ranganadh Velagaleti, Nilesh Zaware and Sudhir Raghavan and Ms. Shruti Choudhary and Mr. Arpit Doshi for their constructive criticism and support which made this dissertation possible.

I would like to thank my family including my sister and brother-in-law for believing in me and also for their precious support. Finally, I would like to express my love and gratitude to my wife, Pranaya Devambatla for her constant support and for standing by me during good times and bad.

TABLE OF CONTENTS

Page

LIST OF ABBREVIATIONS

5,10-CH_2THF	N^5,N^{10}-Methylene tetrahydrofolate
5-FU	5-Fluorouracil
5-F-5'-dCR	5-Fluoro-5'-deoxycytidine
5-F-5'-dUR	5-Fluoro-5'-deoxyuridine
5-F-dUMP	5-Fluoro-2'-deoxyuridine 5'-monophosphate
5-F-dUTP	5-Fluoro-2'-deoxyuridine 5'-triphosphate
5-F-UTP	5-Fluorouridine triphosphate
AICARTFase	5-Aminoimidazole-4-carboxamide ribonucleotide transformylase
AIDS	Acquired immune deficiency syndrome
ABC	ATP-binding cassette
ATP	Adenosine 5'-triphosphate
bFGF	Basic fibroblast growth factor
CA1	Combretastatin A-1
CA1P	Combretastatin A-1 diphosphate
CA4	Combretastatin A-4
CA4P	Combretastatin A-4 phosphate
CAM	Chorioallantoic membrane
CAM	Chorioallantoic membrane
CNS	Central nervous system
dCMP	2'-Deoxycytidine-5'-monophosphate
DFG	Aspartate-Phenylalanine-Glycine
DHF	Dihydrofolate

DHFR	Dihydrofolate reductase
DHPS	Dihydropteroate synthase
DMAP	4-(*N*,*N*-Dimethylamino)pyridine
DMF	Dimethylformamide
DMSO	Dimethyl sulfoxide
DNA	Deoxyribonucleic acid
dTMP	2'-Deoxythymidine-5'-monophosphate
dTTP	2'-Deoxythymidine-5'-triphosphate
dUMP	2'-Deoxyuridine-5'-monophosphate
EGF	Epidermal growth factor
EGFR	Epidermal growth factor receptor
ELISA	Enzyme-linked immunosorbent assay
ERK	Extracellular signal-regulated kinase
FDA	U.S. Food and drug administration
FPGS	Folylpoly-γ-glutamate synthetase
GARTFase	Glycinamide ribonucleotide transformylase
GDP	Guanosine-5'-diphosphate
GTP	Guanosine-5'-triphosphate
HER	human epidermal growth factor receptor
HIV	Human immunodeficiency virus
HPLC	High–performance liquid chromatography
hTS	Human thymidylate synthase
MAP	Microtubule associated protein

MDR	Multidrug resistance
MEK	Mitogen/extracellular signal-regulated kinase
MOE	Molecular Operating Environment
MTOC	Microtubule organizing center
NADPH	Nicotinamide adenine dinucleotide phosphate
NCI	National Cancer Institute
NMP	N-methyl-2-pyrrolodinone
NMR	Nuclear magnetic resonance
PDB	Protein data bank
PDDF	N^{10}-Propargyl-5,8-dideazafolate
PDGF	Platelet-derived growth factor
PDGFR	Platelet-derived growth factor receptor
Pgp	P-glycoprotein
PI3K	Phosphoinositide 3-kinase
PLGF	Placental growth factor
ppm	Parts per million
RFC	Reduced folate carrier
RNA	Ribonucleic acid
RTK	Receptor tyrosine kinase
SRB	Sulforhodamine B
tgTS	*T. gondii* thymidylate synthase
THF	Tetrahydrofuran
TLC	Thin–layer chromatography

TS	Thymidylate synthase
TS–DHFR	Thymidylate synthase–dihydrofolate reductase
VDA	Vascular-disrupting agent
VEGF	Vascular endothelial growth factor
VEGFR	Vascular endothelial growth factor receptor

LIST OF TABLES

LIST OF FIGURES

LIST OF SCHEMES

I. BIOLOGICAL REVIEW

A. Tubulin binding agents

A.1 Microtubules

Microtubules are long, filamentous protein polymers that form one of the major components of the cytoskeleton.[1]

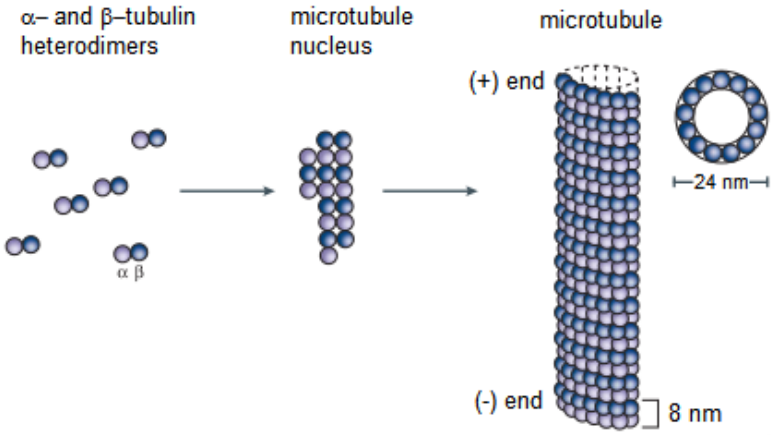

Figure 1. Polymerization of αβ-tubulin heterodimers (modified from ref. 2). αβ-Tubulin heterodimers first form a short microtubule nucleus followed by elongation and arrangement to form a microtubule.

Microtubules are composed of α- and β-tubulin heterodimers each with a molecular weight of about 50 kDa. The αβ-tubulin heterodimers polymerize "head-to-tail" between the α- and β-tubulin to form protofilaments, which are aligned in parallel to form hollow cylindrical microtubule structure (Figure 1).[2] The resulting microtubule has an outer diameter of 24 nm, a wall thickness of 5 nm, and a length extendable to about 25 μm. Each microtubule has α- and β-tubulin on the plus (+) and minus (–) ends, respectively.

A.2 Microtubule dynamics

Microtubules exhibit two major forms of non-equilibrium dynamics, namely dynamic instability and treadmilling.

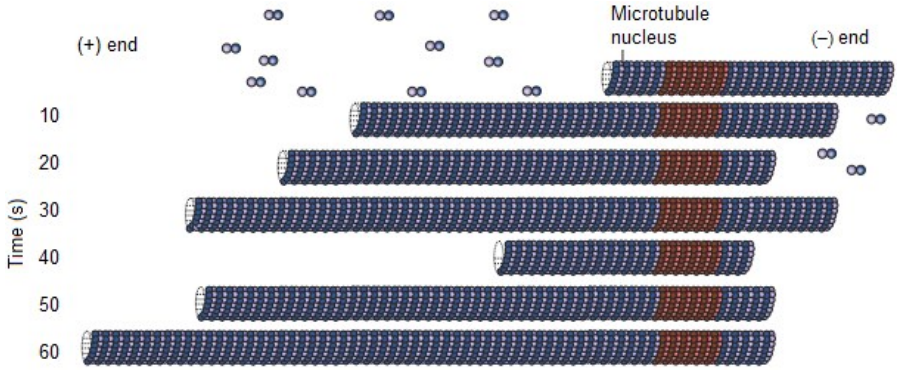

Figure 2. Dynamic instability of microtubules (modified from ref. 2).

In dynamic instability, the individual microtubule ends switch between phases of lengthening and shortening (Figure 2).[3] The growth and shortening of microtubules occur more rapidly and more extensively at the plus (+) end, where the β-tubulin is exposed, than at the minus (–) end, where α-tubulin is exposed. The microtubules undergo relatively long periods of slow lengthening, brief periods of rapid shortening and periods of attenuated dynamics or pause, when the microtubule neither grows nor shortens detectably.[3, 4] Dynamic instability is characterized by four main factors: rate of growth; rate of shrinkage; frequency of switching from the growth stage to shortening (known as ‘‘catastrophe frequency’’) and frequency of switching from shrinkage to growth (known as ‘‘rescue frequency’’).[4]

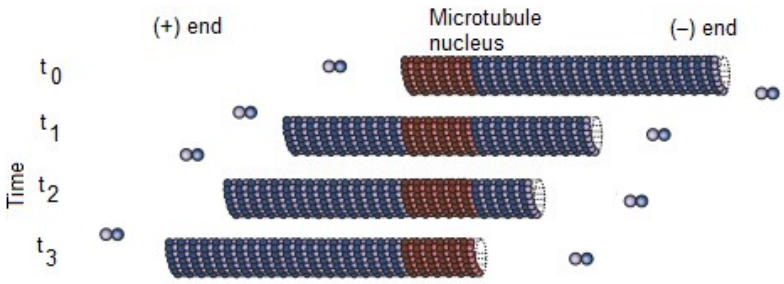

Figure 3. Microtubule treadmilling (modified from ref. 2).

The second dynamic behavior, known as microtubule treadmilling (Figure 3), involves net growth at the plus end of the microtubule and balanced net shortening at the minus end.[4, 5] It results in an intrinsic flow of tubulin subunits from the plus end of the microtubule to the minus end and is particularly important in mitotic spindles.

Microtubule associated proteins (MAPs), proteins associated with microtubules, are important for the formation and stability of microtubules.[6] The two nonequivalent ends of microtubules are structurally well organized. The slow growing minus end is generally anchored at the microtubule organizing center (MTOC) of the centrosome whereas the plus end is highly dynamic and switches between phases of growth and shrinkage.[6]

The polymerization dynamics of microtubules involves binding and/or hydrolysis of guanosine 5'-triphosphate (GTP).[3, 6] Each αβ-tubulin heterodimer has two GTP-binding sites: an exchangeable (E) site on β-tubulin and a non-exchangeable (N) site on α-tubulin that is always filled with GTP. Binding of GTP to the E-site of tubulin is required for microtubule polymerization whereas GTP hydrolysis is required for microtubule depolymerization.[3]

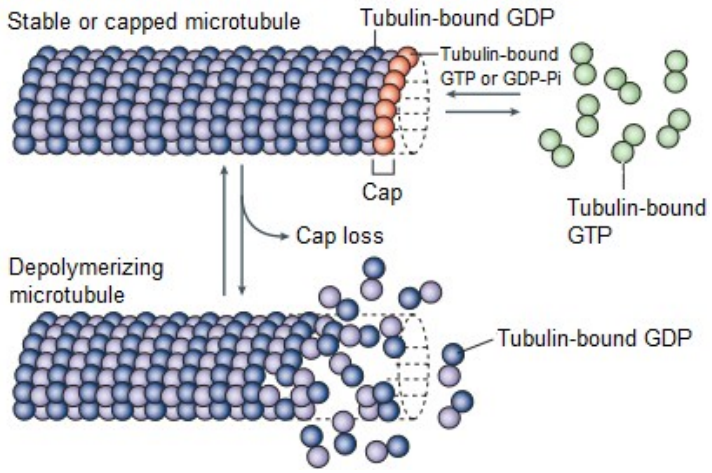

Figure 4. Polymerization dynamics of microtubules (modified from ref. 2). During polymerization, tubulin-bound GTP disassociates as soon as the tubulin-bound GDP binds to the microtubule or shortly thereafter. Depolymerization occurs when the GTP cap is hydrolyzed.

GTP binding to β-tubulin causes straightening of the αβ-tubulin heterodimer to a conformation that promotes polymerization.[7] The GTP-bound heterodimer attaches to the plus end of the microtubule and then the GTP is hydrolyzed to tubulin–GDP and inorganic phosphate (P_i) (Figure 4), providing energy for the addition of another tubulin heterodimer. A microtubule end containing tubulin bound GTP or GDP-P_i is stable or "capped" against depolymerization. Hydrolysis of tubulin-bound GTP and the subsequent release of P_i induce a conformational change in the tubulin that results in microtubule depolymerization. At the final stage of the polymerization process, the GTP cap dissociates and leaves a microtubule core of β-tubulin bound with GDP.

A.3 Role of microtubule dynamics in mitosis

During mitosis, the duplicated chromosomes of cells are divided into two identical sets prior to division into two daughter cells.[8] The correct movements of the

chromosomes and their proper segregation to daughter cells require extremely rapid microtubule dynamics. Their role in mitosis and cell division makes microtubules an important target for anticancer drugs.[1, 9]

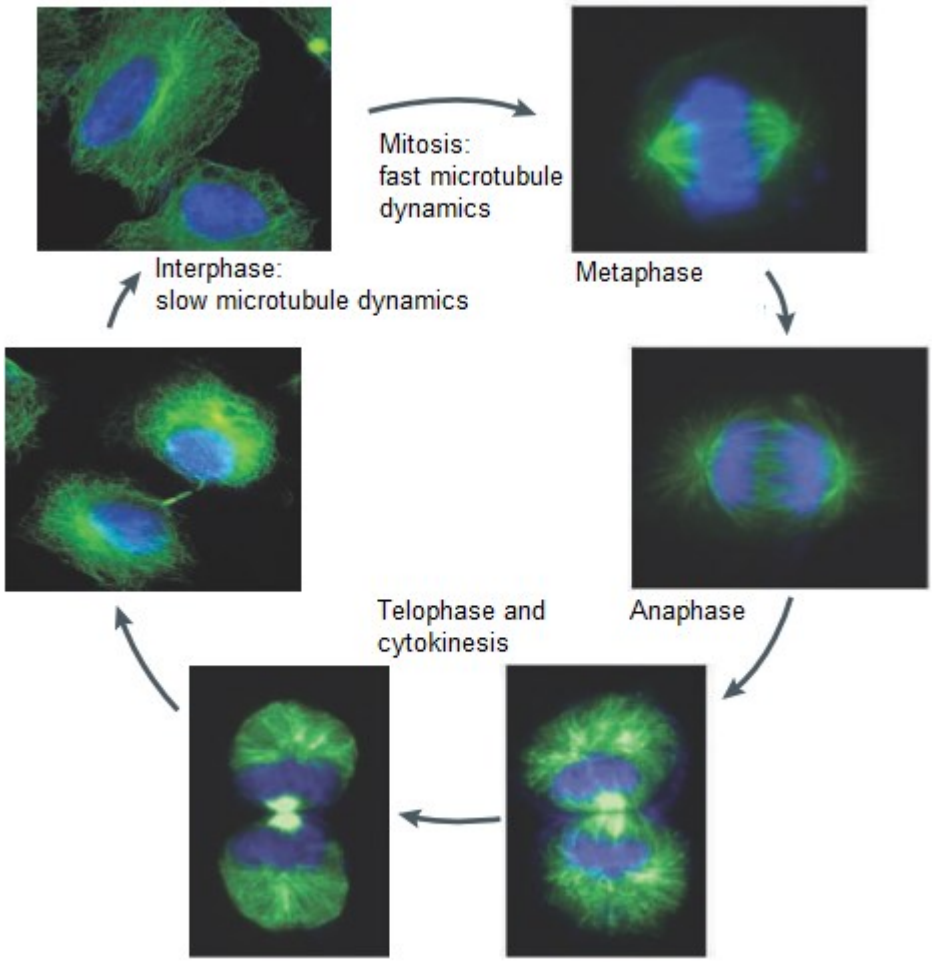

Figure 5. Microtubule dynamics during the cell cycle (modified from ref. 10). Microtubules are shown in green.

Microtubule dynamics vary during the cell cycle, being least dynamic during the interphase and most dynamic during mitosis.[10] Mitosis in most cells progresses rapidly and the highly dynamic microtubules in the spindle are required for all stages of mitosis (Figure 5). During the prophase of mitosis, microtubules become more dynamic and a

bipolar spindle-shaped array of microtubules is assembled outwards from the centrosome. In the prometaphase, the kinetochore microtubules attach to the poles and make vast growing and shortening excursions until they capture the chromosomes. In metaphase, chromosomes are aligned along the equator and have at least two microtubules extending from the kinetochores. When cells enter anaphase, the kinetochore microtubules shorten and pull chromosomes to the poles. During telephase and cytokinesis, the chromosomes arrive at the poles, the mitotic spindle disassembles and the parent cell divides into two daughter cells. As different stages of mitosis are dependent on microtubule dynamics (Figure 5), disruption of microtubule dynamics by microtubule targeting agents results in cell cycle arrest, eventually causing programmed cell death (apoptosis).[10]

A.4 Classification of tubulin binding agents

Tubulin binding agents are structurally highly diverse and are mainly classified into two groups: microtubule-stabilizers and microtubule-destabilizers.[1] Microtubule-stabilizers promote microtubule polymerization at high concentrations and include the taxanes and the epothilones. Microtubule-destabilizers induce microtubule depolymerization at high concentrations and include the vinca alkaloids and colchicine-site binding agents. However, at low antiproliferative concentrations, both these types of agents suppress microtubule dynamics leading to mitotic arrest and subsequent cell death.[1, 8] Tubulin binding agents are widely used for the treatment of both solid tumors and hematological malignancies.[1]

Most microtubule targeting agents are divided into four classes based on their interactions within the taxane,[11] vinca,[12] colchicine,[13] or the newly discovered maytansine site[14] on tubulin.

A.4.1 Taxanes and epothilones:

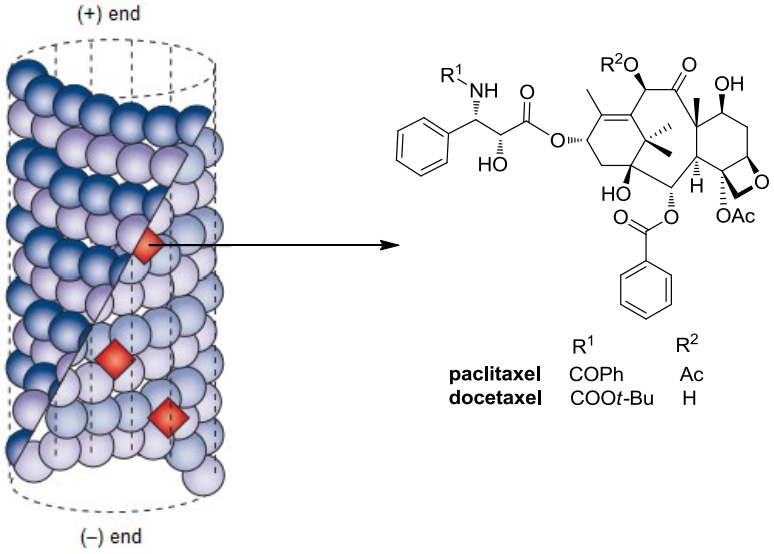

Figure 6. Taxane binding site and representative taxanes (modified from ref. 2).

Paclitaxel (Taxol®), docetaxel (Taxotere®), and the epothilones bind to the β-subunit in the interior of the microtubule, commonly referred to as the taxane site (Figure 6).[11] The binding of paclitaxel leads to the stabilization of microtubules and an increase in net microtubule polymerization. Thus, the ability of the cells to break down the mitotic spindle during mitosis is inhibited by paclitaxel. With the spindle still in place, the parent cell cannot divide into daughter cells resulting in the inhibition of mitosis. Binding of paclitaxel stabilizes the microtubule by inducing a conformational change in β-tubulin which increases its affinity for adjacent tubulin molecules.[12] Low concentrations of Taxol are sufficient to cause cell cycle arrest and induce apoptosis without changing microtubule mass. The IC_{50} of paclitaxel for an antimitotic effect in HeLa cells is 8 nM while the IC_{50} for an increase in microtubule polymerization is 80 nM.[2] The taxoids are widely used in the treatment of breast, non-small cell lung, ovarian, head and neck and prostate cancers.[15]

Most antimitotic agents that induce microtubule polymerization, such as the epothilones, discodermolide and eleutherobin bind to the taxane binding site.[11] Ixabepilone (Ixempra®), which belongs to the epothilone class of taxane-site binders, was approved for the treatment of drug-refractory metastatic breast cancer in 2007.[16]

A.4.2 The vinca alkaloids:

The vinca alkaloids, including vinblastine, vincristine, vindesine, and vinorelbine have a broad spectrum of activity and have been widely used in cancer chemotherapy for lymphomas, non-small-cell lung cancer and pediatric cancers.[1]

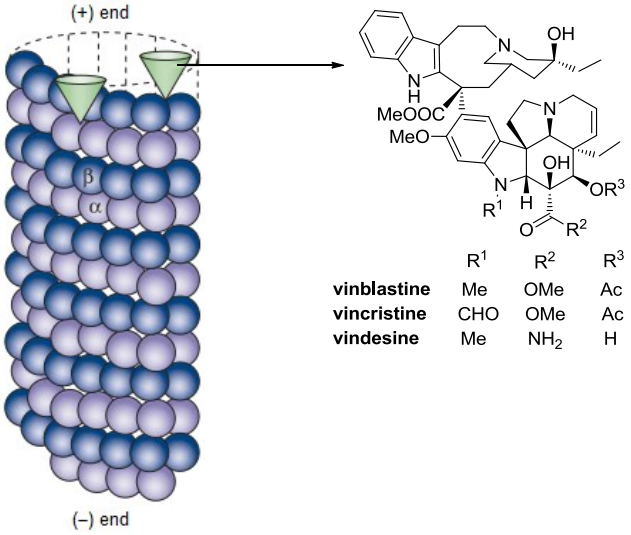

Figure 7. Vinca binding site and representative vinca alkaloids (modified from ref. 2).

The vinca alkaloids bind to the β-subunit on the exterior of the microtubule at a site commonly referred to as the vinca-binding domain (Figure 7). The rapid and reversible binding of vinblastine to soluble tubulin induces a conformational change that leads to tubulin self-association.[12] Vinblastine binds with high affinity to the end of the microtubules but poorly to tubulin that is buried in the tubulin lattice. At high concentrations of 10–100 nM in HeLa cells, vinblastine depolymerizes microtubules and

destroys mitotic spindles. At low concentrations (~1 nM), vinblastine does not depolymerize microtubules, yet it powerfully blocks mitosis by suppression of microtubule dynamics. The binding of one or two molecules of vinblastine per microtubule is sufficient to reduce tubulin dynamics by about 50%, without causing appreciable microtubule depolymerization. Other antitubulin agents such as the halichondrins,[17] cryptophycins,[18] and dolastatins[19] also bind at the vinca binding site. Eribulin mesylate (Halaven®) is a synthetic halichondrin derivative which was approved by the U.S. Food and Drug Administration (FDA) for the treatment of metastatic breast cancer.[20]

A.4.3 Colchicine-site agents:

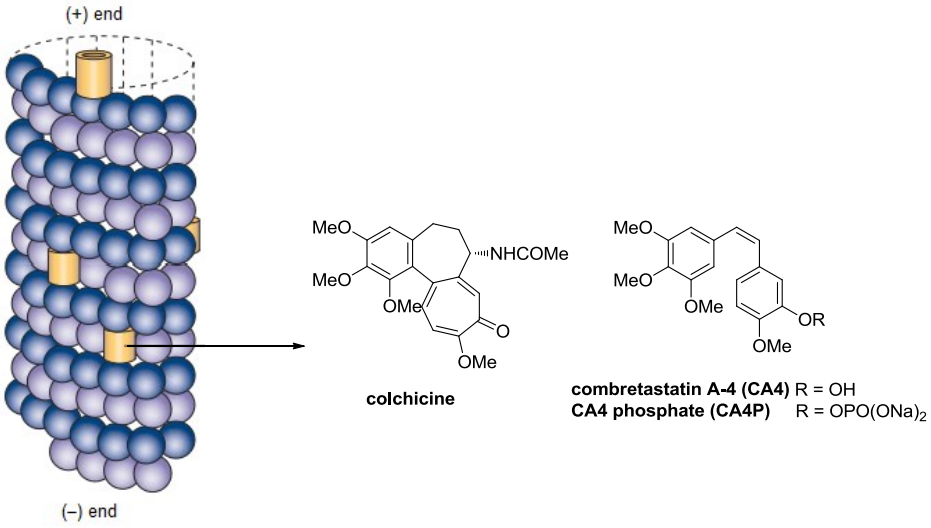

Figure 8. Colchicine binding site and combretastatins (modified from ref. 2).

The third class comprises a diverse collection of small molecules, including colchicine (Figure 8), combretastatins A-1 (CA1) and A-4 (CA4), 2-methoxyestradiol and podophyllotoxin.[21] Colchicine is not used as an antitumor agent due to its toxicity at doses that produce antimitotic effects.[21] However, colchicine (Colcrys®) is useful for the

treatment of gout and familial Mediterranean fever.[22] Colchicine blocks or suppresses cell division by inhibiting the development of spindles when the nuclei are dividing.[21] Therefore it inhibits the division of the nucleus and mitosis. Colchicine binds to soluble tubulin at a distinct site referred to as the colchicine binding site, which is on β-tubulin at the interface between α- and β-tubulins (Figure 8).[12, 13] Colchicine forms a poorly reversible tubulin–colchicine complex with tubulin, which copolymerizes into the microtubule ends along with free tubulin molecules. The ends continue to grow with the complex, but their dynamics are suppressed. These effects lead to cell cycle arrest and apoptotic cell death. Similar to the vinca alkaloids, colchicine site binders depolymerize microtubules at high concentrations but suppress microtubule dynamics at low concentrations. Although there are no clinically approved anticancer agents that bind to the colchicine site, several agents including 2-methoxyestradiol,[23, 24] CA4 phosphate (CA4P, Fosbretabulin®)[25-28] and CA1 diphosphate (CA1P, OXi4503®)[29] have been evaluated in phase 1 and 2 clinical trials as anticancer agents either alone or in combination.

In addition to the antimitotic effect, combretastatins are potent vascular-disrupting agents (VDAs) that target endothelial cells and pericytes of the already established tumor vasculature.[30, 31] CA4P rapidly depolymerizes the microtubules of endothelial cells, reduces blood flow to the tumor by 95% within one hour, increases vascular permeability and hemorrhage of peripheral vessels.[32] Based on this property, both CA4 and CA4P have been evaluated as anti-vascular agents in phase 1 and 2 clinical trials.[30, 33] Importantly, VDAs seem to damage tumor vasculature without significantly harming normal tissues. This selectivity of the VDAs for tumor vasculature can be attributed to

the differences between the mature vasculature of normal tissues and the immature or forming vasculature of tumors.[32, 34] Also, the actin cytoskeleton in endothelial cells of immature tumor vasculature is underdeveloped, which is likely to make the cells more susceptible to damaging agents. In addition, the differences in rates of endothelial cell proliferation may also be a causative factor to the observed tumor selectivity.[32]

A.4.4 Maytansine-site agents:

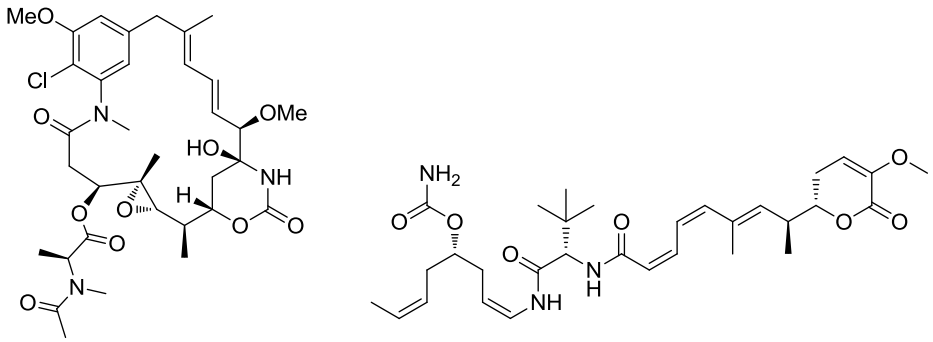

Figure 9. Representative maytansine-site agents.

Recently, Prota *et al.*[14] demonstrated that maytansine (Figure 9) binds to a distinct site on β-tubulin designated as the "maytansine site". Occupancy of this site inhibits tubulin polymerization by preventing the addition of new subunits at the plus ends of the microtubule, thus causing microtubule depolymerization. Phase 1 drug PM060184[35] (Figure 9) and Rhizoxin F[36] are the other microtubule depolymerizing agents that bind to the maytansine site. Maytansine is the cytotoxic component in the antibody drug conjugate Trastuzumab emtansine (Kadcyla®), which was recently approved by the FDA for the treatment of HER2-positive advanced breast cancer.[37]

A.5 Mechanisms of tumor resistance to tubulin binding agents

Multidrug resistance (MDR) severely limits the effectiveness of cancer chemotherapy, including tubulin binding agents.[10, 38] Clinically significant mechanisms of tumor resistance for these agents are drug efflux by ATP-binding cassette (ABC) transporters and expression expression of the βIII-isotype of tubulin.

ABC transporters such as P-glycoprotein (Pgp) are membrane-bound drug efflux proteins that reduce the cellular accumulation of substrates.[39] Drug efflux by Pgp was identified as the chief mechanism of resistance to the vinca alkaloids and taxanes in vitro.[38] For example, the potency of paclitaxel in Pgp overexpressing SKOV3 MDR-1-6/6 cell lines was 800-fold less than in parental SKOV3 cell lines.[40] Overexpression of Pgp has also been reported in the clinical setting in several tumor types, particularly in patients who have received chemotherapy.[41] Furthermore, Pgp expression is considered to be a prognostic indicator in certain cancers and is associated with poor response to chemotherapy.[41, 42] Attempts to reverse Pgp-mediated drug resistance by combining tubulin binding agents with Pgp inhibitors have been disappointing.[43, 44]

The other clinical mechanism of resistance to tubulin binding agents involves the expression of βIII-isotype of tubulin. βIII-Tubulin expression is strongly associated with clinical resistance to taxanes in multiple tumor types such as non-small cell lung,[45, 46] breast,[47] ovarian[48] and gastric cancers.[49] Paclitaxel had 5-fold less activity in βIII-tubulin expressing HeLa cell lines compared to the parental cell line.[40] Also, paclitaxel displayed less suppression of microtubule dynamics in βIII-tubulin expressing cells than in control cells.[50] It was hypothesized that the resistance to taxanes was due to the absence of Ser275 on βIII-tubulin.[51] Paclitaxel is considered to reach its binding site on β-tubulin by

diffusion through the pores in the microtubule wall. This process is stabilized by the formation of a hydrogen bond between 7-hydroxyl of paclitaxel and the -OH of Ser275 of β-tubulin. In βIII-tubulin, Ser275 is replaced by Ala275 thus possibly resulting in decreased binding of paclitaxel to microtubules in βIII-tubulin expressing cell lines. Overexpression of βIII-tubulin is also involved in clinical resistance to Vinca alkaloids in non-small cell lung[45, 52] and ovarian[53] cancers. Colchicine-site binding agents have been shown to circumvent βIII-tubulin resistance,[54, 55] which highlights the advantage of colchicine-site agents over taxanes and vinca alkaloids for cancer chemotherapy.

B. Thymidylate synthase inhibitors

B.1 Thymidylate synthase

Thymidylate synthase (TS), a key enzyme in folate metabolism, is present in almost all living organisms including humans, bacteria and protozoa.[56] It catalyzes the reductive methylation of 2'-deoxyuridine 5'-monophosphate (dUMP) to 2'-deoxythymidine 5'-monophosphate (dTMP) (Figure 10), which is subsequently phosphorylated to 2'-deoxy-thymidine 5'-triphosphate (dTTP) by cellular kinases. The dTTP formed is utilized by deoxyribonucleic acid (DNA) polymerase and is incorporated into DNA. The TS catalyzed reaction is a key step in DNA biosynthesis and the only *de novo* biosynthetic pathway to dTMP.[57] During TS catalysis, N^5,N^{10}-methylene tetrahydrofolate (5,10-CH_2THF) acts as a one-carbon donor and is converted to dihydrofolate (DHF) (Figure 10).

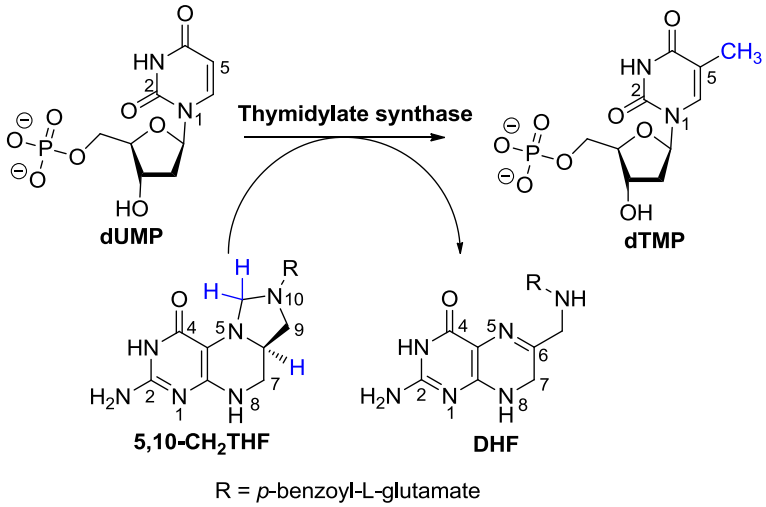

Figure 10. *De novo* synthesis of dTMP by the enzyme TS. TS catalyzes the transfer of methylene group from 5,10-CH_2THF to dUMP resulting in the formation of dTMP and DHF.

B.1.1 Structure of TS

The TS enzyme (EC 2.1.1.45) is a homodimer consisting of two identical subunits each having a molecular weight of 30–35 kDa and a primary sequence of approximately 316 amino acids.[56] It has two active sites, each formed by residues from monomers. The primary structures of several TS enzymes including those of humans, bacteriophages, and plants are known. TS enzymes are highly conserved in different species both in terms of structure and mechanism: 27 amino acids are completely conserved across all species and 165 (80%) are conserved in more than 60% of the organisms. In particular, the active (dUMP) site of TS involves 32 amino acid residues, of which 16 are conserved in all species.

In the protein data bank (PDB),[58] several X-ray crystal structures of TS of various organisms are available in the native enzyme form or as complexes with substrates, products or inhibitors. Notably, the X-ray crystal structures of TS from several

prokaryotic species, including *Escherichia coli* (*E. coli*), and eukaryotes, such as *Homo sapiens*, *Lactobacillus casei* (*L. casei*, lc), and *Pneumocystis carinii (P. carinii)* are known in the literature.[56] Also, X-ray crystal structures of human TS inhibitors such as pemetrexed and raltitrexed are known.[59, 60] The existing crystal structures of TS in the native form or with inhibitors are important for the understanding of both the mechanism and the inhibition of TS.[56] More importantly, they allow a structure-based rational design of TS inhibitors.

Through site-directed mutagenesis, the function of each residue in the substrate-binding site of TS has been studied. Cys198, Asn229, Arg178' and Arg179', Glu60 and Val316 (lcTS numbering) were determined to be the most important residues in dUMP binding site.[56] During the TS catalysis, Cys198 is involved in the nucleophilic attack on C6 of the uracil ring resulting in the formation of a covalent bond between TS and dUMP, thus no mutation is tolerated at Cys198. Asn229 (lcTS numbering), another important residue in the active site, is involved in hydrogen bonding with the 4-oxo of dUMP.[56] Thus substitution of Asn229 by other amino acids resulted in reduced or complete loss of catalytic activity. Asn229 also plays an important role in enzyme specificity. When Asn229 is replaced with Asp229, the enzyme is no longer a deoxyuridylate methylase, but a cytidylate methylase, which catalyzes the methyltranferase reaction with 2'-deoxycytidine 5'-monophosphate (dCMP) instead of dUMP.

Amino acid residues, Arg178' and Arg179' (lcTS numbering), belong to the opposite subunit and bind to the phosphate group of the deoxyribose ring.[56] Replacement of these two amino acids reduced the catalytic activity. The importance of other amino acids in

the active site has also been studied. The C-terminal residue Val316 participates in the conformational change of the enzyme, which occurs after the covalent binding of cofactor 5,10-CH_2THF to the binary complex TS–dUMP.[56] This conformational change is necessary for the catalytic reaction because it positions dUMP and the cofactor to facilitate the transfer of the methyl group. Pro196, Pro197 and His199 (lcTS numbering) are highly conserved amino acids but their substitution with other amino acids is well tolerated.

B.1.2 Catalytic mechanism of TS

The mechanism of catalysis by TS has been examined[61] and is depicted in Figure 11. Sequential binding of substrate (dUMP) and cofactor 5,10-CH_2THF with TS enzyme induces a conformational change to form a non-covalent ternary complex (TS–dUMP–cofactor). In step A, Cys195 of human TS (hTS) attacks C6 of dUMP to form the enol. Protonation at the N^{10}-position of 5,10-CH_2THF results in the formation of the reactive N^5-iminium species in step (**B**). The C5 position of the enol of dUMP reacts with the iminium ion of the activated cofactor to form an unstable covalent ternary complex in step (**C**).[61] The proton at the C5-position of dUMP is abstracted by a base in the active site to provide enol in step (**D**). Abstraction of a proton from O4 of the enol results in the formation of an exocyclic methylene and also the release of the reduced cofactor in step (**E**). The enzymatic reaction is completed by the hydride transfer from C6 of the reduced cofactor to form dTMP. The modified cofactor, which serves as a methylene donor and reductant, is released from the active site of TS followed by release of the product, dTMP.

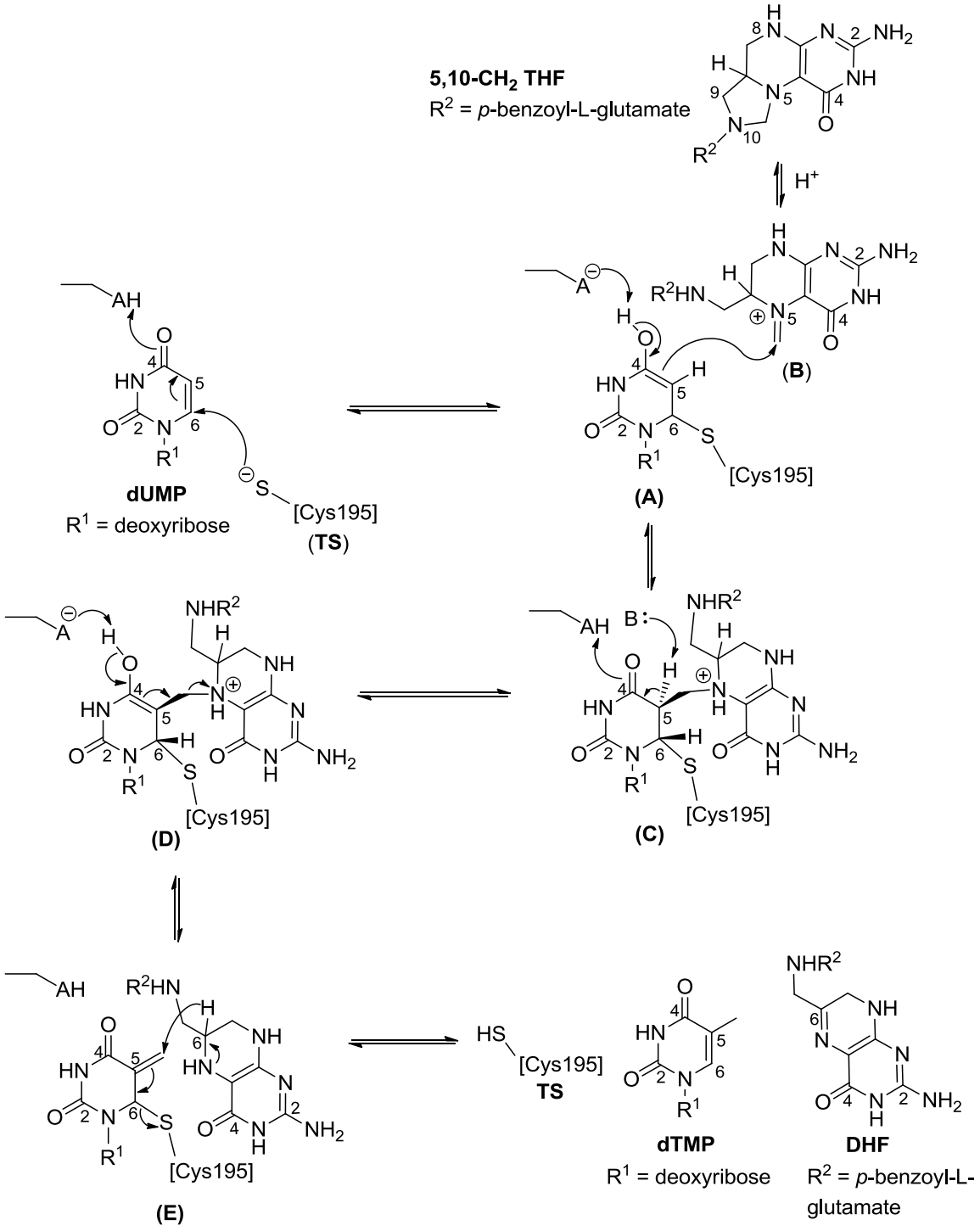

Figure 11. The catalytic mechanism of human TS (modified from ref. 61).

B.2 Inhibition of TS

Inhibition of TS depletes dTTP, one of the four building blocks required for DNA synthesis, thus leading to impaired DNA synthesis and repair.[57] dTTP depletion also perturbs cellular levels of deoxynucleotides resulting in DNA damage.[57, 62] Alternatively, TS inhibition causes accumulation of dUMP, and subsequent misincorporation of dUTP into DNA.[57] These processes result in DNA double-strand breaks that lead to the initiation of apoptotic cell death, commonly referred to as "thymidine-less" cell death.[57]

B.3 TS inhibitors in cancer chemotherapy

Inhibition of TS in tumor cells inhibits DNA biosynthesis resulting in thymidine-less cell death. Normal cells also require TS for DNA synthesis.[56] Nonetheless, TS inhibitors are widely used in cancer chemotherapy and the reason for their tumor selectivity is attributed to differences in transport, metabolism and the rates of cell division for normal and some tumor cells.[57] As tumor cells replicate much more rapidly than normal cells, they have a higher need for synthesis of deoxynucleotides than normal cells. Several TS inhibitors have been rationally designed to target the TS-binding site of either dUMP or cofactor 5,10-CH_2THF. TS inhibitors are classified broadly into two classes: dUMP-based TS inhibitors and antifolates.

B.3.1 dUMP-based TS inhibitors

dUMP-based TS inhibitors are antimetabolites that are analogs of dUMP, one of the substrates in TS catalysis.[57] These inhibitors, upon bioactivation, either inhibit TS or are misincorporated into DNA and/or RNA resulting in the inhibition of DNA and/or RNA synthesis.

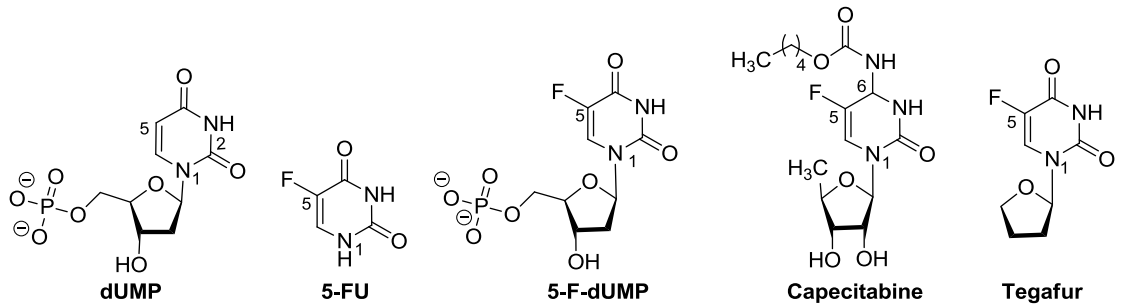

Figure 12. dUMP and representative dUMP-based TS inhibitors.

5-Fluorouracil (5-FU, Figure 12) is a dUMP-based inhibitor and represents the first class of clinically used TS inhibitors.[63] The mechanisms of action of 5-FU include inhibition of TS, incorporation into DNA, and/or incorporation into RNA.[57, 63] 5-FU is a prodrug and must be bioactivated to various active nucleotides such as 5-fluoro-2'-deoxyuridine 5'-monophosphate (5-F-dUMP, Figure 12), 5-fluoro-2'-deoxyuridine 5'-triphosphate (5-F-dUTP) and 5-fluorouridine triphosphate (5-F-UTP). 5-F-dUMP is a mechanism-based inactivator of TS since it forms a covalent complex with TS and the cofactor. Alternatively, 5-F-dUMP can be phosphorylated by a series of enzymatic reactions to 5-F-UTP, which is misincorporated into RNA and causes inhibition of RNA processing and function.

5-FU has been used for more than 50 years in the treatment of colorectal cancer.[57] 5-FU remains one of the most widely used anticancer agents with a broad-spectrum activity against many solid tumors, including pancreas, breast, head and neck, gastric, and ovarian cancers. However, 5-FU causes toxicity to normal cells because the enzymes that activate it are not tumor selective.[64] For instance, 5-FU causes diarrhea because of its activation in the intestines. Moreover, it is rapidly degraded by the dihydropyrimidine dehydrogenases in the liver, thereby limiting its oral bioavailability.

Capecitabine (Xeloda®) and tegafur (Figure 12) are prodrugs that are metabolized to 5-FU, which then gets converted to active nucleotides involved in DNA and RNA damage.[57, 64] Rational drug design of capecitabine exploited the utilization of three tumor-overexpressing enzymes for its metabolism to to 5-FU. Capecitabine is readily absorbed in the gastro-intestinal tract and is converted to 5-fluoro-5'-deoxycytidine (5-F-5'-dCR) by carboxylesterases in the liver. 5-F-5'-dCR is then converted to 5-fluoro-5'-deoxyuridine (5-F-5'-dUR) by cytidine deaminase, which is highly expressed in both liver and tumor tissues. The final step involves the conversion of 5-F-5'-dUR by either thymidine phosphorylase or uridine phosphorylase to form 5-FU. Both thymidine phosphorylase and uridine phosphorylase are highly active in tumors than in normal tissues, thus resulting in tumor specificity to capecitabine. This Medicinal Chemistry approach resulted in capecitabine with improved oral biovailability and tumor selectivity over 5-FU. Capecitabine is used clinically in the treatment of metastatic breast and colorectal cancers.[65] It has also shown promising anticancer activity in patients with prostate, pancreatic, and ovarian cancers. Tegafur (Figure 12) is a prodrug that is bioactivated in the liver by cytochrome P-450 2A6 via 5'-hydroxylation to 5-FU.[57]

B.3.2 Antifolates

Antifolates are classes of compounds that are structurally related to natural cofactor. TS-targeting antifolates are designed to attach to the binding site of the folate cofactor 5,10-CH_2THF, involved in TS catalysis.[57] They are competitive TS inhibitors, but unlike 5,10-CH_2THF, are not bioactivated to form the iminium species. Antifolates are generally divided into two classes: Classical antifolates that contain a benzoyl L-glutamate side-chain and non-classical antifolates that lack the benzoyl L-glutamate.

N^{10}-Propargyl-5,8-dideazafolate (PDDF, Figure 13), was one of the first antifolates to be developed as a specific TS inhibitor.[66] It was also the first quinazoline-containing TS inhibitor that entered phase I clinical trials. However, its development was abondoned due of its renal toxicity resulting from poor water-solubility.[64] Replacement of the 2-amino group of PDDF with a 2-methyl group resulted in improved water solubility and decreased renal toxicity.

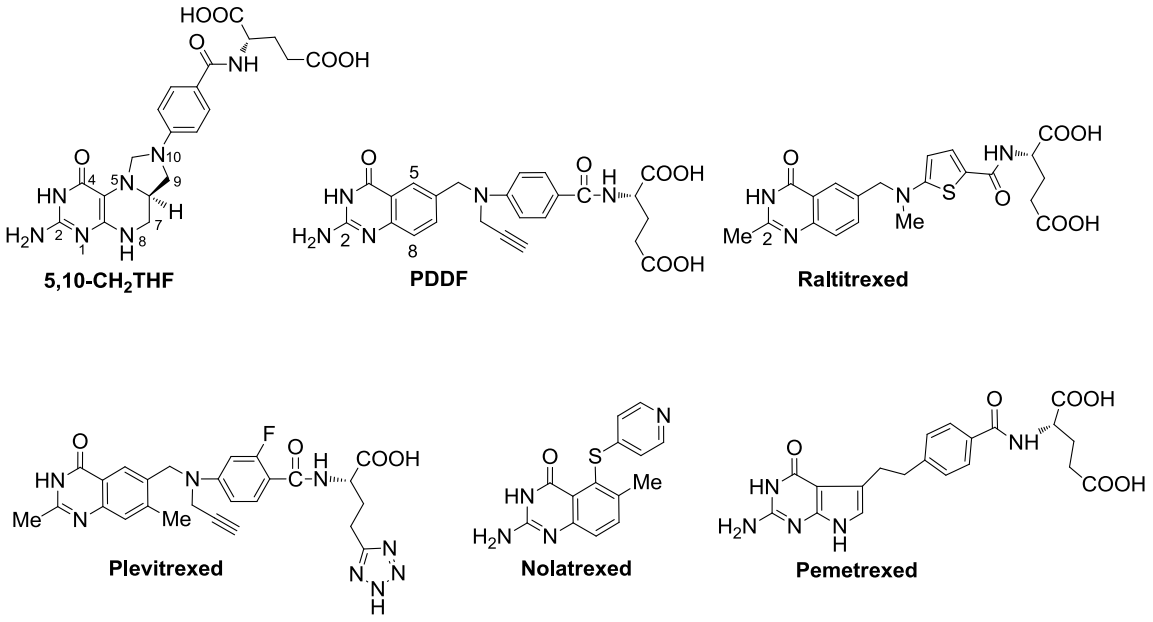

Figure 13. Cofactor 5,10-CH_2THF and representative antifolates as TS inhibitors.

Raltitrexed ((Tomudex®), Figure 13) is the 2-methyl-containing classical antifolate derived from PDDF with decreased renal-toxicity but lower TS-inhibitory potency than PDDF.[67] It is transported into cells via the reduced folate carrier (RFC) and undergoes rapid polyglutamylation by folylpoly-γ-glutamate synthetase (FPGS).[64] Upon polyglutamylation, the potency of raltitrexed is increased by up to 100-fold and cellular retention is significantly prolonged.[64]

In phase II and III trials, raltitrexed had good activity in patients with advanced colorectal and breast cancers.[68] Unfortunately, raltitrexed caused life-threatening toxicity

attributed to gastrointestinal toxicity and myelosuppression. Raltitrexed was approved as first-line therapy for the treatment of advanced colorectal cancer in several European countries, Australia, Canada, and Japan.

Multiple mechanisms of resistance such as decreased uptake by RFC and/or decreased FPGS activity limit the clinical use of classical antifolates.[61] Nonclassical lipophilic antifolates such as nolatrexed (Thymitaq®) and plevitrexed (Figure 13) have been designed to circumvent these resistance mechanisms associated with classical antifolates. Plevitrexed contains a tetrazole moiety instead of the γ-carboxylic acid group and is transported into cells by RFC and passive diffusion but is not a substrate for FPGS.[61] Nolatrexed is the first nonclassical TS inhibitor to reach phase II clinical trials.[69] However, it showed minimal activity in patients with advanced hepatocellular carcinoma.

Pemetrexed ((Alimta®), Figure 13) is a purported multitargeted antifolate that inhibits TS in addition to other folate-dependent enzymes including dihydrofolate reductase (DHFR) (very weakly), 5-aminoimidazole-4-carboxamide ribonucleotide transformylase (AICARTFase), and glycinamide ribonucleotide transformylase (GARTFase) (very weakly).[70] It predominantly enters cells via the RFC under normal pHs and requires polyglutamylation for maximal inhibitory effects.[64] Pemetrexed is approved in the USA for the treatment of advanced nonsquamous non-small cell lung cancer and malignant pleural mesothelioma. The main toxicities associated with pemetrexed are hematologic toxicity, gastrointestinal toxicity, fatigue, and skin rashes.[71]

B.4 Thymidylate synthase inhibition in toxoplasmosis

Toxoplasmosis is a disease that affects the brain and the eyes and is caused by the intracellular parasite *Toxoplasma gondii* (*T. gondii*, tg).[72] Humans generally acquire the

infection by ingestion of food or water that is contaminated with oocysts shed by cats or by eating raw or undercooked meat containing tissue cysts. According to the World Health Organization, the *T. gondii* parasite has infected up to a third of the world's population.[73] While toxoplasmosis is generally benign and goes unnoticed in immunocompetent individuals, it is a major opportunistic infection in immune compromised patients such as those with acquired immune deficiency syndrome (AIDS) and those receiving organ transplants or chemotherapy.[72] *T. gondii* infection is one of the major causes of morbidity and mortality in HIV patients.[74, 75]

Protozoa, including *T. gondii*, contain a bifunctional TS–DHFR enzyme wherein the TS and DHFR exist on the same polypeptide.[76] Recently, Sharma *et al*.[77] solved the first three-dimensional structure of *T. gondii* TS–DHFR (tgTS–DHFR) with a resolution of 3.7 Å. The tgTS–DHFR enzyme is a homodimer in which each monomer has a molecular mass of 69 kDa. Each monomer consists of a TS domain (289 residues) on the C-terminal and a DHFR domain (252 residues) on the N-terminal. TS and DHFR domains are tethered together by a linker region (69 residues). The crystal structure and the overall sequence alignment also indicated that the active site of *T. gondii* TS (tgTS) is highly conserved.[77] Cys489 of the TS domain is involved in the catalysis of dUMP to dTMP. The key residues important for the binding to PDDF (antifolate) are Ile402, Asp513, Leu516, Phe520, Arg603 and Met608. The tgTS–DHFR exhibits substrate channeling i.e. the dihydrofolate is directly transferred from the TS active site to the DHFR active site without entering bulk solution.[77]

T. gondii relies on TS–DHFR for the synthesis of nucleotides essential for its survival. In addition, *T. gondii*, unlike humans, lacks salvage of thymidine thus tgTS

function is necessary for survival of the parasite.[76] Since the TS–DHFR enzyme is crucial for *T. gondii* survival, selective inhibition of tgTS represents a valid target to combat *T. gondii* infection. However, achieving selective inhibition of tgTS over hTS is difficult because TS is highly conserved across species (much more than DHFR) and also there is significant homology between the active site residues of tgTS and hTS as there is across species.[77, 78]

C. Receptor tyrosine kinase inhibitors

C.1 Angiogenesis

Angiogenesis is a complex physiological process in which new blood vessels are formed from existing vasculature.[79] Under normal physiological conditions, angiogenesis is tightly regulated by a balance between proangiogenic and antiangiogenic factors and is only promoted during embryonic and post-embryonic development, reproductive cycle, and wound repair.[80] However, upregulated angiogenesis has been described as one of the hallmarks of cancer, playing a crucial role in tumor growth, invasion, and metastasis. To grow beyond 2–3 mm^3 in size, solid tumors require increased blood supply to fulfill their demand for nutrients, oxygen, and proteolytic enzymes.[81] As a tumor grows in size, it also becomes increasingly hypoxic, and triggers the release of proangiogenic factors such as vascular endothelial growth factor (VEGF), platelet-derived endothelial growth factor (PDGF) and epidermal growth factor (EGF). These growth factors act as proangiogenic signals to initiate angiogenesis.

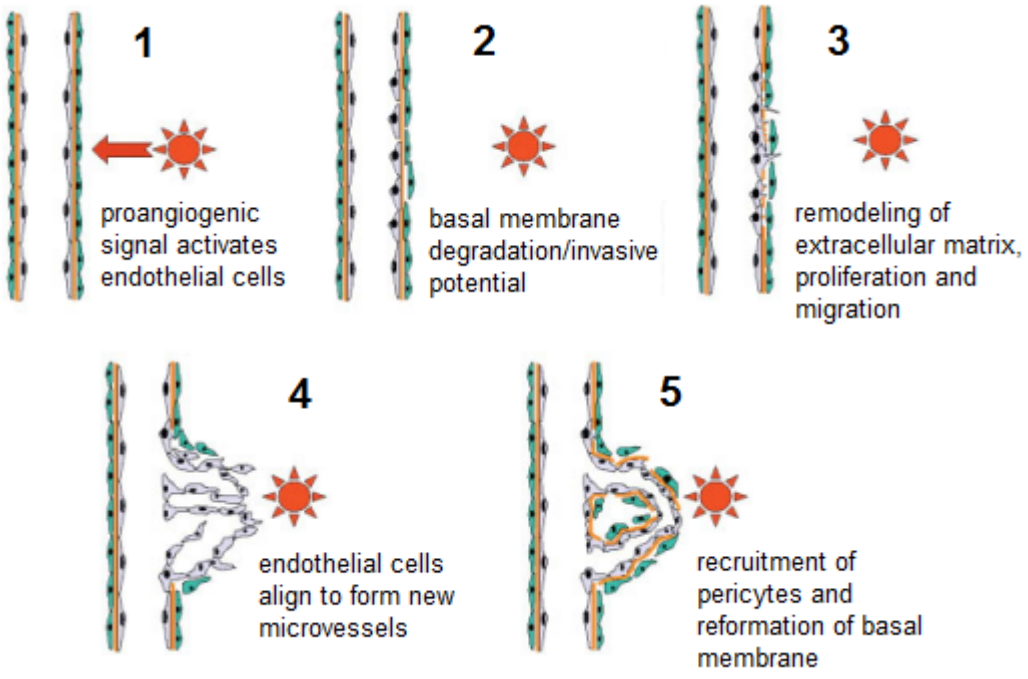

Figure 14. The angiogenic process (modified from ref. 81).

Angiogenesis is initiated when resting endothelial cells are activated by a proangiogenic signal (Figure 14). Endothelial cells release membrane degrading enzymes leading to migration, proliferation and finally differentiation to form new microvessels. A scheme describing the angiogenic process is provided in Figure 14.

The new blood vessels grow and infiltrate into the tumor, thereby providing nutrients and oxygen to sustain tumor proliferation and a route for cancer cell dissemination. This results in tumor progression and metastases.[82] The sustained growth of solid tumors is highly dependent on angiogenesis. Thus antiangiogenic agents have been widely used in the treatment of cancer.[83, 84] The present review will focus on receptor tyrosine kinases (RTKs) as potential targets for the inhibition of angiogenesis.

C.2 Receptor tyrosine kinases

Proangiogenic growth factors such as VEGF, PDGF and EGF bind to their corresponding growth factor receptors, commonly known as receptor tyrosine kinases (RTKs), and initiate signal transduction.[85] The RTKs, namely vascular endothelial growth factor receptor-2 (VEGFR-2), platelet-derived growth factor receptor-β (PDGFR-β) and epidermal growth factor receptor (EGFR), are cell-surface receptors that transfer a phosphate group from adenosine 5'-triphosphate (ATP) to the hydroxyl group of tyrosine of specific proteins inside the cell. The RTKs possess an extracellular domain, a transmembrane domain and an intracellular kinase catalytic domain (Figure 15).

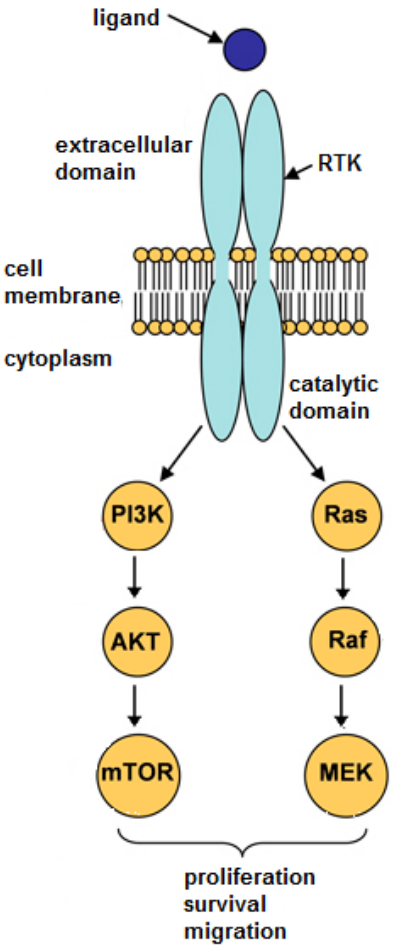

Figure 15. Signaling pathways of RTKs (modified from ref. 86).

Binding of the growth factor to the extracellular domain of RTKs results in receptor dimerization followed by autophosphorylation of the tyrosine residues within the cytoplasmic domain. Autophosphorylation then triggers a cascade of downstream cell signaling pathways (Figure 15) mediated by kinases such as Ras kinase, phosphoinositide 3-kinase (PI3K), mitogen/extracellular signal-regulated kinase (MEK) and extracellular signal-regulated kinase (ERK). Under normal physiological conditions, these signaling pathways are tightly monitored and regulated. Disregulation of these signaling pathways has been linked to malignancy and significantly contributes to the hallmarks of cancer:[87] insensitivity to antigrowth signals, evasion of apoptosis, sustained angiogenesis, tumor invasion and metastases. Thus, inhibition of these RTKs offers a key therapeutic strategy for cancer therapy.[88]

C.3 Inhibitors of receptor tyrosine kinases

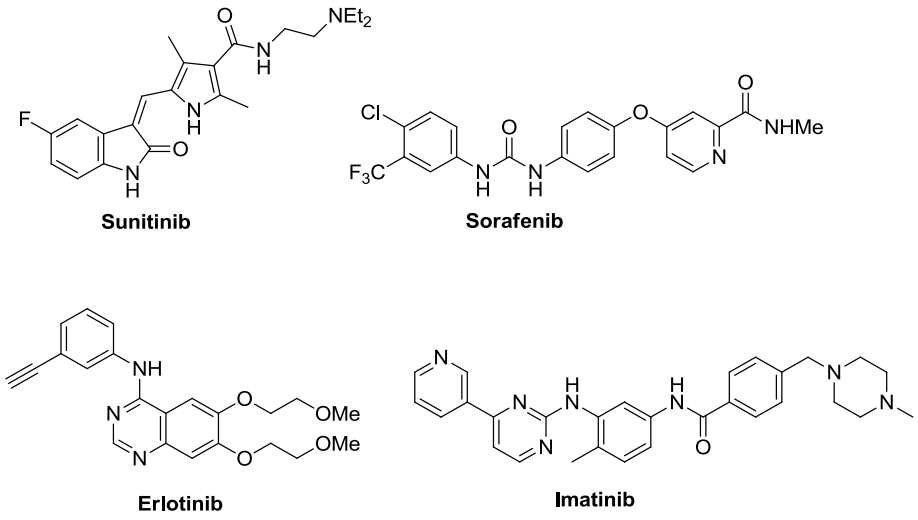

Figure 16. Representative RTK inhibitors in the clinic.

Several antiangiogenic agents such as sunitinib (Sutent®), sorafenib (Nexavar®) and erlotinib (Tarceva®) are currently approved for use in cancer patients (Figure 16).[79]

Imatinib mesylate (Gleevec®, Figure 2) was the first RTK inhibitor approved in the U.S. for chronic myeloid leukemia.[89] A number of RTKs have been recognized to be involved in tumor-induced angiogenesis. The key RTKs in angiogenesis include the VEGFR, PDGFR and EGFR families.

VEGFR. Three types of VEGFRs have been identified, VEGFR-1, VEGFR-2 and VEGFR-3.[90] Among these, VEGFR-2 has been recognized as the principal receptor that mediates VEGF stimulation in angiogenesis. The VEGF family consists of five members, VEGF-A, VEGF-B, VEGF-C, VEGF-D, and placental growth factor (PLGF). VEGF is an important growth factor that is involved in angiogenesis and vasculogenesis (i.e., the formation of the embryonic circulatory system).[91] VEGFRs are almost exclusively expressed on endothelial cells. In addition, VEGFRs are overexpressed in several tumor types with different expression patterns, ligand specificity and cellular/physiological effects of these receptors. Targeted inhibition or disruption of VEGFR-2 produces an abrogation of angiogenesis, decreased endothelial cell survival and decreased tumor growth.[90, 92] Several inhibitors of VEGFR-2 including sunitinib (Figure 16) and semaxanib have displayed antiangiogenic activity.[93, 94] Sunitinib (Sutent®) is a multi-RTK inhibitor (VEGFRs, PDGFRs and c-kit) important in the treatment of renal,[95] pancreatic,[96] and gastrointestinal[97] cancers. Sorafenib (Nexavar®) is also a multi-RTK inhibitor (VEGFR-2, VEGFR-3, PDGFR-β and Raf kinase) used in the treatment of renal,[98] hepatocellular[99] and thyroid[100] cancers.

PDGFR. PDGFR family is comprised of two receptors, PDGFR-α and PDGFR-β, which are activated upon binding to one of the growth factors PDGF-AA, -BB, -CC, -DD, and -AB.[101] PDGFRs are expressed on pericytes, smooth muscle cells that provide

mechanical support to the vasculature. PDGFR plays an important role in angiogenesis by stimulating the formation of microvascular pericytes, thereby stabilizing the newly formed blood vessels. They are also involved in the induction of VEGF secretion and consequently, angiogenesis. Sunitinib and sorafenib are the representative PDGFR-β inhibitors in the clinic.

EGFR. The EGFR family of receptors contains four members: EGFR-1 (later referred to as EGFR; also identified as Erb-B1, or human EGF receptor HER-1), HER-2 (Erb-B2), HER-3 (Erb-B3), and HER-4 (Erb-B4).[102] Among these, HER-2 lacks a known endogeneous ligand and HER-3 lacks kinase activity. The ligand for EGFR, EGF, controls a pathway that is linked to cell proliferation, migration, and differentiation. Overexpression of EGFR, its growth factors, and aberrant EGFR tyrosine kinase activity lead to increased tumor cell proliferation, survival and invasiveness.[103] Inhibition of EGFR signaling has been shown to promote selective apoptosis in tumor endothelial cells.[104] As a result, EGFR has been extensively studied and targeted by small molecule inhibitors and monoclonal antibodies.[102] Erlotinib (Tarceva®) is an EGFR inhibitor used to treat pancreatic[105] and non-small cell lung[106] cancers.

C.4 ATP-binding site of RTKs

Several X-ray crystal structures of RTKs are available in the PDB database.[58] All kinases share a catalytic domain that contains the ATP-binding site. The ATP-binding site of RTKs has been utilized as a promising target for rational drug design. Structural homology and diversity among the ATP-binding sites of kinases has allowed the building of pharmacophore models for rational drug design.[107, 108] The overall three-dimensional structure of the kinase domain is conserved throughout the protein kinase family.[109] The

N-terminal lobe consists of a twisted β-sheet of five antiparallel β-strands and one α-helix. The C-terminal lobe is made up of four β-strands and eight α-helices. Availability of ATP-bound or inhibitor-bound RTK crystal structures has enabled a detailed analysis of the catalytic site, its binding pockets in both active and inactive states as well as the modes of binding of RTK inhibitors.[107]

RTK catalytic cleft. The catalytic cleft of the RTKs usually consists of two regions commonly referred to as the front cleft and the back cleft.[110] While the ATP-binding site occupies the front cleft of the catalytic domain, the back cleft comprises of the elements responsible for the regulation of phosphorylation of peptide substrates. These two regions share a border that includes the aspartate-phenylalanine-glycine (DFG) motif and the β3 segment. A gatekeeper residue and a β3-lysine residue form a gate between the front and back cleft. Access to the back cleft is controlled by kinase gatekeeper residues. Small amino acid residues such as threonine and alanine or bulky gatekeeper residues such as phenylalanine, leucine or methionine control entry to binding in the back pocket and selectivity for inhibitors. The β3-lysine which is conserved in all kinase enzymes can adopt varied conformations in different protein kinases and helps in anchoring the α- and β-phosphates of ATP in the active state.

In a fully active state, protein kinases adopt a DFG-in conformation where the side chain of the DFG aspartate is directed into the ATP-binding site and the aromatic ring of the phenylalanine is positioned in the back cleft.[110] The aspartate in DFG motif chelates with Mg^{2+} and also helps in orienting the γ-phosphate of ATP for its transfer in the active DFG-in conformation.[107, 110] The aromatic side chain of phenylalanine in the active DFG-

in motif is in contact with αC. This contact in many active kinases facilitates the formation of a Lys-Glu ion pair for kinase catalysis.[107]

In the inactive state, the DFG motif is in either a DFG-in or DFG-out conformation.[110] In the DFG-out conformation, the phenylalanine aromatic ring is positioned in the ATP pocket and the aspartate residue of the DFG motif is in the back cleft.[107]

The front cleft. The front cleft includes the ATP-binding site and small, non-ATP contact regions. The ATP site is broadly divided into the following subregions depending on the binding mode (Figure 17).[107]

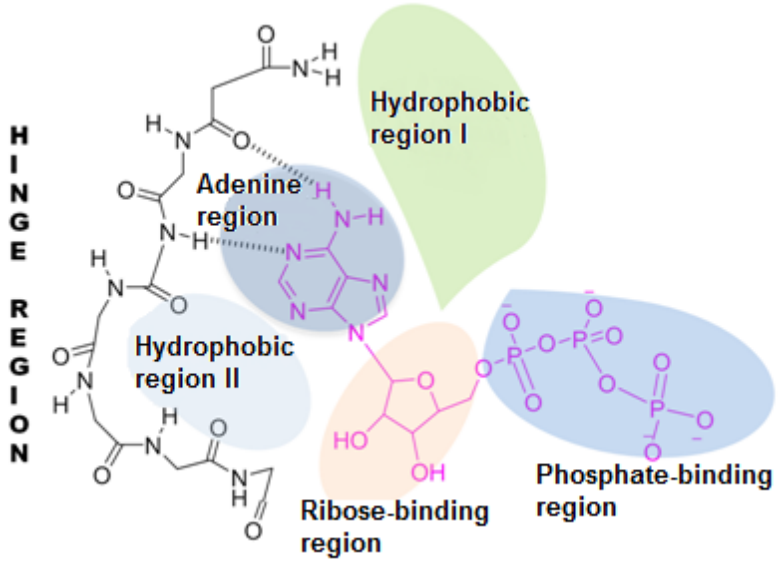

Figure 17. ATP-binding site of RTKs (modified from ref. 111). ATP is shown in magenta.

1. Adenine region: Adenine region is predominantly hydrophobic and is involved in binding various inhibitor scaffolds.[112] This region is bordered by the Hinge region and the gatekeeper. Two key hydrogen bonds are formed by the interaction of the N1 and N6 amino nitrogens of the adenine ring with the NH and carbonyl groups of the peptide

backbone of the hinge region residues of the RTKs. At least one of these key hydrogen bonds are utilized by several RTK inhibitors in binding to the RTKs. Other backbone amide groups in the Hinge region can serve as hydrogen bond donors or acceptors for inhibitor binding.

2. Ribose-binding region: The ribose pocket accommodates the sugar moiety of ATP and is adjacent to a hydrophilic, solvent exposed region. This pocket includes three hydrophobic residues (Ile, Val and Leu) which have been traditionally exploited in the design of EGFR inhibitors.[111]

3. Phosphate-binding region: This region is covered by Asp, Lys and Asn residues and the DFG motif. This region is highly flexible, hydrophilic and solvent exposed, and is therefore considered less important in improving inhibitor affinity and potency.[112]

4. Hydrophobic region II: This pocket is not used by ATP and serves as an entrance for ligand binding. The residues and conformation of this pocket vary depending on the kinase. Thus, this region has been used to obtain selectivity in the design of kinase inhibitors.[112]

The back cleft. In addition to the ATP-binding site, the back cleft provides important binding regions. ATP does not bind in the pockets in the back cleft.[110, 111]

1. Hydrophobic region I: The hydrophobic pocket in the back cleft adjacent to the adenine pocket is called Hydrophobic region I or Back pocket I (BP-I). This pocket has been explored in the design of inhibitors to gain selectivity for kinase targets with small gatekeeper residues.[110]

2. In addition to BP-I, additional binding pockets BP-II, BP-III, and BP-IV can also be accessed by inhibitors depending on the binding state of the RTKs.[107]

Major progress has been made in the rational drug design of RTK inhibitors targeting the ATP-binding site of RTKs. The front catalytic cleft of all kinase enzymes is accessible to ligand binding. Small molecule inhibitors that target the front cleft use a core scaffold to recognize the hinge region. The core scaffold is then substituted to extend into the different pockets of the ATP-binding site resulting in improved binding affinity and selectivity for RTKs.[113]

D. Single agents in combination chemotherapy

Multitargeted single agents or designed multiple ligands are defined as rationally designed single chemical entities that can selectively target two or more biological targets or processes.[114] The most commonly used strategy in the design of multitargeted agents is the hybrid drug design which involves combining structural elements from different compounds that bind to their respective targets. If the pharmacophores for the respective targets overlap, the common structural features of the lead compounds can be "merged" resulting in a multitargeted single agent.

Targeting different pathways in tumor cells using multitargeted agents can increase therapeutic effectiveness, as this strategy may for example prevent cancer cells from developing resistance.[115] Other advantages include a lower risk of drug–drug interactions *in vivo* and improved patient compliance due to less medications required.[116] A challenging factor in the design of multitargeted single agents is optimization of the pharmacokinetics of the lead compound while retaining a balanced target profile (i.e, optimizing the ratio of activities at the different targets and the effects of metabolism to ensure a therapeutic, but non-toxic effect at each of the targets).[114]

Several multitargeted drug strategies have been studied in cancer chemotherapy.[117, 118] One of the clinical strategies that have been successful is the combination of antiangiogenic and cytotoxic agents.[119-124] Multitargeted single agents that combine antiangiogenic effects by RTK inhibition and cytotoxic effects, are reviewed in the following section.

D.1 Dual RTK and TS inhibition

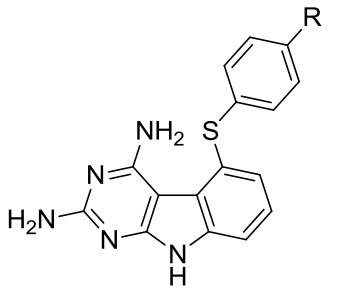

1 R = H
2 R = Me

Figure 18. Single agents with dual RTK and TS inhibitory activity.

2,4-Diamino-5-thioaryl-pyrimido[4,5-*b*]indoles **1** and **2** (Figure 18) have been reported by Gangjee and coworkers[125] as single agents with antiangiogenic and cytotoxic activities. These compounds inhibit VEGFR-2 and PDGFR-β for antiangiogenic effects and TS for cytotoxic effects with inhibitory potencies comparable or better than the standard compounds: semaxanib (VEGFR-2 inhibitor), DMBI (PDGFR-β inhibitor) and raltitrexed (hTS inhibitor). In COLO-205 metastatic colon cancer xenograft mouse models, compound **1** significantly decreased tumor growth, liver metastases and angiogenesis better than DMBI, remarkably without any toxicity.

D.2 Dual RTK and tubulin inhibition

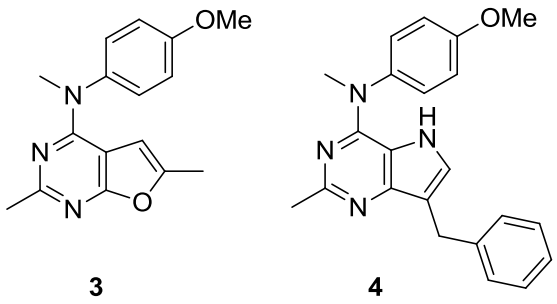

Figure 19. Single agents with dual RTK and tubulin inhibitory activity.

Gangjee and coworkers[55, 126] used hybrid drug design of RTK and tubulin inhibitors that led to the discovery of **3** and **4** (Figure 19) as single agents with antiangiogenic and cytotoxic activities. Both **3** and **4** had cytotoxic activity attributed to the inhibition of tubulin. While compound **3** inhibited both VEGFR-2 and PDGFR-β kinases for antiangiogenic effects, compound **4** had inhibition against VEGFR-2. Compounds **3** and **4** significantly reduced tumor size and vascularity in xenograft and allograft murine models and were superior to docetaxel and sunitinib, without any toxicity.

D.3 Dual RTK and DHFR inhibition

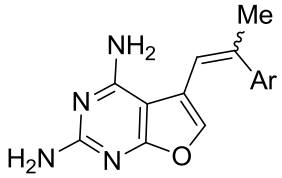

5 Ar = 2'-naphthyl
6 Ar = 2'-OMe-Ph

Figure 20. Single agents with dual RTK and DHFR inhibitory activity.

Gangjee *et al.*[127] reported 5-substituted,2,4-diamino-furo[2,3-*d*]pyrimidines **5** and **6** (Figure 20) as inhibitors of multiple RTKs and DHFR with antiangiogenic and antitumor activities. A 2:1 *E*/*Z* mixture of **5** and the *E*-isomer of **6** demonstrated dual VEGFR-2 and PDGFR-β inhibitory activity comparable to semaxanib and AG1295 as standard compounds, respectively. In a B16 melanoma mouse model, compounds **5** and **6** were as active as the standard antitumor agent methotrexate, both against primary tumors and metastases without any major toxicities.

II. CHEMICAL REVIEW

This section will review the chemistry relevant to the work described in this dissertation. It provides synthetic approaches to the following heterocyclic ring systems.

A. Pyrimido[4,5-*b*]indoles

B. Furo[2,3-*d*]pyrimidines

A. Pyrimido[4,5-*b*]indoles

Methods employed in the synthesis of pyrimido[4,5-*b*]indoles can be broadly divided into three classes:

1. Synthesis of pyrimido[4,5-*b*]indoles from indole precursors

2. Synthesis of pyrimido[4,5-*b*]indoles from pyrimidine precursors

3. Miscellaneous methods

A.1 Synthesis of pyrimido[4,5-*b*]indoles from indole precursors

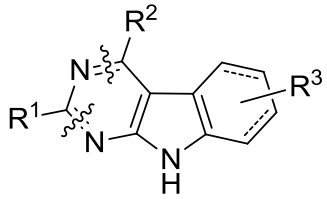

Figure 21. Disconnection strategy for pyrimido[4,5-*b*]indoles from indole precursors.

Different methods used in the synthesis of pyrimido[4,5-*b*]indoles from indoles or tetrahydroindoles utilize a disconnection strategy as shown in Figure 21.

Treatment of 1,2-dichloro-3-nitrobenzene **7** with ethyl cyanoacetate provided **8**,[125] which underwent reductive cyclization to the indole **9** (Scheme 1). Cyclocondensation of

9 with chlorformamidine hydrochloride afforded 2-amino-4-oxo-5-chloro-pyrimido[4,5-*b*]indole **10**.

Scheme 1. Synthesis of 2-amino-pyrimido[4,5-*b*]indoles from indoles

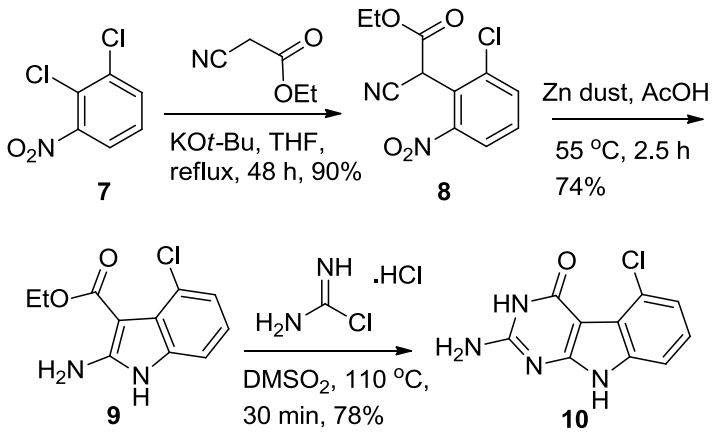

Alternatively, 2-amino-4-oxo-pyrimido[4,5-*b*]indoles can be synthesized by a two-step procedure as shown in Scheme 2 below.[128]

Scheme 2. Sequential two-step synthesis of 2-amino-pyrimido[4,5-*b*]indoles

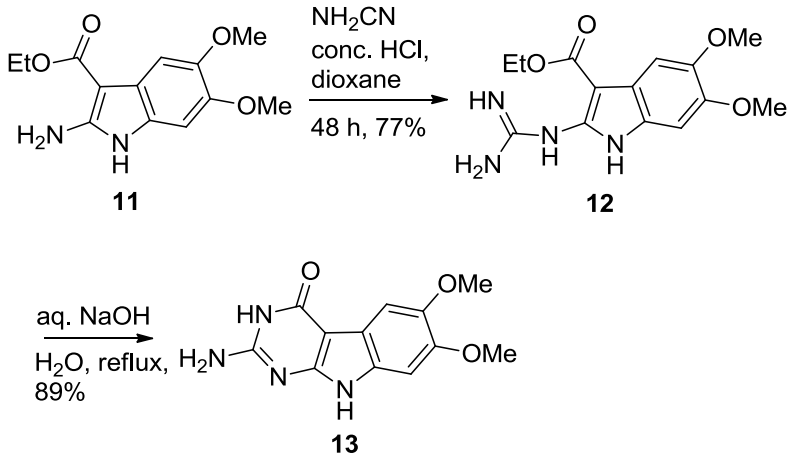

Reaction of the indole **11** (Scheme 2) with cyanamide and conc. HCl provided amidine intermediate **12**, which cyclized under alkaline conditions to 2-amino-4-oxo-6,7-dimethoxy-pyrimido[4,5-*b*]indole **13**.[128]

Scheme 3. Synthesis of the 2-unsubstituted pyrimido[4,5-*b*]indole **17**.

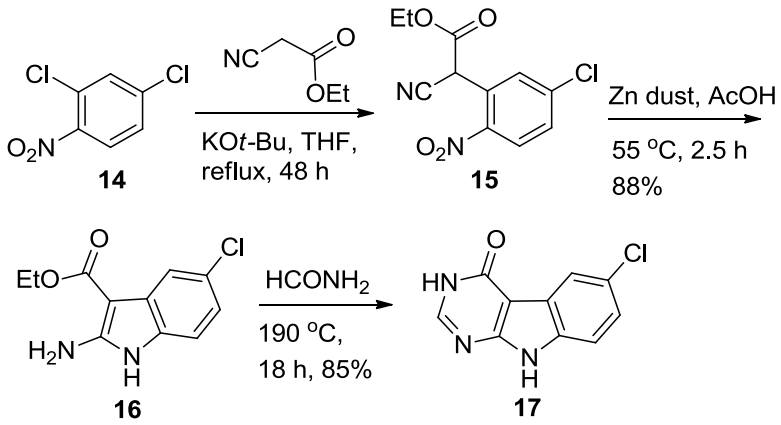

Analogous to 4-chloroindole derivative **9** in Scheme 1, the 5-chloroindole **16** (Scheme 3) was obtained from 1,3-dichloro-4-nitrobenzene **14**.[129] Compound **16** was cyclized using formamide to afford 2-unsubstituted 4-oxo-6-chloro-pyrimido[4,5-*b*]indole **17**.

Scheme 4. Versatile synthesis of 2-substituted pyrimido[4,5-*b*]indoles

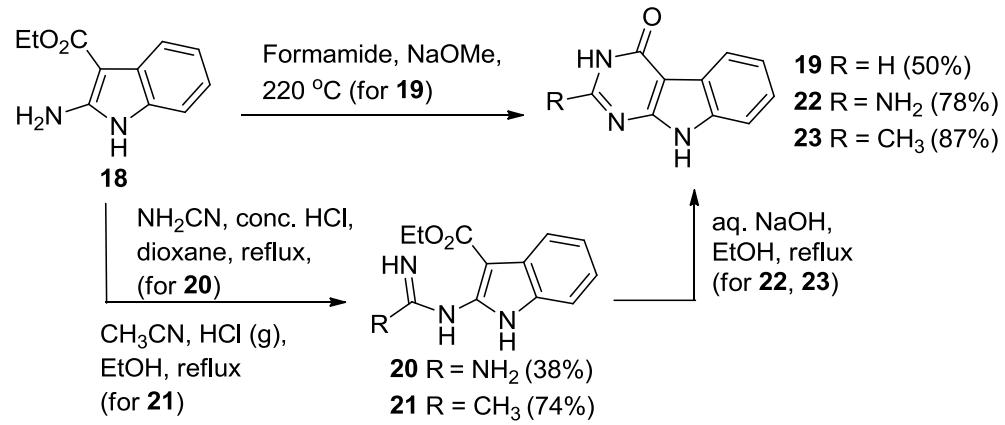

Showalter *et al*.[130] reported a versatile procedure for the preparation of 2-substituted 4-oxo-pyrimido[4,5-*b*]indoles **19**, **22** and **23** from ethyl 2-amino-1*H*-indole-3-carboxylate **18** (Scheme 4). Compound **18** was cyclized using formamide under basic conditions to 2-unsubstituted pyrimido[4,5-*b*]indole **19**. Treatment of **18** with cyanamide and acetonitrile under acidic conditions provided intermediates **20** and **21**, which were cyclized using 1N NaOH to 2-amino- and 2-methyl-pyrimido[4,5-*b*]indoles **22** and **23**, respectively.

Scheme 5. Venugopalan strategy[128] for the synthesis of 2-substituted pyrimido[4,5-*b*]indoles

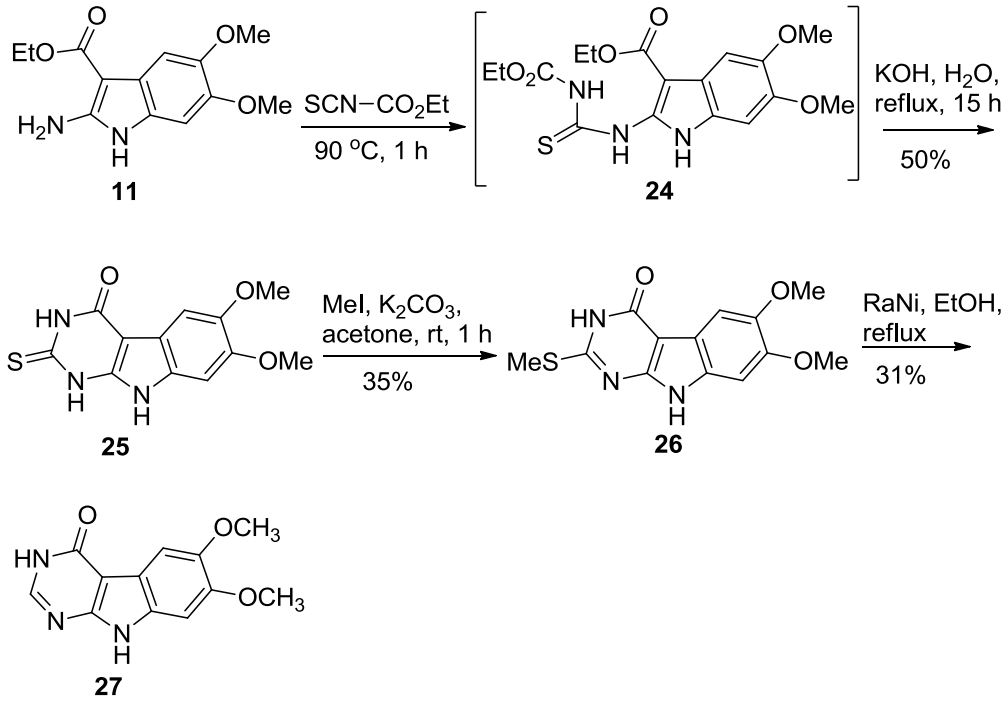

Venugopalan *et al*.[128] reported the synthesis of 2-substituted pyrimido[4,5-*b*]indoles from ethyl 2-amino-4,5-dimethoxy-indole carboxylate **11** (Scheme 5). Treatment of **11** with ethyl carboxyisothiocyanate gave **24**, which cyclized to the 2-thio-4-oxo-pyrimido[4,5-*b*]indole **25** under basic conditions. Methylation of **25** afforded the 2-

methylthio-pyrimido[4,5-*b*]indole **26**, which upon reduction gave the 2-unsubstituted pyrimidoindole **27**. For the synthesis of 2-unsubstituted pyrimido[4,5-*b*]indoles, this strategy presents an alternative to the approach described in Schemes 3 and 4, in which 2-unsubstituted pyrimidoindoles **17** (Scheme 3) and **19** (Scheme 4) were synthesized by a direct reaction of indoles with formamide.

Scheme 6. Synthesis of pyrimido[4,5-*b*]indoles via Pd-catalyzed amidation and cyclization of 2-haloindoles

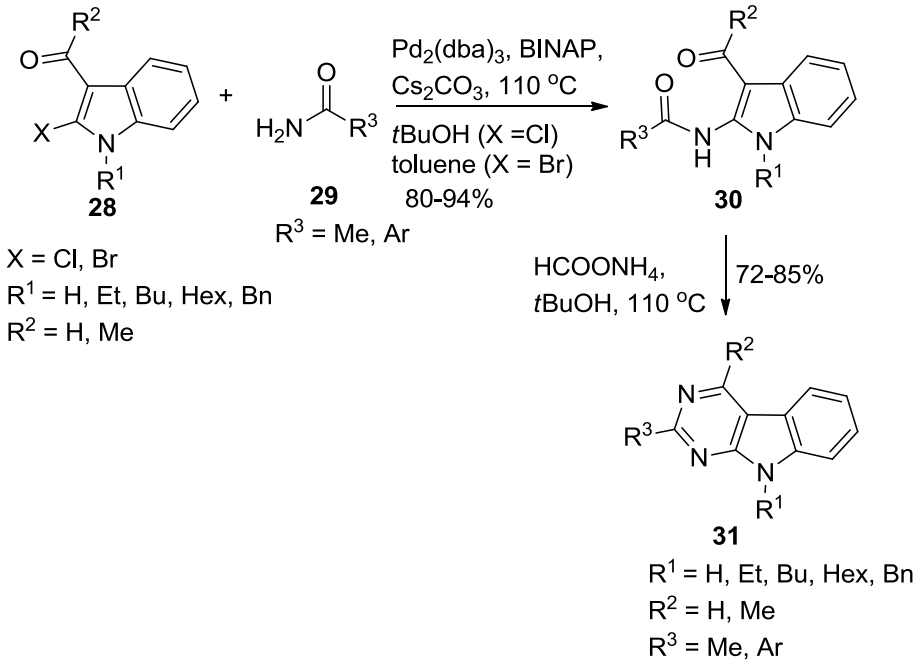

Kumar *et al.*[131] synthesized pyrimido[4,5-*b*]indoles from 2-haloindoles via palladium-catalyzed amidation and cyclization. Coupling of the 3-formyl- or 3-acetyl-2-haloindoles **28** and amides **29** provided **30** in 80–94% yield (Scheme 6). Treatment of **30** with ammonium formate resulted in the formation of pyrimido[4,5-*b*]indoles **31**. According to the proposed mechanism for **30→31**, ammonium formate thermally decomposes and releases ammonia which attacks 3-carbonyl of **30** and generates the

"imine" intermediate, which then cyclizes to provide the desired pyrimido[4,5-*b*]indole **31**.

In Schemes 1–6 above, indoles were utilized to obtain pyrimido[4,5-*b*]indoles. Schemes 7 and 8 below present synthesis of pyrimido[4,5-*b*]indoles from tetrahydroindoles.

Scheme 7. Synthesis of pyrimido[4,5-*b*]indoles from tetrahydroindoles

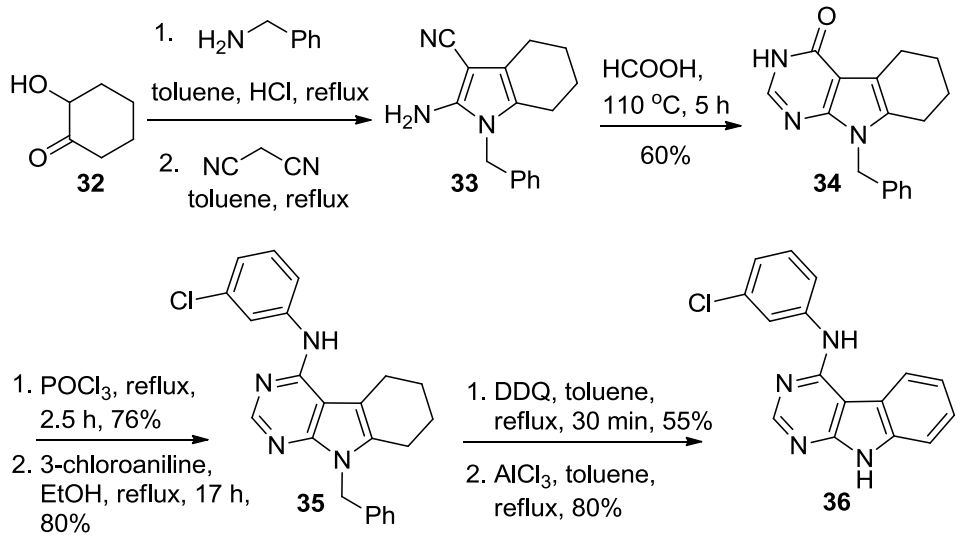

The tetrahydro-1*H*-indole **33** (Scheme 7) was obtained by the treatment of 2-hydroxycyclohexanone **32** with benzylamine and malononitrile.[132] Compound **33** was cyclized using formic acid to the 4-oxo-tetrahydropyrimido[4,5-*b*]indole **34**. Chlorination of the 4-oxo of **34** followed by displacement with 3-chloroaniline afforded **35**. Oxidation of **35** using 2,3-dichloro-5,6-dicyano-1,4-benzoquinone (DDQ) and subsequent removal of the benzyl group provided pyrimido[4,5-*b*]indole **36**.

Müller *et al*.[133] synthesized a series of chiral pyrimido[4,5-*b*]indole derivatives **41** and **42** (Scheme 8). Reaction of chiral tetrahydroindoles **37** with benzonitrile and sodium

methoxide yielded the 2-phenyl-4-amino-tetrahydropyrimido[4,5-*b*]indoles **38**. On the other hand, treatment of **37** with benzoyl chloride provided **40**, which was subsequently cyclized to the 2-phenyl-4-oxo-tetrahydropyrimido[4,5-*b*]indoles **41**. Dehydrogenation of the tetrahydroindoles **38** and **41** furnished the desired pyrimido[4,5-*b*]indoles **39** and **42**, respectively.

Scheme 8. Synthesis of 2-phenyl-pyrimido[4,5-*b*]indoles from tetrahydroindoles

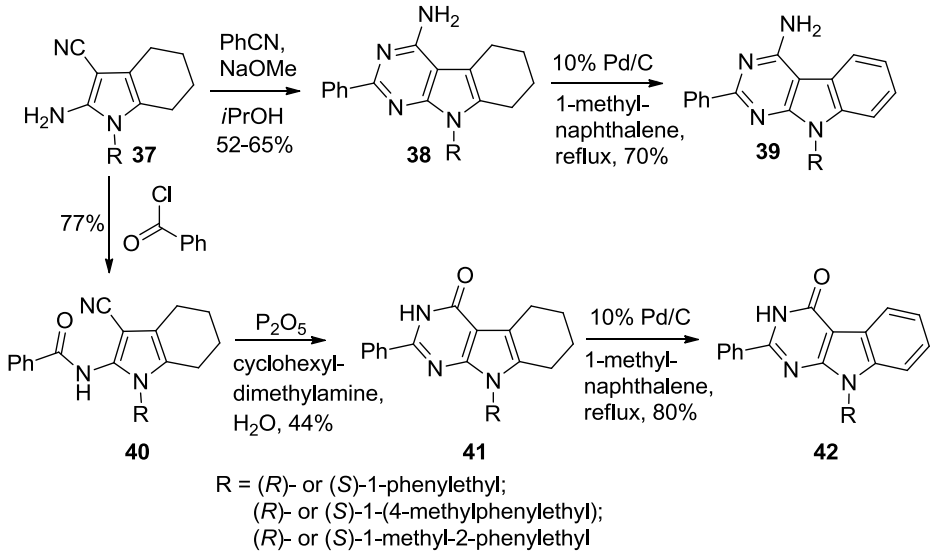

A.2 Synthesis of pyrimido[4,5-*b*]indoles from pyrimidine precursors

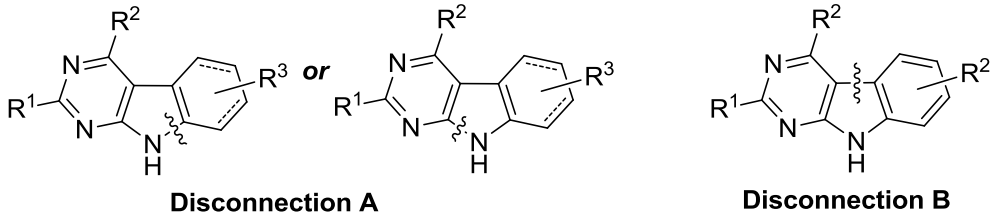

Figure 22. Disconnection strategies for pyrimido[4,5-*b*]indoles from pyrimidine precursors.

Different methods used in the synthesis of pyrimido[4,5-*b*]indoles from pyrimidines employ disconnection strategies A or B as shown in Figure 22.

Scheme 9. Pyrimido[4,5-*b*]indol-2,4-diones from Fischer indole cyclization of 6-(arylhydrazino)uracils

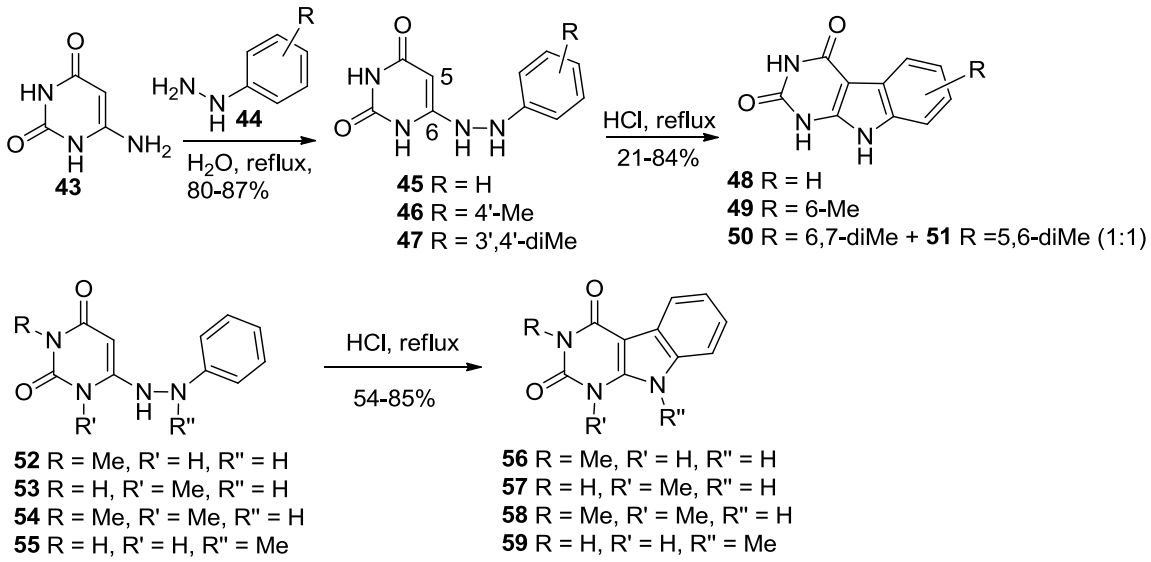

A series of pyrimido[4,5-*b*]indoles using a facile Fischer-type cyclization were synthesized by G. E. Wright (Scheme 9).[134] Treatment of 6-aminouracil **43** with phenyl hydrazines **44** provided 6-(arylhydrazino)uracils **45**–**47**. Compounds **45** and **46** underwent acid–mediated cyclization to **48** and **49** respectively, whereas **47** gave an equal mixture of regioisomers **50** and **51**. The scope of this reaction was extended to the N^1- and/or N^3-methyl 6-(arylhydrazino)uracils **52**–**54** or the *N*-methyl aniline derivative **55**, resulting in the synthesis of pyrimido[4,5-*b*]indol-2,4-diones **56**–**59**, respectively.

The cyclization reaction is analogous to a classical Fischer indole synthesis. The mechanism probably involves N^6-protonation followed by nucleophilic attack by the *ortho* phenyl carbon on the uracil 5-carbon and cleavage of the *N*-*N* bond.

Rearomatization of the phenyl moiety results in the formation of a 5-membered ring by a favored 5-exo-trig cyclization. Finally, the explusion of the uracil amino group gives rise to the pyrimido[4,5-*b*]indole. In the formation of **59** from **55**, the *N*-methyl on the aniline moiety is retained in the product, which indicates that the uracil 6-amino group is expelled as ammonia in the final step of the cyclization.

Scheme 10. Application of Nenitzescu reaction in the synthesis of pyrimido[4,5-*b*]indoles

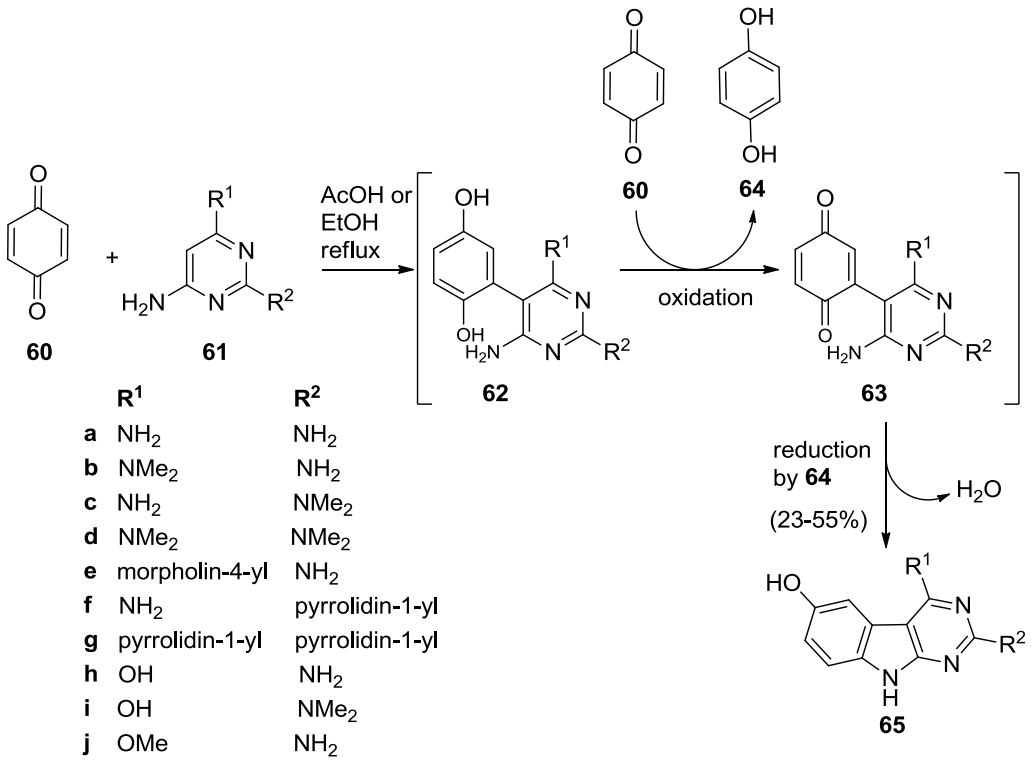

	R^1	R^2
a	NH_2	NH_2
b	NMe_2	NH_2
c	NH_2	NMe_2
d	NMe_2	NMe_2
e	morpholin-4-yl	NH_2
f	NH_2	pyrrolidin-1-yl
g	pyrrolidin-1-yl	pyrrolidin-1-yl
h	OH	NH_2
i	OH	NMe_2
j	OMe	NH_2

The Nenitzescu reaction was utilized by Dotzauer *et al.*[135] to prepare pyrimido[4,5-*b*]indoles via a one-step procedure from 1,4-benzoquinone **60** and 6-aminopyrimidines **61** (Scheme 10). Compounds **61** were treated with excess of 1,4-benzoquinone **60** in boiling glacial acetic acid to provide 6-hydroxy-pyrimido[4,5-*b*]indoles **62** via a mechanism similar to the Nenitzescu reaction. According to the proposed mechanism, the enone of

60 reacts with 6-aminopyrimidine **61** and forms a Michael adduct **62**. Intermediate **62** is oxidized to **63** by benzoquinone **60**, which in turn is reduced to hydroquinone **64**. Intramolecular cyclization of **63** and final hydrogenation by hydroquinone **64** results in the formation of 2,4-disubstituted 6-hydroxy-pyrimido[4,5-*b*]indoles **65**.

Scheme 11. Synthesis of pyrimido[4,5-*b*]indole-2,4-diones from 4-azidouracils

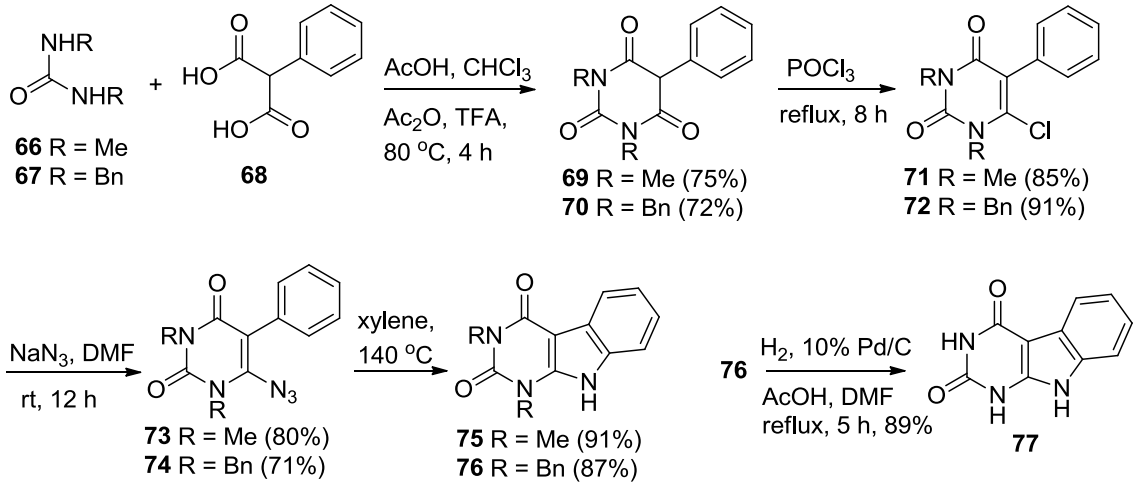

Lapachev *et al*.[136] reported the conversion of 4-azidoouracils to pyrimido[4,5-*b*]indoles (Scheme 11). The synthesis commenced by reacting *N*,*N*-disubstituted ureas **66** and **67** with phenyl malonic acid **68** in the presence of acetic anhydride to obtain 1,3-disubstituted barbituric acids **69** and **70**, respectively. The 4-oxo of **69** and **70** were regiospecifically chlorinated to afford **71** and **72**, which were then converted to 4-azidouracils **73** and **74**, respectively. Thermolysis of the azidouracils **73** and **74** in boiling xylene resulted in the formation of the pyrimido[4,5-*b*]indole-2,4-diones **75** and **76**, respectively. Hydrogenolysis of the *N*-benzyl of **76** afforded the 1,3-unsubstituted pyrimido[4,5-*b*]indole-2,4-dione **77**.

Schemes 12 and 13 below employ disconnection strategy B (Figure 22) for the synthesis of pyrimido[4,5-*b*]indoles via the intramolecular cyclization of arylamino- or cyclohexylamino-substituted pyrimidines.

Scheme 12. Large-scale synthesis of pyrimido[4,5-*b*]indole **85** from trichloropyrimidine

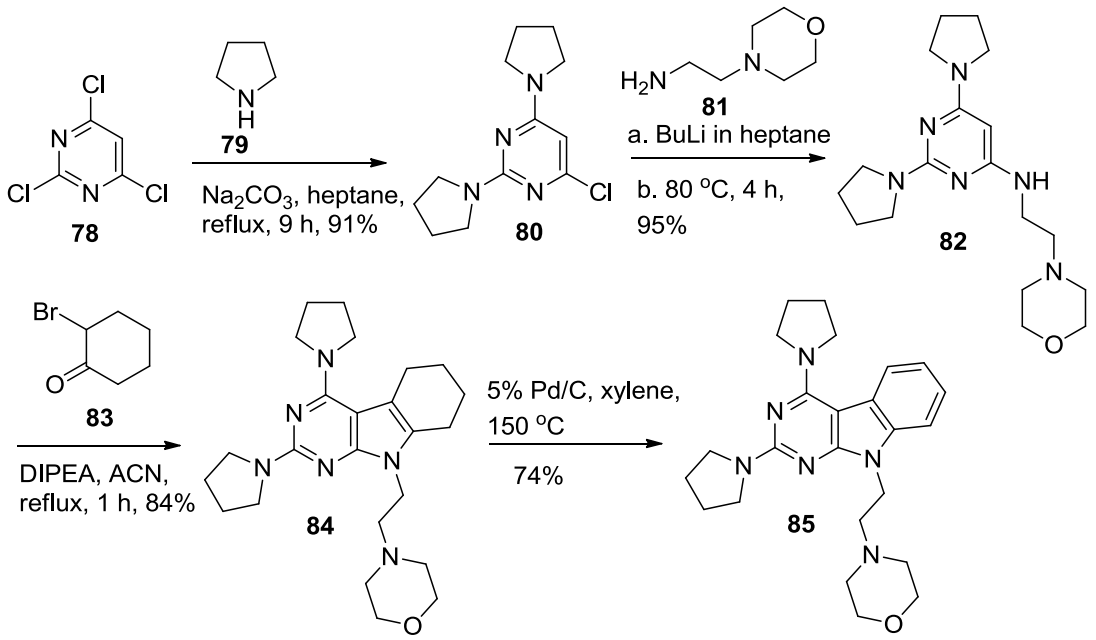

Mauragis *et al*.[137] developed a reliable large-scale process to produce >100 kg of the pyrimido[4,5-*b*]indole **85** (Scheme 12). The synthesis commenced with displacement of the 2- and 4-chloro of 2,4,6-trichloropyrimidine **78** with pyrrolidine **79** to obtain **80**. Displacement of the remaining chloro group in **80** with the lithium amide of **81** provided **82**. Conversion of **82** to the tetrahydropyrimido[4,5-*b*]indole **84** was accomplished by alkylation with bromocyclohexanone **83** and subsequent cyclization. Dehydrogenation of **84** using 5% Pd/C afforded the pyrimido[4,5-*b*]indole **85**.

Zhang *et al*.[138] synthesized various pyrimido[4,5-*b*]indoles via Pd-catalyzed cyclization of 4-anilino-5-iodopyrimidines **88** (Scheme 13). Compounds **88** were

prepared from 4-chloro-5-iodopyrimidine **86** and appropriate anilines **87**. Palladium-catalyzed cyclization of the 5-iodo of **88** provided pyrimido[4,5-*b*]indoles **89** in moderate to good yields.

Scheme 13. Synthesis of pyrimido[4,5-*b*]indoles via palladium-catalyzed cyclization

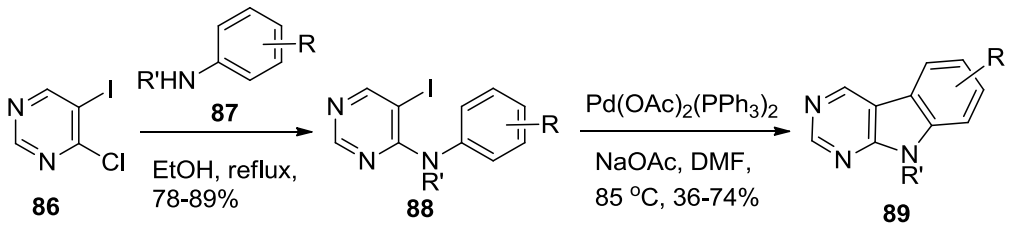

A.3 Miscellaneous methods

Schemes 14–17 discuss the synthesis of pyrimido[4,5-*b*]indoles from oxindoles. Adib *et al*.[139] reported microwave-assisted synthesis of 2,4-diaryl-pyrimido[4,5-*b*]indoles from oxindoles (Scheme 14).

Scheme 14. Microwave-assisted synthesis of pyrimido[4,5-*b*]indoles from oxindoles

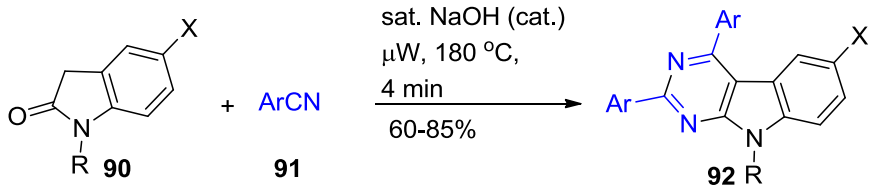

Oxindoles **90** (X = H or Br) react with a variety of aryl nitriles of general structure **91** under microwave irradiation and solvent-free conditions to produce the corresponding pyrimido[4,5-*b*]indoles **92** in good to high yields (Scheme 14).[139]

Scheme 15. Synthesis of 2-substituted pyrimido[4,5-*b*]indoles from oxindole

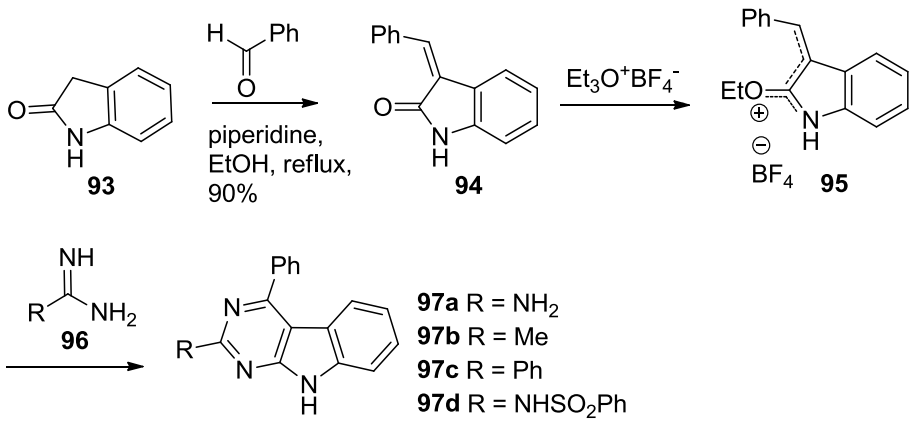

Borovik *et al*.[140] developed a versatile procedure for the synthesis of 2-substituted 4-phenyl-pyrimido[4,5-*b*]indoles **97a**–**d** from oxindole **93** (Scheme 15). Condensation of oxindole **93** with benzaldehyde afforded **94**, which was treated with triethyloxonium tetrafluoroborate to obtain the 2-ethoxy(3-benzylidene)indolenine tetrafluoroborate **95**. Compound **95** was cyclized with substituted amidines **96** to provide 2-substituted 4-phenyl-pyrimido[4,5-*b*]indoles **97a**–**d**.

Scheme 16. Synthesis of 2-substituted pyrimido[4,5-*b*]indoles from 2-amino-pyrimido[4,5-*b*]indole **97a**

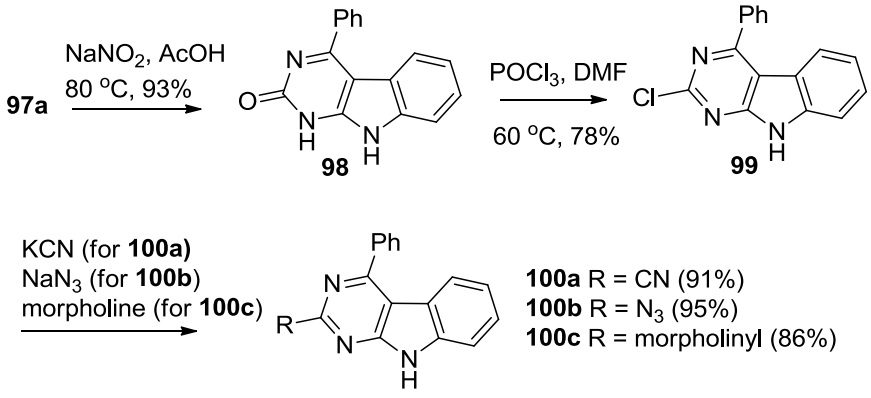

Scheme 16 provides the utilization of 2-amino-4-phenyl-pyrimido[4,5-*b*]indole **97a** in the synthesis of various 2-substituted pyrimido[4,5-*b*]indole**s 98** and **100a**–**c**.[140] Diazotization of 2-amino-pyrimidoindole **97a** furnished 2-oxo-pyrimido[4,5-*b*]indole **98**, which was chlorinated to obtain **99**. Displacement of the 2-chloro of **99** with appropriate nucleophiles afforded 2-substituted pyrimido[4,5-*b*]indole**s 100a**–**c**.

Scheme 17. One-pot multi-component synthesis of pyrimido[4,5-*b*]indoles

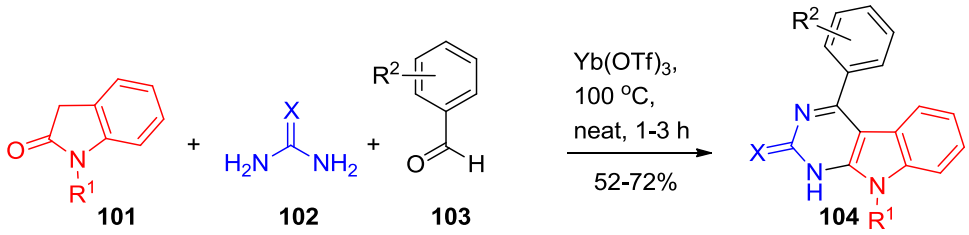

2-Oxo- or 2-thio-substituted 4-aryl-pyrimido[4,5-*b*]indole**s 104** (Scheme 17) were synthesized from a one-pot multi-component reaction of oxindoles **101**, urea or thiourea **102** and aryl aldehyde **103** under solvent-free conditions (Scheme 17).[141] The synthesis employed ytterbium triflate as the catalyst.

Molina *et al*.[142] employed an aza-Wittig type reaction in the synthesis of pyrimido[4,5-*b*]indole **110** (Scheme 18). Diazide **107** was prepared by condensation of *o*-azidobenzaldehyde **105** with ethyl azidoacetate **106**. Staudinger reaction between the diazide **107** and triphenyl phospine gave bis(iminophosphorane) **108**. Treatment of **108** with *p*-tolyl isocyanate in toluene at reflux provided pyrimido[4,5-*b*]indole **110**.

The conversion of **108** to **110** (Scheme 18) can be rationalized in terms of an initial aza-Wittig reaction between the iminophosphorane group linked to the aromatic ring and the isocyanate to give a highly reactive carbodiimide **109a.** Intermediate **109a** undergoes

cyclization by nucleophilic attack by the β-carbon (on the ester side chain) leading to the zwitterionic intermediate **109b**, which undergoes further transformations to indole **109c**. An aza-Wittig reaction of **109c** with a second equivalent of aryl isocyanate gives the carbodiimide **109d**, which subsequently cyclizes to pyrimido[4,5-*b*]indole **110** upon nucleophilic attack of the 2-amino group on the central carbon atom of the carbodiimide moiety.

Scheme 18. Synthesis of pyrimido[4,5-*b*]indole **110** using an aza-Wittig type reaction

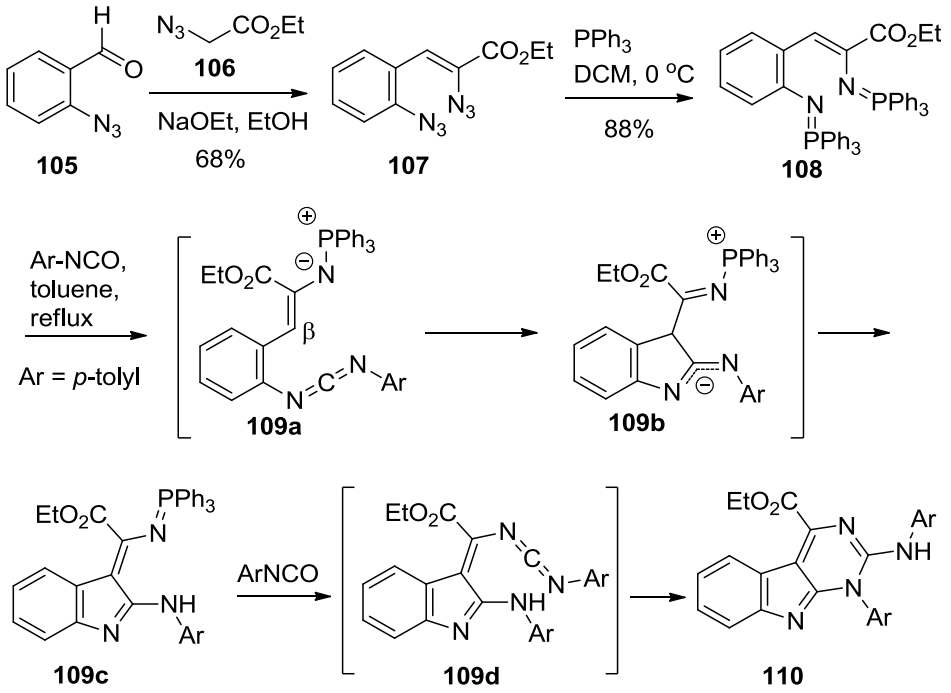

B. Furo[2,3-*d*]pyrimidines

Synthetic strategies that are used in the synthesis of furo[2,3-*d*]pyrimidines can be broadly classified into two strategies:

1. Strategy I: From furan precursors

2. Strategy II: From pyrimidine precursors

B.1. Furo[2,3-*d*]pyrimidines from furan precursors

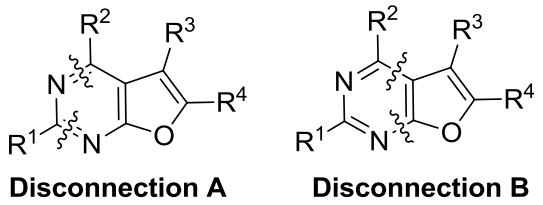

Figure 23. Disconnection strategies for furo[2,3-*d*]pyrimidines from furan precursors.

Different methods used in the synthesis of furo[2,3-*d*]pyrimidines from furan precursors utilize disconnections A or B (Figure 23). For disconnection A, the precursors to cyclization are generally 2-amino-furan-3-nitriles. Disconnection B involves 2-aminofurans and 1,3,5-triazines as precursors.

Scheme 19. Synthesis of 4-amino-furo[2,3-*d*]pyrimidines from 2-amino-furan-3-nitriles

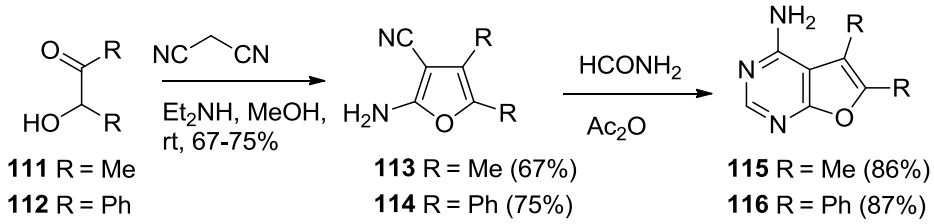

Karl Gewald[143] reported the first synthesis of furo[2,3-*d*]pyrimidines starting from a furan precursor. α-Hydroxy ketones **111** and **112** were treated with malononitrile to afford 2-amino-3-cyanofurans **113** and **114** respectively (Scheme 19). Condensation of **113** and **114** with formamide provided 4-amino-furo[2,3-*d*]pyrimidines **115** and **116** respectively.

The aforementioned strategy to obtain furo[2,3-*d*]pyrimidines from 2-amino-furan-3-nitriles has been utilized by several research groups. Miyazaki and coworkers[144] used this approach to synthesize 4-amino-5-aryl-furo[2,3-*d*]pyrimidines **120** (Scheme 20).

Scheme 20. Synthesis of 4-amino-5-aryl-furo[2,3-*d*]pyrimidines

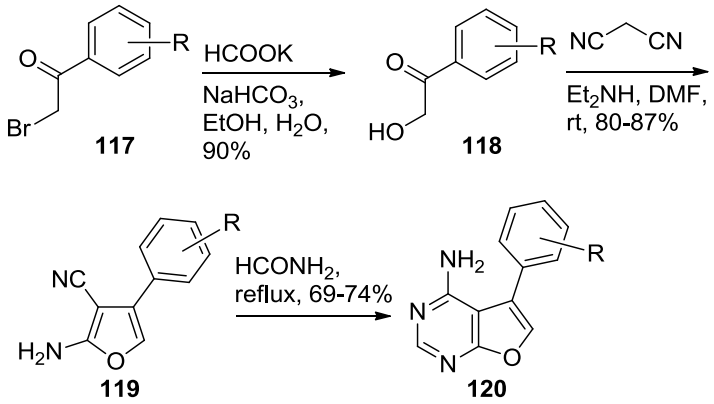

Treatment of 1-aryl-2-bromoethanone **117** (Scheme 20) with potassium formate and aqueous sodium bicarbonate provided **118**.[144] Compound **118** was treated with malononitrile to afford 2-amino-5-aryl-furan-3-nitriles **119**, which were then heated to reflux with formamide to obtain **120** in 69–74% yield.

Scheme 21. Miyazaki strategy[145] for the cyclization of 2-amino-3-cyanofurans to furo[2,3-*d*]pyrimidines

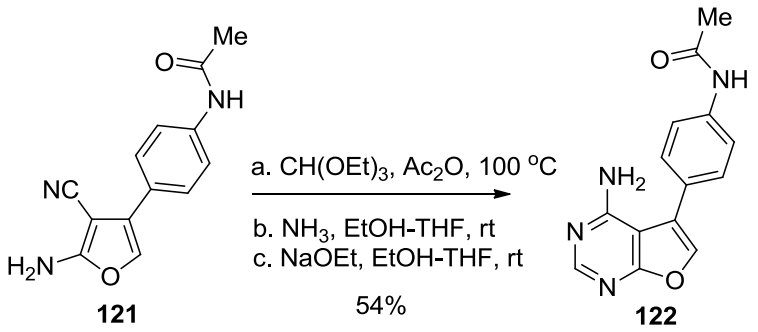

Miyazaki *et al*.[145] reported an alternate synthesis of 2-unsusbstituted 4-amino-5-aryl-furo[2,3-*d*]pyrimidines **122** (Scheme 21) by treating the furan **121** with triethyl orthoformate, followed by amination and base-catalyzed cyclization.

Scheme 22. Dimroth rearrangement in the synthesis of N^4-substituted 5,6-diaryl-furo[2,3-*d*]pyrimidines

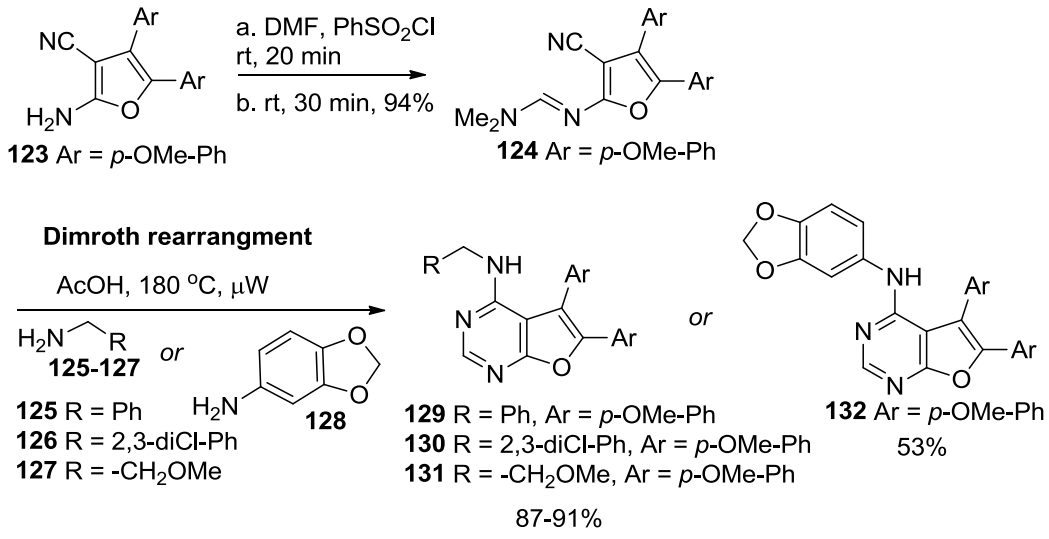

Han and coworkers[146] reported a novel synthesis of N^4-substituted 5,6-diaryl-furo[2,3-*d*]pyrimidines **129**–**132** by microwave irradiation of the formamidine derivative **123** and substituted amines (Scheme 22). Compound **123** was reacted with DMF and benzene sulfonyl chloride to obtain the formamidine derivative **124**. Compound **124** reacts with amines **125**–**127** or benzo[*d*][1,3]dioxol-5-amine **128** and undergoes Dimroth rearrangement to provide **129**–**132**, respectively.

Schemes 19–22 focused on synthesis of furo[2,3-*d*]pyrimidines with no substitution at the 2-position. Scheme 23 below presents the synthesis of 2-methyl-furo[2,3-*d*]pyrimidines by Dave *et al.*[147] Acid-mediated condensation of the furan **114** with acetonitrile afforded 2-methyl-4-amino-5,6-diphenyl-furo[2,3-*d*]pyrimidine **133**.

Scheme 23. Synthesis of 2-methyl-4-amino-furo[2,3-*d*]pyrimidine **133**

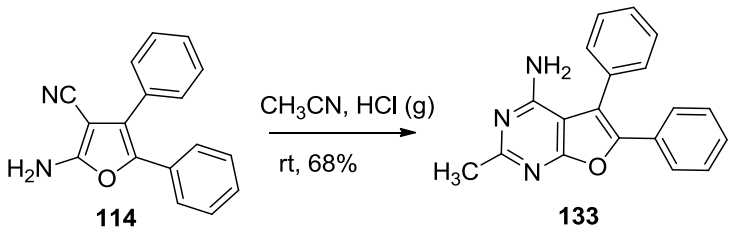

Schemes 19–23 provided strategies for the synthesis of 4-amino-furo[2,3-*d*]pyrimidines. Schemes 24 and 25 below focus on strategies toward the synthesis of 4-oxo-furo[2,3-*d*]pyrimidines.

Scheme 24. Synthesis of 4-oxo-furo[2,3-*d*]pyrimidines

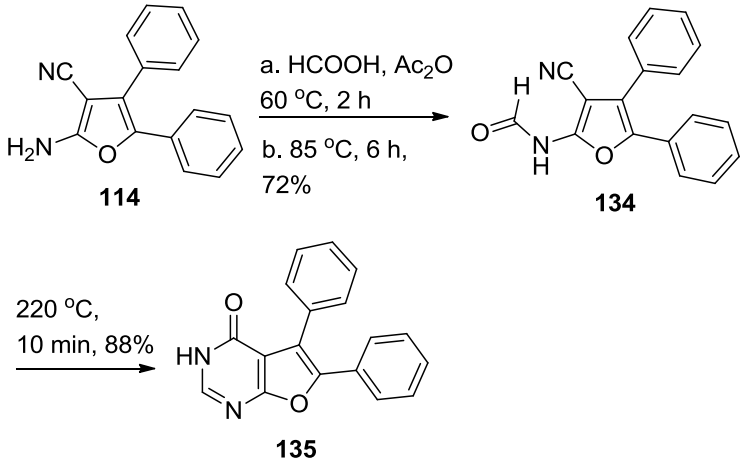

Foloppe and coworkers[148] performed condensation of the furan **114** (Scheme 24) and in situ generated acetic formic anhydride to obtain the *N*-formyl derivative **134**, which underwent thermal cyclization to 4-oxo-5,6-diphenyl-furo[2,3-*d*]pyrimidine **135**.

α-Chloro-β-keto esters **136** and **137** (Scheme 25) reacted with ethyl cyanoacetate under basic conditions to form ketonitriles, which were readily cyclized to tetrasubstituted furans **138** and **139**, respectively.[149] Treatment of **138** and **139** with formamide under acidic conditions afforded furo[2,3-*d*]pyrimidines **140** and **141**,

respectively. Hydrolysis to acids **142** and **143** followed by decarboxylation gave 4-oxo-6-aryl-furo[2,3-*d*]pyrimidines **144** and **145**, respectively. Compounds **144** and **145** represent examples of 5-unsubstituted 6-aryl-furo[2,3-*d*]pyrimidines from furan precursors.

Scheme 25. Synthesis of 6-aryl-furo[2,3-*d*]pyrimidines **144** and **145**

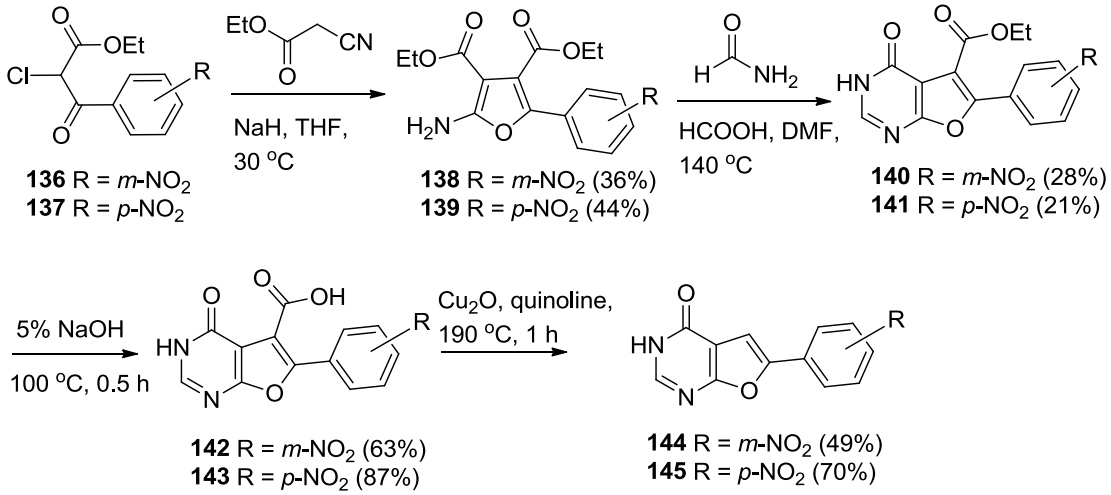

Dang and Liu[150] utilized disconnection strategy B (Figure 23) for the synthesis of furo[2,3-*d*]pyrimidines from 2-aminofurans (Scheme 26).

Scheme 26. Synthesis of furo[2,3-*d*]pyrimidine **148** using Diels–Alder reaction

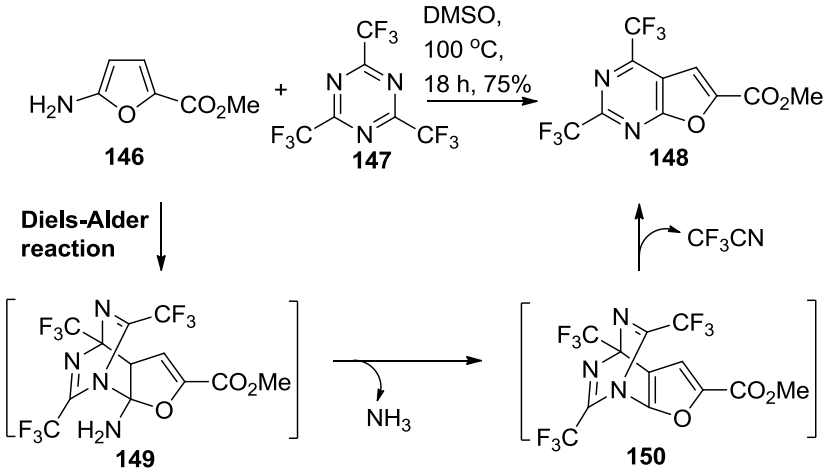

Diels–Alder reaction of 2-aminofuran **146** and 1,3,5-triazine **147** provided furo[2,3-*d*]pyrimidine **148** (Scheme 26). The transformation proceeds through a series of reactions involving Diels–Alder reaction to give intermediate **149**, followed by the elimination of ammonia to afford intermediate **150**, which then undergoes a retro Diels–Alder reaction to **148**.

B.2. Furo[2,3-*d*]pyrimidines from pyrimidine precursors

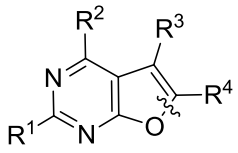

Figure 24. Disconnection strategy for furo[2,3-*d*]pyrimidines from pyrimidine precursors.

Synthesis of furo[2,3-*d*]pyrimidines from pyrimidine precursors utilize 2-hydroxypyrimidines as intermediates (Figure 24). Schemes 27–32 represent examples that utilize 4-hydroxypyrimidines as precursors for the synthesis of furo[2,3-*d*]pyrimidines.

Scheme 27. Synthesis of 2,6-dimethyl-furo[2,3-*d*]pyrimidine **154**

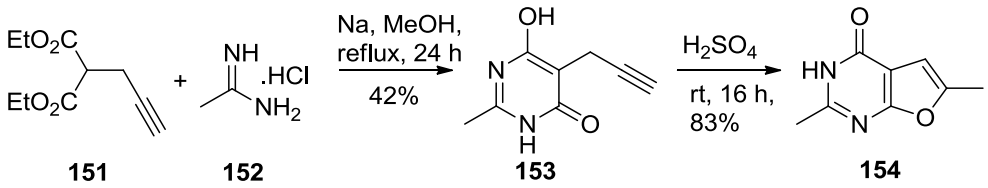

Condensation of diethyl propargyl malonate **151** (Scheme 27) and acetamidine hydrochloride **152** under basic conditions gave 2,4-dihydroxy pyrimidine **153**,[55] which

underwent acid-catalyzed intramolecular cyclization to 2,6-dimethyl-4-oxo-furo[2,3-*d*]pyrimidine **154** in 83% yield.

Scheme 28. Synthesis of 4,6-dimethyl-furo[2,3-*d*]pyrimidines

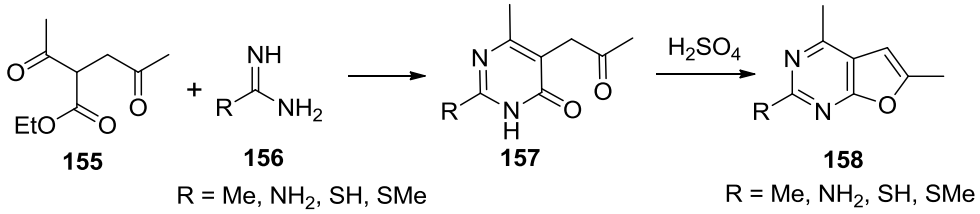

Condensation of β-ketoester **155** (Scheme 28) with amidines **156** afforded 5-acetonyl pyrimidines **157**.[151] Similar to Scheme 27, compound **157** was cyclized under acidic conditions to provide 4,6-dimethyl-2-substituted furo[2,3-*d*]pyrimidines **158**.

Unlike Schemes 27 and 28 that use acid-catalyzed cyclization, Sakamoto and coworkers[152] employed basic conditions for the intramolecular cyclization to obtain the furo[2,3-*d*]pyrimidine **161** (Scheme 29) below.

Scheme 29. Synthesis of furo[2,3-*d*]pyrimidine **161** from 5-iodopyrimidinol

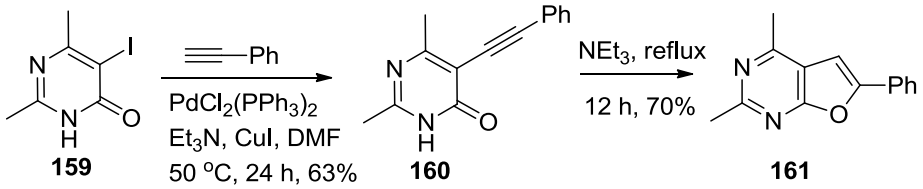

Sonogashira coupling of the 5-iodopyrimidinol **159** and phenylacetylene afforded intermediate **160** (Scheme 29),[152] which was converted to 2,4-dimethyl-6-phenyl-furo[2,3-*d*]pyrimidine **161** using triethylamine. Sonagashira coupling is also a key step in construction of the furan moiety in Schemes 30 and 31 below.

Scheme 30. Versatile synthesis of tetra-substituted furo[2,3-*d*]pyrimidines from 5-iodopyrimidinols

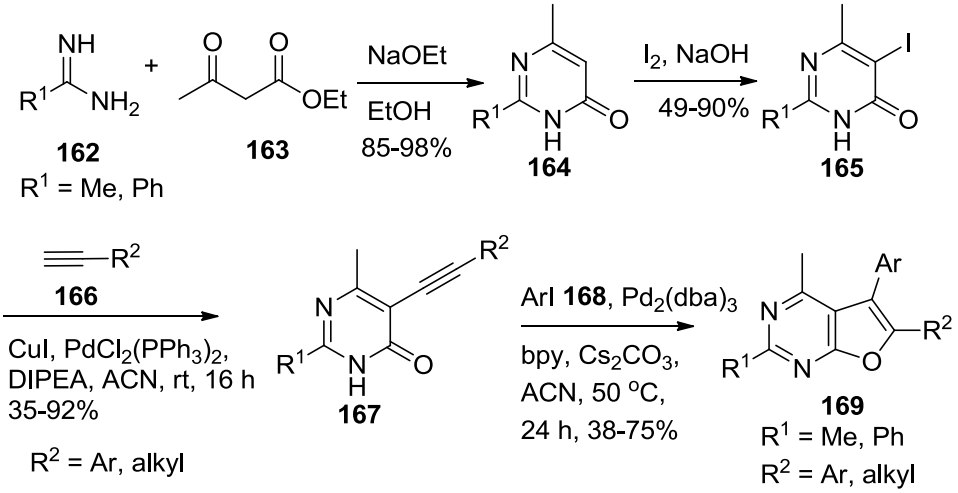

Liu *et al*.[153] employed metal-catalyzed intramolecular cyclization in the synthesis of tetra-substituted furo[2,3-*d*]pyrimidines **169** (Scheme 30). The 2-substituted 5-iodopyrimidinols **165** were obtained by the condensation of amidines **162** with β-ketoester **163** to **164** and subsequent iodination. Sonogashira coupling of iodopyrimidinols **165** and acetylenes **166** provided **167**, which upon Pd-catalyzed intramolecular cyclization with aryl iodides **168** gave **169**.

Scheme 30 above utilizes two metal-catalyzed coupling reactions to obtain furo[2,3-*d*]pyrimidines from 5-iodopyrimidinols. Petricci and coworkers[154] employed microwave irradiation to synthesize furo[2,3-*d*]pyrimidines from 5-iodopyrimidinols in a single step (Scheme 31). Sonagashira coupling of 2,6-disubstituted 5-iodopyrimidinols **170** and propargyl alcohol under microwave conditions provided 2,4,6-trisubstituted furo[2,3-*d*]pyrimidines **172** via intermediate **171**.[154]

Scheme 31. Microwave-assisted Sonagashira coupling in the synthesis of furo[2,3-*d*]pyrimidines

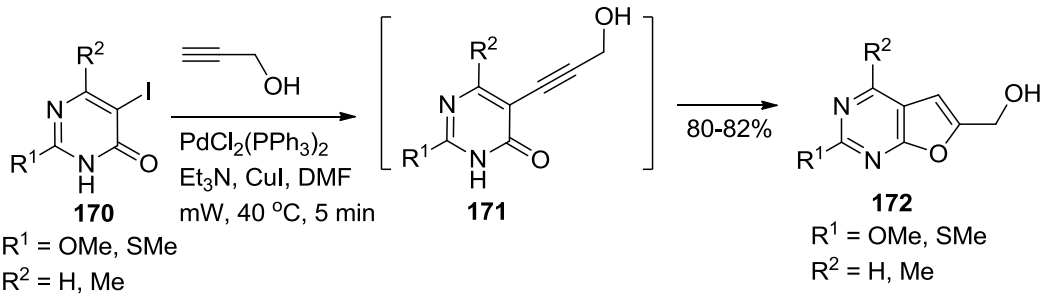

Scheme 32. Synthesis of 2-oxo-furo[2,3-*d*]pyrimidine from uracil

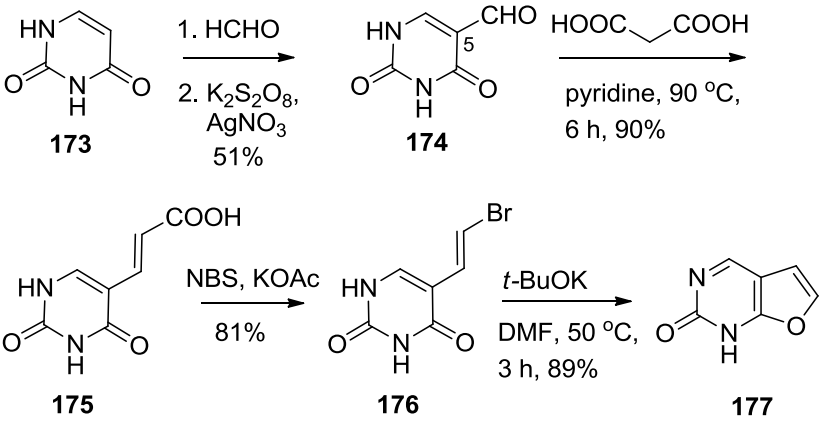

Eger *et al*.[155] reported a novel synthesis of 2-oxo-furo[2,3-*d*]pyrimidine **177** (Scheme 32) via intramolecular cyclocondensation of 5-(2-bromovinyl)-uracil **176**. Uracil **173** was converted to hydroxymethyluracil and subsequently oxidized to 5-formyluracil **174**. Compound **174** was reacted with malonic acid to afford 5-(2-carboxyvinyl)uracil **175**, which was decarboxybrominated to **176**. Cylization of **176** to the 2-oxo-furo[2,3-*d*]pyrimidine **177** was achieved using potassium *tert*-butoxide.

III. STATEMENT OF THE PROBLEM

The present work deals with the following three broad areas:

A. Combination chemotherapy potential in single agents

B. Inhibition of tubulin

C. Selective inhibition of *T.gondii* thymidylate synthase

A. Combination chemotherapy potential in single agents

Angiogenesis – the process of formation of new blood vessels from existing vasculature – is essential for tumor growth and metastasis.[81] When a tumor grows beyond 2 mm^3, it requires nutrients and oxygen for its growth and survival and thus initiates angiogenesis. Under hypoxic conditions, tumors secrete proangiogenic growth factors such as VEGF, PDGF, and EGF, key mediators of angiogenesis. These growth factors bind to their respective RTKs (VEGFR, PDGFR-β and EGFR) and stimulate the process of angiogenesis resulting in tumor growth, survival and metastases. Agents that circumvent angiogenesis by inhibition of RTKs have established a new paradigm in cancer chemotherapy.[79] RTK inhibitors that function by inhibition of a single RTK are prone to resistance by numerous mechanisms including redundant pathways, point mutations in the ATP-binding site and upregulation of additional RTKs.[156, 157] Consequently, multi-RTK inhibition in cancer chemotherapy has emerged as a promising approach and its validity has been highlighted by the approval of several multi-RTK inhibitors including sorafenib (inhibits VEGFR-2, VEGFR-3, PDGFR-β and Raf kinase) and sunitinib (inhibits VEGFRs, PDGFRs and c-kit).[158] However, the antiangiogenic treatment only prevents blood supply to the tumor but does not destroy cancer cells. Thus

antiangiogenic agents need to be combined with radiotherapy or chemotherapy to form an effective therapy and achieve synergistic effects.[159]

Inhibitors of TS and tubulin are widely used cytotoxic agents in cancer chemotherapy. While inhibition of the enzyme TS prevents *de novo* synthesis of nucleotides crucial for DNA synthesis,[57] tubulin inhibitors target microtubule dynamics involved in mitosis.[1]

TS catalyzes the *de novo* synthesis of dTMP from dUMP utilizing 5,10-CH_2THF as the cofactor.[56] Because of its vital role in DNA synthesis and cell growth, TS is a viable target for several clinically used cancer chemotherapeutic agents.[57] Nucleoside–based inhibitors such as 5-FU and capecitabine have found extensive utility in ovarian, breast, colon, and several other cancers alone and in combinations and are a mainstay in cancer chemotherapy.[63, 65] Antifolates, including raltitrexed and pemetrexed, are TS inhibitors clinically used, alone or in combination, in the treatment of mesotheliomas, non-small cell lung and advanced colorectal cancers.[68, 70]

Since microtubule dynamics plays a crucial role in mitosis and cell division,[1] microtubule targeting agents represent an important class of anticancer agents. Tubulin binding agents such as paclitaxel and Vinca alkaloids are widely used to treat solid tumors and hematological malignancies.[1, 8, 9]

Combination chemotherapy with antiangiogenic agents and cytotoxic agents is more effective in cancer treatment than either agent alone.[159, 160] Single agents with dual antiangiogenic and cytotoxic activities significantly decreased tumor growth, tumor metastasis and angiogenesis superior to docetaxel and sunitinib in xenograft mice models, remarkably without any toxicity.[125, 126] Such single agents with multiple mechanisms of

action are commonly referred to as designed multiple ligands and have several pharmacokinetic and pharmacodynamic advantages. These agents could potentially avoid drug–drug interactions and pharmacokinetic problems associated with two or more agents.[116, 161] In addition, they could prevent or delay the emergence of resistance and not cause overlapping toxicities.[116, 162] Most significantly, single agents with dual cytotoxic and antiangiogenic activities simultaneously target rapidly proliferating tumor cells and the tumor vasculature. Also, such single agents could afford synergic effects as they can exert their cytotoxic effect as soon as or even during transient tumor vasculature normalization caused by the antiangiogenic component.[80] As a result, structural design of such multitargeted single agents should allow the cytotoxicity to be manifested as soon as the antiangiogenic effects are operable. Thus the cytotoxic component of these agents need not be as potent as conventional chemotherapeutic agents. Dosing of such an antiangiogenic agent with comparatively lower cytotoxic activity would mimic metronomic chemotherapy, which utilizes more frequent and low-dose administrations of cytotoxic agents compared with conventional chemotherapy.[163] Several clinical trials attest to the safety and efficacy of using antiangiogenic agents such as sunitinib and sorafenib with metronomic doses of cytotoxic agents.[164-167] The single agents offer other advantages such as decreased cost and increased patient compliance,[161] which can play a major part in the clinical success of a therapy.

The antiangiogenic component of single agents targets RTK-overexpressing endothelial cells and as a result, is typically targeted to tumor cells under normal circumstances.[81] In contrast, the cytotoxic component interferes with tumor cell division with less selectivity over rapidly dividing normal cells present in bone marrow, hair and

cells lining the mouth and gut.[168] Therefore, a key challenge in the design of single agents with a cytotoxic component is that the cytotoxic component should only destroy tumor cells that are compromised via the antiangiogenic effect but should not cause toxicity to normal cells not affected by the antiangiogenic effect.[125] As a result, the cytotoxic component of these single agents need not be as potent as conventional chemotherapeutic agents and hence should avoid dose-limiting toxicities[168] associated with cytotoxic agents.

Single agents with dual antiangiogenic and cytotoxic activities significantly decreased tumor growth, tumor metastasis and angiogenesis in xenograft mice models, remarkably without any toxicity.[55, 125-127] The antiangiogenic effects of these compounds were due to inhibition of RTKs and the cytotoxic effects were due to inhibition of thymidylate synthase[125] or tubulin[55, 126] or dihydrofolate reductase[127]. In these studies, VEGFR-2, PDGFR-β and EGFR were chosen as the targets for antiangiogenic effects because of their crucial role in angiogenesis. Additionally, the successful clinical and preclinical combinations of TS inhibitors (for e.g., capecitabine, pemetrexed) or tubulin inhibitors like paclitaxel with antiangiogenic agents was also an important factor in selecting TS and tubulin as the potential cytotoxic targets.[121, 169-172]

A.1 Design of 2,4-diamino-5-arylthio-9*H*-pyrimido[4,5-*b*]indoles as single agents with dual TS and RTK inhibitory potential

Gangjee *et al*.[125] reported pyrimido[4,5-*b*]indoles **1** and **2** (Figure 25) as dual inhibitors of thymidylate synthase and multiple RTKs. In COLO-205 mice xenografts, compounds **1** and **2** significantly inhibited tumor growth, tumor vasculature and liver metastasis better than docetaxel and remarkably with no toxicity.[125] Compounds

178–180[173] (Figure 25) are analogs of **1** with variations at 5-position and were previously synthesized.

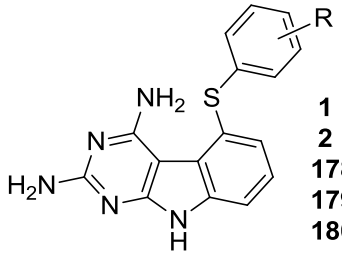

1 R = H
2 R = 4'-Me
178 R = 4'-Cl
179 R = 3',4'-diCl
180 R = 4'-OMe

Figure 25. Lead compounds **1**, **2** and **178–180** as dual TS and RTK inhibitors.

Table 1. Inhibition of TS, RTKs and angiogenesis by **1**, **2** and **178–180**

Compd	**Inhibition of**				
	hTS (μM)	**EGFR (nM)**	**VEGFR-2 (nM)**	**PDGFR-β (nM)**	**CAM angiogenesis (μM)**
1	0.54	15.1 ± 2.5	22.6 ± 2.7	2.8 ± 0.3	28.2 ± 2.9
2	0.39	10.41 ± 1.9	56.3 ± 8.2	40.3 ± 6.7	20.3 ± 5.2
178	0.48	8.3 ± 1.9	29.9 ± 4.8	>200	18.3 ± 3.2
179	n.d.[a]	16.2 ± 3.2	46.7 ± 8.1	>200	1.2 ± 0.04
180	0.14	20.8 ± 3.1	182.2 ± 34.2	60.5 ± 7.2	29.0 ± 3.0
Raltitrexed	0.38				
Sunitinib		172.1 ± 19.4	18.9 ± 2.7	83.1 ± 10.1	1.3 ± 0.07
Erlotinib		1.2 ± 0.2	124.7 ± 18.2		29.1 ± 1.9

[a]n.d. not determined

Table 1 shows inhibitory data for **1**, **2** and **178–180** against human TS and kinases EGFR, VEGFR-2 and PDGFR-β. Kinase inhibition was performed in cell-based assays and therefore, it should be noted that cellular permeability might play a role in the activities of these compounds.

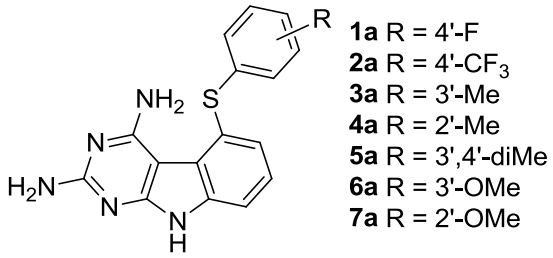

Figure 26. Series I.

Compounds **1a–7a** (Series I, Figure 26) were designed in this study to improve the RTK–inhibitory activity while retaining low submicromolar TS inhibition. Compounds **1a** and **2a** with 4'-F and 4'-CF_3 groups, respectively, were designed to evaluate the contribution of the *para*-electron-withdrawing moiety on biological activity. Compounds **3a** and **4a** were designed to determine the importance of the methyl group at the 4'-position for **2**. In chorioallantoic membrane (CAM) assay, compound **179** with 3',4'-dichloro group had antiangiogenic activity comparable to sunitinib and was 15-fold more active in this assay than the 4'-chloro analog **178**.[173] This increase in activity might be due to either electronics and/or lipophilicity of the additional 3'-chloro group. Novel 3',4'-dimethyl analog **5a** with lipophilicity similar to **179** was designed to evaluate the role of electronics and lipophilicity at 3'-position. The 4'-OMe analog **180** had lower RTK inhibitory activity than the 4'-methyl compound **2**. To determine whether this loss of activity was due to steric intolerance at the 4'-position, compounds **6a** and **7a** with methoxy groups at the 3'- and 2'-positions, respectively, were designed.

Target compounds **1a**–**7a** can be obtained via the synthetic procedure used for lead compounds **1** and **2**. However, the synthesis of **1** and **2** involved seven steps from commercial starting materials and the overall yield was a mere 6%.[125] Hence, it was important to devise an efficient route for the synthesis of the tricyclic target compounds.

Such an efficient synthetic route could also be utilized in the synthesis of lead compounds **1** and **2**, which are required in gram quantities for preclinical studies.

A.2 Design of 4-substituted 5-methyl-furo[2,3-*d*]pyrimidines as single agents with dual tubulin and RTK inhibitory potential

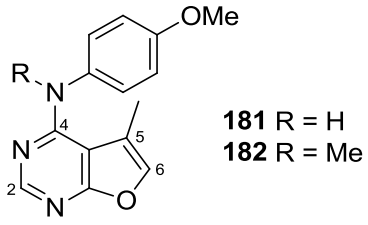

181 R = H
182 R = Me

Figure 27. Lead compounds **181** and **182**.

Gangjee *et al*.[174] reported the 5-methyl-furo[2,3-*d*]pyrimidines **181** and **182** (Figure 27) with variation at N^4-position.

Table 2. Effects of **181** and **182** on cell proliferation, microtubule depolymerization and [^{3}H]-colchicine binding

Compd	**IC_{50} ± SD (MDA-MB-435)**	**EC_{50} for MT depolymerization**	**Inhibition of colchicine binding (% inhibition ± SD)**	
			1 μM	**5 μM**
181	>10 μM	>40 μM	-	-
182	4.3 ± 0.3 nM	23.9 nM	71 ± 6	96 ± 2
CA4	3.4 ± 0.6 nM	13.0 nM	88 ± 2	99 ± 0.2

N^4-Desmethyl **181** was inactive in tubulin assay and in MDA-MB-435 cells (Table 2). On the other hand, the N^4-methyl analog **182** showed potent microtubule depolymerization and inhibition of [^{3}H]-colchicine binding comparable to CA4.[174]

Table 3. RTK inhibitory activity of **181** and **182**

Compd	EGFR inhibition (nM)	VEGFR-2 inhibition (nM)	PDGFR-β inhibition (nM)
181	283.1 ± 40.1	38.1 ± 4.2	57.3 ± 8.0
182	15.5 ± 2.0	9.3 ± 0.72	12.3 ± 2.0
Sunitinib	172.1 ± 19.4	18.9 ± 2.7	83.1 ± 10.1
Erlotinib	1.2 ± 0.2	124.7 ± 18.2	

In the kinase inhibition assays, the N^4-methyl analog **182** was more active than the NH analog **181** (Table 3).[175] More importantly, compound **182** was 2-fold and 7-fold more active than sunitinib in the VEGFR-2 and PDGFR-β kinase assays, respectively.

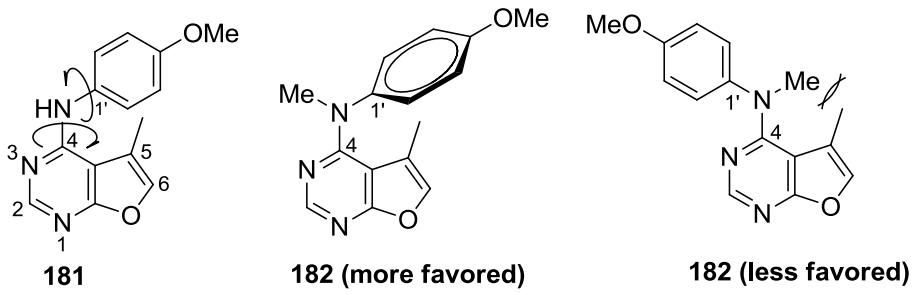

Figure 28. Conformational restriction of C_4-N and N-$C_{1'}$ bonds due to N^4-methyl group.

Compared to the NH analog, the *N*-methyl compound **182** showed spectacular antimitotic and antitumor activities, which could be attributed, in part, to conformational restriction of the bonds connecting the pyrimidine ring and the phenyl ring (Figure 28). In **181**, the C_4-N and N-$C_{1'}$ bonds connecting the pyrimidine and the phenyl moieties are freely rotatable. Whereas in **182**, these bonds are somewhat restricted due to the presence of steric bulk of N^4-methyl group and/or due to steric clash between the N^4-methyl and 5-methyl groups (Figure 28).

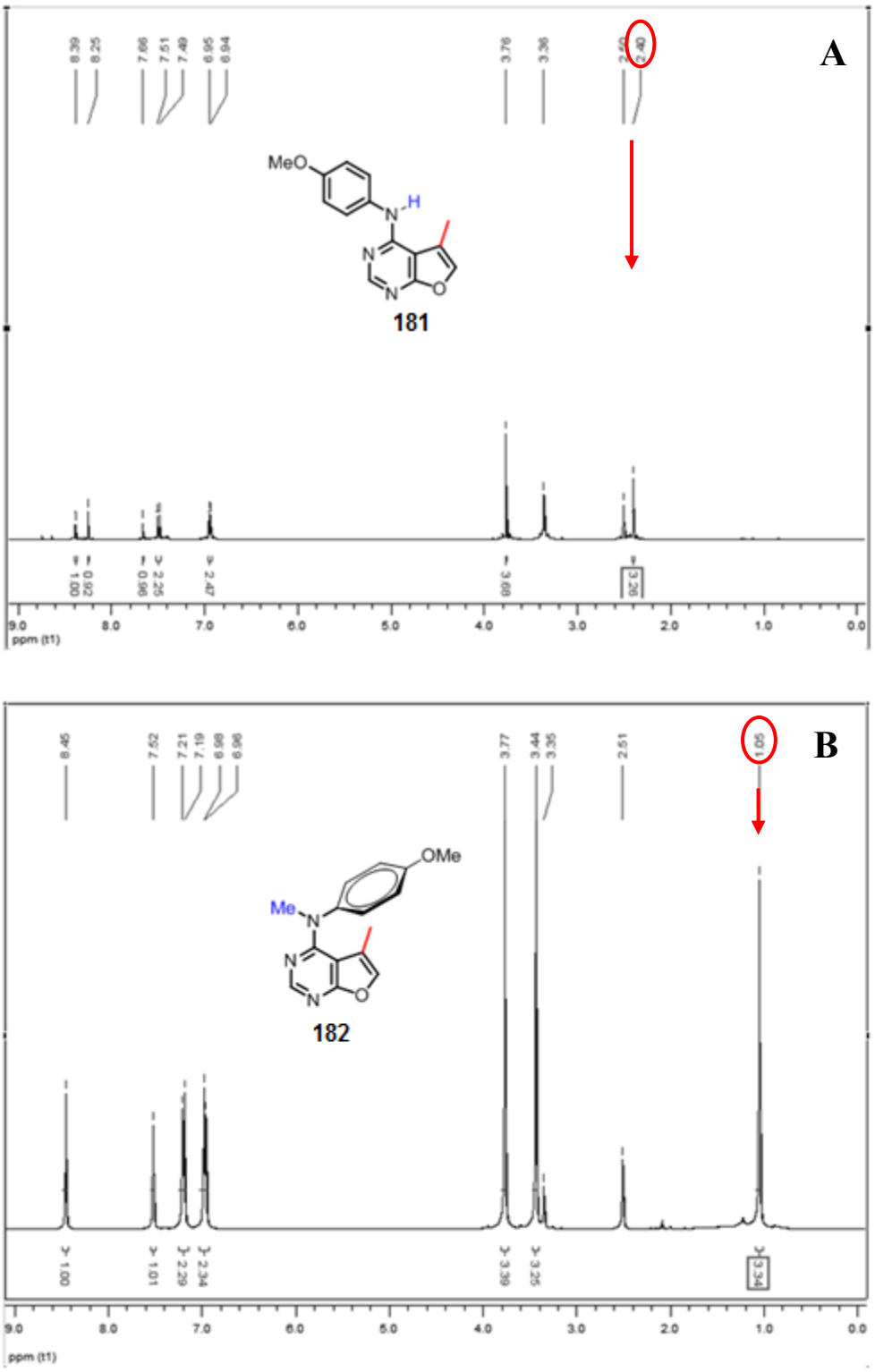

Figure 29. The conformations and ^{1}H NMR analyses of **181** (Fig. A) and **182** (Fig. B).

The ^{1}H NMR spectra of the N^4-desmethyl analog **181** and the N^4-methyl analog **182** provided valuable information related to conformational restriction in **182** (Figure 29).[175] For **181**, the "5-Me" protons appear at δ = 2.40 ppm whereas for **182**, they are significantly shielded at δ = 1.05 ppm. This shielding of the "5-Me" protons in **182** is due to the proximity of a diamagnetic anisotropic cone in **182** arising from the phenyl ring. The steric bulk of the N^4-methyl and/or steric clash between the N^4-methyl and 5-methyl groups in **182** restrict the conformation and thus position the phenyl group on top of the 5-methyl group (as in Figure 29B) resulting in the shielding effect.

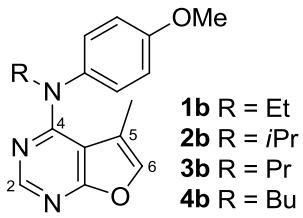

Figure 30. Series II.

Compounds **1b–4b** (Series II, Figure 30) with varying alkyl groups at the N^4-position were designed to determine the steric tolerance at the N^4-position in the colchicine-binding site of tubulin and/or the ATP-binding site of RTKs. In addition, the larger alkyl groups in **1b**–**4b** require greater volume and further restrict the free rotation of the C_4-N and N-C_1' bonds. Introduction of these alkyl groups could improve the RTK-inhibitory activity of **182** by forming additional hydrophobic interactions in the binding site (Figure 31).

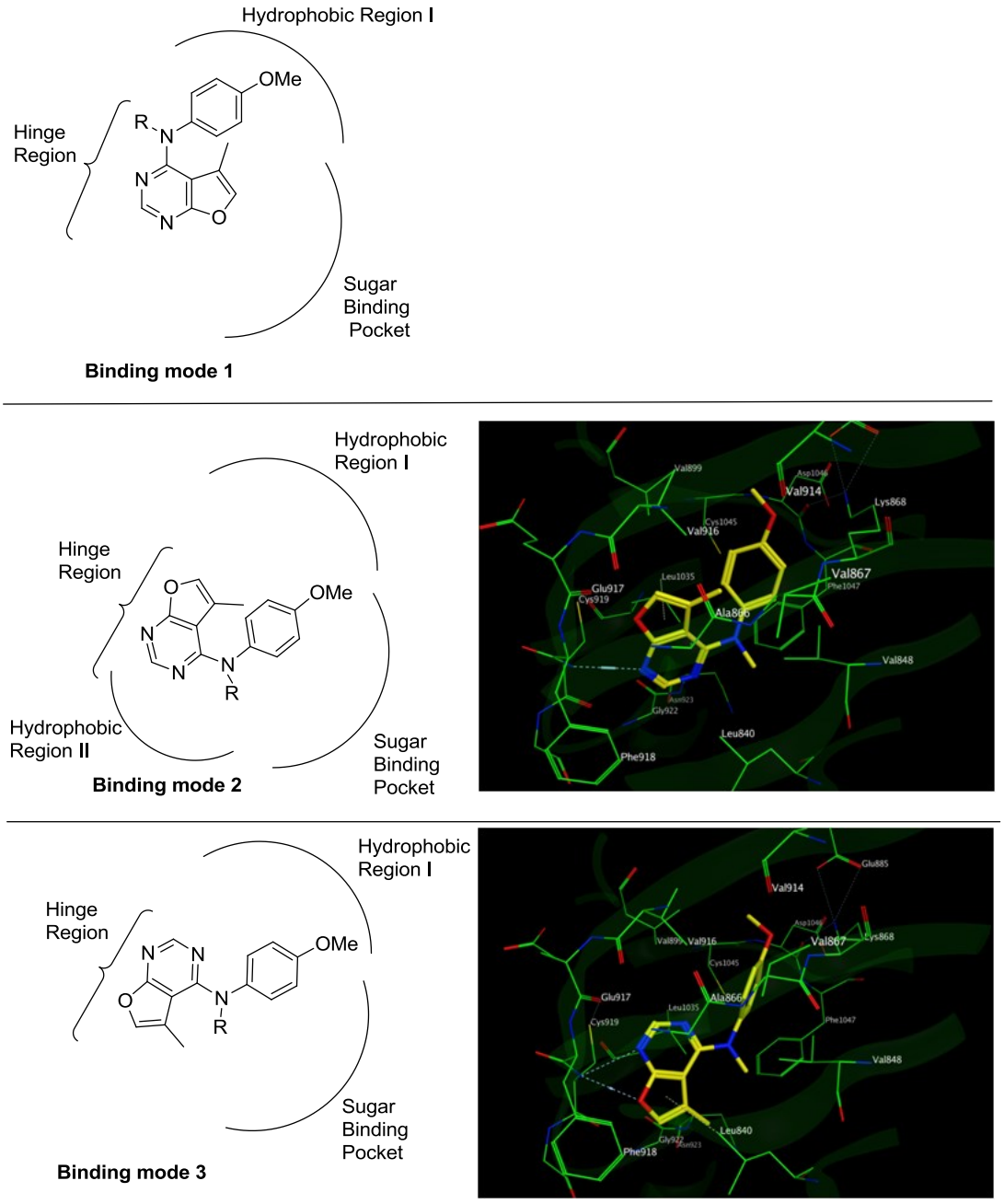

Figure 31. Predicted binding modes of **182** (R = Me) in the ATP-binding site and docked poses of **182** in VEGFR-2 (PDB: 2XIR)[176].

The general RTK pharmacophore model consists of an Adenine region, a Sugar binding pocket and a Phosphate binding region which binds the adenine ring, the sugar moiety and the triphosphate moiety of ATP, respectively. Additionally, there are two

Hydrophobic regions I and II, neither of which are utilized by ATP for binding. The furo[2,3-*d*]pyrimidine ring of **182** and the designed compounds **1b**–**4b** could bind to the Adenine region similar to heterocyclic scaffold inhibitors such as quinazolines and pyrrolo[2,3-*d*]pyrimidines.[177] If the furo[2,3-*d*]pyrimidines (exemplified by **182**) occupy binding mode 1 (Figure 31), alkylation at N^4-position might not be sterically tolerated. Alternatively, the furo[2,3-*d*]pyrimidines could adopt binding mode 2 in which the compounds are rotated around the 2-H–C_2 bond. In this mode, the *N*-alkyl group could orient towards the Sugar binding pocket or Hydrophobic region II and the 4-anilino group could occupy Hydrophobic region I. These compounds could also adopt binding mode 3 in which the molecule is rotated by 60° (from mode 2). In this mode, the *N*-alkyl and the 4-anilino groups could occupy the Sugar binding pocket and Hydrophobic region I, respectively. Docking studies performed on the X-ray crystal structure of VEGFR2 (pdb: 2XIR)[176] suggested the possibility of several binding modes. Representative low energy binding modes (-6.39 kcal/mol for binding mode 3) and (-4.16 kcal/mol for binding mode 2) are shown in Figure 31. In both binding modes, compound **182** (R = Me) makes a hydrogen bond interaction with the backbone NH of cysteine in the hinge region.

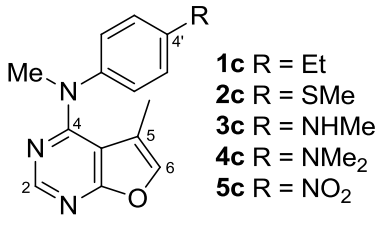

Figure 32. Series III.

Compounds **1c**–**5c** (Series III, Figure 32) were designed to determine the importance of the 4'-methoxy group for tubulin and RTK inhibition. Compounds **1c**, **2c** and **4c** were designed to examine the role of 4'-methoxy group as a hydrogen-bond acceptor.

Compound **3c** with a 4'-NHMe group was designed to determine if a hydrogen-bond donor is tolerated at this position. Compound **5c** containing the 4'-NO_2 group was designed to know whether an electron-withdrawing group is tolerated at this position for RTK inhibitory activity. On the basis of the previous SAR on related pyrimidine-fused scaffolds,[55, 178] compound **5c** is not expected to have antitubulin activity.

Gram-scale synthesis of **182** was required for further preclinical evaluations including toxicity and xenograft studies in mice.

B. Inhibition of tubulin

Tubulin binding agents disrupt microtubule dynamics leading to mitotic arrest and cell death. Half of all human tumors have mutations in the p53 gene, and the most effective drugs in p53 mutant cell lines are tubulin binding agents.[179, 180] Tubulin binding agents such as taxanes and vinca alkaloids are widely used for the treatment of solid tumors and hematological malignancies.[1, 8, 9]

However, the enormous clinical success of taxanes and vinca alkaloids has been compromised by two major mechanisms of tumor resistance: Overexpression of Pgp and the expression of the βIII-tubulin.[181] Pgp overexpression is clinically observed in many tumor cell lines, particularly in patients who have received chemotherapy.[41] Overexpression of Pgp resulted in poor response to taxol-based chemotherapy in patients with non-small cell lung cancer.[41, 42] Use of Pgp inhibitors in overcoming Pgp-mediated resistance was not successful due to intolerable side effects.[44] Tubulin binding agents that are not substrates of Pgp (for e.g. epothilones)[181] represent a viable alternate strategy for circumventing Pgp-mediated resistance. Such agents would be extremely useful for patients that develop resistance due to Pgp overexpression.[39, 42, 181]

The expression of βIII-tubulin is involved in clinical resistance to taxanes and Vinca alkaloids in non-small cell lung,[45, 46, 52] breast,[47] ovarian[48, 53] and gastric[49] cancers. Colchicine-site binding agents were not susceptible to βIII-tubulin mediated resistance,[54, 55] which demonstrates the importance of developing anticancer drugs that bind to the colchicine-site. Although there are no colchicine-site agents in the clinic, several agents including CA4P (Fosbretabulin®)[25-28] and CA1P (OXi4503)[29] are currently in phase 1 and 2 clinical trials. Development of tubulin binding agents that are less sensitive to Pgp and/or βIII-tubulin mediated resistance could result in broader antitumor activity and improved rates of survival.

B.1 Design of N^4-aryl-5-chloro-2,4-diamino-pyrimido[4,5-*b*]indoles as inhibitors of tubulin

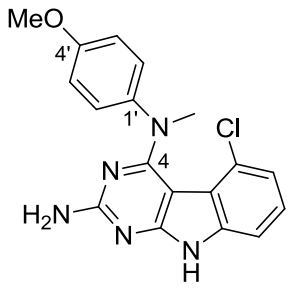

183

Figure 33. Tubulin inhibitor **183**.

Pyrimido[4,5-*b*]indole **183** (Figure 33) is a potent microtubule depolymerizing agent that inhibited the growth of cancer cells with GI_{50} values in the submicromolar range.[182] It was discovered to be a colchicine-site binding agent and also overcame the Pgp and βIII-tubulin mediated drug resistance clinically observed with paclitaxel and vinca alkaloids.

Table 4. Compound **183** inhibits cell proliferation and tubulin assembly

Compd	**IC_{50} ± SD (MDA-MB-435)**	**Inhibition of tubulin assembly**
183	183 nM	7.1 ± 0.8 μM
CA4	3.4 nM	1.0 ± 0.09 μM

Compound **183** had a 7-fold lower inhibition of tubulin assembly than the standard colchicine site agent CA4 (Table 4).[182] It showed a 60-fold higher IC_{50} value than CA4 in MDA-MB-435 cancer cell lines. Compound **183** represented the first example of pyrimido[4,5-*b*]indoles as a potent tubulin inhibitor. It was of interest to identify the structural features of the tricyclic pyrimido[4,5-*b*]indoles that contribute to antitubulin activity. Hence, compounds **1d**–**6d** (Series IV, Figure 34) were designed as potential inhibitors of tubulin.[182]

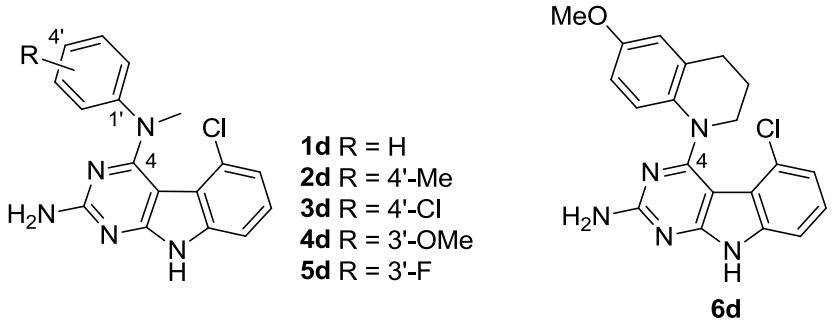

Figure 34. Series IV.

Compound **1d** (Figure 34) was designed to determine the importance of the 4'-methoxy group to tubulin inhibition. Compounds **2d** and **3d** are designed to evaluate the role of electron-donating and electron-withdrawing groups at 4'-position. The 3'-methoxy analog **4d** was designed to explore the effect of a methoxy group at this position to

antitubulin activity. Compound **5d** was designed to evaluate the effect of electron-withdrawing group at the 3'-position.

Compound **6d** (Figure 34) was designed as a conformationally restricted analog by incorporating the bicyclic 6-methoxy-tetrahydroquinoline moiety onto the 4-position of the pyrimido[4,5-*b*]indole. Compared to the *N*-methylanilines, the tetrahydroquinoline moiety eliminates the rotation around the "N-Ph" bond thereby restricting the conformation of the phenyl ring. The restricted confirmation of the phenyl group in **5d** results in a much more rigid structure than **183** but still maintains the phenyl and alkyl substitutions on the N^4-position as in **183**.

B.2 Design of 2,4-substituted pyrimido[4,5-*b*]indoles as inhibitors of tubulin

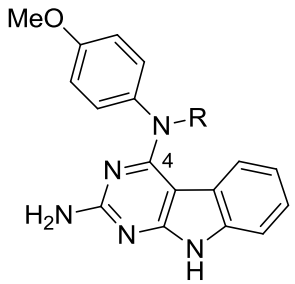

184 R = H
185 R = Me

Figure 35. Pyrimido[4,5-*b*]indoles **184** and **185**.

Gangjee *et al*.[178] reported the pyrimido[4,5-*b*]indoles **184** and **185** (Figure 35) which vary in substitution at the N^4-position. The 4-NH analog **184** was inactive in MDA-MB-435 cell lines and in the microtubule depolymerization assay (Table 5). The *N*-methyl analog **185** is a colchicine-site agent, which inhibited cell proliferation about 4-fold less than CA4. Also, compound **185** circumvented clinically relevant mechanisms of tumor resitance of paclitaxel due to Pgp and βIII-tubulin.

Table 5. Effects of **184** and **185** on proliferation of MDA-MB-435 cells, microtubule depolymerization and [^{3}H]-colchicine binding

Compd	IC_{50} ± SD (MDA-MB-435)	EC_{50} microtubule depolymerization	Inhibition of colchicine binding (% inhibition ± SD) at 5 μM
184		>40 μM	
185	14.7 ± 1.5 nM	105 ± 12 nM	84 ± 0.5
CA4	3.4 ± 0.6 nM	13.0 nM	99 ± 0.2

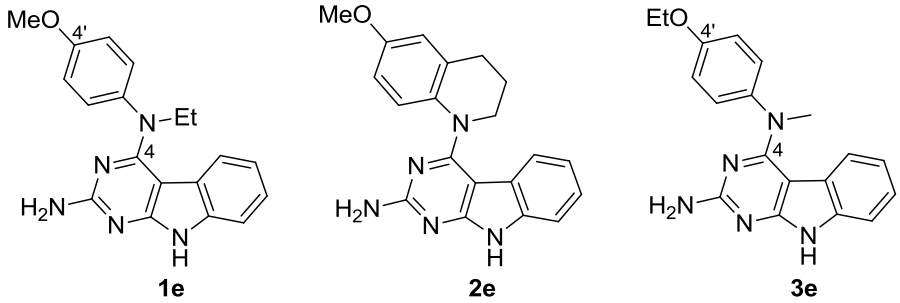

Figure 36. Series V.

Compounds **1e**–**3e** (Figure 36) with variations at N^4-position were proposed to improve the tubulin inhibitory activity of **185**. Compound **1e** with a larger ethyl group at the N^4-position was designed to determine the effect of size at the N^4-position on antitubulin activity. Compound **2e** contains **a** 6-methoxy-tetrahydroquinoline moiety at the 4-position of the pyrimido[4,5-*b*]indole. It was designed to evaluate the effect of conformational restriction of the phenyl group on tubulin inhibition. The 4'-ethoxy analog **3e** was designed based on molecular modeling (Figure 37).

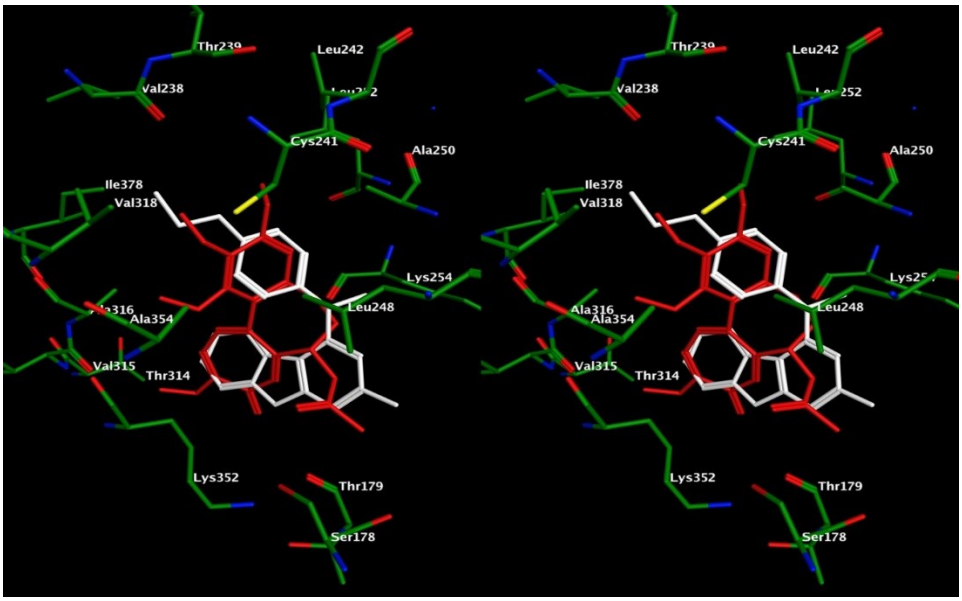

Figure 37. Stereoview. Superimposition of the docked conformation of **3e** (white) overlaid with colchicine (red) in the colchicine-site of tubulin (PDB: 1SA0)[183].

Figure 37 shows the docked conformation[178] of **3e** (-7.75 kcal/mol) in the colchicine site of tubulin (PDB: 1SA0)[183] obtained using MOE 2013.08.[184] The oxygen atom of the 4'-OEt group of **3e** forms hydrogen bonding with Cysβ241 of tubulin. Also, the 4'-OEt group forms hydrophobic interactions with Valα318 and Ileβ378, which were absent in colchicine and **185**. Compound **3e** was designed based on the hypothesis that the replacement of 4'-OMe of **185** with the larger 4'-OEt group would allow additional interactions with the hydrophobic residues in the colchicine-site of tubulin.

Compound **1f** (Figure 38) is designed by the bioisostere replacement of the 4'-OMe group in **185** with 4'-SMe group. This modification was found to improve antitubulin activity in the cyclopenta[*d*]pyrimidines[185] and the furo[2,3-*d*]pyrimidines.[186]

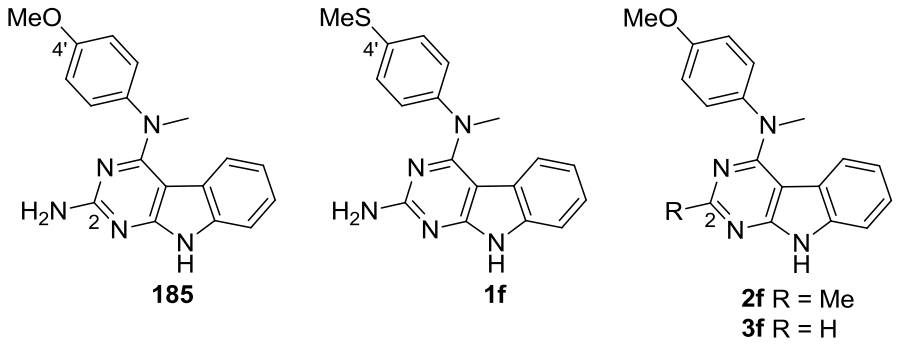

Figure 38. Lead compound **185** and target compounds **1f**–**3f** (Series VI).

Compounds **2f** and **3f** (Figure 38) with 2-Me and 2-H substitutions are designed to evaluate the importance of the 2-NH_2 group in antitubulin activity. These substitutions are well tolerated and afforded increased antitubulin activity in pyrimidine-fused bicyclic systems.[185, 186]

Bulk syntheses of potent tubulin inhibitors **183** and **185** were carried out for further preclinical evaluations.

C. Selective inhibition of *T.gondii* thymidylate synthase

Infection by the parasite *T. gondii* can lead to toxoplasmosis in immune compromised patients such as organ transplant, patients undergoing chemotherapy for cancer and HIV/AIDS patients.[72]

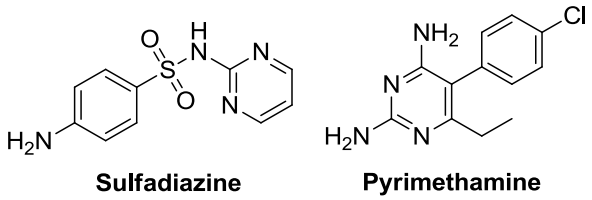

Figure 39. Representative drugs in the treatment of *T. gondii* infection.

Standard therapy for the treatment of toxoplasmosis involves a combination of sulfa drugs like sulfadiazine (Figure 39) and DHFR inhibitors such as pyrimethamine along

with folinic acid for rescue of bone marrow toxicity caused by pyrimethamine.[187] Pyrimethamine selectively targets *T. gondii* DHFR where as sulfadiazine inhibits dihydropteroate synthase (DHPS) which catalyzes the *de novo* folate biosynthesis, a pathway absent in humans. The current therapies are limited by drug intolerance,[188, 189] central nervous system (CNS)-related side effects[190] associated with sulfonamides and treatment failures[191] owing to resistance. Pyrimethamine with clindamycin therapy may be used an alternative in patients allergic to sulfa drugs.[189] Although this therapy resulted in lower allergic reactions than pyrimethamine-sulfadiazine therapy, 30% of patients did not respond to the treatment.[188] Drug resistance and treatment failures to these very similar first-line agents indicate an urgent need for new agents.

The TS–DHFR enzyme is crucial for dTMP synthesis in *T. gondii* and hence represents a valid target to combat *T. gondii* infection.[76] However, inhibitors selective for *T. gondii* TS (tgTS) over human TS (hTS) are not known at the time this research project was conceived. This is mainly due to the significant homology between the active site residues of tgTS and hTS.[78] Availability of selective tgTS inhibitors would avoid the aforementioned drawbacks associated with current therapies.

C.1 Synthesis of 2-amino-4-oxo-5-thioaryl-9*H*-pyrimido[4,5-*b*]indoles as selective inhibitors of *T. gondii* thymidylate synthase

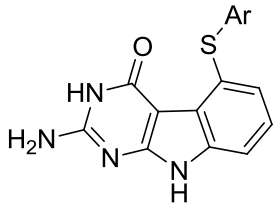

1g Ar = Ph
2g Ar = 2'-naphthyl
3g Ar = 4'-Me-Ph
4g Ar = 1'-naphthyl
5g Ar = 4'-OMe-Ph
6g Ar = 4'-F-Ph
7g Ar = 4'-OPh-Ph

Figure 40. 2-Amino-4-oxo-pyrimido[4,5-*b*]indoles **1g**–**7g** (Series VII).

Gangjee *et al*.[192] serendipitously discovered 2-amino-4-oxo-5-arylthio-pyrimido[4,5-*b*]indoles **1g**–**6g** (Figure 40) as selective inhibitors of tgTS. Remarkably, compounds **1g**–**4g** displayed 10-fold selectivity for tgTS over hTS compared to 0.2- and 3-fold selectivities for clinically used raltitrexed and pemetrexed, respectively (Table 6). The 5-thionaphthyl analogs **2g** and **4g** had low two-digit nanomolar tgTS inhibitory activities.

Table 6. TS inhibitory activity of **1g**–**6g**

Compd	**Human TS** (μM) (**A**)	***T. gondii* TS** (μM) (**B**)	**Selectivity Ratio** (**A/B**)
1g	2.7	0.13	20.8
2g	0.21	0.012	17.5
3g	1.3	0.13	10
4g	0.27	0.027	10
5g	0.75	0.23	3.3
6g	1.8	0.65	2.7
Raltitrexed	0.38	1.8	0.2
Pemetrexed	9.5	2.8	3.4

Encouraged by the preliminary data, additional quantities of **1g**–**6g** were required for further preclinical evaluation including X-ray crystal and *T. gondii* culture studies and for pharmacokinetic studies. Compounds **1g**–**6g** have been previously synthesized albeit in poor yields (2–6%) from commercially available starting materials.[192] The unprecedented tgTS selectivity of **1g**–**6g** (Table 6) prompted the design of an efficient synthetic strategy for preparing these compounds. This synthetic strategy can also be utilized for preparing novel analogs related to Series VII. Compound **7g** is one such analog which was designed based on molecular modeling (Figure 41).

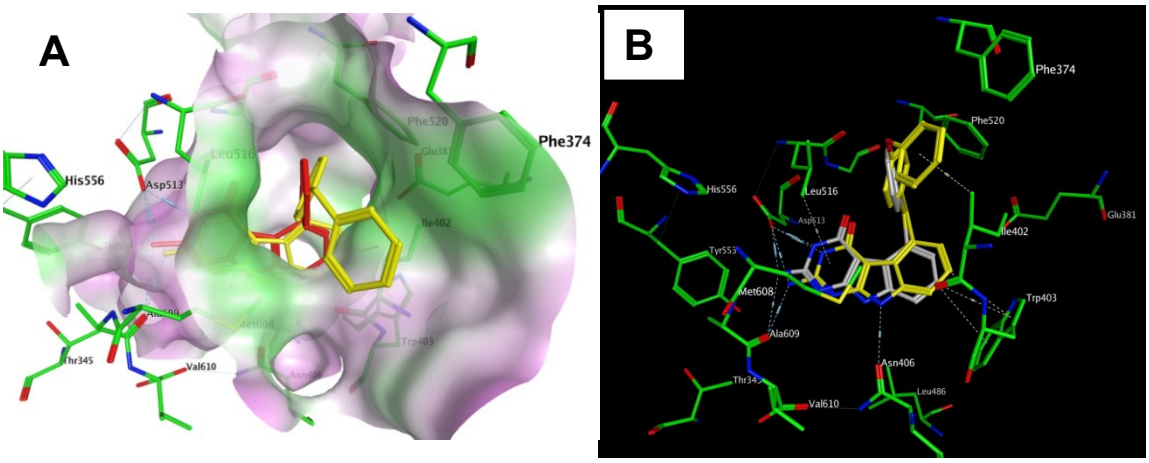

Figure 41. Compounds **1g** and **7g** in the active site of tgTS. (A) Surface map of tgTS active site occupied by **1g** (red) and **7g** (yellow) (PDB: 4KY4)[193]. Hydrophobic and polar surfaces are colored green and magenta, respectively. (B) Key interactions between tgTS residues and **1g** or **7g**.

Compounds **1g** and **7g** were docked in the X-ray crystal structure of tgTS (PDB: 4KY4)[193] using LeadIT.[194] The 5-thiophenyl substitution of **1g** accesses a hydrophobic pocket formed by Ile402, Leu516, Phe374 and Phe530 (Figure 41A). Since the phenyl ring does not occupy the large hydrophobic pocket, it was of interest to append a 4'-phenoxy group in target compound **7g** in an attempt to gain additional interactions with Phe374 and therefore improve the tgTS activity. Figure 41B provides key interactions made by **1g** and **7g** in the active site of tgTS. The 2-NH_2 of both **1g** and **7g** forms hydrogen bonding with Ala609 and Asp513 of tgTS whereas the 3-NH forms hydrogen bonding with the Asp513. The tricyclic scaffold is stabilized by hydrophobic interaction with Leu516 and Trp403. Compound **7g** forms additional hydrophobic interactions with Ile402, Phe374 and Phe520 and hydrogen bonding (indole NH) with Asn406. Also, the 4'-phenoxy **7g** would probe the hydrophobic pocket and thus help us know whether hydrophobic residues are involved in selectivity for tgTS over hTS.

Compounds **1g**–**6g** had poor water solubility and thus, to improve water-solubility, HCl salts of two most tgTS selective compounds, **1g** and **2g**, were also synthesized.

IV. CHEMICAL DISCUSSION

Synthesis of 5-thioaryl-9*H*-pyrimido[4,5-*b*]indole-2,4-diamines 1a–7a and lead compounds 1 and 2

Target compounds **1a**–**7a** can be synthesized utilizing the synthetic procedure for lead compounds **1** and **2**. However, the synthesis of **1** and **2** from commercially available 1,2-dichloro-3-nitrobenzene required seven steps and had a mere 6% overall yield.[125] Hence, it was important to devise an efficient high-yielding strategy for the synthesis of target compounds **1a**–**7a**. It was our intention that the synthetic scheme devised should also be adaptable to gram-scale synthesis of lead compounds **1** and **2** for preclinical evaluation.

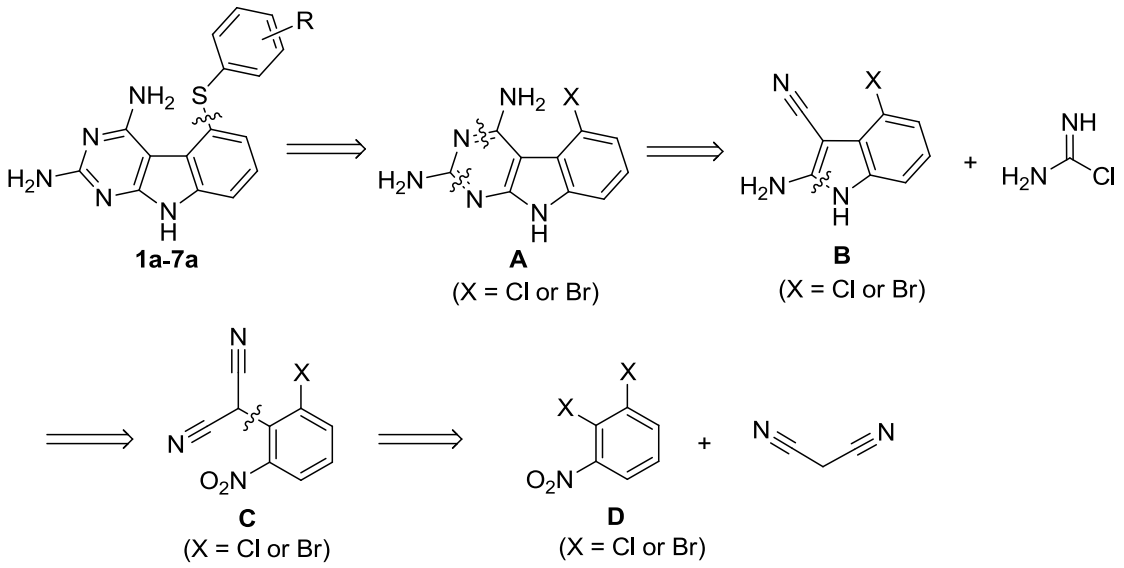

Figure 42. Retrosynthesis of target compounds **1a**–**7a**.

The synthesis of target compounds **1a**–**7a** was envisioned *via* a nucleophilic displacement reaction[125] of 5-chloro- or 5-bromo-pyrimido[4,5-*b*]indoles of general structure **A** (Figure 42), which could be prepared by condensation[125] of substituted

indoles **B** with chlorformamidine. Indoles **B** can in turn be synthesized via reductive cyclization[125] of appropriately substituted nitrobenzenes **C**, which could be obtained by electrophilic aromatic substitution[125] of 1,2-dichloro- or 1,2-dibromo-3-nitrobenzene **D** with malononitrile.

In an effort to develop this method, initially the synthesis of lead compounds **1** and **2** was undertaken (Scheme 33), with the plan to extend the new scheme, if successful, to the target compounds **1a**–**7a**, which contain electron-withdrawing or sterically demanding thioaryl groups at 5-position.

Scheme 33. Efficient gram-scale synthesis of lead compounds **1** and **2**

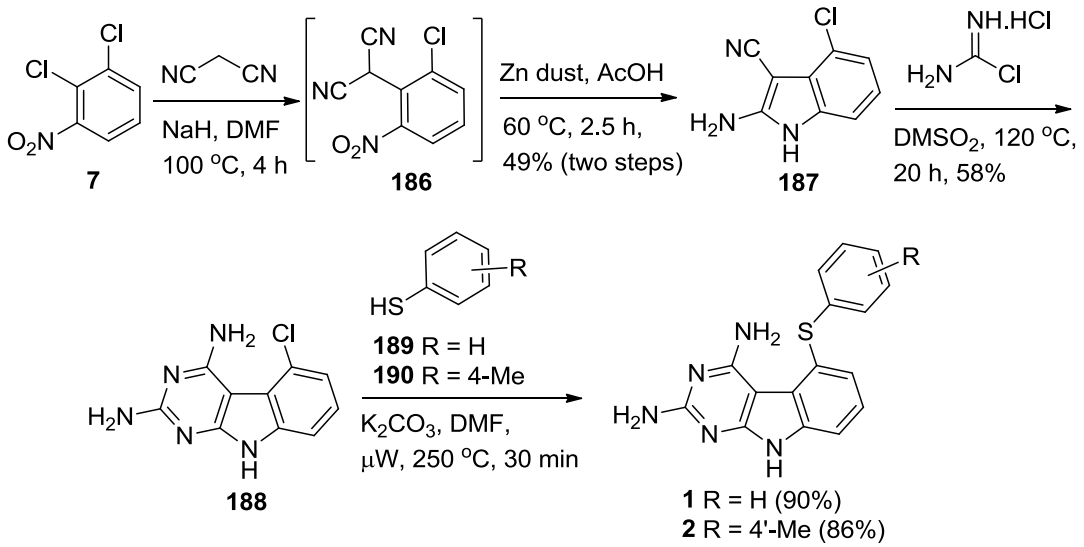

Displacement of 1,2-dichloro-3-nitro-benzene **7** with the sodium salt of malononitrile anion provided 2-(2-chloro-6-nitrophenyl)malononitrile **186** (Scheme 33). Several reaction conditions such as varying the solvent (THF, DMF) and/or the base (potassium *tert*-butoxide, sodium hydride) and/or temperature (75 °C to 120 °C) were screened for this step. The reaction did not go to completion [monitored by thin–layer chromatography (TLC)] when potassium *tert*-butoxide was employed as the base. Using

THF as solvent also did not result in complete utilization of the reactant **7** even after 48 h. With DMF/NaH as the solvent/base combination, reactions were performed at temperatures of 75 ºC, 100 ºC and 120 ºC. Optimum temperature was found to be 100 ºC for improved yields and less side products (based on TLC).

Reductive cyclization of **186** using zinc dust in acetic acid furnished 2-amino-4-chloro-1*H*-indole-3-carbonitrile **187** (Scheme 33). The ^{1}H NMR of **187** showed the presence of the indole NH peak at 10.98 ppm and the 2-NH_2 peak at 6.91 ppm and both these peaks exchanged in the presence of D_2O. This confirmed the formation of the indole **187** and inturn indicated that the 2-chloro group in **7**, and not the 3-chloro, was displaced by the malononitrile anion to provide **186**. Cyclocondensation of **187** with carbamimidic chloride hydrochloride[195] afforded the 2,4-diamino-5-chloro-pyrimido[4,5-*b*]indole **188**[125] in 45% yield. The reactant **187** was completely utilized after 2 h and two spots (1:1 ratio) were observed on TLC (5% MeOH in $CHCl_3$). It was assumed that one of the products might be the uncyclized analog of **188**. Upon prolonging the reaction time to 20 h, only one spot was observed on TLC indicating that the other spot initially observed was probably an uncyclized analog of **188**.

This synthetic strategy offers an effective route for the synthesis of the valuable 5-chloro intermediate **188** from 1,2-dichloro-3-nitro-benzene **7**. It provided **188** in three steps with an overall yield of 22% compared to the reported procedure[125] which gave **188** in six steps with 5% overall yield. Compound **188** was then treated with aryl thiols **189** and **190** to provide 1 g of **1** and **2** respectively.[125]

Scheme 34. Attempted synthesis of target compound **1a**

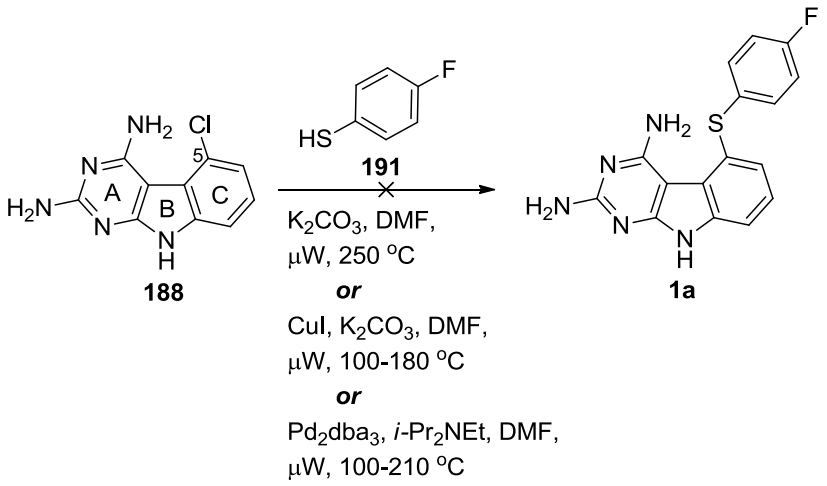

However, similar reaction of **188** with arylthiols containing electron-withdrawing substituents (e.g. **191**) resulted in no S_NAr reaction (e.g. **1a**) (Scheme 34). This decreased reactivity can be attributed to the reduced nucleophilicity of these arylthiols due to the negative inductive effect associated with the electron withdrawing substituents that make the electrons on the sulfur less available for a nucleophilic attack. In addition to this, the 5-chloro group in **188** is not a good leaving group in the S_NAr reaction first due to the absence of activation, and second due to the presence of an indole nitrogen meta to the chlorine which can donate electrons into the C-ring making it electron rich, and hence, making the 5-carbon less electrophilic. One of the ways to facilitate the reaction between **188** and **191** is to employ metal-catalyzed coupling.[173, 196, 197] Copper-catalyzed coupling ($CuI/K_2CO_3/DMF$)[173, 197] between **188** and **191** did not give any new product (based on TLC). Palladium-catalyzed coupling[173, 196] between **188** and electron-withdrawing arylthiols such as **191** also failed (Scheme 34). Another alternative for improving the reactivity is by increasing the electrophilicity of the 5-carbon of **188**, which can be

obtained by replacing the 5-chloro of **188** with a 5-bromo group. The bromo group at the 5-position is easier to displace than a chloro group because of its higher electronegativity.

Scheme 35. Synthesis of target compounds **1a**–**6a**

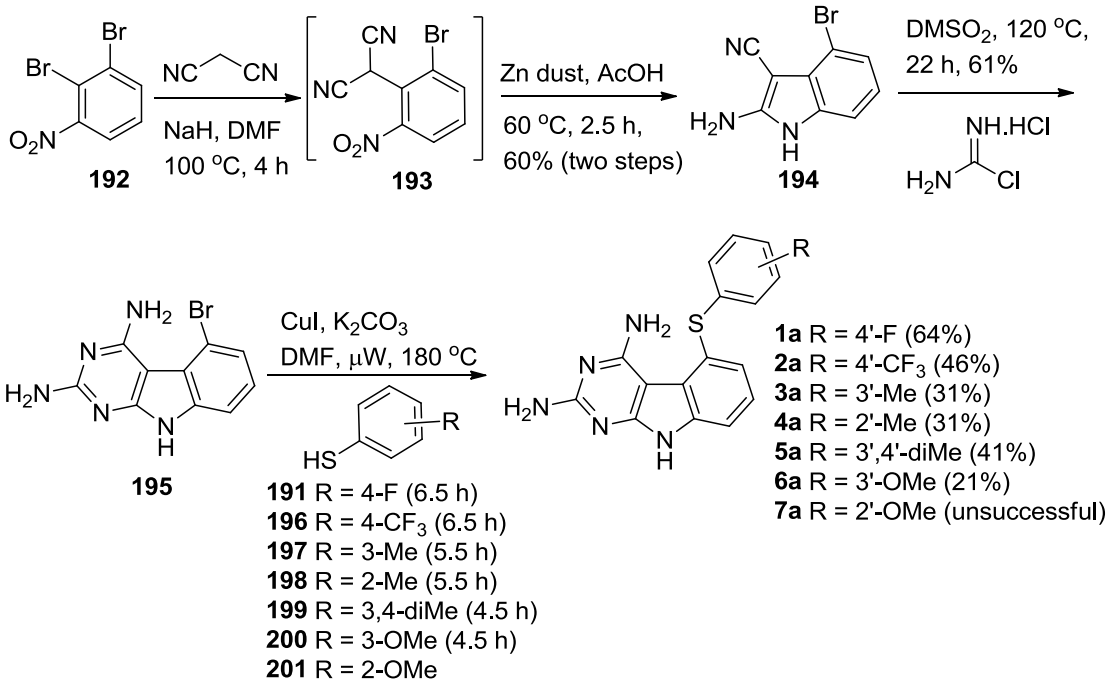

Thus, synthesis of target compounds **1a**–**6a** started from 2,3-dibromonitrobenzene **192**[198] (Scheme 35) that was synthesized by nitration of 1,2-dibromobenzene (the major product is 1,2-dibromo-4-nitrobenzene; purification was accomplished by column chromatography). Displacement of the 2-bromo of **192** with malononitrile using sodium hydride provided **193**. The use of potassium *tert*-butoxide resulted in only 60% utilization of **192**. Reductive cyclization[125] of **193** using zinc dust furnished **194**, which upon cyclocondensation with carbamimidic chloride hydrochloride[195] afforded the 2,4-diamino-5-bromo-pyrimido[4,5-*b*]indole **195**. Ullmann coupling of **195** with appropriate arylthiols **191**, **196**–**200** using CuI, K_2CO_3 under microwave conditions furnished the target compounds **1a**–**6a** in 21–64% yield. Column chromatography of **1a**–**6a** should not

be carried out using a CombiFlash® Rf system because the compounds stick to the silica gel and do not elute out. Ullmann coupling of **195** and **201** using similar conditions resulted in partial utilization of the reactant **195** and/or formation of multiple side products (TLC). Hence, it was decided to perform Ullmann coupling either at lower temperatures or by using other copper catalysts (Scheme 36).

Scheme 36. Synthesis of target compound **7a**

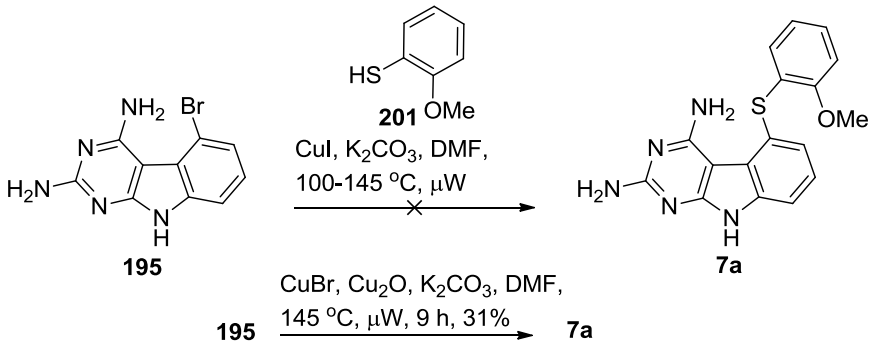

Ullmann coupling of **195** and **201** (Scheme 36) at lower temperatures (100–145 °C) resulted in only 50–60% utilization of reactant **195** (based on TLC). As the strategy of coupling at lower temperatures did not work, the next option considered was to attempt other copper catalysts. Copper catalysts Cu_2O/CuBr have been successfully employed[199] for Ullmann coupling in the synthesis of nolatrexed. Ullmann coupling of **195** and **201** using CuBr/Cu_2O resulted in **7a** in 31% yield (Scheme 36).

Synthesis of *N*,*N*-disubstituted-5-methylfuro[2,3-*d*]pyrimidin-4-amines 1b–4b and 1e–5e

Target compounds **1b**–**4b** were synthesized as described in Scheme 37. Compound **203**[143] was obtained by reacting hydroxyacetone **202** with malononitrile in the presence of triethylamine and was used without purification for the next step. Treatment of **203**

with formamidine (obtained by stirring formamidine hydrochloride with sodium ethoxide) in ethanol provided 4-amino-5-methyl-furo[2,3-*d*]pyrimidine **204**.[174] ^{1}H NMR of **204** showed the presence of the 4-NH_2 as a broad singlet at 7.02 ppm and the C_2-CH as a singlet at 8.13 ppm. Ullmann coupling of **204** and 4-iodo anisole **205** using copper iodide and L-proline afforded **181** in 33% yield.[174] N^4-Alkylation[174] of **181** with alkyl iodides **206**–**209** furnished **1b**–**4b** in 57-85% yield.

Scheme 37. Synthesis of target compounds **1b**–**4b**

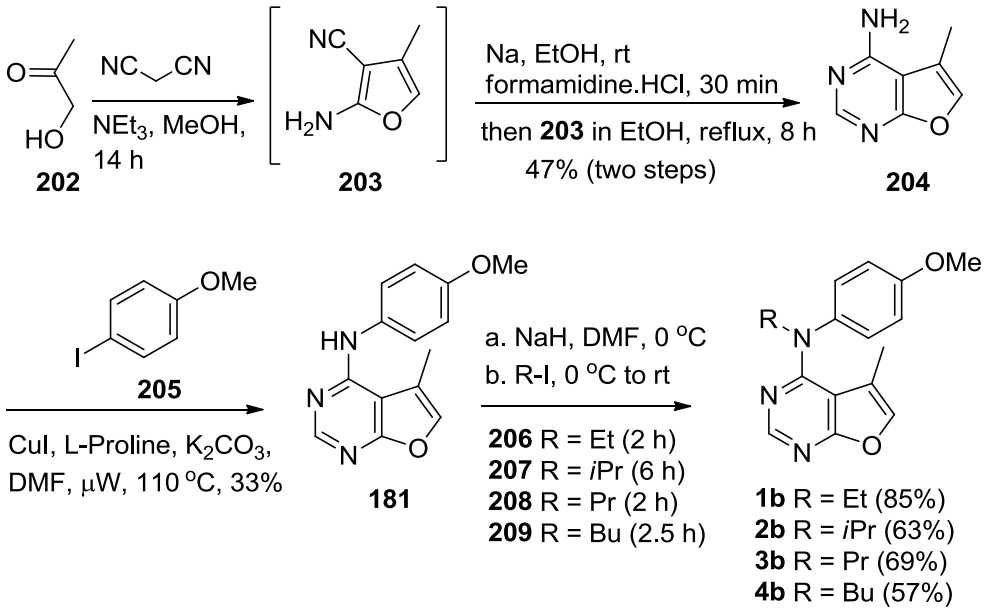

Scheme 38. Synthesis of target compound **1c**

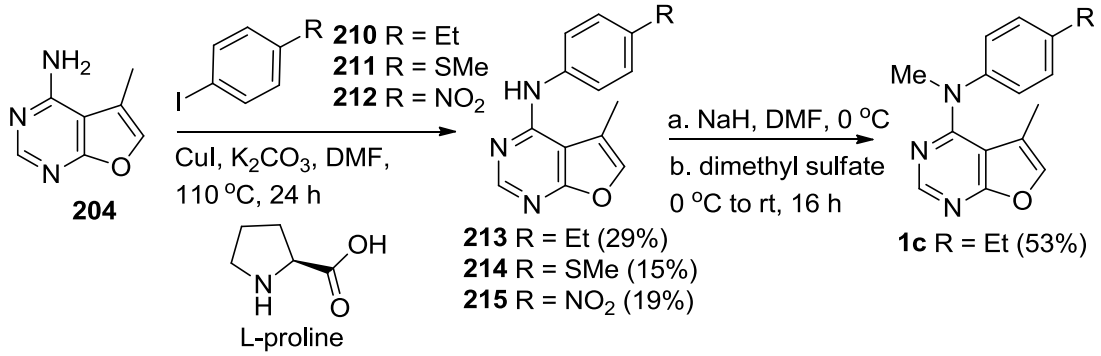

Ullmann coupling[200] of **204** and *p*-ethyl phenyl iodide **210** (Scheme 38) using copper iodide and L-proline afforded **213** in 29% yield. Compound **213** was N^4-methylated using dimethyl sulfate to furnish target compound **1c** in 53% yield. Ullmann coupling of **204** with aryl iodides **211** and **212** using copper iodide and L-proline provided **214** and **215** in poor yields. In these reactions, it was observed that 50-60% of **204** was unreacted (based on TLC). Using higher (2–3) equivalents of CuI and/or L-proline did not improve the reactivity of **204**. The reactivity of **204** (or the reaction yield) also did not improve under higher reaction temperatures (120–150 ^oC) and/or microwave conditions. To improve the reactivity of **204** as well as the reaction yield, it was decided to change the ligand "L-proline" and/or the catalyst "copper iodide". Guo, X. *et al*.[201] successfully utilized pipecolinic acid as the ligand for *N*-arylation of electron-deficient aromatic systems. Hence, pipecolinic acid, instead of L-proline, was employed as the ligand for Ullmann coupling of **204** and aryl iodides **211** or **212** (Scheme 39).

Scheme 39. Synthesis of target compounds **2c**–**5c**

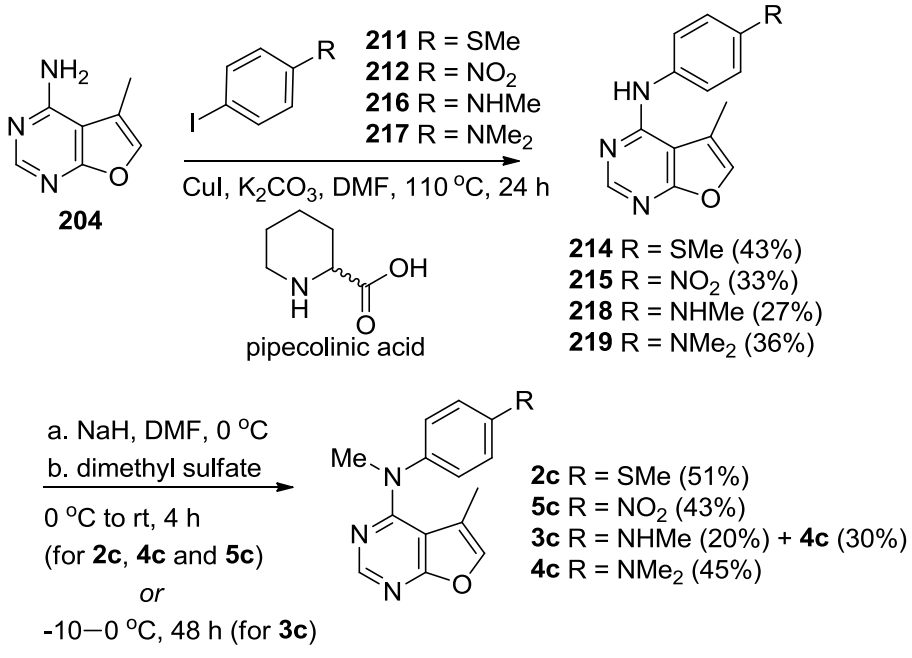

Ullmann coupling[201] of **204** with aryl iodides **211** and **212** using pipecolinic acid as the ligand provided significantly better yields for **214** and **215** (Scheme 39), respectively, than when L-proline was the ligand. Similarly, treatment of **204** with *p*-iodo anilines **216**[202] and **217**[202] afforded **218** and **219**, respectively in moderate yields. N^4-Methylation of **214**, **215** and **219** using dimethyl sulfate at room temperature afforded target compounds **2c**, **5c** and **4c**, respectively, in 43-51% yield. Similar conditions for the N^4-methylation of **218** resulted in the methylation of both 4- and 4'-nitrogens to give the 4'-NMe_2 analog **4c** instead of desired compound **3c**. Reaction at rt or the use of more than one equivalent of NaH gave predominantly **4c**. Hence, compound **218** was treated with NaH (1.1 equivalents) and dimethyl sulfate (1.1 equivalents) at -10–0 °C to furnish the desired compound **3c** in 20% yield and **4c** in 30% yield.

Retrosynthetic strategies for 2,4,5-trisubstituted pyrimido[4,5-*b*]indoles

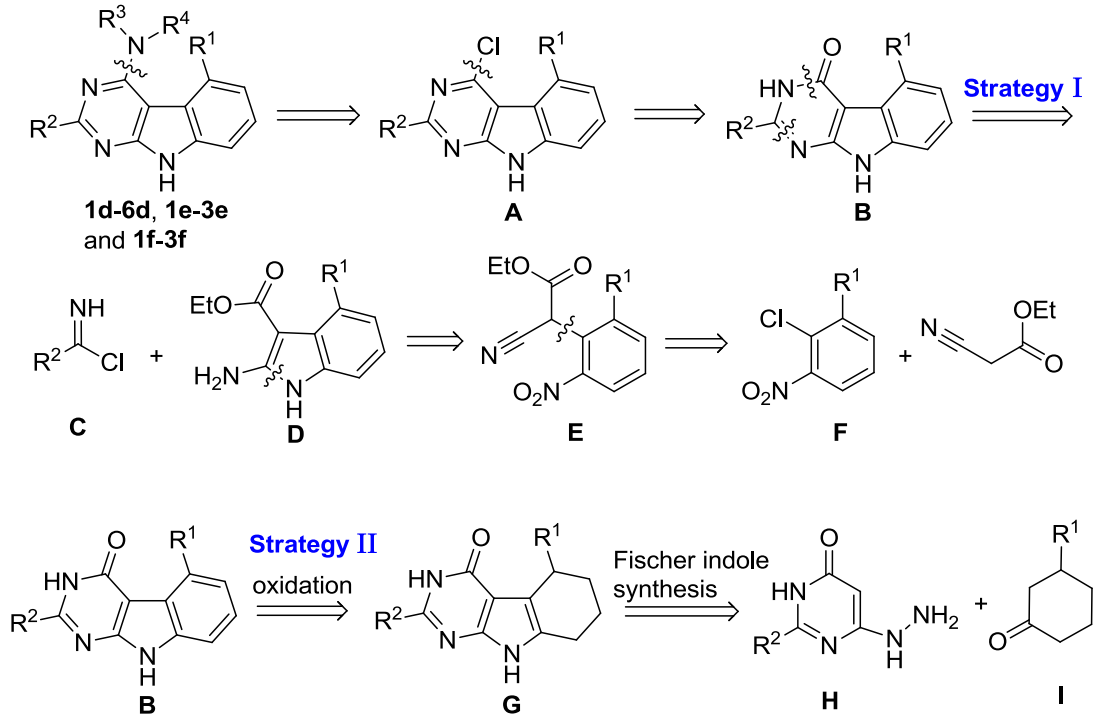

Figure 43. Retrosynthetic strategies for target compounds **1d–6d**, **1e–3e** and **1f–3f**.

The synthesis of target compounds **1d–6d**, **1e–3e** and **1f–3f** was envisioned *via* nucleophilic displacement reactions[125] of 4-chloro-pyrimido[4,5-*b*]indoles with general structure **A** (Figure 43), which could be prepared from 4-oxo- pyrimido[4,5-*b*]indoles **B**. Compounds of general structure **B** can be synthesized using either of the two strategies. Strategy 1 involves condensation[125] of substituted indoles **D** with chlorformamidine type reagents **C**. Indoles **D** can be synthesized via reductive cyclization[125] of appropriately substituted nitrobenzenes **E**, which could be obtained by treating[125] *o*-chloro-nitrobenzenes **D** with malononitrile. Alternatively, 4-oxo- pyrimido[4,5-*b*]indoles **B** can be prepared via strategy II that utilizes a Fischer indole synthesis of **G** from aryl hydrazines **H** and cyclohexanones **I**.

Synthesis of N^4-aryl-5-chloro-2,4-diamino-pyrimido[4,5-*b*]indoles 1d–6d

Disconnection strategy I (Figure 43) was utilized for the synthesis of target compounds **1d–6d**. Displacement of the 2-chloro group of 1,2-dichloro-3-nitro-benzene **7** by the ethyl cyanoacetate anion provided **8**[125] as a viscous yellow liquid in 96% yield (Scheme 40). Reduction of the nitro group of **8** followed by cyclization furnished **9**[125] as a pink solid in 74% yield.[125] ^{1}H NMR indicated the formation of the indole **9**: a one–proton singlet at 10.97 ppm (indole NH) and a two–proton broad singlet at 6.87 ppm (2-NH_2 group) and both these peaks exchanged in the presence of D_2O. Cyclocondensation of **9** with carbamimidic chloride hydrochloride[195] afforded the tricyclic compound **10**[125] after workup as a pale brown solid in 64% yield. Protection of the 2-amino group of **10** using pivalic anhydride provided **220**[125] in 60% yield, better than the reported method[125] which utilized pivalic anhydride, 4-(*N*,*N*-dimethylamino)pyridine (DMAP) and triethylamine to give **220** in 40% yield. The

pivaloyl protection of the 2-amino group increases the solubility of the compound in organic solvents for the chlorination step; a direct chlorination of unprotected **10** with phosphorus oxychloride resulted in no reaction.

Scheme 40. Synthesis of target compounds **1d**–**6d**

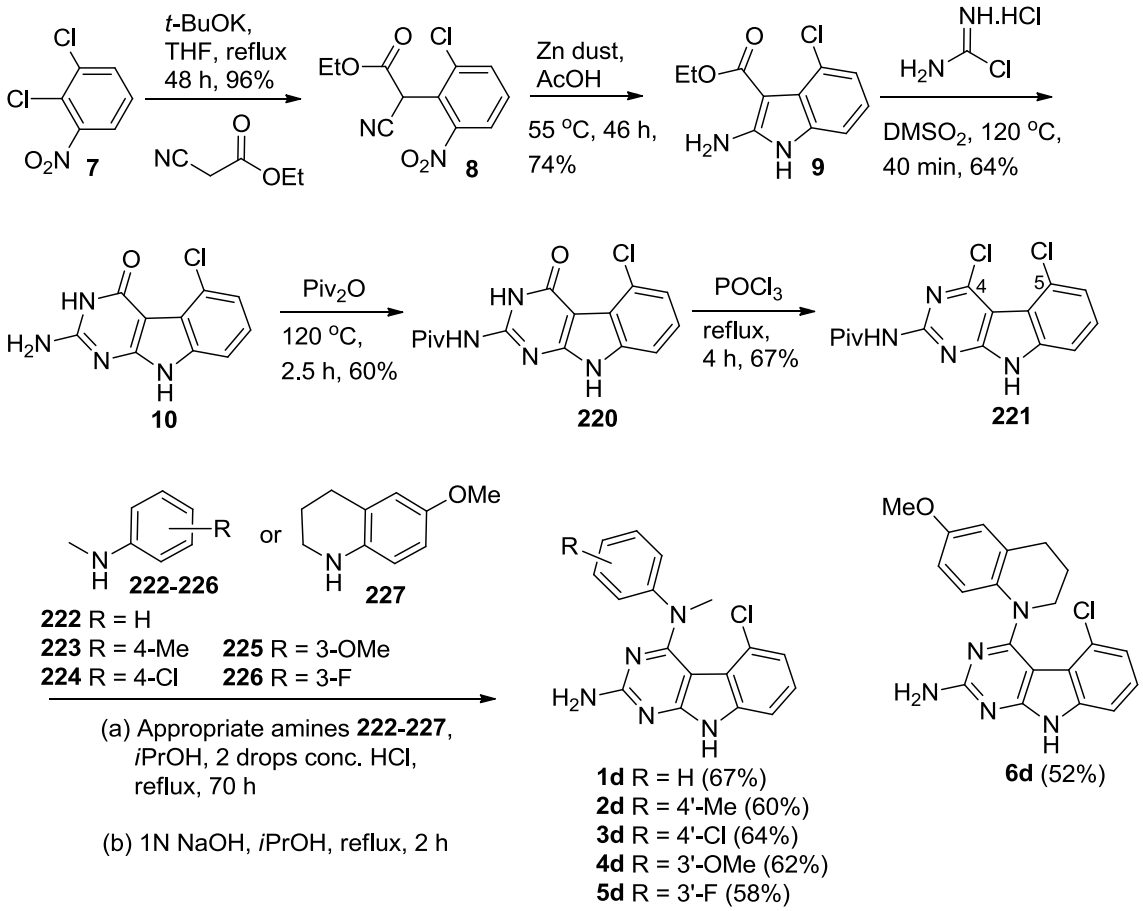

Compound **221**[125] was obtained by treating **220** with phosphorus oxychloride (Scheme 40). Displacement[203] of the 4-chloro group in **221** with *N*-methyl anilines **222**–**226** or 6-methoxy-1,2,3,4-tetrahydroquinoline **227** followed by base–mediated deprotection of the 2-amino group provided target compounds **1d**–**6d** respectively in 52–67% yield.[182] The amines **222**–**227** regiospecifically displaced the 4-chloro of **221**

rather than the 5-chloro group because the 4-position is more electrophilic than the 5-position owing to the presence of the adjacent 3-nitrogen atom.

Synthesis of 2,4-disubstituted-9*H*-pyrimido[4,5-b]indole-4-amines 1e–3e and 1f–3f

Target compounds **1e**–**3e** and **1f**–**3f** were synthesized by employing the disconnection strategy II (Figure 43), which involves a "Fisher indole synthesis" as the key step in the construction of pyrimido[4,5-*b*]indole ring.

Scheme 41. Synthesis of target compounds **1e** and **2e**

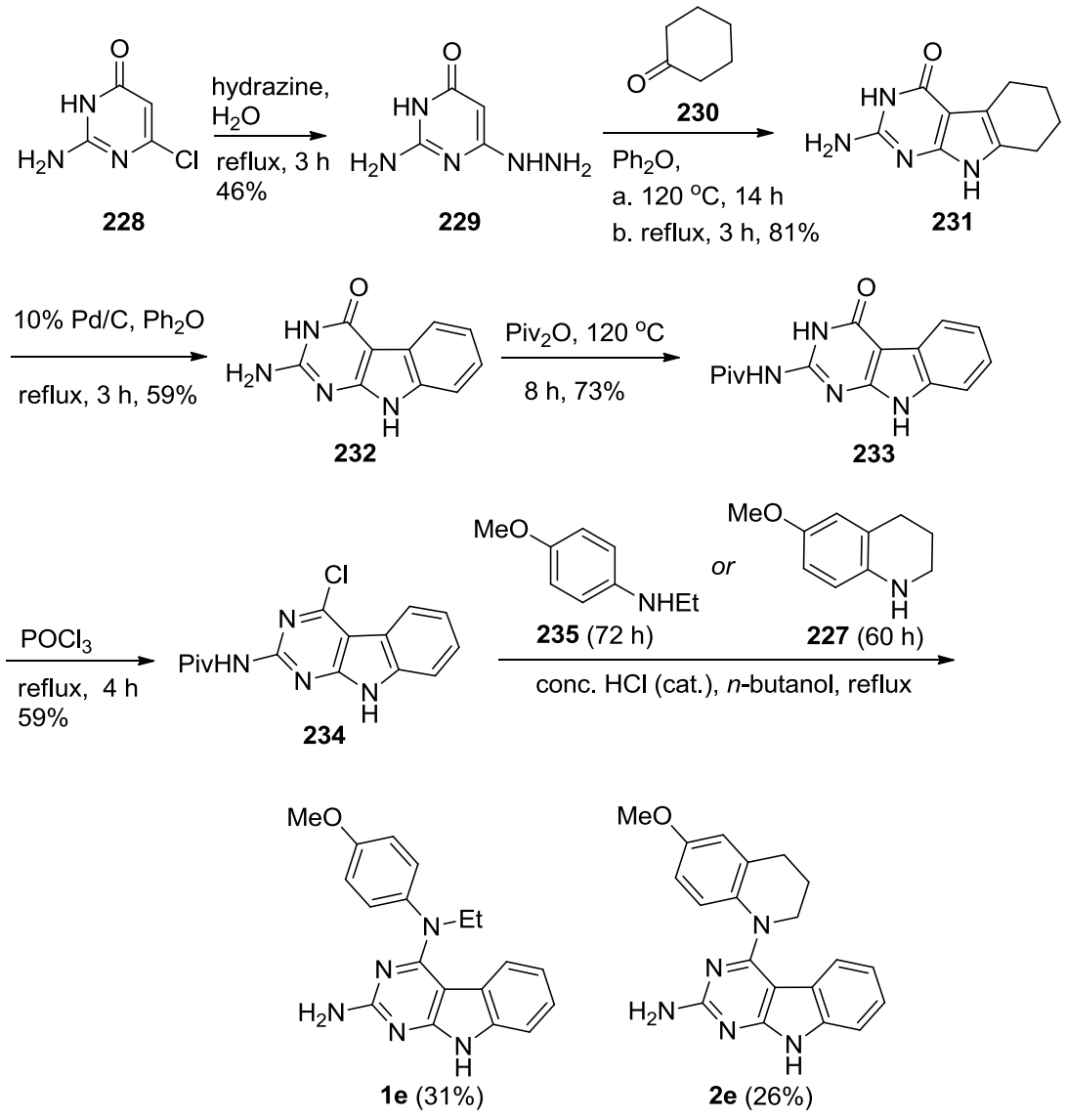

Displacement of the 6-chloro of 2-amino-6-chloropyrimidin-4(3*H*)-one **228** with hydrazine using a reported method[204] afforded **229** in 46% yield (Scheme 41). Fischer indole cyclization of the 6-hydrazinopyrimidin-3-one **229** with cyclohexanone **230** furnished the tricyclic scaffold **231**.[178] This reaction required reflux in diphenyl ether (250 ^{o}C) to facilitate the cyclization to **231**. The ^{1}H NMR of **231** showed the presence of a D_2O-exchangeable indole NH peak at 10.50 ppm and four pairs of aliphatic CH_2 peaks at 1.64–1.69, 2.42 and 2.53 ppm. This structural data confirmed the formation of the indole **231**. The partially saturated ring in **231** was oxidized using 10% Pd/C to provide **232**[178] in 57% yield. The 2-amino moiety of **232** was pivaloyl protected to give **233**,[178] which upon chlorination afforded the common intermediate **234**.[178] Attempts to displace the 4-chloro of **234** with anilines **235**[205] and 6-methoxy-1,2,3,4-tetrahydroquinoline **227** in isopropanol at reflux were unsuccessful. After 72 h, less than 5% of **234** was utilized (based on TLC). Hence, *n*-butanol, that has higher boiling point than isopropanol, was chosen as the solvent for the synthesis of **1e** and **2e**. Compound **234** was treated with **235** and **227** in *n*-butanol to afford **1e**[178] and **2e**, respectively, after simultaneous deprotection of the 2-amino group.

Scheme 42. Synthesis of target compound **3e**

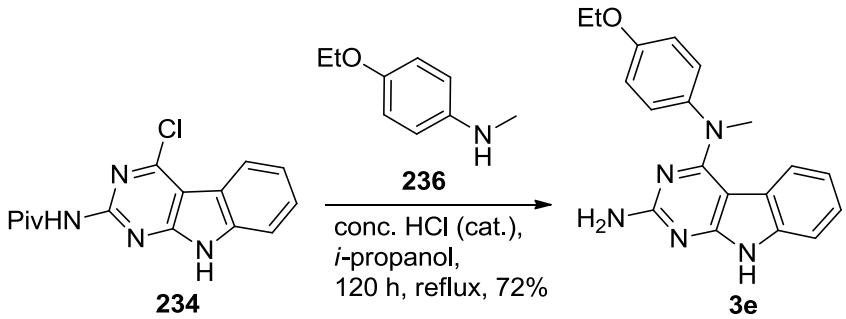

Compound **3e** was obtained from nucleophilic displacement of **234** with 4-ethoxy-*N*-methylaniline **236**[206] and simultaneous deprotection of the 2-amino group (Scheme 42).[178] Unlike the displacement of the 4-chloro of **234** with **235** and **227** (Scheme 41) which required heating in *n*-butanol at reflux, the displacement of **234** with **236** worked in isopropanol at reflux. This can be attributed to lower reactivity of the sterically hindered amines **235** and **227** compared to **236**.

Scheme 43. Synthesis of target compound **1f**

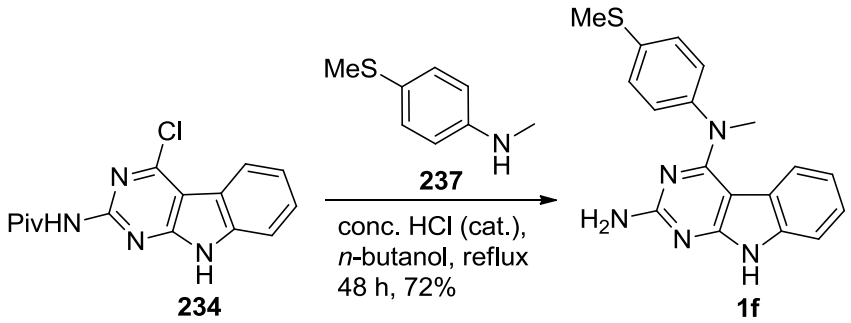

Displacement of the 4-chloro of **234** with 4-thiomethyl-*N*-methylaniline **237**[206] followed by simultaneous deprotection of the 2-amino group in *n*-butanol at reflux provided **1f** in 72% yield (Scheme 43).[178] *n*-Butanol was chosen as the solvent for **1f** because the reaction of **234** with **237** in isopropanol at reflux resulted in less than 5% completion after 72 h (based on TLC).

The synthesis of target compound **2f** commenced from commercially available 1-chloro-2-nitrobenzene **238** (Scheme 44). Displacement of the chloro of **238** by the ethyl cyanoacetate anion provided **239** in 86% yield. Reduction of the nitro group of **239** followed by cyclization furnished **18** in a yield of 74%.[129] Bubbling anhydrous HCl gas through a solution of **18** in acetonitrile afforded **21**.[130] Compound **21** was then treated with aqueous NaOH solution in ethanol at reflux to obtain **23**.[130] Proton NMR of **23**

confirmed the formation of 2-methyl-4-oxo-pyrimido[4,5-*b*]indole: a three-proton singlet (2-Me) at 2.41 ppm, two D_2O-exchangeable singlets (3-NH and 9-NH) at 11.98 ppm and 12.12 ppm and 4 aryl protons (between 7.18 and 7.94 ppm). Compound **23** was chlorinated[178] using phosphorus oxychloride to afford **240** in 79% yield. Displacement of the 4-chloro of **240** with 4-methoxy-*N*-methyl aniline **241** provided target compound **2f** in 78% yield.

Scheme 44. Synthesis of target compound **2f**

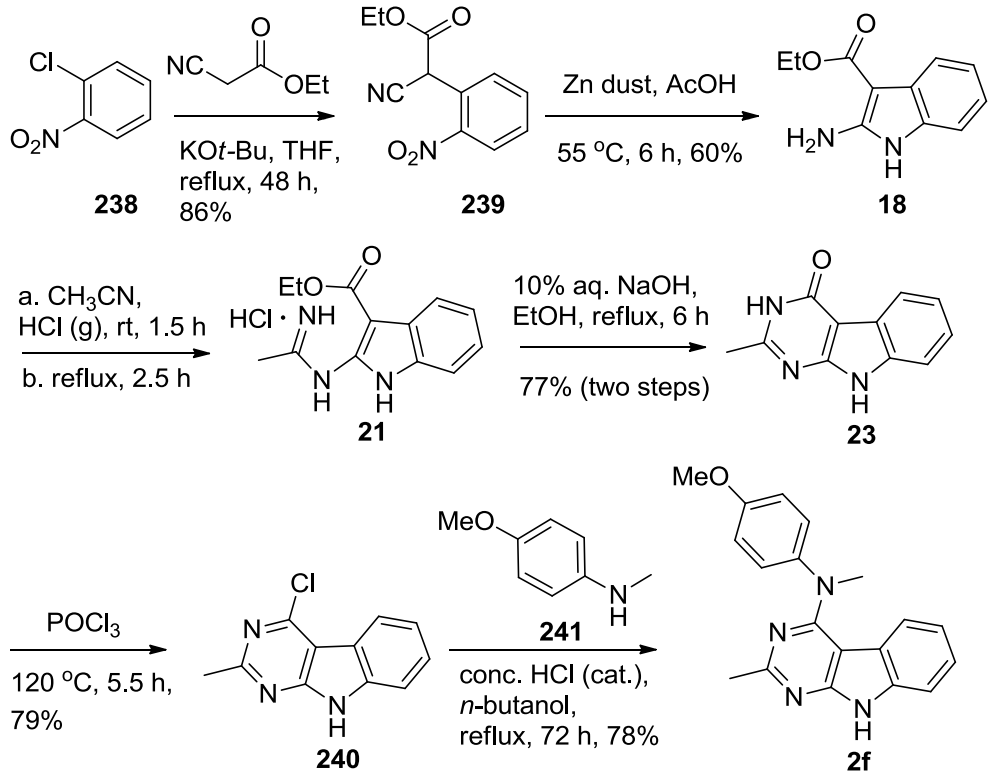

The target compound **3f** was synthesized using Scheme 45. 2-Amino-indole-3-nitrile **18** (Scheme 44) was reacted with neat formamide to afford pyrimido[4,5-*b*]indole **242** (Scheme 45).[129] The 4-oxo of **242** was converted to the 4-chloro **243** by treating with phosphorus oxychloride. Nucleophilic displacement of **243** with 4-methoxy-*N*-methyl aniline **241** provided target compound **3f** in 38% yield.

Scheme 45. Synthesis of target compound **3f**

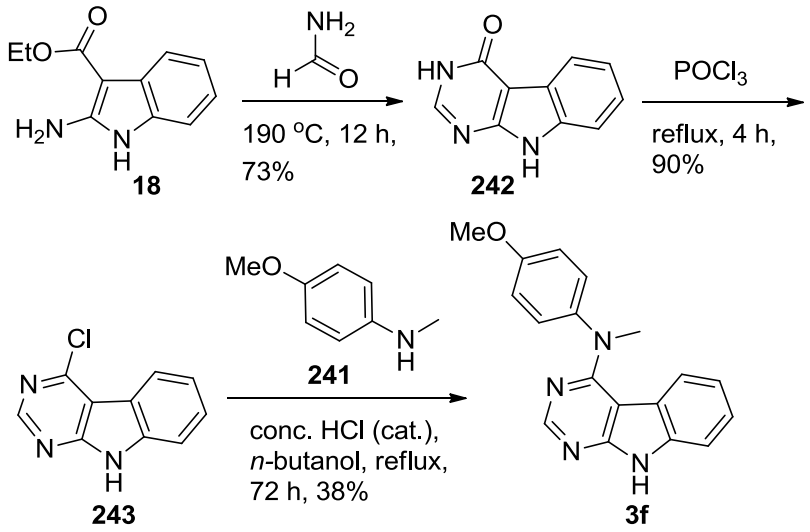

Synthesis of 2-amino-4-oxo-5-thioaryl-9*H*-pyrimido[4,5-*b*]indoles 1g–7g

Scheme 46. Synthesis of **1g**–**6g** and novel compound **7g**

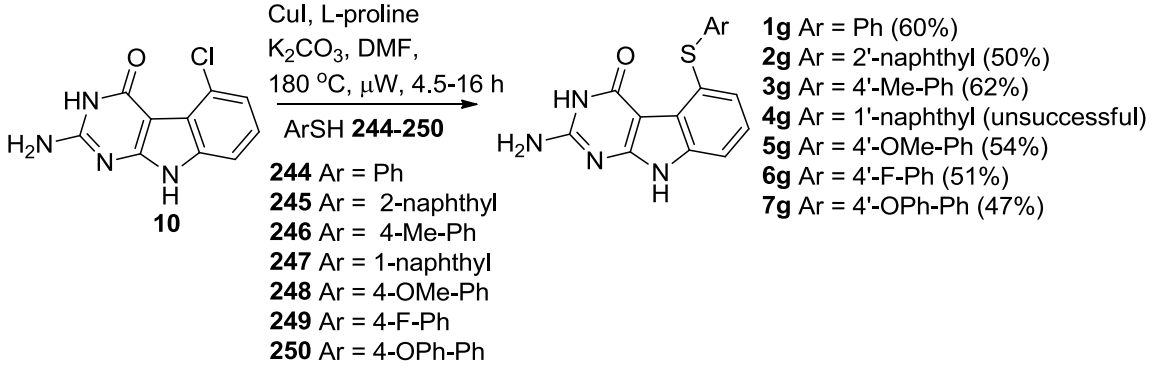

Compounds **1g**–**6g** have been previously synthesized albeit in very poor yields (2–6%) from commercial starting materials.[192] To improve the yield, Ullmann coupling[197] of **10** with aryl thiols **244**−**249** was attempted with copper iodide as the catalyst (Scheme 46). Several temperatures (145–200 °C), solvents (DMF, NMP) with/without ligand (L-proline) were screened. The optimal method is described in Scheme 46. Compound **10**[125] was obtained in 45% yield from commercial starting materials in three steps (Scheme

40). Ullmann coupling of **10** with **244**−**246**, **248**−**250** using CuI and L-proline at 180 °C under microwave conditions provided **1g**−**3g** and **5g**−**7g** in 47-62% yield. Similar displacement of **10** with 1-naphthyl thiol **247** was unsuccessful probably due to steric hindrance. Column chromatography of **1g**−**3g** and **5g**−**7g** should not be carried out with a CombiFlash® Rf system because the compounds stick to the silica gel and do not elute out. Optimization of this reaction resulted in the synthesis of **1g**−**3g**, **5g** and **6g** in 23–28% overall yield from commercial starting materials, which is a significant improvement over the previous method which gave a mere 2–6% yield.

Scheme 47. Synthesis of **1g**·HCl and **2g**·HCl

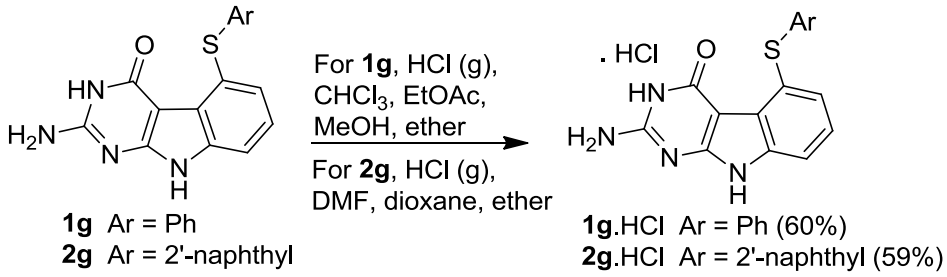

Hydrochloride salts **1g**·HCl and **2g**·HCl were synthesized to improve the water solubility of **1g** and **2g** (Scheme 47). The HCl salt of **1g** (**1g**·HCl) was obtained by bubbling anhydrous HCl gas through a solution of **1g** in chloroform, ethyl acetate, diethyl ether and methanol. The HCl salt of **2g** (**2g**·HCl) was prepared by treating **2g** in DMF, dioxane and diethyl ether with anhydrous HCl gas.

V. EXPERIMENTAL

All evaporations were carried out in vacuum with a rotary evaporator. Analytical samples were dried in vacuo (0.2 mm Hg) in a CHEM-DRY drying apparatus over P_2O_5 at 50 °C. Thin–layer chromatography (TLC) was performed on Whatman® Sil G/UV254 silica gel plates and the spots were visualized by irradiation with ultraviolet light (254 and 366 nm). Proportions of solvents used for TLC are by volume. All analytical samples were homogeneous on TLC in at least two different solvent systems. Column chromatography was performed on a 70−230 mesh silica gel (Fisher Scientific) column. Flash chromatography was carried out using CombiFlash® Rf 200 (Teledyne ISCO) automated flash chromatography system with pre-packed RediSep® Rf normal–phase flash columns (230−400 mesh). The amount (weight) of silica gel for column chromatography was in the range of 50−100 times the amount (weight) of the crude compounds being separated. Columns were wet-packed with appropriate solvent unless specified otherwise. Melting points were determined using a digital MEL-TEMP II melting point apparatus with FLUKE 51 K/J electronic thermometer or using an MPA100 OptiMelt automated melting point system and are uncorrected. Nuclear magnetic resonance spectra for proton (^{1}H NMR) were recorded on Bruker Avance II 400 (400 MHz) and 500 (500 MHz) NMR systems and were analyzed using MestReC NMR data processing software. The chemical shift (δ) values are expressed in ppm (parts per million) relative to tetramethylsilane as an internal standard: s, singlet; d, doublet; t, triplet; q, quartet; m, multiplet; br, broad singlet; exch, protons exchangeable by addition of D_2O.

Elemental analyses or high-performance liquid chromatography (HPLC)/mass analysis were used to determine the purities of the target compounds. Elemental analyses were

performed by Atlantic Microlab, Inc., Norcross, GA. Elemental compositions are within ±0.4% of the calculated values and indicate >95% purity. Fractional moles of water or organic solvents frequently found in some analytical samples could not be prevented despite 24−48 h of drying in vacuo and were confirmed where possible by their presence in the ^{1}H NMR spectra. Mass spectrum data were acquired on an Agilent G6220AA TOF LC/MS system using the nano ESI (Agilent chip tube system with infusion chip). HPLC analysis was performed on a Waters HPLC system using XSelect® CSH C18 column. Peak area of the major peak w.r.t other peaks was used to determine the purity. All solvents and chemicals were purchased from Sigma–Aldrich Co. or Fisher Scientific Inc. and were used as received.

2-(2-Chloro-6-nitrophenyl)malononitrile (186).

To an ice-cold solution of malononitrile (10.3 g, 156 mmol) in anhydrous DMF (500 mL) under argon atmosphere was added sodium hydride (3.75 g, 156 mmol). The resulting white suspension was stirred for 15 min and then 1,2-dichloro-3-nitrobenzene **7** (10 g, 52 mmol) was added. An orange color was observed within 2-3 minutes after adding **7**. The mixture was stirred at 100 °C for 4 h. After cooling the reaction mixture, 200 mL H_2O was added, and the aqueous mixture was acidified to pH 2.0 with conc. HCl. The mixture was extracted with diethyl ether (500 mL × 3) and the combined organic phases were dried using anhydrous sodium sulfate and concentrated to give **186** as dark brown oil. TLC R_f = 0.72 (hexane/EtOAc, 1:1); ^{1}H NMR (500 MHz, DMSO-d_6): δ = 6.22 (s, 1H, CH); 7.72–7.75 (m, 1H, Ar); 7.92–7.93 (m, 1H, Ar); 8.18–8.20 (m, 1H, Ar). This material was used directly for the next step without further purification.

2-Amino-4-chloro-1*H*-indole-3-carbonitrile (187).

A solution of **186** (1 g, 4.5 mmol) in glacial acetic acid (60 mL) was treated with 3 g of zinc dust. The mixture was stirred at 60 °C for 45 min and then recharged with zinc dust (1 g). After heating for another 105 min, the mixture was filtered through a pad of Celite. The pad was washed with 60 mL AcOH, the filtrate was concentrated and then neutralized with saturated Na_2CO_3 solution. The resulting precipitate was then purified by column chromatography, eluting sequentially with 0% and 1% MeOH in $CHCl_3$. Fractions containing the product (TLC) were pooled and evaporated to afford 490 mg (49%, two steps) of **187** as a pink solid. TLC R_f = 0.25 ($CHCl_3$/MeOH, 10:1 with 2 drops of conc. NH_4OH); mp 240.1–240.9 °C. ^{1}H NMR (500 MHz, DMSO-d_6): δ = 6.84–6.88 (m, 1H, Ar); 6.91 (br, 2H, 2-NH_2, exch); 6.92–6.94 (m, 1H, Ar); 7.07–7.09 (m, 1H, Ar); 10.98 (s, 1H, 1-NH, exch). Elemental analysis calculated (%) for $C_9H_6ClN_3 \cdot 0.09CH_3COCH_3$: C, 56.56; H, 3.35; N, 21.35; Cl, 18.01. Found: C, 56.36; H, 3.39; N, 21.31; Cl, 17.94.

5-Chloro-9*H*-pyrimido[4,5-*b*]indole-2,4-diamine (188).

Compound **187** (0.8 g, 4.16 mmol), carbamimidic chloride hydrochloride[195] (0.8 g) and methyl sulfone (8 g, 10 equivalents) were taken in a 100 mL evaporation flask and was heated at 120 °C for 20 h. About 10 mL of ammonia in methanol was added to neutralize the reaction mixture. Solvent was removed under reduced pressure and the product was purified by column chromatography, sequentially eluting with 1% and 5% methanol in chloroform. Fractions containing the product (TLC) were pooled and evaporated to afford 0.57 g (58%) of **188** as a brown solid. TLC R_f = 0.53 ($CHCl_3$/MeOH, 5:1 with 2 drops of

conc. NH_4OH); mp 243.2–243.8 ºC (lit.[125] 245.2–246.3 ºC). ^1H NMR (400 MHz, DMSO-d_6): δ = 6.07 (s, 2H, 4-NH_2, exch); 6.80 (bs, 2H, 2-NH_2, exch); 7.06–7.13 (m, 2H, Ar); 7.21–7.23 (m, 1H, Ar); 11.49 (s, 1H, 9-NH, exch). ^1H NMR agreed well with the literature reported[125] values.

General procedure for the synthesis of 5-(substituted phenylthio)-9*H*-pyrimido[4,5-*b*]indole-2,4-diamines 1 and 2.

Compound **188** (50 mg, 1 equivalent), potassium carbonate (4 equivalents) and appropriate aryl thiol (4 equivalents) were weighed and added to a Biotage® microwave vial. *N*-methyl pyrrolidine-2-one (NMP, 3 mL) was added as solvent and the vial was sealed. The reaction was run in a Biotage® initiator at very high absorption for 30 minutes at 250 °C. The reaction mixture was transferred to the top of a 15 g silica gel column and was sequentially eluted with 1% and 3% methanol in chloroform. Fractions containing the product (TLC) were pooled and evaporated to give the desired product which was further purified by washing with diethyl ether.

5-(Phenylthio)-9*H*-pyrimido[4,5-*b*]indole-2,4-diamine (1).

Using the general procedure described above, compound **188** (50 mg, 0.22 mmol) was treated with benzene thiol **189** (95 mg, 0.86 mmol) to yield 60 mg (90%) of **1** as a brown solid. TLC R_f = 0.62 ($CHCl_3$/MeOH, 5:1 with 2 drops of conc. NH_4OH); mp 251.1-252.0 °C (lit.[125] 251 ºC). ^1H NMR (400 MHz, DMSO-d_6): δ = 6.02 (s, 2H, 4-NH_2, exch); 7.03–7.04 (m, 2H, Ar); 7.13–7.15 (m, 1H, Ar); 7.22–7.25 (m, 3H, Ar), 7.24 (s, 2H, 2-NH_2, exch); 7.32–7.33 (m, 1H, Ar); 7.40–7.42 (m, 1H, Ar); 11.48 (s, 1H, 9-NH, exch).

Elemental analysis calculated (%) for $C_{16}H_{13}N_5S \cdot 0.47CH_3OH$: C, 61.35; H, 4.65; N, 21.72; S, 9.95. Found: C, 61.32; H, 4.41; N, 21.66; S, 9.89. ^{1}H NMR agreed well with the literature reported[125] values.

5-(4-Methylphenylthio)-9*H*-pyrimido[4,5-*b*]indole-2,4-diamine (2).

Using the general procedure described above, compound **188** (50 mg, 0.22 mmol) was treated with *p*-toluene thiol **190** (95 mg, 0.86 mmol) to provide 59 mg (86%) of **2** as a brown solid. TLC R_f = 0.60 ($CHCl_3$/MeOH, 5:1 with 2 drops of conc. NH_4OH); mp >250 ^oC (lit.[125] >250 ^oC). ^{1}H NMR (400 MHz, DMSO-d_6): δ = 2.20 (s, 3H, CH_3), 6.03 (bs, 2H, 4-NH_2, exch), 6.96–6.98 (m, 2H, Ar), 7.06–7.08 (m, 2H, Ar), 7.18–7.22 (m, 1H, Ar), 7.20 (bs, 2H, 4-NH_2, exch), 7.29–7.31 (m, 1H, Ar), 7.37–7.39 (m, 1H, Ar), 11.47 (s, 1H, 9-NH, exch). Elemental analysis calculated (%) for $C_{17}H_{15}N_5S$: C, 63.53; H, 4.70; N, 21.79; S, 9.98. Found: C, 63.13; H, 4.85; N, 21.51; S, 9.87. ^{1}H NMR agreed well with the literature reported[125] values.

2-Amino-4-bromo-1*H*-indole-3-carbonitrile (194).

To an ice-cold solution of malononitrile (4.76 g, 72 mmol) in anhydrous DMF (500 mL) under argon atmosphere was added sodium hydride (2.6 g, 104 mmol). Thus formed white suspension was stirred for 15 min and then 1,2-dibromo-3-nitrobenzene **192**[198] (10 g, 36 mmol) was added. Orange color was observed within 2-3 minutes after adding **192**. The mixture was stirred at 100 °C for 4 h. After cooling the reaction mixture, 200 mL H_2O was added, and the resulting aqueous mixture was acidified to pH 2.0 with conc. HCl. The mixture was extracted with diethyl ether (500 mL × 3) and then the combined

organic phases were dried using anhydrous sodium sulfate and concentrated to give (2-Bromo-6-nitrophenyl)-malononitrile **193** as dark-brown oil. TLC R_f = 0.42 ($CHCl_3$/MeOH, 10:1); ^{1}H NMR (400 MHz, DMSO-d_6): δ = 6.18 (s, 1H, CH); 7.62–7.66 (m, 1H, Ar); 8.07–8.09 (m, 1H, Ar); 8.19–8.21 (m, 1H, Ar). The material was used directly for the next step.

A solution of **193** (3.92 g, 14.6 mmol) in glacial acetic acid (500 mL) was treated with a single charge of zinc dust (6.84 g, 2 parts by weight). The mixture was stirred at 60 °C for 45 min, then recharged with zinc dust (3.92 g, 1 part by weight). After heating for another 105 min, the mixture was filtered through a pad of Celite. The pad was washed with glacial acetic acid, the filtrate was concentrated and then washed with saturated Na_2CO_3 solution. The precipitate was collected and then dissolved in methanol. Silica gel (5 g) was added to make the plug and was then purified by column chromatography, eluting sequentially with 0% and 1% MeOH in $CHCl_3$. The fractions containing the pure product (TLC) were pooled and evaporated to give 2.52 g of **197** as a pink solid. The overall yield from **192** to **194** was 60%. TLC R_f = 0.25 ($CHCl_3$/MeOH, 10:1 with 2 drops of conc. NH_4OH); mp 231.1–231.9 ºC. ^{1}H NMR (400 MHz, DMSO-d_6): δ = 6.78–6.82 (m, 1H, Ar); 6.89 (bs, 2H, NH_2, exch); 7.07–7.08 (m, 1H, Ar); 7.10–7.12 (m, 1H, Ar); 10.98 (s, 1H, NH, exch). Elemental analysis calculated (%) for $C_9H_6BrN_3$: C, 45.79; H, 2.56; N, 17.80; Br, 33.84. Found: C, 45.89; H, 2.59; N, 17.57; Br, 33.56.

5-Bromo-9*H*-pyrimido[4,5-*b*]indole-2,4-diamine (195).

A mixture of 2-amino-4-bromo-1*H*-indole-3-carbonitrile **194** (3 g, 12.7 mmol), carbamimidic chloride hydrochloride[195] (1.6 g, 13.9 mmol) and methyl sulfone (30 g) was stirred and stirred at 120 °C for 8 h, after which it was recharged with carbamimidic chloride hydrochloride[195] (1.6 g, 13.9 mmol) and stirred for another 14 h. The reaction mixture was cooled and 50 mL of ammonia in methanol was added to neutralize the reaction mixture. Solvents were evaporated and the crude mixture was purified by column chromatography, eluting sequentially with 1% and 5% methanol in chloroform. Fractions containing the desired product (TLC) were pooled and evaporated to afford 2.16 g (61%) of **195** as an off-white solid. TLC R_f = 0.27 ($CHCl_3$/MeOH, 10:1 with 2 drops of conc. NH_4OH); mp 239.8–240.1 ºC. ^{1}H NMR (400 MHz, DMSO-d_6): δ = 6.05 (bs, 2H, 2-NH_2, exch); 6.95 (br, 2H, 4-NH_2, exch); 7.01–7.05 (m, 1H, Ar); 7.24–7.26 (m, 2H, Ar); 11.49 (br, 1H, 9-NH, exch). HRMS (ESI): *m*/*z* calculated for $C_{10}H_8BrN_5$ + H^+ [M+H^+]: 278.0036, 280.0016. Found: 278.0029, 280.0005.

General procedure for the synthesis of 5-(substituted phenylthio)-9*H*-pyrimido[4,5-*b*]indole-2,4-diamines 1a–6a.

Compound **195** (1 equivalent), appropriate aryl thiol (4 equivalents), copper iodide (4 equivalents) and potassium carbonate (8 equivalents) were added to a Biotage® microwave vial. DMF (3 mL) was added as the solvent and the vial was sealed. The reaction was run in a Biotage® Initiator at 180 °C for 4.5–6.5 h (depending on the aryl thiol). After cooling to room temperature, silica gel (0.3 g) was added and DMF was removed under reduced pressure and the crude product was purified by column

chromatography, sequentially eluting with 1%, 2% and 3% methanol in chloroform. Fractions containing the product (TLC) were pooled and evaporated to afford the product.

5-(4-Fluorophenylthio)-9*H*-pyrimido[4,5-*b*]indole-2,4-diamine (1a).

Using the general procedure described above, the reaction of **195** (40 mg, 0.14 mmol) with 4-fluorophenylthiol **191** (0.06 mL, 0.56 mmol), copper iodide (110 mg, 0.56 mmol) and potassium carbonate (159 mg, 1.12 mmol) for 6.5 hours afforded 33 mg (64%) of **1a** as a brown solid. TLC R_f = 0.65 ($CHCl_3$/MeOH, 5:1 with 2 drops of conc. NH_4OH); mp 267.9–268.9 °C. ^{1}H NMR (400 MHz, DMSO-d_6): δ = 6.08 (s, 2H, 2-NH_2, exch), 7.11–7.41 (m, 9H, Ar and 4-NH_2), 11.52 (s, 1H, 9-NH, exch). Elemental analysis calculated (%) for $C_{16}H_{12}FN_5S{\cdot}0.26CH_3OH$: C, 58.52; H, 3.94; N, 20.99; S, 9.61; F, 5.69. Found: C, 58.35; H, 3.85; N, 21.06; S, 9.84; F, 5.54.

5-(4-Trifluoromethylphenylthio)-9*H*-pyrimido[4,5-*b*]indole-2,4-diamine (2a).

Using the general procedure described above, the reaction of **195** (50 mg, 0.18 mmol), 4-trifluoromethylphenylthiol **196** (0.2 mL, 0.72 mmol), copper iodide (137.5 mg, 0.72 mmol) and potassium carbonate (198.75 mg, 1.44 mmol) for 6.5 hours afforded 32 mg (46%) of **2a** as a brown solid. TLC R_f = 0.65 ($CHCl_3$/MeOH, 5:1 with 2 drops of conc. NH_4OH); mp >250 °C. ^{1}H NMR (400 MHz, DMSO-d_6): δ = 6.04 (s, 2H, 2-NH_2, exch); 7.12–7.29 (d, 4H, Ar); 7.35–7.48 (m, 3H, Ar and 4-NH_2); 7.59–7.61 (d, 2H, Ar); 11.57 (s, 1H, 9-NH, exch). Elemental analysis calculated (%) for $C_{17}H_{12}F_3N_5S{\cdot}0.32CH_3OH$: C,

53.94; H, 3.47; N, 18.16; S, 8.32; F, 14.78. Found: C, 54.25; H, 3.32; N, 17.96; S, 8.32; F, 14.55.

5-(*m*-Tolylthio)-9*H*-pyrimido[4,5-*b*]indole-2,4-diamine (3a).

Using the general procedure described above, the reaction of **195** (50 mg, 0.175 mmol) with *m*-toluene thiol **197** (0.09 mL, 0.7 mmol), copper iodide (137.5 mg, 0.7 mmol) and potassium carbonate (198.7 mg, 1.4 mmol) for 5.5 hours afforded 18 mg (31%) of **3a** as a brown solid. TLC R_f = 0.65 ($CHCl_3$/MeOH, 5:1 with 2 drops of conc. NH_4OH); mp 228.0–228.5 °C. ^{1}H NMR (400 MHz, DMSO-d_6): δ = 2.19 (s, 3H, 3'-Me), 6.04 (s, 2H, 2-NH_2, exch), 6.75–6.77 (m, 1H, Ar), 6.93–6.97 (m, 3H, Ar and 4-NH_2), 7.11–7.24 (m, 3H, Ar), 7.29–7.32 (m, 1H, Ar), 7.39–7.41 (m, 1H, Ar), 11.49 (s, 1H, 9-NH, exch). Elemental analysis calculated (%) for $C_{17}H_{15}N_5S{\cdot}0.28CH_3OH$: C, 68.67; H, 6.44; N, 14.13; S, 9.05. Found: C, 68.61; H, 6.45; N, 13.79; S, 9.05.

5-(*o*-Tolylthio)-9*H*-pyrimido[4,5-*b*]indole-2,4-diamine (4a).

Using the general procedure described above, the reaction of **195** (50 mg, 0.175 mmol) with *o*-toluene thiol **198** (0.09 mL, 0.7 mmol), copper iodide (137.5 mg, 0.7 mmol) and potassium carbonate (198.7 mg, 1.4 mmol) for 5.5 hours afforded 18 mg (31%) of **4a** as a brown solid. TLC R_f = 0.65 ($CHCl_3$/MeOH, 5:1 with 2 drops of conc. NH_4OH); mp decomposes at 284.7–285.8 °C. ^{1}H NMR (400 MHz, DMSO-d_6): δ = 2.39 (s, 3H, 2'-Me), 6.08 (s, 2H, 2-NH_2, exch), 6.43–6.45 (d, 1H, Ar), 6.95–7.07 (m, 3H, Ar), 7.23–7.25 (m, 4H, Ar and 4-NH_2), 7.41–7.43 (m, 1H, Ar), 11.53 (s, 1H, 9-NH, exch). Elemental

analysis calculated (%) for $C_{17}H_{15}N_5S \cdot 0.34CH_3OH$: C, 62.67; H, 4.96; N, 21.08; S, 9.65. Found: C, 62.35; H, 4.69; N, 21.23; S, 9.88.

5-(3,4-Dimethylphenylthio)-9*H*-pyrimido[4,5-*b*]indole-2,4-diamine (5a).

Using the general procedure described above, the reaction of **195** (40 mg, 0.14 mmol) with 3,4-dimethylphenylthiol **199** (0.07 mL, 0.56 mmol), copper iodide (110 mg, 0.56 mmol) and potassium carbonate (159 mg, 1.12 mmol) for 4.5 hours afforded 21 mg (41%) of **5a** as a brown solid. TLC R_f = 0.65 ($CHCl_3$/MeOH, 5:1 with 2 drops of conc. NH_4OH); mp decomposes at 252.8–253.8 ºC. ^{1}H NMR (400 MHz, DMSO-d_6): δ = 2.10–2.11 (d, 6H, 3'-Me and 4'-Me), 6.03 (s, 2H, 2-NH_2, exch), 6.73–6.75 (d, 1H, Ar), 6.94–7.02 (m, 3H, Ar and 4-NH_2), 7.17–7.38 (m, 4H, Ar), 11.46 (s, 1H, 9-NH, exch). Elemental analysis calculated (%) for $C_{18}H_{17}N_5S \cdot 0.58CH_3OH$: C, 63.04; H, 5.50; N, 19.78; S, 9.06. Found: C, 63.07; H, 5.17; N, 19.61; S, 9.00.

5-(3-Methoxyphenylthio)-9*H*-pyrimido[4,5-*b*]indole-2,4-diamine (6a).

Using the general procedure described above, the reaction of **195** (40 mg, 0.14 mmol) with 3-methoxyphenylthiol **200** (0.07 mL, 0.56 mmol), copper iodide (110 mg, 0.56 mmol) and potassium carbonate (159 mg, 1.12 mmol) for 4.5 hours afforded 20 mg (21%) of **6a** as a brown solid. TLC R_f = 0.65 ($CHCl_3$/MeOH, 5:1 with 2 drops of conc. NH_4OH); mp decomposes at 190.4–191.3 ºC. ^{1}H NMR (400 MHz, DMSO-d_6): δ = 3.64 (s, 3H, OCH_3), 6.14 (bs, 2H, 2-NH_2, exch), 6.53–6.56 (d, 2H, Ar), 6.71–6.74 (d, 1H, Ar), 7.15–7.44 (m, 6H, Ar and 4-NH_2), 11.55 (s, 1H, 9-NH, exch). HRMS (ESI): *m/z* calculated for $C_{17}H_{15}N_5OS + H^+$ [M+H$^+$]: 338.1076. Found: 338.1078. HPLC analysis:

retention time = 41.89 min; peak area, 97.46%; eluent A, H_2O; eluent B, ACN; gradient elution (100% H_2O to 10% H_2O) over 60 min with a flow rate of 0.5 mL/min and detection at 254 nm; column temperature, rt.

5-(*o*-Methoxyphenylthio)-9*H*-pyrimido[4,5-*b*]indole-2,4-diamine (7a).

Compound **195** (50 mg, 0.18 mmol), 2-methoxyphenyl thiol **201** (76 mg, 0.54 mmol), copper bromide (16 mg, 0.14 mmol), copper oxide (16 mg, 0.14 mmol) and potassium carbonate (75 mg, 0.72 mmol) were added to a Biotage® microwave vial. DMF (3 mL) was added as solvent and the vial was sealed. The reaction was run in a Biotage® initiator at 145 °C for 9 h. After cooling to room temperature, silica gel (0.3 g) was added and DMF was removed under reduced pressure. The crude product was purified by column chromatography, sequentially eluting with 1%, 2% and 3% methanol in chloroform. Fractions containing the product (TLC) were pooled and evaporated to afford 20 mg (31%) of **7a** as a brown solid. TLC R_f = 0.65 ($CHCl_3$/MeOH, 5:1 with 2 drops of conc. NH_4OH); mp >250 °C. ^{1}H NMR (400 MHz, DMSO-d_6): δ = 3.34 (s, 3H, 4-NH_2, exch); 3.89 (s, 3H, OCH_3); 6.14 (br, 2H, 2-NH_2, exch); 6.31–6.33 (d, 1H, Ar); 6.70–6.74 (t, 1H, Ar); 7.03–7.05 (m, 1H, Ar); 7.10–7.13 (m, 1H, Ar); 7.23–7.31 (m, 2H, Ar); 7.42–7.44 (d, 1H, Ar); 11.57 (br, 1H, 9-NH, exch). HRMS (ESI): *m/z* calculated for $C_{17}H_{16}N_5OS + H^+$ [M+H$^+$]: 338.1070. Found: 338.1064. HPLC analysis: retention time = 31.33 min; peak area, 95.86%; eluent A, H_2O; eluent B, ACN; gradient elution (100% H_2O to 10% H_2O) over 60 min with a flow rate of 0.5 mL/min and detection at 254 nm; column temperature, rt. Elemental analysis calculated (%) for $C_{17}H_{15}N_5OS{\cdot}0.225CHCl_3$: C, 56.80; H, 4.21; N, 19.23; S, 8.80. Found: C, 56.92; H, 4.52; N, 18.94; S, 8.62.

2-Amino-4-methylfuran-3-carbonitrile (203).

To a solution of malononitrile (1.46 g, 22.1 mmol) in 20 mL anhydrous MeOH was added triethylamine (2.23 g, 22.1 mmol) under argon atmosphere. To this solution at 0 °C was added a solution of hydroxyacetone **202** (1.64 g, 1.08 g/mL, 22.1 mmol) in 10 mL anhydrous MeOH. The solution was warmed to rt and stirred for 14 h. The solvents were evaporated to give **203** as a brown-colored crude solid. TLC R_f = 0.60 (hexane/EtOAc, 10:1). ^{1}H NMR (400 MHz, $CDCl_3$): δ = 2.01 (s, 3H, 4-CH_3), 4.75 (br, 2H, 2-NH_2), 6.61 (s, 1H, C5-CH). ^{1}H NMR agreed well with the literature reported[143] values. This material was used directly for the next step without purification.

5-Methylfuro[2,3-*d*]pyrimidin-4-amine (204).

In a 500 mL round bottom flask, sodium metal (2.3 g, 100 mmol) was added cautiously to stirred anhydrous ethanol (5.8 mL, 100 mmol) over 10 min at room temperature. After stirring for another 5 min, formamidine hydrochloride (8.05 g, 100 mmol) was added. The resulting slurry was stirred at room temperature for 30 min after which solution of **203** (13 g crude, ≈ 100 mmol) in 200 mL anhydrous ethanol was added. The mixture was heated to reflux for 8 h. After cooling the reaction mixture to room temperature, silica gel (25 g) was added and the solvents were evaporated under reduced pressure to obtain a plug. Purification was done by flash chromatography using 1% methanol in chloroform. Fractions containing the product (TLC) were pooled and evaporated to provide 7.1 g (47%, two steps) of **204** as lustrous pink crystals. TLC R_f = 0.29 ($CHCl_3$/MeOH, 10:1); mp 241.9–242.2 °C (lit.[174] 240.2–242.5 °C). ^{1}H NMR (400 MHz, DMSO-d_6): δ = 2.288–2.292 (d, 3H, CH_3, J = 1.4 Hz), 7.02 (br, 2H, NH_2, exch), 7.533–5.536 (d, 1H, C6-

CH, J = 1.4 Hz), 8.13 (s, 1H, C2-CH). ^{1}H NMR agreed well with the literature reported[174] values.

_N_-(4-Methoxyphenyl)-5-methylfuro[2,3-_d_]pyrimidin-4-amine (181).

A 50 mL round bottom flask was charged with copper iodide (66.5 mg, 0.35 mmol), anhydrous potassium carbonate (480 mg, 3.5 mmol), L-proline (80 mg, 0.7 mmol), compound **204** (150 mg, 1 mmol) and 4-iodo anisole **205** (350 mg, 3.5 mmol). The flask was connected to vacuum for 3 min followed by addition of anhydrous DMF (15 mL) using syringe. The flask was purged with argon for 5 min and then heated in an oil bath maintained at 110 ^{o}C. On heating, the color of the suspension turned blueish grey which lasted for about 2 h. The reaction was stirred for another 22 h at 110 ^{o}C at the end of which the mixture was allowed to cool to room temperature. Ethyl acetate (25 mL) was added and the mixture was poured into water (100 mL). The product was extracted with ethyl acetate (100 mL × 2). The combined organic extracts were washed with brine (100 mL) and dried (anhydrous sodium sulfate) and concentrated under reduced pressure. Silica gel (500 mg) was added and the solvent evaporated to obtain a plug. Purification by flash chromatography using hexanes and ethyl acetate (10:1 to 2:1) afforded 87.5 mg (33%) of **181** as a light brown solid. TLC R_f = 0.77 ($CHCl_3$/MeOH, 10:1); mp 101.0–101.7 ^{o}C (lit.[174] 99.0–101.6 ^{o}C). ^{1}H NMR (400 MHz, DMSO-d_6): δ = 2.383–2.386 (d, 3H, CH_3, J = 1.2 Hz), 3.75 (s, 3H, OCH_3), 6.92–6.94 (d, 2H, Ar, J = 8.8 Hz), 7.47–7.49 (d, 2H, Ar, J = 8.8 Hz), 7.650–7.653 (d, 1H, C6-CH, J = 1.2 Hz), 8.23 (s, 1H, C2-CH), 8.38 (s, 1H, 4-NH, exch). ^{1}H NMR agreed well with the literature reported[174] values.

General procedure for the synthesis of substituted furo[2,3-*d*]pyrimidines 1b–4b.

In a 25 mL round bottom flask, compound **181** (1 equivalent) and DMF (2 mL) were added to afford a solution. The flask was purged with argon for 5 min followed by cooling down to 0 ^{o}C using ice bath. To the solution at 0 ^{o}C was added sodium hydride (3 equivalents) and stirred for 20 min under argon atmosphere. Appropriate alkyl iodide (3-4 equivalents) was injected to the reaction mixture and the flask was warmed to room temperature. The mixture was stirred at room temperature until the TLC showed completion of the reactant **181**. Aqueous 1N HCl solution was added dropwise to quench the reaction followed by water (20 mL) to afford a precipitate. The product was extracted with ethyl acetate (10 mL × 3). The combined organic extracts were washed with brine (10 mL), dried (anhydrous sodium sulfate) and concentrated under reduced pressure. Silica gel (200 mg) was added and the solvent was evaporated to obtain a silica gel plug. The silica gel plug was purified by flash chromatography using hexanes and ethyl acetate (5:1). Fractions containing the product (TLC) were pooled and concentrated to obtain **1b**–**4b** in yields of 57–85%.

***N*-Ethyl-*N*-(4-methoxyphenyl)-5-methylfuro[2,3-*d*]pyrimidin-4-amine (1b).**

Using the general procedure described above, ethyl iodide **206** (61.70 mg or 0.1 mL, 1.2 mmol) was added to an ice-cold solution of **181** (100 mg, 0.4 mmol) and NaH (28.8 mg, 1.2 mmol) in 2 mL DMF and the reaction was run at room temperature for 2 h, to provide 94 mg (85%) of **1b** as an off-white solid. TLC R_f = 0.88 ($CHCl_3$/MeOH, 15:1); mp 77.8–78.3 ^{o}C. ^{1}H NMR (400 MHz, $CDCl_3$): δ = 1.064–1.067 (d, 3H, 5-CH_3, J = 1.2 Hz), 1.22 (t, 3H, CH_3, J = 7 Hz), 3.82 (s, 3H, OCH_3), 4.06–4.11 (q, 2H, NCH_2, J = 7 Hz),

6.88–6.91 (d, 2H, Ar, J = 8.9 Hz), 7.074–7.077 (d, 1H, C6-CH, J = 1.2 Hz), 7.09–7.11 (d, 2H, Ar, J = 8.9 Hz), 8.48 (s, 1H, C2-CH). Elemental analysis calculated (%) for $C_{16}H_{17}N_3O_2$: C, 67.83; H, 6.05; N, 14.83. Found: C, 67.53; H, 6.05; N, 14.77.

***N*-Isopropyl-*N*-(4-methoxyphenyl)-5-methylfuro[2,3-*d*]pyrimidin-4-amine (2b).**

Using the general procedure described above, isopropyl iodide **207** (266.36 mg, 1.6 mmol) was added to an ice-cold solution of **181** (100 mg, 0.4 mmol) and NaH (38.4 mg, 1.6 mmol) in 2 mL DMF and the reaction was run at room temperature for 6 h, to provide 75 mg (63%) of **2b** as an off-white solid. TLC R_f = 0.88 ($CHCl_3$/MeOH, 15:1); mp 95.8–96.6 °C. ^{1}H NMR (400 MHz, $CDCl_3$): δ = 1.02 (d, 3H, 5-CH_3, J = 1.3 Hz), 1.14–1.16 (d, 6H, two CH_3, J = 6.8 Hz), 3.79 (s, 3H, OCH_3), 5.30–5.37 (m, 1H, N-CH), 6.85–6.87 (d, 2H, Ar, J = 8.9 Hz), 7.000–7.004 (d, 1H, C6-CH, J = 1.3 Hz), 7.02–7.04 (d, 2H, Ar, J = 8.9 Hz), 8.42 (s, 1H, C2-CH). Elemental analysis calculated (%) for $C_{17}H_{19}N_3O_2$: C, 68.67; H, 6.44; N, 14.13. Found: C, 68.61; H, 6.45; N, 13.79.

***N*-(4-Methoxyphenyl)-5-methyl-*N*-propylfuro[2,3-*d*]pyrimidin-4-amine (3b).**

Using the general procedure described above, propyl iodide **208** (199 mg or 0.12 mL, 1.2 mmol) was added to an ice-cold solution of **181** (100 mg, 0.4 mmol) and NaH (28.8 mg, 1.2 mmol) in 2 mL DMF and the reaction was run at room temperature for 2 h, to provide 80 mg (69%) of **3b** as an off-white solid. TLC R_f = 0.88 ($CHCl_3$/MeOH, 15:1); mp 113.5–114.2 °C. ^{1}H NMR (400 MHz, $CDCl_3$): δ = 0.94–0.97 (t, 3H, CH_3), 1.095–1.098 (d, 3H, 5-CH_3, J = 1.2 Hz), 1.70–1.74 (m, 2H, CH_2), 3.84 (s, 3H, OCH_3), 3.96–3.99 (m, 2H, N-CH_2), 6.89–6.91 (d, 2H, Ar, J = 8.95 Hz), 7.092–7.095 (d, 1H, C6-CH, J = 1.2

Hz), 7.10–7.12 (d, 2H, Ar, J = 9.0 Hz), 8.49 (s, 1H, C2-CH). Elemental analysis calculated (%) for $C_{17}H_{19}N_3O_2$: C, 68.67; H, 6.44; N, 14.13. Found: C, 68.72; H, 6.41; N, 14.16.

***N*-Butyl-*N*-(4-methoxyphenyl)-5-methylfuro[2,3-*d*]pyrimidin-4-amine (4b).**

Using the general procedure described above, butyl iodide **209** (216.26 mg or 0.13 mL, 1.2 mmol) was added to an ice-cold solution of **181** (100 mg, 0.4 mmol) and NaH (28.8 mg, 1.2 mmol) in 2 mL DMF and the reaction was run at room temperature for 2.5 h to provide 70 mg (57%) of **4b** as a semisolid. TLC R_f = 0.88 ($CHCl_3$/MeOH, 15:1); ^{1}H NMR (400 MHz, $CDCl_3$): δ = 0.88–0.92 (t, 3H, CH_3), 1.06 (s, 3H, 5-CH_3), 1.30–1.39 (m, 2H, CH_2), 1.59–1.67 (m, 2H, CH_2), 3.81 (s, 3H, OCH_3), 3.96–4.00 (m, 2H, N-CH_2), 6.86–6.88 (d, 2H, Ar, J = 8.9 Hz), 7.06–7.09 (m, 3H, Ar and C6-CH), 8.45 (s, 1H, C2-CH). HRMS (ESI): *m/z* calculated for $C_{18}H_{21}N_3O_2$ + H^+ [M+H^+]: 312.1712. Found: 312.1709. HPLC analysis: retention time = 38.76 min; peak area, 97.33%; eluent A, H_2O; eluent B, ACN; gradient elution (100% H_2O to 10% H_2O) over 60 min with a flow rate of 0.5 mL/min and detection at 254 nm; column temperature, rt.

General procedure for the synthesis of *N*-(4-substituted phenyl)-5-methylfuro[2,3-*d*]pyrimidin-4-amines 213–215 using L-proline as the ligand.

A 50 mL round bottom flask was charged with copper iodide (66.5 mg, 0.35 mmol), anhydrous potassium carbonate (480 mg, 3.5 mmol), L-proline (80 mg, 0.7 mmol), compound **204** (150 mg, 1 mmol) and appropriate iodobenzene (3.5 mmol). The flask was connected to vacuum for 3 min followed by addition of anhydrous DMF (15 mL)

using syringe. The flask was purged with argon for 5 min and then heated in an oil bath maintained at 110 °C. On heating, the color of the suspension turned blueish grey which lasted for about 2 h. The reaction was stirred for additional 22 h at 110 °C at the end of which the mixture was allowed to cool to room temperature. Ethyl acetate (25 mL) was added and the mixture was poured into water (100 mL). The product was extracted with ethyl acetate (100 mL × 2). The combined organic extracts were washed with brine (100 mL) and dried (anhydrous sodium sulfate) and concentrated under reduced pressure. Silica gel (500 mg) was added and the solvent evaporated to obtain a plug. Purification was performed by flash chromatography using hexanes and ethyl acetate (10:1 to 2:1). Fractions containing the product (TLC) were pooled and evaporated to afford the product.

***N*-(4-Ethylphenyl)-5-methylfuro[2,3-*d*]pyrimidin-4-amine (213).**

Using the general procedure described above, reaction between **204** (150 mg, 1 mmol) and 1-ethyl-4-iodobenzene **210** (350 mg, 3.5 mmol) provided 74 mg (29%) of **213** as a brown semisolid. TLC R_f = 0.78 ($CHCl_3$/MeOH, 10:1); ^{1}H NMR (400 MHz, $CDCl_3$): δ = 1.23–1.27 (t, 3H, CH_3), 2.421–2.423 (d, 3H, 5-CH_3, J = 0.9 Hz), 2.65–2.69 (q, 2H, CH_2), 6.85 (s, 1H, 4-NH, exch), 7.21–7.23 (d, 2H, Ar, J = 8.3 Hz), 7.296–7.298 (d, 1H, C6-CH, J = 0.9 Hz), 7.51–7.53 (d, 2H, Ar, J = 8.3 Hz), 8.45 (s, 1H, C2-CH). Elemental analysis calculated (%) for $C_{15}H_{15}N_3O \cdot 0.1CH_3CO_2C_2H_5$: C, 70.57; H, 6.08; N, 16.03. Found: C, 70.79; H, 6.20; N, 15.75.

5-Methyl-*N*-(4-(methylthio)phenyl)furo[2,3-*d*]pyrimidin-4-amine (214).

Using the general procedure described above, reaction between **204** (150 mg, 1 mmol) and 4-iodo-thioanisole **211** (350 mg, 3.5 mmol) afforded 40 mg (15%) of **214** as a semisolid. TLC R_f = 0.83 ($CHCl_3$/MeOH, 10:1); ^{1}H NMR (400 MHz, $CDCl_3$): δ = 2.41 (s, 3H, SCH_3), 2.51 (s, 3H, 5-CH_3), 7.02 (s, 1H, 4-NH, exch), 7.28–7.34 (m, 3H, Ar and C6-CH), 7.57–7.59 (d, 2H, Ar), 8.47 (s, 1H, C2-CH).

***N*-(4-Nitrophenyl)-5-methylfuro[2,3-*d*]pyrimidin-4-amine (215).**

Using the general procedure described above, reaction between **204** (150 mg, 1 mmol) and 4-iodo-nitrobenzene **212** (250 mg, 3.5 mmol) provided 51 mg (19%) of **215** as a brown solid. TLC R_f = 0.79 ($CHCl_3$/MeOH, 10:1); ^{1}H NMR (400 MHz, $CDCl_3$): δ = 2.474–2.476 (d, 3H, CH_3), 7.835–7.838 (d, 1H, C6-CH), 7.98–8.00 (d, 2H, Ar), 8.25–8.27 (d, 2H, Ar), 8.54 (s, 1H, C2-CH), 9.16 (s, 1H, 4-NH, exch). HRMS (ESI): *m/z* calculated for $C_{13}H_{11}N_4O_3 + H^+$ [M+H$^+$]: 271.0831. Found: 271.0836.

***N*-Methyl-*N*-(4-ethylphenyl)-5-methylfuro[2,3-*d*]pyrimidin-4-amine (1c).**

In a 25 mL round bottom flask, compound **213** (40 mg, 0.16 mmol, 1 equivalent) and DMF (2 mL) were added to afford a solution. The flask was purged with argon for 5 min followed by cooling down to 0 ºC using ice bath. To the solution at 0 ºC was added sodium hydride (11.5 mg, 0.48 mmol) and stirred for 20 min. Dimethyl sulfate (0.04 mL, 0.48 mmol) was injected to the reaction mixture and the flask was warmed to room temperature. The mixture was stirred at room temperature for 16 h and the TLC showed complete utilization of the reactant **213**. Aqueous 1N HCl solution was added dropwise to

quench the reaction followed by water (20 mL) to afford a precipitate. The product was extracted with ethyl acetate (10 mL × 3). The combined organic extracts were washed with brine (10 mL), dried (anhydrous sodium sulfate) and concentrated under reduced pressure. Silica gel (200 mg) was added and the solvent was evaporated to obtain a plug which was purified by flash chromatography using hexanes and ethyl acetate (10:1) to obtain 23 mg (53%) of **1c** as a white solid. TLC R_f = 0.77 ($CHCl_3$/MeOH, 10:1); mp 116.3–116.8 °C. ^{1}H NMR (400 MHz, $CDCl_3$): δ = 1.09 (s, 3H, 5-CH_3), 1.24–1.28 (t, 3H, CH_3), 2.64–2.70 (q, 2H, CH_2), 3.57 (s, 3H, NCH_3), 7.10–7.12 (d, 3H, Ar), 7.19–7.21 (m, 2H, Ar and C6-CH), 8.56 (s, 1H, C2-CH). Elemental analysis calculated (%) for $C_{16}H_{17}N_3O \cdot 0.07CH_3CO_2C_2H_5$: C, 71.50; H, 6.47; N, 15.36. Found: C, 71.29; H, 6.28; N, 15.55.

General procedure for the synthesis of *N*-(4-substitutedphenyl)-5-methylfuro[2,3-*d*]pyrimidin-4-amines 214, 215, 218 and 219 using pipecolinic acid as the ligand.

A 50 mL round bottom flask was charged with compound **204** (1 equivalent), copper iodide (0.4–0.5 equivalents), anhydrous potassium carbonate (2–4 equivalents), pipecolinic acid (0.8–1.0 equivalents) and appropriate iodobenzene (2–3 equivalents). The flask was connected to vacuum for 3 min followed by addition of anhydrous DMF using syringe. The flask was purged with argon for 5 min and then heated in an oil bath maintained at 110 °C. On heating, the color of the suspension turned orange/pink suspension which lasted for about 2 h. The reaction was stirred for additional 22 h at 110 °C at the end of which the mixture was allowed to cool to room temperature. Ethyl acetate (25 mL) was added and the mixture was poured into water (100 mL). The product

was extracted with ethyl acetate (100 mL × 2). The combined organic extracts were washed with brine (100 mL) and dried (anhydrous sodium sulfate) and concentrated under reduced pressure. Silica gel (500 mg) was added and the solvent evaporated to obtain a plug. Purification was performed by flash chromatography using hexanes and ethyl acetate (10:1 to 2:1). Fractions containing the product (TLC) were pooled and evaporated to afford the product.

5-Methyl-*N*-(4-(methylthio)phenyl)furo[2,3-*d*]pyrimidin-4-amine (214).

Using the general procedure described above, reaction between **204** (149 mg, 1 mmol) and 4-iodo-thioanisole **211** (500 mg, 2 mmol) in the presence of copper iodide (76 mg, 0.4 mmol), pipecolinic acid (103 mg, 0.8 mmol), anhydrous potassium carbonate (277 mg, 2 mmol) and anhydrous DMF (15 mL) afforded 120 mg (43%) of **214** as a brownish red solid. TLC R_f = 0.83 ($CHCl_3$/MeOH, 10:1); mp 112.8–113.0 °C. ^{1}H NMR (400 MHz, DMSO-d_6): δ = 2.431–2.434 (d, 3H, 5-CH_3, J = 1.2 Hz), 2.49 (s, 3H, SCH_3), 7.28–7.30 (d, 2H, Ar, J = 8.6 Hz), 7.62–7.63 (d, 2H, Ar, J = 8.6 Hz), 7.705–7.708 (d, 1H, C6-CH, J = 1.2 Hz), 8.33 (s, 1H, C2-CH), 8.48 (s, 1H, 4-NH, exch). Elemental analysis calculated (%) for $C_{14}H_{13}N_3OS \cdot 0.07CH_3(CH_2)_4CH_3$: C, 62.44; H, 5.08; N, 15.15; S, 11.77. Found: C, 62.41; H, 5.13; N, 15.02; S, 11.74.

***N*-(4-Nitrophenyl)-5-methylfuro[2,3-*d*]pyrimidin-4-amine (215).**

Using the general procedure described above, reaction between **204** (149 mg, 1 mmol) and 4-iodo-nitrobenzene **212** (500 mg, 2 mmol) in the presence of copper iodide (76 mg, 0.4 mmol), pipecolinic acid (103 mg, 0.8 mmol), anhydrous potassium carbonate (277

mg, 2 mmol) and anhydrous DMF (15 mL) afforded 90 mg (33%) of **215** as yellow crystals. TLC R_f = 0.79 ($CHCl_3$/MeOH, 10:1); mp decomposes at 157.6–158.2 °C. ^{1}H NMR (400 MHz, DMSO-d_6): δ = 2.472–2.474 (d, 3H, 5-CH_3, J = 1.0 Hz), 7.832–7.835 (d, 1H, C6-CH, J = 1.2 Hz), 7.98–8.00 (d, 2H, Ar, J = 9.2 Hz), 8.25–8.27 (d, 2H, Ar, J = 9.2 Hz), 8.54 (s, 1H, C2-CH), 9.14 (s, 1H, 4-NH, exch). Elemental analysis calculated (%) for $C_{13}H_{10}N_4O_3 \cdot 0.09CH_3(CH_2)_4CH_3$: C, 58.50; H, 4.08; N, 20.15. Found: C, 58.18; H, 4.17; N, 19.82.

N^1-Methyl-N^4-(5-methylfuro[2,3-*d*]pyrimidin-4-yl)benzene-1,4-diamine (218).

Using the general procedure described above, reaction between **204** (298 mg, 2 mmol) and 4-iodo-*N*-methyl aniline **216** (700 mg, 6 mmol) in the presence of copper iodide (190 mg, 1 mmol), pipecolinic acid (258 mg, 2 mmol), anhydrous potassium carbonate (1100 mg, 8 mmol) and anhydrous DMF (30 mL) provided 136 mg (27%) of **218** as a light brown solid. TLC R_f = 0.73 ($CHCl_3$/MeOH, 10:1); mp 161.4–162.2 °C. ^{1}H NMR (400 MHz, DMSO-d_6): δ = 2.355–2.357 (d, 3H, 5-CH_3, J = 1.0 Hz), 2.68–2.69 (d, 3H, 4'-NCH_3, J = 5.0 Hz), 5.56–5.60 (q, 1H, 4'-NH, exch), 6.53–6.56 (d, 2H, Ar, J = 8.7 Hz), 7.23–7.26 (d, 2H, Ar, J = 8.7 Hz), 7.618–7.621 (d, 1H, C6-CH, J = 1.2 Hz), 8.19 (s, 1H, C2-CH), 8.26 (s, 1H, 4-NH, exch). Elemental analysis calculated (%) for $C_{14}H_{14}N_4O$: C, 66.13; H, 5.55; N, 22.03. Found: C, 66.14; H, 5.57; N, 21.90.

N^1,N^1-Dimethyl-N^4-(5-methylfuro[2,3-*d*]pyrimidin-4-yl)benzene-1,4-diamine (219).

Using the general procedure described above, reaction between **204** (298 mg, 2 mmol) and 4-iodo-*N*,*N*-dimethyl aniline **217** (741 mg, 6 mmol) in the presence of copper iodide

(190 mg, 1 mmol), pipecolinic acid (258 mg, 2 mmol), anhydrous potassium carbonate (1100 mg, 8 mmol) and anhydrous DMF (30 mL) provided 191 mg (36%) of **219** as a brown solid. TLC R_f = 0.77 ($CHCl_3$/MeOH, 10:1); mp decomposes at 196.8–197.2 °C. ^{1}H NMR (400 MHz, DMSO-d_6): δ = 2.379–2.382 (d, 3H, 5-CH_3, J = 1.1 Hz), 2.89 (s, 6H, 4'-$N(CH_3)_2$), 6.74–6.76 (d, 2H, Ar, J = 8.98 Hz), 7.36–7.38 (d, 2H, Ar, J = 8.93 Hz), 7.637–7.640 (d, 1H, C6-CH, J = 1.2 Hz), 8.21 (s, 1H, C2-CH), 8.30 (s, 1H, 4-NH, exch). Elemental analysis calculated (%) for $C_{15}H_{16}N_4O \cdot 0.1CH_3(CH_2)_4CH_3$: C, 67.66; H, 6.33; N, 20.23. Found: C, 67.48; H, 6.14; N, 19.92.

General procedure for the synthesis of substituted furo[2,3-*d*]pyrimidines 2c, 4c and 5c.

In a 25 mL round bottom flask, appropriate furo[2,3-*d*]pyrimidine (1 equivalent) and DMF (2 mL) were added to afford a solution. The flask was purged with argon for 5 min followed by cooling down to 0 °C using ice bath. To the solution at 0 °C was added sodium hydride (3 equivalents) and stirred for 20 min under argon atmosphere. Dimethyl sulfate (3 equivalents) was injected to the reaction mixture and the flask was warmed to room temperature. The mixture was stirred at room temperature for 4 h after which aqueous 1N HCl solution was added dropwise to quench the reaction followed by water (20 mL) to afford a precipitate. The product was extracted with ethyl acetate (10 mL × 3) and the combined organic extracts were washed with brine (10 mL), dried (anhydrous sodium sulfate) and concentrated under reduced pressure. Silica gel (200 mg) was added and the solvent was evaporated to obtain a plug. The plug was purified by flash

chromatography eluting with hexanes and ethyl acetate (5:1) to obtain **2c**, **4c** and **5c** in yields of 43-51%.

***N*,5-Dimethyl-*N*-(4-(methylthio)phenyl)furo[2,3-*d*]pyrimidin-4-amine (2c).**

Using the general procedure described above, reaction between **212** (105 mg, 0.4 mmol) and dimethylsulfate (0.08 mL, 1.2 mmol) in 8 mL DMF in the presence of sodium hydride (28.8 mg, 1.2 mmol) provided 56 mg (51%) of **2c** as a brown solid. TLC R_f = 0.88 ($CHCl_3$/MeOH, 10:1); mp 95.8–96.2 °C. ^{1}H NMR (400 MHz, DMSO-d_6): δ = 1.109–1.112 (d, 3H, 5-CH_3, J = 1.1 Hz), 2.48 (s, 3H, SCH_3), 3.47 (s, 3H, NCH_3), 7.20–7.22 (d, 2H, Ar, J = 8.65 Hz), 7.28–7.30 (d, 2H, Ar, J = 8.66 Hz), 7.567–7.570 (d, 1H, C6-CH, J = 1.2 Hz), 8.50 (s, 1H, C2-CH). Elemental analysis calculated (%) for $C_{15}H_{15}N_3OS$: C, 63.13; H, 5.30; N, 14.72; S, 11.24. Found: C, 63.17; H, 5.41; N, 14.76; S, 11.14.

***N*^{1},*N*^{1},*N*^{4}-Trimethyl-*N*^{4}-(5-methylfuro[2,3-*d*]pyrimidin-4-yl)benzene-1,4-diamine (4c).**

Using the general procedure described above, reaction between **219** (107.3 mg, 0.4 mmol) and dimethylsulfate (0.08 mL, 1.2 mmol) in 8 mL DMF in the presence of sodium hydride (28.8 mg, 1.2 mmol) provided 54 mg (45%) of **4c** as a white solid. TLC R_f = 0.85 ($CHCl_3$/MeOH, 10:1); mp 142.1–142.8 °C. ^{1}H NMR (400 MHz, DMSO-d_6): δ = 1.071–1.073 (d, 3H, 5-CH_3, J = 0.9 Hz), 2.90 (s, 6H, 4'-$N(CH_3)_2$), 3.41 (s, 3H, 4-NCH_3), 6.73–6.75 (d, 2H, Ar, J = 8.9 Hz), 7.07–7.09 (d, 2H, Ar, J = 8.9 Hz), 7.482–7.484 (d, 1H, C6-CH, J = 0.9 Hz), 8.41 (s, 1H, C2-CH). Elemental analysis calculated (%) for

$C_{16}H_{18}N_4O \cdot 0.22(C_2H_5)_2O$: C, 67.89; H, 6.82; N, 18.76. Found: C, 68.16; H, 6.60; N, 18.64.

_N_,5-Dimethyl-_N_-(4-nitrophenyl)furo[2,3-_d_]pyrimidin-4-amine (5c).

Using the general procedure described above, reaction between **215** (48.5 mg, 0.18 mmol) and dimethylsulfate (0.04 mL, 0.54 mmol) in 4 mL DMF in the presence of sodium hydride (13 mg, 0.54 mmol) provided 22 mg (43%) of **5c** as a yellow solid. TLC R_f = 0.83 ($CHCl_3$/MeOH, 10:1); mp 190.6–191.0 °C. ^{1}H NMR (400 MHz, DMSO-d_6): δ = 1.44 (s, 3H, 5-CH_3), 3.63 (s, 3H, NCH_3), 7.29–7.31 (d, 2H, Ar, J = 9.03 Hz), 7.82 (s, 1H, C6-CH), 8.16–8.18 (d, 2H, Ar, J = 9.07 Hz), 8.74 (s, 1H, C2-CH). ^{1}H NMR (400 MHz, $CDCl_3$): δ = 1.442–1.444 (d, 3H, 5-CH_3, J = 0.9 Hz), 3.67 (s, 3H, NCH_3), 7.08–7.11 (d, 2H, Ar, J = 9.1 Hz), 7.305–7.307 (d, 1H, C6-CH, J = 0.9 Hz), 8.14–8.16 (d, 2H, Ar, J = 9.1 Hz), 8.69 (s, 1H, C2-CH). Elemental analysis calculated (%) for $C_{14}H_{12}N_4O_3 \cdot 0.33CH_3CO_2C_2H_5$: C, 58.72; H, 4.71; N, 17.88. Found: C, 59.04; H, 4.72; N, 17.82.

_N_^{1},_N_^{4}-Dimethyl-_N_^{1}-(5-methylfuro[2,3-_d_]pyrimidin-4-yl)benzene-1,4-diamine (3c).

In a 25 mL round bottom flask, compound **218** (50.8 mg, 0.2 mmol, 1 equivalent) and DMF (3 mL) were added to afford a solution. The flask was purged with argon for 5 min followed by cooling down to 0 °C using ice bath. To the solution at 0 °C was added sodium hydride (5.3 mg, 0.22 mmol) and stirred for 20 min at 0 °C. Dimethyl sulfate (0.02 mL, 0.22 mmol) was injected to the reaction mixture and the mixture was stirred at -10–0 °C for 48 h after which TLC showed complete utilization of the reactant **218**.

Aqueous 1N HCl solution was added dropwise to quench the reaction followed by water (5 mL) to afford a precipitate. The product was extracted with ethyl acetate (10 mL × 3). The combined organic extracts were washed with brine (10 mL), dried (anhydrous sodium sulfate), added silica gel (200 mg) and concentrated under reduced pressure to obtain a plug. Purification was done by flash chromatography eluting with hexanes and ethyl acetate (10:1) to obtain 12.5 mg (20%) of **3c** as a brown solid and 18 mg (30%) of undesired product **4c**. TLC R_f = 0.82 ($CHCl_3$/MeOH, 10:1); mp 122.1–122.9 °C. ^{1}H NMR (400 MHz, DMSO-d_6): δ = 1.103–1.105 (d, 3H, 5-CH_3, J = 1.1 Hz), 2.67–2.68 (d, 3H, 4'-NCH_3, J = 5.0 Hz), 3.39 (s, 3H, 4-NCH_3), 5.80–5.84 (q, 1H, 4'-NH, exch), 6.54–6.56 (d, 2H, Ar, J = 8.7 Hz), 6.98–7.00 (d, 2H, Ar, J = 8.7 Hz), 7.474–7.477 (d, 1H, C6-CH, J = 1.2 Hz), 8.39 (s, 1H, C2-CH). Elemental analysis calculated (%) for $C_{15}H_{16}N_4O \cdot 0.6C_4H_8O$: C, 67.07; H, 6.73; N, 17.98. Found: C, 67.32; H, 6.58; N, 17.91.

Ethyl(2-chloro-2-nitrophenyl)(cyano)acetate (8).

To an ice cold solution of ethyl cyanoacetate (10.9 mL, 102.4 mmol) in anhydrous THF (170 mL) under nitrogen, was added potassium *tert*–butoxide (12.7 g, 107.5 mmol). The formed white suspension was stirred for 15 min, then treated with 1,2–dichloro-3-nitro-benzene **7** (9.83 g , 51.2 mmol). The suspension was heated to reflux for 48 hours. The resulting reddish brown solution was poured in to 50 mL water, and the aqueous mixture was then acidified to pH 2 with conc. HCl. The mixture was extracted with ether (150 mL × 3) and then the combined organic phase was dried using anhydrous Na_2SO_4 and then concentrated to give a dark yellow–colored semisolid. Column chromatography in a column packed with silica gel, four times the weight of the dark oil using 10:1

hexane:ethyl acetate as the eluent provided 13.2 g (96%) of **8** as a viscous yellow liquid. TLC R_f = 0.32 (hexane/EtOAc, 3:1). ^{1}H NMR (500 MHz, DMSO-d_6): δ = 1.18–1.21 (t, 3H, CH_3), 4.19–4.24 (q, 2H, CH_2), 6.37 (s, 1H, CH), 7.7–8.15 (m, 3H, Ar). ^{1}H NMR and mp agreed well with the literature reported[125] values.

Ethyl-2-amino-4-chloro-1*H*-indole-3-carboxylate (9).

To a solution of **8** (6 g, 22.34 mmol) in 230 mL glacial acetic acid was added 6 g of zinc dust. The mixture was heated to 55 °C for 1 h and then 2 g of Zn dust was added. Zinc dust (2 g) was added for every 10 hours. After stirring at 55 °C for another 45 hrs, the yellow mixture was filtered through a pad of Celite. The pad was washed with acetic acid and the filtrate was concentrated to a residue that was distributed between chloroform and water. The organic phase was washed with 5% $NaHCO_3$ solution to provide a pink precipitate which was filtered, dried over P_2O_5, dissolved in acetone, added silica gel (equal to the quantity of the precipitate) and converted to a silica gel plug by removing the solvent under reduced pressure. The plug was transferred on top of a column packed with silica gel, twenty times the weight of plug, eluted with 1% methanol in $CHCl_3$. Fractions containing the product (TLC) were pooled and evaporated to give 3.94 g (74%) of **9** as a pink solid. TLC R_f = 0.40 ($CHCl_3$/MeOH, 10:1); mp 141.4–142.0 °C (lit.[125] 140.0–142.0 °C). ^{1}H NMR (500 MHz, DMSO-d_6): δ = 1.26–1.29 (t, 3H, CH_3), 4.16–4.21 (q, 2H, CH_2), 6.87 (s, 2H, 2-NH_2, exch), 6.83–7.08 (m, 3H, Ar), 10.93 (s, 1H, 9-NH, exch). ^{1}H NMR agreed well with the literature reported[125] values.

2-Amino-5-chloro-3,9-dihydro-4*H*-pyrimido[4,5-*b*]indol-4-one (10).

Methyl sulfone (30 g), compound **9** (4 g, 16.7 mmol) and carbamimidic chloride hydrochloride[195] (2.12 g, 18.4 mmol) were taken in a round-botttomed flask and then 3 g of methyl sulfone was added on top of the mixture. Heating to 120 °C with stirring, the mixture was dissolved completely following which the reaction was continued for 40 minutes. About 100 mL water was added to quench the reaction. Neutralization of the reaction mixture with conc. NH_4OH solution resulted in a brown precipitate. The precipitate was filtered, dried under P_2O_5 to provide 2.52 g (64%) of **10** as a dark brown solid. This material was used for the next step without further purification. TLC R_f = 0.43 ($CHCl_3$/MeOH, 5:1); mp >250 ºC (lit.[125] >250 ºC). ^{1}H NMR (500 MHz, DMSO-d_6): δ = 6.57 (br, 2H, 2-NH_2 , exch), 7.04–7.17 (m, 3H, Ar), 10.41 (s, 1H, 9-NH, exch), 11.64 (s, 1H, 3-NH, exch). ^{1}H NMR agreed well with the literature reported[125] values.

***N*-(5-Chloro-4-oxo-4,9-dihydro-3*H*-pyrimido[4,5-*b*]indol-2-yl)-2,2-dimethyl propan-amide (220).**

Compound **10** (2 g, 8.5 mmol) and 150 mL of pivalic anhydride were taken in a 250 mL round bottomed flask. The reaction mixture was stirred at 120 °C for 2.5 h. Then, hexane was added under room temperature which resulted in precipitation of pale brown colored solid. The solid was filtered, washed with hexane and used without further purification for the next step. The filtrate was then concentrated and a plug was made, using silica gel three times the product. The plug was transferred on top of a column packed with silica gel, twenty times the weight of plug and eluted with 1% methanol in chloroform. Fractions containing the product (TLC) were pooled and evaporated to afford 1.6 g (60%)

of **220** as a brown solid. TLC R_f = 0.80 ($CHCl_3$/MeOH, 5:1); mp 189.2–189.8 °C (lit.[125] 185.8–190.1 °C). ^{1}H NMR (500 MHz, DMSO-d_6): δ = 1.26 (s, 9H, $C(CH_3)_3$), 7.19–7.37 (m, 3H, Ar), 11.16 (s, 1H, 2-NH, exch), 11.93 (s, 1H, 3-NH, exch), 12.11 (s, 1H, 9-NH, exch). ^{1}H NMR agreed well with the literature reported[125] values.

***N*-(4,5-Dichloro-9*H*-pyrimido[4,5-*b*]indol-2-yl)-2,2-dimethyl propanamide (221).**

Compound **220** (1 g, 3.137 mmol) was treated with 200 mL of $POCl_3$ in a 500 mL round bottom flask. The reaction mixture was heated to reflux for 4 hours. The $POCl_3$ was evaporated and the mixture was neutralized using conc. NH_4OH solution (28-30 wt% in water). The aqueous mixture was filtered (the precipitate being the compound) and the precipitate was dried. To the solution was added silica and solvent was removed under reduced pressure to provide a silica gel plug. The plug was transferred on top of a column packed with silica gel, twenty times the weight of plug, eluted with chloroform and 1% methanol in chloroform. Fractions containing the product (TLC) were pooled and evaporated to provide 710 mg (67%) of **221** as a brown solid. TLC R_f = 0.86 ($CHCl_3$/MeOH, 5:1); mp 245.9–246.5 °C (lit.[125] 245.6–246.1 °C). ^{1}H NMR (500 MHz, DMSO-d_6): δ = 1.24 (s, 9H, $C(CH_3)_3$), 7.36–7.50 (m, 3H, Ar), 10.30 (s, 1H, 9-NH, exch), 12.96 (s, 1H, 2-NH, exch). ^{1}H NMR agreed well with the literature reported[125] values.

General procedure for the synthesis of 5-chloro-N^4-methyl-9*H*-pyrimido[4,5-*b*]indole-2,4-diamines 1d–6d.

To a solution of **221** (1 equivalent) in 40 mL of *i*-propanol was added *N*-methyl anilines **222**–**226** or 6-methoxy-1,2,3,4-tetrahydroquinoline **227** and 2 drops of conc. HCl. The

reaction mixture was heated to reflux for 70 h, cooled to room temperature and then neutralized with 4 mL of 1N sodium hydroxide solution. The reaction was then heated to reflux for 2 h. The solvent was then evaporated to obtain a dark brown colored solid. The resulting precipitate was then dissolved in chloroform and methanol. To the solution was added silica gel, four times the weight of the reaction mixture, and the solvent was removed under reduced pressure to provide a plug. The plug was transferred on top of a column packed with silica gel, twenty times the weight of plug and was eluted with 1% methanol in chloroform. Fractions containing the product (TLC) were pooled and evaporated to give a solid which was further purified by washing with hexane.

5-Chloro-N^4-methyl-N^4-phenyl-9*H*-pyrimido[4,5-*b*]indole-2,4-diamine (1d).

Using the general procedure described above, compound **221** (100 mg, 0.30 mmol) was treated with *N*-methyl aniline **222** (95 mg, 0.90 mmol) to afford 64 mg (67%) of **1d** as a brown solid. TLC R_f = 0.42 ($CHCl_3$/MeOH, 15:1); mp 228.1–229.1 °C. ^{1}H NMR (400 MHz, DMSO-d_6): δ = 3.34 (s, 3H, NCH_3), 6.61 (s, 2H, NH_2, exch), 6.76–6.80 (m, 3H, Ar), 7.02–7.04 (m, 1H, Ar), 7.12–7.21 (m, 3H, Ar), 7.27–7.29 (m, 1H, Ar), 11.81 (s, 1H, 9-NH, exch). Elemental analysis calculated (%) for $C_{17}H_{14}ClN_5$: C, 63.06; H, 4.36; N, 21.63; Cl, 10.95. Found: C, 63.06; H, 4.25; N, 21.62; Cl, 10.86.

5-Chloro-N^4-methyl-N^4-*p*-tolyl-9*H*-pyrimido[4,5-*b*]indole-2,4-diamine (2d).

Using the general procedure described above, compound **221** (100 mg, 0.30 mmol) was treated with *N*-methyl-*p*-toluidine **223** (108 mg, 0.90 mmol) to provide 60 mg (60%) of **2d** as a brown solid. TLC R_f = 0.38 ($CHCl_3$/MeOH, 15:1); mp 231.9–232.8 °C. ^{1}H NMR

(400 MHz, DMSO-d_6): δ = 2.19 (s, 3H, CH_3), 3.32 (s, 3H, NCH_3), 6.53 (s, 2H, NH_2, exch), 6.70–6.72 (m, 2H, Ar), 6.94–6.96 (m, 2H, Ar), 7.00–7.02 (m, 1H, Ar), 7.16–7.19 (m, 1H, Ar), 7.25–7.27 (m, 1H, Ar), 11.74 (s, 1H, 9-NH, exch). Elemental analysis calculated (%) for $C_{18}H_{16}ClN_5$: C, 63.99; H, 4.77; N, 20.73; Cl, 10.49. Found: C, 63.85; H, 4.83; N, 20.44; Cl, 10.56.

5-Chloro-*N*^{4}-(4-chlorophenyl)-*N*^{4}-methyl-9*H*-pyrimido[4,5-*b*]indole-2,4-diamine (3d).

Using the general procedure described above, compound **221** (100 mg, 0.30 mmol) was treated with 4-chloro-*N*-methyl aniline **224** (126 mg, 0.90 mmol) to afford 68 mg (64%) of **3d** as a brown solid. TLC R_f = 0.39 ($CHCl_3$/MeOH, 15:1); mp 226.4–227.2 ^oC. ^1H NMR (400 MHz, DMSO-d_6): δ = 3.35 (s, 3H, NCH_3), 6.66 (s, 2H, NH_2, exch), 6.75–6.77 (m, 2H, Ar), 7.04–7.06 (m, 1H, Ar), 7.16–7.19 (m, 3H, Ar), 7.28–7.30 (m, 1H, Ar), 11.86 (s, 1H, 9-NH, exch). Elemental analysis calculated (%) for $C_{17}H_{13}Cl_2N_5 \cdot 1.0CH_3OH$: C, 55.40; H, 4.39; N, 17.94; Cl, 18.17. Found: C, 55.34; H, 4.33; N, 18.04; Cl, 18.06.

5-Chloro-*N*^{4}-3-methoxyphenyl-*N*^{4}-methyl-9*H*-pyrimido[4,5-*b*]indole-2,4-diamine (4d).

Using the general procedure described above, compound **221** (100 mg, 0.30 mmol) was treated with 3-methoxy-*N*-methyl aniline **225** (122 mg, 0.90 mmol) to give 65 mg (62%) of **4d** as a brown solid. TLC R_f = 0.39 ($CHCl_3$/MeOH, 15:1); mp 226.8–227.2 ^oC. ^1H NMR (400 MHz, DMSO-d_6): δ = 3.34 (s, 3H, OCH_3), 3.59 (s, 3H, NCH_3), 6.28–6.38 (m, 3H, Ar), 6.63 (s, 2H, NH_2, exch), 7.00–7.05 (m, 2H, Ar), 7.18–7.22 (m. 1H, Ar);

7.28–7.30 (m. 1H, Ar); 11.82 (s, 1H, 9-NH, exch). Elemental analysis calculated (%) for $C_{18}H_{16}ClN_5O \cdot 0.23CH_3COCH_3$: C, 61.14; H, 4.77; N, 19.07; Cl, 9.66. Found: C, 60.88; H, 4.57; N, 19.14; Cl, 9.38.

5-Chloro-*N*^{4}-3-fluorophenyl-*N*^{4}-methyl-9*H*-pyrimido[4,5-*b*]indole-2,4-diamine (5d). Using the general procedure described above, compound **221** (100 mg, 0.30 mmol) was treated with 3-fluoro-*N*-methyl aniline **226** (122 mg, 0.90 mmol) to yield 59 mg (58%) of **5d** as a brown solid. TLC R_f = 0.39 ($CHCl_3$/MeOH, 15:1); mp 217.1–217.9 °C. ^{1}H NMR (400 MHz, DMSO-d_6): δ = 3.31 (s, 3H, NCH_3), 6.49–6.56 (m, 3H, Ar), 6.71 (s, 2H, NH_2, exch), 7.05–7.07 (d, 1 H, Ar), 7.09–7.11 (m, 1H, Ar), 7.20–7.24 (t, 1H, Ar), 7.29–7.31 (d, 1H, Ar), 11.89 (s, 1H, 9-NH, exch). HRMS (ESI): *m/z* calculated for $C_{17}H_{14}N_5ClF + H^+$ [M+H$^+$]: 342.0916. Found: 342.0911. HPLC analysis: retention time = 39.47 min; peak area, 96.40%; eluent A, H_2O; eluent B, ACN; gradient elution (100% H_2O to 10% H_2O) over 60 min with a flow rate of 0.5 mL/min and detection at 254 nm; column temperature, rt.

5-Chloro-4-(6-methoxy-3,4-dihydroquinolin-1(2*H*)-yl)-9*H*-pyrimido[4,5-*b*]indol-2-amine (6d). Using the general procedure described above, compound **221** (100 mg, 0.30 mmol) was treated with 6-methoxy-1,2,3,4-tetrahydroquinoline **227** (145 mg, 0.90 mmol) to provide 59 mg (52%) of **6d** as a brown solid. TLC R_f = 0.30 ($CHCl_3$/MeOH, 15:1); mp 187.1–187.9 °C. ^{1}H NMR (400 MHz, DMSO-d_6): δ = 1.78–1.79 (m, 1H, CH), 1.98–1.99 (m, 1H, CH), 2.78–2.81 (m, 2H, CH_2), 3.57 (m, 1H, CH), 3.66 (s, 3H, OCH_3), 3.85–3.86 (m,

1H, CH), 6.42 (s, 2H, 2-NH_2, exch), 6.46–6.49 (m, 1H, Ar), 6.52–6.54 (m, 1H, Ar), 6.65–6.66 (d, 1H, Ar), 7.02–7.03 (m, 1H, Ar), 7.15–7.18 (t, 1H, Ar), 7.25–7.26 (m, 1H, Ar), 11.70 (s, 1H, 9-NH, exch). Elemental analysis calculated (%) for $C_{20}H_{18}ClN_5O$: C, 63.24; H, 4.78; N, 18.44; Cl, 9.33. Found: C, 63.24; H, 4.97; N, 18.15; Cl, 9.31.

2-Amino-6-hydrazinopyrimidin-4(3*H*)-one (229).

To a stirred suspension of **228** (15 g, 103 mmol) in 250 mL water was added anhydrous hydrazine (12 g, 375 mmol), and the mixture was heated to reflux for 3 h. The resulting clear solution was cooled, and the precipitate that separated was collected by filtration, washed with water followed by ethanol and dried to give 6.6 g (46%) of **229** as a white solid. mp decomposes at 313.0 °C (lit.[207] 314.0–315.0 °C). This material was used without further purification for the next step.

2-Amino-3,5,6,7,8,9-hexahydro-4*H*-pyrimido[4,5-*b*]indol-4-one (231).

A mixture of 2-amino-6-hydrazinopyrimidin-4(3*H*)-one **229** (3.5 g, 25 mmol) and cyclohexanone **230** (2.45 g, 25 mmol) in diphenyl ether (300 mL) was stirred at 120 °C for 14 h and then heated to reflux (250 °C) for 3 h. After cooling to room temperature, hexane (600 mL) was added, and the precipitated solid was collected by filtration. The solid was dried over P_2O_5, dissolved in methanol, and silica gel (three times the weight of solid) was added, following which the solvent was removed under reduced pressure to obtain a dry plug. The plug was loaded on top of a column packed with silica in chloroform. The weight of silica in the column was thirty times the weight of the plug. Flash chromatography using 20% methanol in chloroform afforded 4.1 g (81%) of **231**[178]

as an yellow solid. TLC R_f = 0.35 ($CHCl_3$/MeOH, 5:1); mp >300 °C. ^{1}H NMR (500 MHz, DMSO-d_6): δ = 1.64–1.69 (m, 4H, 6-CH_2 and 7-CH_2), 2.42 (m, 2H, 5-CH_2), 2.53 (m, 2H, 8-CH_2), 5.88 (s, 2H, 2-NH_2, exch), 10.02 (s, 1H, 3-NH, exch), 10.50 (s, 1H, 9-NH, exch). This material was used without further purification for the next step.

2-Amino-3,9-dihydro-4*H*-pyrimido[4,5-*b*]indol-4-one (232).

A mixture of **231** (1 g, 5 mmol) and 10% palladium on carbon (480 mg, 0.5 mmol) in diphenyl ether (50 mL) was heated to reflux for 3 h. The reaction mixture was cooled to room temperature, and DMF (50 mL) was added to dissolve the product. The catalyst was removed by filtration through Celite, washed with DMF and silica gel (3 g) was added. Solvent was removed under reduced pressure to afford a plug, which was loaded on top of a silica gel column in chloroform (the silica was thirty times the weight of the plug). The column was eluted with 20% methanol in chloroform to afford 560 mg (59%) of **232**[178] as an off-white solid. TLC R_f = 0.32 ($CHCl_3$/MeOH, 5:1); mp >300 °C. ^{1}H NMR (500 MHz, DMSO-d_6): δ = 6.51 (s, 2H, 2-NH_2), 7.03–7.10 (m, 2H, Ar), 7.22–7.25 (m, 1H, Ar), 7.68–7.70 (m, 1H, Ar), 10.47 (s, 1H, 3-NH, exch), 11.35 (s, 1H, 9-NH, exch). This material was used without further purification for the next step.

2,2-Dimethyl-*N*-(4-oxo-4,9-dihydro-3*H*-pyrimido[4,5-*b*]indol-2-yl)propanamide (233).

Compound **232** (0.5 g, 2.5 mmol) and 20 mL of pivalic anhydride were taken in a 100 mL round-bottomed flask. The reaction mixture was stirred at 120 °C for 8 hours. Then, hexane (60 mL) was added to the reaction mixture at room temperature leading to the

formation of a brown colored precipitate. The precipitate was filtered, washed with hexane and dried to give 0.52 g (73%) of **233**[178] as a brown solid. TLC R_f = 0.6 ($CHCl_3$/MeOH, 10:1); mp >300 °C. ^{1}H NMR (500 MHz, DMSO-d_6): δ = 1.26 (s, 9H, $C(CH_3)_3$), 7.17–7.21 (m, 1H, Ar), 7.24–7.28 (m, 1H, Ar), 7.43–7.45 (m, 1H, Ar), 7.86–7.88 (m, 1H, Ar), 11.12 (s, 1H, NH, exch), 11.85 (s, 1H, NH, exch), 12.03 (s, 1H, NH, exch). This material was used without further purification for the next step.

***N*-(4-Chloro-9*H*-pyrimido[4,5-*b*]indol-2-yl)-2,2-dimethylpropanamide (234).**

To a 50 mL round-bottomed flask was added **233** (56 mg, 0.17 mmol) and phosphorus oxychloride (15 mL). The mixture was stirred and heated to reflux for 4 h. The phosphoryl trichloride was removed by evaporation under reduced pressure using a vacuum aspirator. The resulting residue was cooled in an ice and water mixture and neutralized with ammonium hydroxide solution to yield a precipitate that was filtered and dried over P_2O_5. The filtrate was extracted with chloroform and dried over sodium sulfate. The dry precipitate and filtrate were combined and dried under vacuum to provide 35 mg (59%) of **234**[178] as a brown solid. TLC R_f = 0.65 ($CHCl_3$/MeOH, 10:1); mp 234.1–234.6 °C. ^{1}H NMR (400 MHz, DMSO-d_6): δ = 1.24 (s, 9H, $C(CH_3)_3$), 7.34–7.38 (m, 1H, Ar), 7.53–7.55 (m, 2H, Ar), 8.15–8.17 (m, 1H, Ar), 10.25 (s, 1H, 2-NH, exch), 12.55 (s, 1H, 9-NH, exch). This material was used without further purification for the next step.

General procedure for the synthesis of N^4-substituted-9*H*-pyrimido[4,5-*b*]indole-2,4-diamines 1e and 2e:

To a 100 mL round-bottomed flask were added **234** (1 equivalent), appropriate aryl amine (3 equivalents), *n*-butanol and catalytic amount of conc. HCl. The resulting mixture was heated to reflux until the TLC showed completion of the reactant **234**. The solvent was removed under reduced pressure to obtain a mixture that was dissolved in methanol, basified with ammonia in methanol, and silica gel was added. The solvent was removed by evaporation to yield a dry plug which was purified by flash chromatography using 1% methanol in chloroform. Fractions containing the desired product (TLC) were pooled and evaporated to obtain compounds **1e** and **2e**.

N^4-Ethyl-N^4-(4-methoxyphenyl)-9*H*-pyrimido[4,5-*b*]indole-2,4-diamine (1e).

Using the general procedure described above, compound **234** (80 mg, 0.26 mmol), *N*-ethyl-4-methoxyaniline **235** (120 mg, 0.78 mmol) and 1 drop of conc. HCl were heated to reflux in 50 mL of *n*-butanol for 72 h to afford 30 mg (31%) of **1e**[178] as a white solid. TLC R_f = 0.50 ($CHCl_3$/MeOH, 15:1); mp 223.9–224.6 °C. ^{1}H NMR (400 MHz, DMSO-d_6): δ = 1.15–1.19 (t, 3H, J = 6.9 Hz, CH_3), 3.74 (s, 3H, OCH_3), 4.09–4.13 (q, 2H, J = 6.9 Hz, N-CH_2), 5.66–5.68 (d, 1H, Ar), 6.15 (s, 2H, 2-NH_2, exch), 6.50–6.54 (t, 1H, Ar), 6.90–6.97 (m, 3H, Ar), 7.12–7.16 (m, 3H, Ar), 11.20 (s, 1H, 9-NH, exch). Elemental analysis calculated (%) for $C_{19}H_{19}N_5O{\cdot}0.90CH_3OH$: C, 65.98; H, 6.29; N, 19.33. Found: C, 65.81; H, 6.15; N, 19.31.

4-(6-Methoxy-3,4-dihydroquinolin-1(2*H*)-yl)-9*H*-pyrimido[4,5-*b*]indol-2-amine (2e). Using the general procedure described above, compound **234** (80 mg, 0.26 mmol), 6-methoxy-1,2,3,4-tetrahydroquinoline **227** (120 mg, 0.78 mmol) and 1 drop of conc. HCl were heated to reflux in 30 mL of *n*-butanol for 60 h to provide 24.5 mg (26%) of **2e** as an yellow solid. TLC R_f = 0.48 ($CHCl_3$/MeOH, 15:1); mp 172.8–174.0 °C. ^{1}H NMR (400 MHz, DMSO-d_6): δ = 1.95–2.01 (m, 2H, *J* = 6.2 and 6.6 Hz, CH_2), 2.84–2.87 (t, 2H, *J* = 6.6 Hz, CH_2), 3.69 (s, 3H, OCH_3), 3.87–3.90 (t, 2H, *J* = 6.2 Hz, N-CH_2), 6.19–6.21 (d, 1H, Ar), 6.26 (s, 2H, 2-NH_2, exch), 6.46–6.48 (m, 1H, Ar), 6.57–6.58 (m, 1H, Ar), 6.71–6.74 (t, 1H, Ar), 6.868–6.874 (m, 1H, Ar), 7.04–7.07 (t, 1H, Ar), 7.21–7.23 (m, 1H, Ar), 11.31 (s, 1H, 9-NH, exch). Elemental analysis calculated (%) for $C_{20}H_{19}N_5O \cdot 0.40CH_3OH$: C, 68.39; H, 5.79; N, 19.55. Found: C, 68.20; H, 5.55; N, 19.53.

N^4-(4-Ethoxyphenyl)-N^4-methyl-9*H*-pyrimido[4,5-*b*]indole-2,4-diamine (3e).

In a 100 mL round-bottomed flask, compound **234** (80 mg, 0.26 mmol), 4-ethoxy-*N*-methylaniline **236** (120 mg, 0.78 mmol) and 1 drop of conc. HCl in 30 mL isopropanol were heated to reflux for 120 h. After cooling to rt, silica gel (500 mg) was added, and isopropanol was removed under reduced pressure. The dry residue was dissolved in methanol, basified with ammonia in methanol, and silica gel was added. The solvent was removed by evaporation to yield a silica gel plug. The plug was loaded on top of a silica gel column in chloroform (the weight of the silica was 15 times that of the plug). Purification was performed by flash chromatography using 0.5% methanol in chloroform and the fractions containing the product (TLC) were pooled and the solvent was evaporated to afford to provide 63 mg (72%) of **3e**[178] as a white solid. TLC R_f = 0.43

($CHCl_3$/MeOH, 15:1); mp 238.8−239.6 °C. ^{1}H NMR (400 MHz, DMSO-d_6): δ = 1.29–1.32 (t, 3H, J = 6.9 Hz, CH_3), 3.50 (s, 3H, N-CH_3), 3.97–4.02 (q, 2H, J = 6.9 Hz, CH_2), 5.76–5.78 (d, 1H, Ar), 6.22 (s, 2H, 2-NH_2, exch), 6.53–6.57 (t, 1H, Ar), 6.88–6.90 (m, 2H, Ar), 6.95–6.98 (t, 1H, Ar), 7.13–7.15 (m, 3H, Ar), 11.24 (s, 1H, 9-NH, exch). Elemental analysis calculated (%) for $C_{19}H_{19}N_5O$: C, 68.45; H, 5.74; N, 21.01. Found: C, 68.40; H, 5.61; N, 21.01.

N^4-Methyl-N^4-(4-(methylthio)phenyl)-9*H*-pyrimido[4,5-*b*]indole-2,4-diamine (1f).

In a round bottom flask, compound **234** (110 mg, 0.36 mmol), *N*-methyl-4-(methylthio)aniline **237** (223 mg, 1.45 mmol) and 2 drops of conc. HCl in 50 mL of *n*-butanol were heated to reflux for 48 h. After cooling to rt, silica gel (500 mg) was added, and isopropanol was removed under reduced pressure. The dry residue was dissolved in methanol, basified with ammonia in methanol, and silica gel was added. The solvent was removed by evaporation to yield a silica gel plug. Purification was performed by flash chromatography using 0.5% methanol in chloroform and the fractions containing the product (TLC) were pooled and the solvent was evaporated to afford to provide 86 mg (72%) of **1f** as an off-white solid. TLC R_f = 0.44 ($CHCl_3$/MeOH, 15:1); mp 248.2–248.8 °C. ^{1}H NMR (400 MHz, DMSO-d_6): δ = 2.44 (s, 3H, SCH_3), 3.54 (s, 3H, NCH_3), 5.90–5.92 (d, 1H, Ar), 6.23 (s, 2H, 2-NH_2, exch), 6.57–6.59 (t, 1H, Ar), 6.99–7.03 (m, 1H, Ar), 7.12–7.14 (m, 2H, Ar), 7.17–7.19 (m, 1H, Ar), 7.22–7.24 (m, 2H, Ar), 11.31 (s, 1H, 9-NH, exch). Elemental analysis calculated (%) for $C_{18}H_{17}N_5S$: C, 64.45; H, 5.11; N, 20.88; S, 9.56. Found: C, 64.22; H, 5.18; N, 20.88; S, 9.38.

Ethyl 2-(2-nitrophenyl)-2-cyanoacetate (239).

To an ice cold solution of ethyl cyanoacetate (14.36 g, 126.94 mmol) in anhydrous THF (170 mL) under argon atmosphere, was added potassium *tert*-butoxide (14.24 g, 126.94 mmol). Thus formed white suspension was stirred for 15 min and then 1-chloro-2-nitro-benzene **238** (10.00 g, 63.47 mmol) was added. The suspension was heated to reflux for 48 h after which 200 mL water was added and acidified to pH 2 with conc. HCl. The mixture was extracted with ether (250 mL × 3) and then the combined organic phase was dried (anhydrous sodium sulfate) and concentrated to give a dark yellow colored liquid. Flash chromatography using 10:1 hexane:ethyl acetate in a column packed with silica gel, four times the weight of the dark oil, provided 12.75 g (86%) of **239** as a viscous yellow liquid. TLC R_f = 0.32 (hexane/EtOAc, 3:1). ^{1}H NMR (400 MHz, DMSO-d_6): δ = 1.23–1.26 (t, 3H, CH_3), 4.16–4.24 (q, 2H, CH_2), 5.58 (s, 1H, CH), 7.58–7.62 (m, 1H, Ar), 7.68–7.72 (m, 2H, Ar), 8.15–8.17 (d, 1H, Ar). ^{1}H NMR agreed well with the literature reported[129] values.

Ethyl 2-amino-1*H*-indole-3-carboxylate (18).

Compound **239** (12.75 g, 54.44 mmol) in 230 mL glacial acetic acid, was treated with a single charge of 8.5 g of zinc dust. The mixture was heated at 55 °C for 2 h and 4 g of Zn dust was added. After stirring at 55 °C for another 4 h, the reaction mixture was cooled and filtered through a pad of Celite. The pad was washed with acetic acid and the filtrate was concentrated to a residue that was neutralized with saturated Na_2CO_3 solution. The precipitate was filtered, dried over P_2O_5 and was dissolved in acetone. To this solution was added 15 g silica gel and the solvent was removed under reduced pressure to afford a

silica gel plug. Purification was done by flash chromatography eluting with 1% methanol in $CHCl_3$. Fractions containing the product (TLC) were pooled and evaporated to give 6.67 g (60%) of **18** as an off-white solid. TLC R_f = 0.65 ($CHCl_3$/MeOH, 10:1); mp 178.9–180.1 °C (lit.[208] 179.0–181.0 °C). ^{1}H NMR (400 MHz, DMSO-d_6): δ = 1.31–1.34 (t, 3H, CH_3), 4.20–4.25 (q, 2H, CH_2), 6.67 (s, 2H, 2-NH_2, exch), 6.86–6.88 (t, 1H, Ar), 6.89–6.97 (t, 1H, Ar), 7.10–7.12 (d, 1H, Ar), 7.54–7.56 (d, 1H, Ar), 10.64 (s, 1H, 1-NH, exch). Elemental analysis calculated (%) for $C_{11}H_{12}N_2O_2$: C, 64.69; H, 5.92; N, 13.72. Found: C, 64.64; H, 6.08; N, 13.66. ^{1}H NMR agreed well with the literature reported[208] values.

2-[(1-Iminoethyl)amino]-1*H*-indole-3-carboxylic acid ethyl ester, hydrochloride (21). Dry HCl gas was bubbled into a suspension of **18** (1.0 g, 4.9 mmol) and CH_3CN (65 mL) for 1.5 h. The mixture was then heated to reflux for 2.5 h and then cooled to 25 °C. The precipitate was collected and dried to give 1.2 g of **21** as a white hygroscopic solid. mp >300 °C (lit.[130] >300 °C). ^{1}H NMR (400 MHz, DMSO-d_6): δ = 1.32-1.36 (t, 3H, CH_3, J = 7.1 Hz), 2.43 (br, 3H, CH_3), 4.26–4.32 (q, 2H, CH_2, J = 7.1 Hz), 7.24–7.32 (m, 2H, Ar), 7.49–7.51 (d, 1H, Ar, J = 7.56 Hz), 8.04–8.06 (d, 1H, Ar, J = 7.51 Hz), 9.0 (br, 1H, 2-NH), 10.05 (br, 1H, 1-NH, exch), 12.06 (br, 1H, 1'-NH, exch), 12.75 (br, 1H, HCl, exch). ^{1}H NMR agreed well with the literature reported[130] values. This material was used directly for the next step without further purification.

2-Methyl-3*H*-pyrimido[4,5-*b*]indol-4(9*H*)-one (23).

A solution of **21** (1.2 g, 4.3 mmol), EtOH (350 mL), and 10% aq NaOH (35 mL) was

heated to reflux for 6 h. The cooled solution was concentrated to a residue that was diluted with 25 mL of H_2O. The solution was adjusted to pH 2 with 3N HCl solution and then stored at 25 °C for 30 min. The precipitated solid was collected, dissolved in methanol and then was added 2.5 g of silica gel. The solvent was removed under reduced pressure to provide a silica gel plug, which was purified by flash chromatography eluting with 2% and 3% methanol in chloroform. Fractions containing the product (TLC) were pooled and evaporated to give 0.96 g (77% over two steps) of **23** as a white solid. TLC R_f = 0.51 ($CHCl_3$/MeOH, 10:1); mp >275 °C (lit.[130] >275 °C). ^{1}H NMR (400 MHz, DMSO-d_6): δ = 2.41 (s, 3H, 2-CH_3), 7.18–7.22 (t, 1H, Ar), 7.27–7.31 (t, 1H, Ar), 7.43–7.45 (d, 1H, Ar), 7.93–7.94 (d, 1H, Ar), 11.98 (s, 1H, 3-NH, exch), 12.12 (s, 1H, 9-NH, exch). Elemental analysis calculated (%) for $C_{11}H_9N_3O \cdot 0.39CH_3OH$: C, 64.62; H, 5.03; N, 19.85. Found: C, 64.73; H, 4.88; N, 19.64. ^{1}H NMR agreed well with the literature reported[130] values.

4-Chloro-2-methyl-9*H*-pyrimido[4,5-*b*]indole (240).

In a 250 mL round-bottomed flask was added **23** (1.04 g, 4.9 mmol) and 150 mL of $POCl_3$. The reaction mixture was heated at 120 °C for 5.5 h. The $POCl_3$ was evaporated and the mixture was neutralized using aqueous NH_4OH solution leading to a precipitate. The precipitate was filtered, washed with cold water, dried and was dissolved in methanol. To the solution was added silica and solvent was removed under reduced pressure to provide a silica gel plug. The plug was purified by flash chromatography using chloroform and 1% methanol in chloroform as the eluent. Fractions containing the product (TLC) were pooled and evaporated to give 650 mg (79%) of **240** as an off-white

solid. TLC R_f = 0.69 ($CHCl_3$/MeOH, 10:1); mp 286.0−286.4 °C. ^{1}H NMR (400 MHz, DMSO-d_6): δ = 2.69 (s, 3H, 2-CH_3), 7.38–7.42 (m, 1H, Ar), 7.57–7.62 (m, 2H, Ar), 8.22–8.23 (d, 1H, Ar), 12.56 (s, 1H, 9-NH, exch). Elemental analysis calculated (%) for $C_{11}H_8ClN_3$: C, 60.70; H, 3.70; N, 19.31; Cl, 16.29. Found: C, 60.68; H, 3.81; N, 19.11; Cl, 16.35.

_N_-(4-Methoxyphenyl)-_N_,2-dimethyl-9_H_-pyrimido[4,5-_b_]indol-4-amine (2f).

To a round-bottomed flask were added **240** (120 mg, 0.55 mmol), 4-methoxy-*N*-methylaniline **241** (302.5 mg, 2.2 mmol), 2 drops of conc. HCl and 25 mL of *n*-butanol. The reaction mixture was heated to reflux for 72 h. After cooling to rt, silica gel (500 mg) was added, and *n*-butanol was removed under reduced pressure to afford a silica gel plug. Flash chromatography was done using 0.5% and 1% methanol in chloroform. Fractions containing the product (TLC) were pooled and the solvent was evaporated to afford 137 mg (78%) of **2f** as an off-white solid. TLC R_f = 0.82 ($CHCl_3$/MeOH, 5:1); mp 239.1−239.9 °C. ^{1}H NMR (400 MHz, DMSO-d_6): δ = 2.59 (s, 3H, 2-CH_3), 3.59 (s, 3H, OCH_3), 3.75 (s, 3H, NCH_3), 5.89–5.90 (d, 1H, C5-CH), 6.66–6.69 (t, 1H, Ar), 6.92–6.94 (d, 2H, Ar), 7.14–7.17 (m, 1H, Ar), 7.19–7.21 (d, 2H, Ar), 7.31–7.33 (d, 1H, Ar), 11.85 (s, 1H, 9-NH, exch). Elemental analysis calculated (%) for $C_{19}H_{18}N_4O$: C, 71.68; H, 5.70; N, 17.60. Found: C, 71.91; H, 5.70; N, 17.69.

3_H_-Pyrimido[4,5-_b_]indol-4(9_H_)-one (242).

Compound **18** (400 mg, 1.96 mmol) and formamide (6 ml, 150 mmol) were taken in a 25 mL round bottom flask. The reaction mixture was stirred at 190 °C for 12 h. The reaction

mixture was cooled down, filtered, washed well with water and dried under reduced pressure. The dried precipitate was dissolved in 3 mL DMF and then precipitated using 30 mL Et_2O. The precipitate was collected, washed with Et_2O and dried over P_2O_5 to give 292 mg (73%) of **242** as a brown solid. TLC R_f = 0.48 ($CHCl_3$/MeOH, 5:1); mp >300 °C (lit.[129] >300 °C). ^{1}H NMR (400 MHz, DMSO-d_6): δ = 2.74 (s, 0.3H, "DMF" N-CH_3), 2.89 (s, 0.3H, "DMF" NCH_3), 7.22–7.25 (m, 1H, Ar), 7.31–7.35 (m, 1H, Ar), 7.47–7.49 (d, 1H, Ar), 7.96 (s, 0.1H, "DMF" H), 7.98–8.00 (d, 1H, Ar), 8.12 (s, 1H, C2-CH), 12.19 (s, 1H, 3-NH, exch), 12.22 (br, 1H, 9-NH, exch). Elemental analysis calculated (%) for $C_{10}H_7N_3O \cdot 0.2HCON(CH_3)_2$: C, 63.72; H, 4.24; N, 22.43. Found: C, 63.70; H, 4.07; N, 22.16. ^{1}H NMR agreed well with the literature reported[129] values.

4-Chloro-9*H*-pyrimido[4,5-*b*]indole (243).

In a 100 mL round bottom flask was added **242** (340 mg, 1.70 mmol) and 35 mL of $POCl_3$. The reaction mixture was heated to reflux for 4 h. The $POCl_3$ was evaporated and the mixture was neutralized using aqueous NH_4OH solution leading to a precipitate. The precipitate was filtered, washed with cold water, dried and was dissolved in methanol. To the solution was added silica and solvent was removed under reduced pressure to provide a silica gel plug. Flash chromatography was done using chloroform and 1% methanol in chloroform. Fractions containing the product (TLC) were pooled and evaporated to give 310 mg (90%) of **243** as an off-white solid. TLC R_f = 0.64 ($CHCl_3$/MeOH, 10:1); mp >250 °C. ^{1}H NMR (400 MHz, DMSO-d_6): δ = 7.42–7.46 (m, 1H, Ar), 7.64–7.65 (m, 2H, Ar), 8.29–8.31 (d, 1H, Ar), 8.79 (s, 1H, C2-CH), 12.80 (s, 1H, 9-NH, exch). ^{1}H NMR agreed well with the literature reported[129] values.

***N*-(4-Methoxyphenyl)-*N*-methyl-9*H*-pyrimido[4,5-*b*]indol-4-amine (3f).**

To a 100 mL round bottom flask were added **243** (102 mg, 0.5 mmol), 4-methoxy-*N*-methylaniline **241** (274 mg, 2 mmol), 2 drops of conc. HCl and 30 mL of *n*-butanol. The reaction mixture was heated to reflux for 72 h. After cooling to rt, silica gel (500 mg) was added, and *n*-butanol was removed under reduced pressure. Purification was performed by flash chromatography using 1% methanol in chloroform as the eluent and the fractions containing the product (TLC) were pooled and the solvent was evaporated to afford 58 mg (38%) of **3f** as an off-white solid. TLC R_f = 0.74 ($CHCl_3$/MeOH, 10:1); mp >250 ºC. ^{1}H NMR (400 MHz, DMSO-d_6): δ = 3.61 (s, 3H, OCH_3), 3.76 (s, 3H, NCH_3), 5.95–5.96 (d, 1H, C5-CH), 6.70–6.73 (t, 1H, Ar), 6.93–6.95 (m, 2H, Ar), 7.19–7.23 (m, 3H, Ar), 7.36–7.37 (d, 1H, Ar), 8.57 (s, 1H, C2-CH), 12.07 (s, 1H, 9-NH, exch). Elemental analysis calculated (%) for $C_{18}H_{16}N_4O$: C, 71.04; H, 5.30; N, 18.41. Found: C, 70.92; H, 5.33; N, 18.24.

General procedure for the synthesis of 5-(aryl sulfanyl)-9*H*-pyrimido[4,5-*b*]indole-2,4-diamines 1g−3g and 5g−7g.

Compound **10** (50 mg, 0.21 mmol), the appropriate thiol (0.84 mmol), copper iodide (162 mg, 0.84 mmol), L-proline (98 mg, 0.84 mmol) and potassium carbonate (118 mg, 0.84 mmol) were added to a Biotage® microwave vial. Around 3.5–4 mL DMF was added as solvent and the tube was sealed. The reaction was run in a microwave at 180 °C until the TLC showed completion of the reactant **10**. After cooling to room temperature, the reaction mixture was transferred on top of a silica gel column and eluted with 1%, 2%,

3% and 4% methanol in chloroform. Fractions containing the product (TLC) were pooled and evaporated to afford **1g**–**3g** and **5g**–**7g** in 47–62% yield.

2-Amino-5-(phenylsulfanyl)-3,9-dihydro-4*H*-pyrimido[4,5-*b*]indol-4-one (1g). Using the general procedure described above, the reaction of **10** with benzene thiol **244** for 12 h afforded 39 mg (60%) of **1g** as a brown solid. TLC R_f = 0.39 ($CHCl_3$/MeOH, 5:1 with 2 drops of conc. NH_4OH); mp 247.0–247.4 °C (lit.[193] 247 °C). ^{1}H NMR (400 MHz, DMSO-d_6): δ = 6.51–6.54 (d, 1H, C6-CH), 6.52 (br, 2H, 2-NH_2, exch), 6.95–6.98 (t, 1H, J = 6.0 Hz, C7-CH), 7.07–7.09 (d, 1H, J = 6.0 Hz, C8-CH), 7.31–7.39 (m, 5H, Ar), 10.35 (s, 1H, 3-NH, exch), 11.55 (s, 1H, 9-NH, exch). Elemental analysis calculated (%) for $C_{16}H_{12}N_4OS{\cdot}0.23CH_3OH$: C, 61.74; H, 4.12; N, 17.75; S, 10.16. Found: C, 61.50; H, 4.03; N, 17.81; S, 10.54. ^{1}H NMR agreed well with the literature reported[193] values.

2-Amino-5-(2-naphthylsulfanyl)-3,9-dihydro-4*H*-pyrimido[4,5-*b*]indol-4-one (2g). Using the general procedure described above, the reaction of **10** with naphthalene-2-thiol **245** for 4.5 h afforded 38 mg (50%) of **2g** as an off-white solid. TLC R_f = 0.47 ($CHCl_3$/MeOH, 5:1 with 2 drops of conc. NH_4OH); mp >250 °C (lit.[193] >250 °C). ^{1}H NMR (400 MHz, DMSO-d_6): δ = 6.54 (br, 2H, 2-NH_2, exch), 6.55–6.57 (d, 1H, C6-CH), 6.94–6.97 (t, 1H, C7-CH), 7.09–7.11 (d, 1H, C8-CH), 7.426–7.429 (d, 1H, Ar), 7.52–7.54 (m, 2H, Ar), 7.87–7.93 (m, 3H, Ar), 7.981–7.983 (d, 1H, Ar), 10.36 (s, 1H, 3-NH, exch), 11.58 (s, 1H, 9-NH, exch). Elemental analysis calculated (%) for $C_{20}H_{14}N_4OS{\cdot}0.6CH_3OH$: C, 65.52; H, 4.38; N, 14.84; S, 8.49. Found: C, 65.31; H, 4.35; N, 14.99; S, 8.87. ^{1}H NMR agreed well with the literature reported[193] values.

2-Amino-5-(*p*-tolylthio)-3*H*-pyrimido[4,5-*b*]indol-4(9*H*)-one (3g).

Using the general procedure described above, the reaction of **10** with 4-methoxyphenyl thiol **246** for 16 h afforded 43 mg (62%) of **3g** as a brown solid. TLC R_f = 0.42 ($CHCl_3$/MeOH, 5:1 with 2 drops of conc. NH_4OH); mp >250 °C (lit.[192] >250 °C). ^1H NMR (400 MHz, DMSO-d_6): δ = 2.34 (s, 3H, CH_3), 6.36–6.38 (d, 1H, C6-CH), 6.52 (br, 2H, 2-NH_2, exch), 6.90–6.93 (t, 1H, C7-CH), 7.01–7.03 (d, 1H, *J* = 6.0 Hz, C8-CH), 7.23–7.25 (d, 2H, Ar), 7.33–7.34 (d, 2H, Ar), 10.37 (s, 1H, 3-NH, exch), 11.54 (s, 1H, 9-NH, exch). Elemental analysis calculated (%) for $C_{17}H_{14}N_4OS{\cdot}0.3CH_3OH$: C, 62.59; H, 4.61; N, 16.88; S, 9.66. Found: C, 62.24; H, 4.42; N, 17.00; S, 9.81. ^1H NMR agreed well with the literature reported[209] values.

2-Amino-5-((4-methoxyphenyl)thio)-3H-pyrimido[4,5-b]indol-4(9*H*)-one (5g).

Using the general procedure described above, the reaction of **10** with 4-methoxyphenyl thiol **248** for 16 h afforded 39 mg (54%) of **97** as a brown solid. TLC R_f = 0.47 ($CHCl_3$/MeOH, 5:1 with 2 drops of conc. NH_4OH); mp >250 °C (lit.[192] >250 °C). ^1H NMR (400 MHz, DMSO-d_6): δ = 3.81 (s, 3H, CH_3), 6.23–6.24 (d, 1H, *J* = 6.8 Hz, C6-CH), 6.52 (br, 2H, 2-NH_2, exch), 6.87–6.91 (t, 1H, *J* = 7.6 Hz, C7-CH), 6.96–6.98 (d, 1H, *J* = 6.8 Hz, C8-CH), 7.02–7.05 (d, 2H, *J* = 8.8 Hz, Ar), 7.43–7.45 (d, 2H, *J* = 8.8 Hz, Ar), 10.40 (s, 1H, 3-NH, exch), 11.50 (s, 1H, 9-NH, exch). HPLC analysis: retention time = 27.99 min; peak area, 95.21%; eluent A, H_2O; eluent B, ACN; gradient elution (100% H_2O to 10% H_2O) over 60 min with a flow rate of 0.5 mL/min and detection at 254 nm; column temperature, rt. ^1H NMR agreed well with the literature reported[209] values.

2-Amino-5-((4-fluorophenyl)thio)-3*H*-pyrimido[4,5-*b*]indol-4(9*H*)-one (6g).

Using the general procedure described above, the reaction of **10** with 4-fluorophenyl thiol **249** for 16 h afforded 35 mg (51%) of **95** as a brown solid. TLC R_f = 0.47 ($CHCl_3$/MeOH, 5:1 with 2 drops of conc. NH_4OH); mp >300 °C (lit.[192] >300 °C). ^{1}H NMR (400 MHz, DMSO-d_6): δ = 6.42 (d, 1H, J = 8.0 Hz, C7-CH), 6.52 (br, 2H, 2-NH_2, exch), 6.94 (t, 1H, J = 8.0 Hz, C6-CH), 7.04–7.06 (m, 1H, C8-CH), 7.21–7.26 (m, 2H, Ar), 7.42–7.46 (m, 2H, Ar), 10.36 (s, 1H, 3-NH, exch), 11.54 (s, 1H, 9-NH, exch). ^{1}H NMR agreed well with the literature reported[209] values.

2-Amino-5-((4-phenoxyphenyl)thio)-3*H*-pyrimido[4,5-*b*]indol-4(9*H*)-one (7g).

Using the general procedure described above, the reaction of **10** with 4-phenoxybenzene thiol **250** for 12 h afforded 40 mg (47%) of **7g** as a brown solid. TLC R_f = 0.46 ($CHCl_3$/MeOH, 5:1 with 2 drops of conc. NH_4OH); mp >300 °C. ^{1}H NMR (400 MHz, DMSO-d_6): δ = 6.41–6.43 (d, 1H, C6-CH); 6.56 (br, 2H, 2-NH_2, exch); 6.94–6.98 (t, 1H, Ar); 7.02–7.05 (m, 3H, Ar); 7.09–7.11 (m, 2H, Ar); 7.18–7.21 (t, 1H, Ar); 7.42–7.46 (m, 4H, Ar); 10.40 (s, 1H, 3-NH, exch); 11.54 (s, 1H, 9-NH, exch). Elemental analysis calculated (%) for $C_{22}H_{16}N_4O_2S \cdot 0.26NH_4OH \cdot 0.40HCl$: C, 62.30; H, 4.21; N, 14.07; S, 7.56; Cl, 3.35. Found: C, 62.30; H, 4.30; N, 14.04; S, 7.64; Cl, 3.73.

2-Amino-5-(phenylthio)-3*H*-pyrimido[4,5-*b*]indol-4(9*H*)-one hydrochloride (1g·HCl).

Compound **1g** (50 mg) was dissolved in chloroform (2 mL), ethyl acetate (5 mL), methanol (0.2 mL) and diethyl ether (2 mL), and then HCl gas was bubbled into the solution till precipitation ceased. The yellow solid was collected by filtration and dried

over P_2O_5 to afford 32 mg of **1g**·HCl in 60% yield. Mp >300 °C. ^{1}H NMR (400 MHz, DMSO-d_6): δ = 6.52–6.54 (m, 1H, Ar), 6.60 (br, 3H, 2-NH_3^+, exch), 6.98–7.00 (m, 1H, Ar), 7.11–7.13 (m, 1H, Ar), 7.38–7.39 (m, 5H, Ar), 10.61 (s, 1H, 3-NH, exch), 11.72 (s, 1H, 9-NH, exch). HRMS (ESI): *m/z* calculated for $C_{16}H_{13}N_4OS$·HCl + H^+ [M+H^+]: 309.0810. Found: 309.0804. HPLC analysis: retention time = 24.80 min; peak area, 96.09%; eluent A, H_2O; eluent B, ACN; gradient elution (100% H_2O to 10% H_2O) over 60 min with a flow rate of 0.5 mL/min and detection at 254 nm; column temperature, rt.

2-Amino-5-(naphthalen-2-ylthio)-3*H*-pyrimido[4,5-*b*]indol-4(9*H*)-one hydrochloride (2g·HCl**).**

Compound **2g** (50 mg) was dissolved in *N*,*N*-dimethylformamide (2 mL), dioxane (2 mL) and diethyl ether (20 mL), and then HCl gas was bubbled into the solution till precipitation ceased. The white solid was collected by filtration and dried over P_2O_5 to afford 30 mg of **2g**·HCl in 59% yield. Mp >300 °C. ^{1}H NMR (400 MHz, DMSO-d_6): δ = 6.56–6.58 (m, 1 H, Ar), 6.70 (br, 3H, 2-NH_3^+, exch), 6.95–6.99 (m, 1H, Ar), 7.12–7.14 (m, 1H, Ar), 7.41–7.43 (m, 1H, Ar), 7.52–7.55 (m, 2H, Ar), 7.87–7.99 (m, 4H, Ar), 10.59 (s, 1H, 3-NH, exch), 11.72 (s, 1H, 9-NH, exch). Elemental analysis calculated (%) for $C_{20}H_{15}ClN_4OS$·0.14$C_4H_8O_2$·0.05HCl: C, 60.37; H, 3.98; N, 13.70; Cl, 9.10; S, 7.84 Found: C, 60.19; H, 4.00; N, 13.88; Cl, 9.01; S, 7.78.

VI. SUMMARY

This dissertation describes the design and synthesis of following structural classes of compounds either as single agents with combination chemotherapy potential or as tubulin inhibitors or as selective *T. gondii* TS inhibitors:

1. 2,4-Diamino-5-thioaryl-9*H*-pyrimido[4,5-*b*]indoles
2. *N*,*N*-Disubstituted-5-methylfuro[2,3-*d*]pyrimidin-4-amines
3. N^4-Aryl-5-chloro-2,4-diamino-pyrimido[4,5-*b*]indoles
4. 2,4-Disubstituted-9*H*-pyrimido[4,5-b]indole-4-amines
5. 2-Amino-4-oxo-5-thioaryl-9*H*-pyrimido[4,5-*b*]indoles

From these projects, a total of forty two novel compounds were synthesized and characterized, and among them, thirty six target compounds were submitted for various biological assays. In addition, five selective *T. gondii* TS inhibitors were resynthesized and submitted for further preclinical and X-ray crystallographic studies. These compounds are as follows:

1. 5-(4-Fluorophenylthio)-9*H*-pyrimido[4,5-*b*]indole-2,4-diamine (**1a**)
2. 5-(4-Trifluoromethylphenylthio)-9*H*-pyrimido[4,5-*b*]indole-2,4-diamine (**2a**)
3. 5-(*m*-Tolylthio)-9*H*-pyrimido[4,5-*b*]indole-2,4-diamine (**3a**)
4. 5-(*o*-Tolylthio)-9*H*-pyrimido[4,5-*b*]indole-2,4-diamine (**4a**)
5. 5-(3,4-Dimethylphenylthio)-9*H*-pyrimido[4,5-*b*]indole-2,4-diamine (**5a**)
6. 5-(3-Methoxyphenylthio)-9*H*-pyrimido[4,5-*b*]indole-2,4-diamine (**6a**)
7. 5-(*o*-Methoxyphenylthio)-9*H*-pyrimido[4,5-*b*]indole-2,4-diamine (**7a**)
8. *N*-Ethyl-*N*-(4-methoxyphenyl)-5-methylfuro[2,3-*d*]pyrimidin-4-amine (**1b**)
9. *N*-Isopropyl-*N*-(4-methoxyphenyl)-5-methylfuro[2,3-*d*]pyrimidin-4-amine (**2b**)

10. *N*-(4-Methoxyphenyl)-5-methyl-*N*-propylfuro[2,3-*d*]pyrimidin-4-amine (**3b**)
11. *N*-Butyl-*N*-(4-methoxyphenyl)-5-methylfuro[2,3-*d*]pyrimidin-4-amine (**4b**)
12. *N*-Methyl-*N*-(4-ethylphenyl)-5-methylfuro[2,3-*d*]pyrimidin-4-amine (**1c**)
13. *N*,5-Dimethyl-*N*-(4-(methylthio)phenyl)furo[2,3-*d*]pyrimidin-4-amine (**2c**)
14. N^1,N^4-Dimethyl-N^1-(5-methylfuro[2,3-*d*]pyrimidin-4-yl)benzene-1,4-diamine (**3c**)
15. N^1,N^1,N^4-Trimethyl-N^4-(5-methylfuro[2,3-*d*]pyrimidin-4-yl)benzene-1,4-diamine (**4c**)
16. *N*,5-Dimethyl-*N*-(4-nitrophenyl)furo[2,3-*d*]pyrimidin-4-amine (**5c**)
17. 5-Chloro-N^4-methyl-N^4-phenyl-9*H*-pyrimido[4,5-*b*]indole-2,4-diamine (**1d**)
18. 5-Chloro-N^4-methyl-N^4-*p*-tolyl-9*H*-pyrimido[4,5-*b*]indole-2,4-diamine (**2d**)
19. 5-Chloro-N^4-(4-chlorophenyl)-N^4-methyl-9*H*-pyrimido[4,5-*b*]indole-2,4-diamine (**3d**)
20. 5-Chloro-N^4-3-methoxyphenyl-N^4-methyl-9*H*-pyrimido[4,5-*b*]indole-2,4-diamine (**4d**)
21. 5-Chloro-N^4-3-fluorophenyl-N^4-methyl-9*H*-pyrimido[4,5-*b*]indole-2,4-diamine (**5d**)
22. 5-Chloro-4-(6-methoxy-3,4-dihydroquinolin-1(2*H*)-yl)-9*H*-pyrimido[4,5-*b*]indol-2-amine (**6d**)
23. N^4-Ethyl-N^4-(4-methoxyphenyl)-9*H*-pyrimido[4,5-*b*]indole-2,4-diamine (**1e**)
24. 4-(6-Methoxy-3,4-dihydroquinolin-1(2*H*)-yl)-9*H*-pyrimido[4,5-*b*]indol-2-amine (**2e**)
25. N^4-(4-Ethoxyphenyl)-N^4-methyl-9*H*-pyrimido[4,5-*b*]indole-2,4-diamine (**3e**)
26. N^4-Methyl-N^4-(4-(methylthio)phenyl)-9*H*-pyrimido[4,5-*b*]indole-2,4-diamine (**1f**)
27. *N*-(4-Methoxyphenyl)-*N*,2-dimethyl-9*H*-pyrimido[4,5-*b*]indol-4-amine (**2f**)
28. *N*-(4-Methoxyphenyl)-*N*-methyl-9*H*-pyrimido[4,5-*b*]indol-4-amine (**3f**)
29. 2-Amino-5-(phenylsulfanyl)-3,9-dihydro-4*H*-pyrimido[4,5-*b*]indol-4-one (**1g**)
30. 2-Amino-5-(2-naphthylsulfanyl)-3,9-dihydro-4*H*-pyrimido[4,5-*b*]indol-4-one (**2g**)

31. 2-Amino-5-(*p*-tolylthio)-3*H*-pyrimido[4,5-*b*]indol-4(9*H*)-one (**3g**)

32. 2-Amino-5-((4-methoxyphenyl)thio)-3H-pyrimido[4,5-b]indol-4(9H)-one (**5g**)

33. 2-Amino-5-((4-fluorophenyl)thio)-3*H*-pyrimido[4,5-*b*]indol-4(9*H*)-one (**6g**)

34. 2-Amino-5-((4-phenoxyphenyl)thio)-3*H*-pyrimido[4,5-*b*]indol-4(9*H*)-one (**7g**)

35. 2-Amino-5-(phenylthio)-3*H*-pyrimido[4,5-*b*]indol-4(9*H*)-one hydrochloride (**1g**·HCl).

36. 2-Amino-5-(naphthalen-2-ylthio)-3*H*-pyrimido[4,5-*b*]indol-4(9*H*)-one hydrochloride (**2g**·HCl).

37. *N*-(4-Ethylphenyl)-5-methylfuro[2,3-*d*]pyrimidin-4-amine (**213**).

38. 5-Methyl-*N*-(4-(methylthio)phenyl)furo[2,3-*d*]pyrimidin-4-amine (**214**).

39. *N*-(4-Nitrophenyl)-5-methylfuro[2,3-*d*]pyrimidin-4-amine (**215**).

40. N^1-Methyl-N^4-(5-methylfuro[2,3-*d*]pyrimidin-4-yl)benzene-1,4-diamine (**218**).

41. N^1,N^1-Dimethyl-N^4-(5-methylfuro[2,3-*d*]pyrimidin-4-yl)benzene-1,4-diamine (**219**).

During this study, a novel synthetic route was successfully optimized for the synthesis of target compounds **1a**–**7a**. Also, it led to the resynthesis of gram quantities of lead compounds **1** and **2** with significant improvement in overall yield over the reported procedure. Ullmann coupling conditions were explored and successfully employed as a key step to obtain target compounds **2c**–**5c**. Optimization of Ullmann coupling resulted in the resynthesis of **1g**–**3g**, **5g** and **6g** with highly improved yields over previous methods.

Compounds **1a**–**7a**, **1b**–**4b** and **1c**–**5c** were designed and synthesized as single agents which combine cytostatic mechanism (via RTK inhibition) with a cytotoxic mechanism (via TS or tubulin inhibition). Pyrimido[4,5-*b*]indoles **1a**–**7a** were evaluated against multiple RTKs using whole cell assays and the 4'-CF_3 analog **2a** and the 3',4'-

diMe analog **5a** were the most potent inhibitors of VEGFR-2 and EGFR kinases. Furo[2,3-*d*]pyrimidines **1b**–**4b** and **1c**–**5c** were tested as inhibitors of tubulin and multiple RTKs (whole cell assays). Compounds **1b**, **3b** and **2c**–**4c** had potent multi-RTK inhibition along with potent anti-tubulin activity, thus making them single agents with combination chemotherapy potential. Compounds **2b** (N^4-*i*Pr-4'-OMe) and **1c** (N^4-Me-4'-Et) had potent RTK inhibition with weak microtubule depolymerizing activity. Therefore, compounds **2b** and **1c** can be used in anticancer chemotherapy either alone as RTK inhibitors or in combination chemotherapy with other cytotoxic agents.

4-Anilino-pyrimido[4,5-*b*]indoles **1d**–**6d**, **1e**–**3e** and **1f**–**3f** were evaluated as tubulin inhibitors and as agents that can overcome Pgp and βIII-tubulin mediated drug resistance. Structural requirements of pyrimido[4,5-*b*]indoles for tubulin inhibition are: alkyl group at N^4-position, hydrogen at 5-position and alkoxy group at 4'-position.

2-Amino-4-oxo-5-thioaryl-pyrimido[4,5-*b*]indoles **1g**–**7g** were tested in tgTS, hTS and *T. gondii* cell culture assays. Compounds **1g**, **4g** and **7g** are nanomolar inhibitors of tgTS with up to a remarkable 122-fold selectivity for tgTS over hTS. These compounds are the only tgTS-selective inhibitors known till date and also provide a new target (TS) to combat *T. gondii* infection.

Pyrimido[4,5-*b*]indoles described in this dissertation represent one of the unique classes of molecules with diverse biological targets. 2-Amino-5-thioaryl-pyrimido[4,5-*b*]indoles with 4-amino substitution are anticancer agents which inhibit TS and multiple RTKs where as those with 4-oxo substitution were tgTS-selective antiparasitic agents. 4-Anilino-pyrimido[4,5-*b*]indoles are anticancer agents which inhibit tubulin and/or multiple RTKs.

VII. BIBLIOGRAPHY

1. Dumontet, C.; Jordan, M. A. Microtubule-binding agents: A dynamic field of cancer therapeutics. *Nat. Rev. Drug Discov.* **2010**, *9*, 790-803.
2. Jordan, M. A.; Wilson, L. Microtubules as a target for anticancer drugs. *Nat. Rev. Cancer* **2004**, *4*, 253-265.
3. Bowne-Anderson, H.; Zanic, M.; Kauer, M.; Howard, J. Microtubule dynamic instability: A new model with coupled GTP hydrolysis and multistep catastrophe. *Bioessays* **2013**, *35*, 452-461.
4. Gardner, M. K.; Zanic, M.; Howard, J. Microtubule catastrophe and rescue. *Curr. Opin. Cell Biol.* **2013**, *25*, 14-22.
5. Jordon, M. A.; Kamath, K. How do microtubule-targeted drugs work? An overview. *Curr. Cancer Drug Targets* **2007**, *7*, 730-742.
6. Etienne-Manneville, S. From signaling pathways to microtubule dynamics: The key players. *Curr. Opin. Cell Biol.* **2010**, *22*, 104-111.
7. Quiniou, E.; Guichard, P.; Perahia, D.; Marco, S.; Mouawad, L. An atomistic view of microtubule stabilization by GTP. *Structure* **2013**, *21*, 833-843.
8. Risinger, A. L.; Giles, F. J.; Mooberry, S. L. Microtubule dynamics as a target in oncology. *Cancer Treat. Rev.* **2009**, *35*, 255-261.
9. Stanton, R. A.; Gernert, K. M.; Nettles, J. H.; Aneja, R. Drugs that target dynamic microtubules: A new molecular perspective. *Med. Res. Rev.* **2011**, *31*, 443-481.
10. Kavallaris, M. Microtubules and resistance to tubulin-binding agents. *Nat. Rev. Cancer* **2010**, *10*, 194-204.

11. Field, Jessica J.; Díaz, José F.; Miller, John H. The binding sites of microtubule-stabilizing agents. *Chem. Biol.* **2013**, *20*, 301-315.

12. Amos, L. A. What tubulin drugs tell us about microtubule structure and dynamics. *Semin. Cell Dev. Biol.* **2011**, *22*, 916-926.

13. Massarotti, A.; Coluccia, A.; Silvestri, R.; Sorba, G.; Brancale, A. The tubulin colchicine domain: A molecular modeling perspective. *ChemMedChem* **2012**, *7*, 33-42.

14. Prota, A. E.; Bargsten, K.; Diaz, J. F.; Marsh, M.; Cuevas, C.; Liniger, M.; Neuhaus, C.; Andreu, J. M.; Altmann, K.-H.; Steinmetz, M. O. A new tubulin-binding site and pharmacophore for microtubule-destabilizing anticancer drugs. *Proc. Natl. Acad. Sci.* **2014**, *111*, 13817-13821.

15. Altmann, K.-H. Microtubule-stabilizing agents: A growing class of important anticancer drugs. *Curr. Opin. Chem. Biol.* **2001**, *5*, 424-431.

16. Puhalla, S.; Brufsky, A. Ixabepilone: A new chemotherapeutic option for refractory metastatic breast cancer. *Biologics* **2008**, *2*, 505-515.

17. Ortega, V.; Cortés, J. Potential clinical applications of halichondrins in breast cancer and other neoplasms. *Breast Cancer* **2012**, *4*, 9-19.

18. Smith, C. D.; Zhang, X. Mechanism of action of cryptophycin: Interaction with the Vinca alkaloid domain of tubulin. *J. Biol. Chem.* **1996**, *271*, 6192-6198.

19. Cormier, A.; Marchand, M.; Ravelli, R. B. G.; Knossow, M.; Gigant, B. Structural insight into the inhibition of tubulin by vinca domain peptide ligands. *EMBO Rep.* **2008**, *9*, 1101-1106.

20. Menis, J.; Twelves, C. Eribulin (Halaven): A new, effective treatment for women with heavily pretreated metastatic breast cancer. *Breast Cancer* **2011**, *3*, 101-111.

21. Lu, Y.; Chen, J.; Xiao, M.; Li, W.; Miller, D. An overview of tubulin inhibitors that interact with the colchicine binding site. *Pharm. Res.* **2012**, *29*, 2943-2971.

22. Yang, L. P. H. Oral colchicine (Colcrys®). *Drugs* **2010**, *70*, 1603-1613.

23. Harrison, M.; Hahn, N.; Pili, R.; Oh, W.; Hammers, H.; Sweeney, C.; Kim, K.; Perlman, S.; Arnott, J.; Sidor, C.; Wilding, G.; Liu, G. A phase II study of 2-methoxyestradiol (2ME2) NanoCrystal® dispersion (NCD) in patients with taxane-refractory, metastatic castrate-resistant prostate cancer (CRPC). *Invest. New Drugs* **2011**, *29*, 1465-1474.

24. Bruce, J.; Eickhoff, J.; Pili, R.; Logan, T.; Carducci, M.; Arnott, J.; Treston, A.; Wilding, G.; Liu, G. A phase II study of 2-methoxyestradiol nanocrystal colloidal dispersion alone and in combination with sunitinib malate in patients with metastatic renal cell carcinoma progressing on sunitinib malate. *Invest. New Drugs* **2012**, *30*, 794-802.

25. Liu, P. Q., Y.; Wu, L.; Yang, S.; Li, N.; Wang, H.; Xu, H.; Sun, K.; Zhang, S.; Han, X.; Sun, Y.; Shi, Y A phase I clinical trial assessing the safety and tolerability of combretastatin A4 phosphate injections. *Anticancer Drugs* **2014**, *25*, 462-471.

26. Ng, Q.-S.; Mandeville, H.; Goh, V.; Alonzi, R.; Milner, J.; Carnell, D.; Meer, K.; Padhani, A. R.; Saunders, M. I.; Hoskin, P. J. Phase Ib trial of radiotherapy in combination with combretastatin-A4-phosphate in patients with non-small-cell lung cancer, prostate adenocarcinoma, and squamous cell carcinoma of the head and neck. *Ann. Oncol.* **2012**, *23*, 231-237.

27. Zweifel, M.; Jayson, G. C.; Reed, N. S.; Osborne, R.; Hassan, B.; Ledermann, J.; Shreeves, G.; Poupard, L.; Lu, S.-P.; Balkissoon, J.; Chaplin, D. J.; Rustin, G. J. S. Phase II trial of combretastatin A4 phosphate, carboplatin, and paclitaxel in patients with platinum-resistant ovarian cancer. *Ann. Oncol.* **2011**, *22*, 2036-2041.

28. Nathan, P.; Zweifel, M.; Padhani, A. R.; Koh, D.-M.; Ng, M.; Collins, D. J.; Harris, A.; Carden, C.; Smythe, J.; Fisher, N.; Taylor, N. J.; Stirling, J. J.; Lu, S.-P.; Leach, M. O.; Rustin, G. J. S.; Judson, I. Phase I trial of combretastatin A4 phosphate (CA4P) in combination with bevacizumab in patients with advanced cancer. *Clin. Cancer Res.* **2012**, *18*, 3428-3439.

29. Patterson, D. M.; Zweifel, M.; Middleton, M. R.; Price, P. M.; Folkes, L. K.; Stratford, M. R. L.; Ross, P.; Halford, S.; Peters, J.; Balkissoon, J.; Chaplin, D. J.; Padhani, A. R.; Rustin, G. J. S. Phase I clinical and pharmacokinetic evaluation of the vascular-disrupting agent OXi4503 in patients with advanced solid tumors. *Clin. Cancer Res.* **2012**, *18*, 1415-1425.

30. Siemann, D. W.; Chaplin, D. J.; Walicke, P. A. A review and update of the current status of the vasculature-disabling agent combretastatin-A4 phosphate (CA4P). *Expert Opin. Investig. Drugs* **2009**, *18*, 189-197.

31. Mita, M. M.; Sargsyan, L.; Mita, A. C.; Spear, M. Vascular-disrupting agents in oncology. *Expert Opin. Investig. Drugs* **2013**, *22*, 317-328.

32. Tozer, G. M.; Prise, V. E.; Wilson, J.; Cemazar, M.; Shan, S.; Dewhirst, M. W.; Barber, P. R.; Vojnovic, B.; Chaplin, D. J. Mechanisms associated with tumor vascular shut-down induced by combretastatin A-4 phosphate: Intravital

microscopy and measurement of vascular permeability. *Cancer Res.* **2001**, *61*, 6413-6422.

33. Nagaiah, G.; Remick, S. C. Combretastatin A4 phosphate: A novel vascular disrupting agent. *Future Oncol.* **2010**, *6*, 1219-1228.

34. Prise, V. E. H., D. J.; Stratford, M. R.; Wilson, J.; Tozer, G. M. The vascular response of tumor and normal tissues in the rat to the vascular targeting agent, combretastatin A-4-phosphate, at clinically relevant doses. *Int. J. Oncol.* **2002**, *21*, 717-726.

35. Pera, B.; Barasoain, I.; Pantazopoulou, A.; Canales, A.; Matesanz, R.; Rodriguez-Salarichs, J.; García-Fernandez, L. F.; Moneo, V.; Jiménez-Barbero, J.; Galmarini, C. M.; Cuevas, C.; Peñalva, M. A.; Díaz, J. F.; Andreu, J. M. New interfacial microtubule inhibitors of marine origin, PM050489/PM060184, with potent antitumor activity and a distinct mechanism. *ACS Chem. Biol.* **2013**, *8*, 2084-2094.

36. Hanauske, A. R.; Catimel, G.; Aamdal, S.; ten Bokkel Huinink, W.; Paridaens, R.; Pavlidis, N.; Kaye, S. B.; te Velde, A.; Wanders, J.; Verweij, J. Phase II clinical trials with rhizoxin in breast cancer and melanoma. The EORTC Early Clinical Trials Group. *Br. J. Cancer* **1996**, *73*, 397-399.

37. Verma, S.; Miles, D.; Gianni, L.; Krop, I. E.; Welslau, M.; Baselga, J.; Pegram, M.; Oh, D.-Y.; Diéras, V.; Guardino, E.; Fang, L.; Lu, M. W.; Olsen, S.; Blackwell, K. Trastuzumab emtansine for HER2-positive advanced breast cancer. *N. Engl. J. Med.* **2012**, *367*, 1783-1791.

38. Fojo, A. T.; Menefee, M. Microtubule targeting agents: Basic mechanisms of multidrug resistance (MDR). *Semin. Oncol.* **2005**, *32*, S3-S8.

39. Leonard, G. D.; Fojo, T.; Bates, S. E. The role of ABC transporters in clinical practice. *Oncologist* **2003**, *8*, 411-424.

40. Gangjee, A.; Zhao, Y.; Lin, L.; Raghavan, S.; Roberts, E. G.; Risinger, A. L.; Hamel, E.; Mooberry, S. L. Synthesis and discovery of water-soluble microtubule targeting agents that bind to the colchicine site on tubulin and circumvent Pgp mediated resistance. *J. Med. Chem.* **2010**, *53*, 8116-8128.

41. Chiou, J. F.; Liang, J. A.; Hsu, W. H.; Wang, J. J.; Ho, S. T.; Kao, A. Comparing the relationship of taxol-based chemotherapy response with P-glycoprotein and lung resistance-related protein expression in non-small cell lung cancer. *Lung* **2003**, *181*, 267-273.

42. Fojo, T.; Menefee, M. Mechanisms of multidrug resistance: The potential role of microtubule-stabilizing agents. *Ann. Oncol.* **2007**, *18*, 3-8.

43. Lhommé, C.; Joly, F.; Walker, J. L.; Lissoni, A. A.; Nicoletto, M. O.; Manikhas, G. M.; Baekelandt, M. M. O.; Gordon, A. N.; Fracasso, P. M.; Mietlowski, W. L.; Jones, G. J.; Dugan, M. H. Phase III study of Valspodar (PSC 833) combined with paclitaxel and carboplatin compared with paclitaxel and carboplatin alone in patients with stage IV or suboptimally debulked stage III epithelial ovarian cancer or primary peritoneal cancer. *J. Clin. Oncol.* **2008**, *26*, 2674-2682.

44. Binkhathlan, Z.; Lavasanifar, A. P-glycoprotein inhibition as a therapeutic approach for overcoming multidrug resistance in cancer: Current status and future perspectives. *Curr. Cancer Drug Targets* **2013**, *13*, 326-346.

45. Resell, R.; Scagliotti, G.; Danenberg, K. D.; Lord, R. V. N.; Bepler, G.; Novello, S.; Cooc, J.; Crino, L.; Sanchez, J. J.; Taron, M.; Boni, C.; Marinis, F. D.; Tonato, M.;

Marangolo, M.; Gozzelino, F.; Costanzo, F. D.; Rinaldi, M.; Salonga, D.; Stephens, C. Transcripts in pretreatment biopsies from a three-arm randomized trial in metastatic non-small-cell lung cancer. *Oncogene* **2003**, *22*, 3548-3553.

46. Dumontet, C. I., S.; Souquet, P. -J.; Bejui-Thivolet, F.; Pacheco, Y.; Peloux, N.; Frankfurter, A.; Luduena, R.; Perol, M. Expression of class III beta tubulin in non-small cell lung cancer is correlated with resistance to taxane chemotherapy. *Bull. Cancer* **2005**, *92*, 25-30.

47. Tommasi, S.; Mangia, A.; Lacalamita, R.; Bellizzi, A.; Fedele, V.; Chiriatti, A.; Thomssen, C.; Kendzierski, N.; Latorre, A.; Lorusso, V.; Schittulli, F.; Zito, F.; Kavallaris, M.; Paradiso, A. Cytoskeleton and paclitaxel sensitivity in breast cancer: The role of β-tubulins. *Int. J. Cancer* **2007**, *120*, 2078-2085.

48. Mozzetti, S.; Ferlini, C.; Concolino, P.; Filippetti, F.; Raspaglio, G.; Prislei, S.; Gallo, D.; Martinelli, E.; Ranelletti, F. O.; Ferrandina, G.; Scambia, G. Class III β-tubulin overexpression is a prominent mechanism of paclitaxel resistance in ovarian cancer patients. *Clin. Cancer Res.* **2005**, *11*, 298-305.

49. Hwang, J.-E.; Hong, J.-Y.; Kim, K.; Kim, S.-H.; Choi, W.-Y.; Kim, M.-J.; Jung, S.-H.; Shim, H.-J.; Bae, W.-K.; Hwang, E.-C.; Lee, K.-H.; Lee, J.-H.; Cho, S.-H.; Chung, I.-J. Class III β-tubulin is a predictive marker for taxane-based chemotherapy in recurrent and metastatic gastric cancer. *BMC Cancer* **2013**, *13*, 431-431.

50. Kamath, K.; Wilson, L.; Cabral, F.; Jordan, M. A. βIII-Tubulin induces paclitaxel resistance in association with reduced effects on microtubule dynamic instability. *J. Biol. Chem.* **2005**, *280*, 12902-12907.

51. Freedman, H.; Huzil, J. T.; Luchko, T.; Ludueña, R. F.; Tuszynski, J. A. Identification and characterization of an intermediate taxol binding site within microtubule nanopores and a mechanism for tubulin isotype binding selectivity. *J. Chem. Inf. Model.* **2009**, *49*, 424-436.

52. Sève, P.; Isaac, S.; Trédan, O.; Souquet, P.-J.; Pachéco, Y.; Pérol, M.; Lafanéchère, L.; Penet, A.; Peiller, E.-L.; Dumontet, C. Expression of class III β-tubulin is predictive of patient outcome in patients with non–small cell lung cancer receiving vinorelbine-based chemotherapy. *Clin. Cancer Res.* **2005**, *11*, 5481-5486.

53. Ferrandina, G.; Zannoni, G. F.; Martinelli, E.; Paglia, A.; Gallotta, V.; Mozzetti, S.; Scambia, G.; Ferlini, C. Class III β-tubulin overexpression is a marker of poor clinical outcome in advanced ovarian cancer patients. *Clin. Cancer Res.* **2006**, *12*, 2774-2779.

54. Stengel, C.; Newman, S. P.; Leese, M. P.; Potter, B. V. L.; Reed, M. J.; Purohit, A. Class III β-tubulin expression and in vitro resistance to microtubule targeting agents. *Brit. J. Cancer* **2010**, *102*, 316-324.

55. Zhang, X.; Raghavan, S.; Ihnat, M.; Thorpe, J. E.; Disch, B. C.; Bastian, A.; Bailey-Downs, L. C.; Dybdal-Hargreaves, N. F.; Rohena, C. C.; Hamel, E.; Mooberry, S. L.; Gangjee, A. The design and discovery of water soluble 4-substituted-2,6-dimethylfuro[2,3-*d*]pyrimidines as multitargeted receptor tyrosine kinase inhibitors and microtubule targeting antitumor agents. *Bioorg. Med. Chem.* **2014**, *22*, 3753-3772.

56. Costi, M. P. F., S.; Venturelli, A.; Calo, S.; Tondi, D.; Barlocco, D. Thymidylate synthase structure, function and implication in drug discovery. *Curr. Med. Chem.* **2005**, *12*, 2241-2258.

57. Wilson, P. M.; Danenberg, P. V.; Johnston, P. G.; Lenz, H.-J.; Ladner, R. D. Standing the test of time: Targeting thymidylate biosynthesis in cancer therapy. *Nat. Rev. Clin. Oncol.* **2014**, *11*, 282-298.

58. Berman, H. M.; Westbrook, J.; Feng, Z.; Gilliland, G.; Bhat, T. N.; Weissig, H.; Shindyalov, I. N.; Bourne, P. E. The Protein Data Bank. *Nucleic Acids Res.* **2000**, *28*, 235-242.

59. Sayre, P. H.; Finer-Moore, J. S.; Fritz, T. A.; Biermann, D.; Gates, S. B.; MacKellar, W. C.; Patel, V. F.; Stroud, R. M. Multi-targeted antifolates aimed at avoiding drug resistance form covalent closed inhibitory complexes with human and Escherichia coli thymidylate synthases. *J. Mol. Biol.* **2001**, *313*, 813-829.

60. Phan, J.; Koli, S.; Minor, W.; Dunlap, R. B.; Berger, S. H.; Lebioda, L. Human thymidylate synthase is in the closed conformation when complexed with dUMP and raltitrexed, an antifolate drug. *Biochemistry* **2001**, *40*, 1897-1902.

61. Gmeiner, W. H. Novel chemical strategies for thymidylate synthase inhibition. *Curr. Med. Chem.* **2005**, *12*, 191-202.

62. Houghton, J. A.; Tillman, D. M.; Harwood, F. G. Ratio of 2'-deoxyadenosine-5'-triphosphate/thymidine-5'-triphosphate influences the commitment of human colon carcinoma cells to thymineless death. *Clin. Cancer Res.* **1995**, *1*, 723-730.

63. Longley, D. B.; Harkin, D. P.; Johnston, P. G. 5-Fluorouracil: Mechanisms of action and clinical strategies. *Nat. Rev. Cancer* **2003**, *3*, 330-338.

64. Garg, D.; Henrich, S.; Salo-Ahen, O. M. H.; Myllykallio, H.; Costi, M. P.; Wade, R. C. Novel approaches for targeting thymidylate synthase to overcome the resistance and toxicity of anticancer drugs. *J. Med. Chem.* **2010**, *53*, 6539-6549.

65. Walko, C. M.; Lindley, C. Capecitabine: A review. *Clin. Ther.* **2005**, *27*, 23-44.

66. Gangjee, A.; Jain, H. D.; Kurup, S. Recent advances in classical and non-classical antifolates as antitumor and antiopportunistic infection agents: Part II. *Anticancer Agents Med. Chem.* **2008**, *8*, 205-231.

67. Chu, E.; Callender, M.; Farrell, M.; Schmitz, J. Thymidylate synthase inhibitors as anticancer agents: From bench to bedside. *Cancer Chemother. Pharmacol.* **2003**, *52*, 80-89.

68. Van Cutsem, E.; Cunningham, D.; Maroun, J.; Cervantes, A.; Glimelius, B. Raltitrexed: Current clinical status and future directions. *Ann. Oncol.* **2002**, *13*, 513-522.

69. Jhawer, M.; Rosen, L.; Dancey, J.; Hochster, H.; Hamburg, S.; Tempero, M.; Clendeninn, N.; Mani, S. Phase II trial of nolatrexed dihydrochloride [ThymitaqTM, AG 337] in patients with advanced hepatocellular carcinoma. *Invest. New Drugs* **2007**, *25*, 85-94.

70. Paz-Ares, L.; Bezares, S.; Tabernero, J. M.; Castellanos, D.; Cortes-Funes, H. Review of a promising new agent—Pemetrexed disodium. *Cancer* **2003**, *97*, 2056-2063.

71. Exinger, D.; Exinger, F.; Mennecier, B.; Limacher, J.-M.; Dufour, P.; Kurtz, J.-E. Multitargeted antifolate (Pemetrexed): A comprehensive review of its mechanisms of action, recent results and future prospects. *Cancer Ther.* **2003**, *1*, 315-322.

72. Saadatnia, G.; Golkar, M. A review on human toxoplasmosis. *Scand. J. Infect. Dis.* **2012**, *44*, 805-814.

73. Montoya, J. G.; Liesenfeld, O. Toxoplasmosis. *Lancet* **2004**, *363*, 1965-1976.

74. Durand, C. M.; Flexner, C. HIV cure: Knocking on the door. *Clin. Pharmacol. Ther.* **2013**, *93*, 382-384.

75. Centers for Disease Control and Prevention (CDC). Toxoplasmosis (*Toxoplasma* infection). http://www.cdc.gov/parasites/toxoplasmosis (accessed January 8, 2015).

76. Hyde, J. E. Targeting purine and pyrimidine metabolism in human apicomplexan parasites. *Curr. Drug Targets.* **2007**, *8*, 31-47.

77. Sharma, H.; Landau, M. J.; Vargo, M. A.; Spasov, K. A.; Anderson, K. S. First three-dimensional structure of *Toxoplasma gondii* thymidylate synthase–dihydrofolate reductase: Insights for catalysis, interdomain interactions, and substrate channeling. *Biochemistry* **2013**, *52*, 7305-7317.

78. Ferrari, S.; Losasso, V.; Costi, M. P. Sequence-based identification of specific drug target regions in the thymidylate synthase enzyme family. *ChemMedChem* **2008**, *3*, 392-401.

79. El-Kenawi, A. E.; El-Remessy, A. B. Angiogenesis inhibitors in cancer therapy: Mechanistic perspective on classification and treatment rationales. *Br. J. Pharmacol.* **2013**, *170*, 712-729.

80. Jain, R. K. Normalizing tumor microenvironment to treat cancer: Bench to bedside to biomarkers. *J. Clin. Oncol.* **2013**, *31*, 2205-2218.

81. Quesada, A. R.; Muñoz-Chápuli, R.; Medina, M. A. Anti-angiogenic drugs: From bench to clinical trials. *Med. Res. Rev.* **2006**, *26*, 483-530.

82. Joyce, J. A.; Pollard, J. W. Microenvironmental regulation of metastasis. *Nat. Rev. Cancer* **2009**, *9*, 239-252.

83. Zhang, C.; Tan, C.; Ding, H.; Xin, T.; Jiang, Y. Selective VEGFR inhibitors for anticancer therapeutics in clinical use and clinical trials. *Curr. Pharm. Des.* **2012**, *18*, 2921-2935.

84. Sun, W. Angiogenesis in metastatic colorectal cancer and the benefits of targeted therapy. *J. Hematol. Oncol.* **2012**, *5*, 1-9.

85. Zwick, E. B., J.; Ullrich, A. Receptor tyrosine kinases as targets for anticancer drugs. *Trends Mol. Med.* **2002**, *8*, 17-23.

86. Heymann, D.; Redini, F. Targeted therapies for bone sarcomas. *BoneKEy Rep.* **2013**, *2*, Article number: 378 (2013).

87. Floor, S. L. D., J. E.; Maenhaut, C.; Raspe, E. Hallmarks of cancer: Of all cancer cells, all the time? . *Trends Mol. Med.* **2012**, *18*, 509-515.

88. Levitzki, A. Tyrosine kinase inhibitors: Views of selectivity, sensitivity, and clinical performance. *Annu. Rev. Pharmacol. Toxicol.* **2013**, *53*, 161-185.

89. Cohen, M. H.; Williams, G.; Johnson, J. R.; Duan, J.; Gobburu, J.; Rahman, A.; Benson, K.; Leighton, J.; Kim, S. K.; Wood, R.; Rothmann, M.; Chen, G.; U, K. M.; Staten, A. M.; Pazdur, R. Approval summary for imatinib mesylate capsules in the treatment of chronic myelogenous leukemia. *Clin. Cancer Res.* **2002**, *8*, 935-942.

90. Shibuya, M. Vascular endothelial growth factor and its receptor system: Physiological functions in angiogenesis and pathological roles in various diseases. *J. Biochem.* **2013**, *153*, 13-19.

91. Holmes, K.; Roberts, O. L.; Thomas, A. M.; Cross, M. J. Vascular endothelial growth factor receptor-2: Structure, function, intracellular signalling and therapeutic inhibition. *Cell. Signal.* **2007**, *19*, 2003-2012.

92. Musumeci, F.; Radi, M.; Brullo, C.; Schenone, S. Vascular endothelial growth factor (vegf) receptors: Drugs and new inhibitors. *J. Med. Chem.* **2012**, *55*, 10797-10822.

93. Zhang, C. T., C.; Ding, H.; Xin, T.; Jiang, Y. Selective VEGFR inhibitors for anticancer therapeutics in clinical use and clinical trials. *Curr. Pharm. Des.* **2012**, *18*, 2921-2935.

94. Zhang, J. S., Y.; Pan, X.; He, L. Recent advances in antiangiogenic agents with VEGFR as target. *Mini Rev. Med. Chem.* **2011**, *11*, 920-946.

95. Motzer, R. J.; Hutson, T. E.; Tomczak, P.; Michaelson, M. D.; Bukowski, R. M.; Rixe, O.; Oudard, S.; Negrier, S.; Szczylik, C.; Kim, S. T.; Chen, I.; Bycott, P. W.; Baum, C. M.; Figlin, R. A. Sunitinib versus interferon alfa in metastatic renal-cell carcinoma. *N. Engl. J. Med.* **2007**, *356*, 115-124.

96. Raymond, E.; Dahan, L.; Raoul, J.-L.; Bang, Y.-J.; Borbath, I.; Lombard-Bohas, C.; Valle, J.; Metrakos, P.; Smith, D.; Vinik, A.; Chen, J.-S.; Hörsch, D.; Hammel, P.; Wiedenmann, B.; Van Cutsem, E.; Patyna, S.; Lu, D. R.; Blanckmeister, C.; Chao, R.; Ruszniewski, P. Sunitinib malate for the treatment of pancreatic neuroendocrine tumors. *N. Engl. J. Med.* **2011**, *364*, 501-513.

97. Demetri, G. D.; van Oosterom, A. T.; Garrett, C. R.; Blackstein, M. E.; Shah, M. H.; Verweij, J.; McArthur, G.; Judson, I. R.; Heinrich, M. C.; Morgan, J. A.; Desai, J.; Fletcher, C. D.; George, S.; Bello, C. L.; Huang, X.; Baum, C. M.; Casali, P. G.

Efficacy and safety of sunitinib in patients with advanced gastrointestinal stromal tumour after failure of imatinib: A randomised controlled trial. *Lancet* **2006**, *368*, 1329-1338.

98. Escudier, B.; Eisen, T.; Stadler, W. M.; Szczylik, C.; Oudard, S.; Siebels, M.; Negrier, S.; Chevreau, C.; Solska, E.; Desai, A. A.; Rolland, F.; Demkow, T.; Hutson, T. E.; Gore, M.; Freeman, S.; Schwartz, B.; Shan, M.; Simantov, R.; Bukowski, R. M. Sorafenib in advanced clear-cell renal-cell carcinoma. *N. Engl. J. Med.* **2007**, *356*, 125-134.
99. Llovet, J. M.; Ricci, S.; Mazzaferro, V.; Hilgard, P.; Gane, E.; Blanc, J.-F.; de Oliveira, A. C.; Santoro, A.; Raoul, J.-L.; Forner, A.; Schwartz, M.; Porta, C.; Zeuzem, S.; Bolondi, L.; Greten, T. F.; Galle, P. R.; Seitz, J.-F.; Borbath, I.; Häussinger, D.; Giannaris, T.; Shan, M.; Moscovici, M.; Voliotis, D.; Bruix, J. Sorafenib in advanced hepatocellular carcinoma. *N. Engl. J. Med.* **2008**, *359*, 378-390.
100. Brose, M. S.; Nutting, C. M.; Jarzab, B.; Elisei, R.; Siena, S.; Bastholt, L.; de la Fouchardiere, C.; Pacini, F.; Paschke, R.; Shong, Y. K.; Sherman, S. I.; Smit, J. W. A.; Chung, J.; Kappeler, C.; Peña, C.; Molnár, I.; Schlumberger, M. J. Sorafenib in radioactive iodine-refractory, locally advanced or metastatic differentiated thyroid cancer: a randomised, double-blind, phase 3 trial. *Lancet* **2014**, *384*, 319-328.
101. Heldin, C.-H. Targeting the PDGF signaling pathway in tumor treatment. *Cell Commun. Signal.* **2013**, *11*, 97.
102. Patel, R. Y. L., H. Targeting the EGFR-family for therapy: Biological challenges and clinical perspective. *Curr. Pharm. Des.* **2012**, *18*, 2672-2679.

103. Scagliotti, G.; Govindan, R. Targeting angiogenesis with multitargeted tyrosine kinase inhibitors in the treatment of non-small cell lung cancer. *Oncologist* **2010**, *15*, 436-446.

104. Seshacharyulu, P. P., M. P.; Haridas, D.; Jain, M.; Ganti, A. K.; Batra, S. K. Targeting the EGFR signaling pathway in cancer therapy. *Expert Opin. Ther. Targets* **2012**, *16*, 15-31.

105. Welch, S. A.; Moore, M. J. Erlotinib: Success of a molecularly targeted agent for the treatment of advanced pancreatic cancer. *Future Oncol.* **2007**, *3*, 247-254.

106. Shepherd, F. A.; Rodrigues Pereira, J.; Ciuleanu, T.; Tan, E. H.; Hirsh, V.; Thongprasert, S.; Campos, D.; Maoleekoonpiroj, S.; Smylie, M.; Martins, R.; van Kooten, M.; Dediu, M.; Findlay, B.; Tu, D.; Johnston, D.; Bezjak, A.; Clark, G.; Santabárbara, P.; Seymour, L. Erlotinib in previously treated non–small-cell lung cancer. *N. Engl. J. Med.* **2005**, *353*, 123-132.

107. Liao, J. J. A., R. C. Targeting protein multiple conformations: A structure-based strategy for kinase drug design. *Curr. Top. Med. Chem.* **2007**, *7*, 1394-1407.

108. Scapin, G. Structural biology in drug design: Selective protein kinase inhibitors. *Drug Discov. Today* **2002**, *7*, 601-611.

109. Mendrola, J. M.; Shi, F.; Park, J. H.; Lemmon, M. A. Receptor tyrosine kinases with intracellular pseudokinase domains. *Biochem. Soc. Trans.* **2013**, *41*, 1029-1036.

110. Morphy, R. Selectively nonselective kinase inhibition: Striking the right balance. *J. Med. Chem.* **2009**, *53*, 1413-1437.

111. Liu, Y.; Gray, N. S. Rational design of inhibitors that bind to inactive kinase conformations. *Nat. Chem. Biol.* **2006**, *2*, 358-364.

112. Fabbro, D.; Ruetz, S.; Buchdunger, E.; Cowan-Jacob, S. W.; Fendrich, G.; Liebetanz, J.; Mestan, J.; O'Reilly, T.; Traxler, P.; Chaudhuri, B.; Fretz, H.; Zimmermann, J.; Meyer, T.; Caravatti, G.; Furet, P.; Manley, P. W. Protein kinases as targets for anticancer agents: From inhibitors to useful drugs. *Pharmacol. Ther.* **2002**, *93*, 79-98.

113. Levitzki, A. Tyrosine kinase inhibitors: Views of selectivity, sensitivity, and clinical performance. *Annu. Rev. Pharmacol. Toxicol.* **2013**, *53*, 161-185.

114. Costantino, L. B., D. Designed multiple ligands: Basic research vs clinical outcomes *Curr. Med. Chem.* **2012**, *19*, 3353-3387.

115. Melisi, D. P., G.; Tamburrino, A.; Carbone, C.; Tortora, G. Rationale and clinical use of multitargeting anticancer agents. *Curr. Opin. Pharmacol.* **2013**, *13*, 536-542.

116. Morphy, R.; Rankovic, Z. Designed multiple ligands. An emerging drug discovery paradigm. *J. Med. Chem.* **2005**, *48*, 6523-6543.

117. Arooj, M. S., S.; Cao, G. p.; Lee, K. W. An innovative strategy for dual inhibitor design and its application in dual inhibition of human thymidylate synthase and dihydrofolate reductase enzymes. *PLoS ONE* **2013**, *8*, e60470.

118. Azmi, A. S. Network pharmacology for cancer drug discovery: Are we there yet? . *Future Med. Chem.* **2012**, *4*, 939-941.

119. Markman, M. Combination cytotoxic and antiangiogenic therapy in the management of epithelial ovarian cancer. *Comb. Prod. Ther.* **2012**, *1*, 1-7.

120. Bischof, M.; Abdollahi, A.; Gong, P.; Stoffregen, C.; Lipson, K. E.; Debus, J. ü.; Weber, K. J.; Huber, P. E. Triple combination of irradiation, chemotherapy (pemetrexed), and VEGFR inhibition (SU5416) in human endothelial and tumor cells. *Int. J. Radiat. Oncol. Biol. Phys.* **2004**, *60*, 1220-1232.

121. Bello, E.; Taraboletti, G.; Colella, G.; Zucchetti, M.; Forestieri, D.; Licandro, S. A.; Berndt, A.; Richter, P.; D'Incalci, M.; Cavalletti, E.; Giavazzi, R.; Camboni, G.; Damia, G. The tyrosine kinase inhibitor E-3810 combined with paclitaxel inhibits the growth of advanced-stage triple-negative breast cancer xenografts. *Mol. Cancer Ther.* **2013**, *12*, 131-140.

122. Boere, I. A.; Hamberg, P.; Sleijfer, S. It takes two to tango: Combinations of conventional cytotoxics with compounds targeting the vascular endothelial growth factor–vascular endothelial growth factor receptor pathway in patients with solid malignancies. *Cancer Sci.* **2010**, *101*, 7-15.

123. Jo, M. Y. K., Y. G.; Kim, Y.; Lee, S. J.; Kim, M. H.; Joo, K. M.; Kim, H. H.; Nam, D. H. Combined therapy of temozolomide and ZD6474 (vandetanib) effectively reduces glioblastoma tumor volume through anti-angiogenic and anti-proliferative mechanisms. *Mol. Med. Rep.* **2012**, *6*, 88-92.

124. Liu, J.; Guo, W.; Xu, B.; Ran, F.; Chu, M.; Fu, H.; Cui, J. Angiogenesis inhibition and cell cycle arrest induced by treatment with Pseudolarix acid B alone or combined with 5-fluorouracil. *Acta Biochim. Biophys. Sin.* **2012**, *44*, 490-502.

125. Gangjee, A.; Zaware, N.; Raghavan, S.; Ihnat, M.; Shenoy, S.; Kisliuk, R. L. Single agents with designed combination chemotherapy potential: Synthesis and evaluation of substituted pyrimido[4,5-*b*]indoles as receptor tyrosine kinase and

thymidylate synthase inhibitors and as antitumor agents. *J. Med. Chem.* **2010**, *53*, 1563-1578.

126. Gangjee, A.; Pavana, R. K.; Ihnat, M. A.; Thorpe, J. E.; Disch, B. C.; Bastian, A.; Bailey-Downs, L. C.; Hamel, E.; Bai, R. Discovery of antitubulin agents with antiangiogenic activity as single entities with multitarget chemotherapy potential. *ACS Med. Chem. Lett.* **2014**, *5*, 480-484.
127. Gangjee, A.; Zeng, Y.; Ihnat, M.; Warnke, L. A.; Green, D. W.; Kisliuk, R. L.; Lin, F.-T. Novel 5-substituted, 2,4-diaminofuro[2,3-*d*]pyrimidines as multireceptor tyrosine kinase and dihydrofolate reductase inhibitors with antiangiogenic and antitumor activity. *Bioorg. Med. Chem.* **2005**, *13*, 5475-5491.
128. Venugopalan, B.; Desai, P. D.; De Souza, N. J. Synthesis of 6,7-dimethoxypyrimido[4,5-*b*]-indoles as potential antihypertensive agents. *J. Heterocycl. Chem.* **1988**, *25*, 1633-1639.
129. Tichý, M.; Pohl, R.; Xu, H. Y.; Chen, Y.-L.; Yokokawa, F.; Shi, P.-Y.; Hocek, M. Synthesis and antiviral activity of 4,6-disubstituted pyrimido[4,5-*b*]indole ribonucleosides. *Bioorg. Med. Chem.* **2012**, *20*, 6123-6133.
130. Showalter, H. D. H.; Bridges, A. J.; Zhou, H.; Sercel, A. D.; McMichael, A.; Fry, D. W. Tyrosine kinase inhibitors. 16. 6,5,6-Tricyclic benzothieno[3,2-*d*]pyrimidines and pyrimido[5,4-*b*]- and -[4,5-*b*]indoles as potent inhibitors of the epidermal growth factor receptor tyrosine kinase. *J. Med. Chem.* **1999**, *42*, 5464-5474.
131. Kumar, A. S.; Amulya Rao, P. V.; Nagarajan, R. Synthesis of pyrido[2,3-*b*]indoles and pyrimidoindoles via Pd-catalyzed amidation and cyclization. *Org. Biomol. Chem.* **2012**, *10*, 5084-5093.

132. Traxler, P. M.; Furet, P.; Mett, H.; Buchdunger, E.; Meyer, T.; Lydon, N. 4-(Phenylamino)pyrrolopyrimidines: Potent and selective, ATP site directed inhibitors of the EGF-receptor protein tyrosine kinase. *J. Med. Chem.* **1996**, *39*, 2285-2292.

133. Müller, C. E.; Geis, U.; Grahner, B.; Lanzner, W.; Eger, K. Chiral pyrrolo[2,3-*d*]pyrimidine and pyrimido[4,5-*b*]indole derivatives: Structure−activity relationships of potent, highly stereoselective A1-adenosine receptor antagonists. *J. Med. Chem.* **1996**, *39*, 2482-2491.

134. Wright, G. E. 9*H*-Pyrimido[4,5-*b*]indole-2,4-diones. The acid-catalyzed cyclization of 6-(phenylhydrazino)uracils. *J. Heterocycl. Chem.* **1976**, *13*, 539-544.

135. Dotzauer, B.; Troschütz, R. Synthesis of medicinally interesting 2,4-diamino-9*H*-pyrimido[4,5-*b*]indol-6-ols via extension of the Nenitzescu reaction. *Synlett* **2004**, 1039-1043.

136. Lapachev, V.; Stadlbauer, W.; Kappe, T. 4-Aminouracils and pyrimido[4,5-*b*]indolediones from 4-azidouracils. *Monatsh. Chem.* **1988**, *119*, 97-102.

137. Mauragis, M. A.; Veley, M. F.; Lipton, M. F. Evaluation and rapid scale-up of the synthesis of the pyrrolopyrimidines U-101033E and U-104067F. *Org. Process Res. Dev.* **1997**, *1*, 39-44.

138. Zhang, Y.-M.; Razler, T.; Jackson, P. F. Synthesis of pyrimido[4,5-*b*]indoles and benzo[4,5]furo[2,3-*d*]pyrimidines via palladium-catalyzed intramolecular arylation. *Tetrahedron Lett.* **2002**, *43*, 8235-8239.

139. Adib, M.; Mohammadi, B.; Bijanzadeh, H. R. A novel and simple synthesis of 9*H*-pyrimido[4,5-*b*]indoles under microwave irradiation and solvent-free conditions. *Synlett* **2008**, 177-180.

140. Borovik, V. P.; Shkurko, O. P. Synthesis of functional 2-substituted 4-phenyl-9*H*-pyrimido[4,5-*b*]indoles. *Russ. Chem. Bull.* **2002**, *51*, 2129-2133.

141. Majumder, S.; Bhuyan, P. J. One-pot multi-component synthesis of pyrimido[4,5-*b*]indoles in solvent-free condition. *J. Iran. Chem. Soc.* **2014**, *11*, 993-996.

142. Molina, P.; Arques, A.; Alías, A.; Vinader, M. V. Iminophosphorane-mediated synthesis of functionalized indoles and 1,3-benzodiazepines. *Tetrahedron Lett.* **1991**, *32*, 4401-4404.

143. Gewald, K. Heterocycles from CH-acidic nitriles. IX. Reaction of α-hydroxy ketones with malononitrile. *Chem. Ber.* **1966**, *99*, 1002-1007.

144. Miyazaki, Y.; Matsunaga, S.; Tang, J.; Maeda, Y.; Nakano, M.; Philippe, R. J.; Shibahara, M.; Liu, W.; Sato, H.; Wang, L.; Nolte, R. T. Novel 4-amino-furo[2,3-*d*]pyrimidines as Tie-2 and VEGFR2 dual inhibitors. *Bioorg. Med. Chem. Lett.* **2005**, *15*, 2203-2207.

145. Miyazaki, Y.; Maeda, Y.; Sato, H.; Nakano, M.; Mellor, G. W. Rational design of 4-amino-5,6-diaryl-furo[2,3-d]pyrimidines as potent glycogen synthase kinase-3 inhibitors. *Bioorg. Med. Chem. Lett.* **2008**, *18*, 1967-1971.

146. Han, Y.; Ebinger, K.; Vandevier, L. E.; Maloney, J. W.; Nirschl, D. S.; Weller, H. N. Efficient and library-friendly synthesis of furo- and thieno[2,3-*d*]pyrimidin-4-amine derivatives by microwave irradiation. *Tetrahedron Lett.* **2010**, *51*, 629-632.

147. Dave, K. G. S., C. J.; Devani, M. B.; Kalyanaraman, R.; Ananthan, S.; Ullas, G. V.; Bhadti, V. S. Reaction of nitriles under acidic conditions. Part I. A general method of synthesis of condensed pyrimidines. *Heterocycl. Chem.* **1980**, *17*, 1497-1500.

148. Foloppe, N.; Fisher, L. M.; Howes, R.; Kierstan, P.; Potter, A.; Robertson, A. G. S.; Surgenor, A. E. Structure-based design of novel Chk1 Inhibitors: Insights into hydrogen bonding and protein−ligand affinity. *J. Med. Chem.* **2005**, *48*, 4332-4345.

149. Martin-Kohler, A.; Widmer, J.; Bold, G.; Meyer, T.; Séquin, U.; Traxler, P. Furo[2,3-*d*]pyrimidines and oxazolo[5,4-*d*]pyrimidines as inhibitors of receptor tyrosine kinases (RTK). *Helv. Chim. Acta* **2004**, *87*, 956-975.

150. Dang, Q.; Liu, Y. An efficient entry to furo[2,3-*d*]pyrimidines via inverse electron demand Diels–Alder reactions of 2-aminofurans with 1,3,5-triazines. *Tetrahedron Lett.* **2009**, *50*, 6758-6760.

151. Bisagni, E. M., J. P.; Andre-Louisfert, J. 2,3-Disubstituted furans and pyrroles. VI. Synthesis of some new pyrimidines and their transformation into furo- and pyrrolo[2,3-*d*]pyrimidines. *Bull. Soc. Chim. Fr.* **1969**, *3*, 803-811.

152. Sakamoto, T.; Kondo, Y.; Yamanaka, H. Studies on pyrimidine derivatives. XXIX. Synthesis of pyrimidines fused with five-membered heterocycles by cross-coupling of 5-iodopyrimidines with phenylacetylene and styrene. *Chem. Pharm. Bull.* **1982**, *30*, 2417-2420.

153. Liu, Z.; Li, D.; Li, S.; Bai, D.; He, X.; Hu, Y. Synthesis of novel 5,6-substituted furo[2,3-*d*]pyrimidines via Pd-catalyzed cyclization of alkynylpyrimidinols with aryl iodides. *Tetrahedron* **2007**, *63*, 1931-1936.

154. Petricci, E.; Radi, M.; Corelli, F.; Botta, M. Microwave-enhanced Sonogashira coupling reaction of substituted pyrimidinones and pyrimidine nucleosides. *Tetrahedron Lett.* **2003**, *44*, 9181-9184.

155. Eger, K.; Jalalian, M.; Schmidt, M. Steric fixation of bromovinyluracil: Synthesis of furo[2,3-*d*]pyrimidine nucleosides. *J. Heterocycl. Chem.* **1995**, *32*, 211-218.

156. Sennino, B.; McDonald, D. M. Controlling escape from angiogenesis inhibitors. *Nat. Rev. Cancer* **2012**, *12*, 699-709.

157. Ribatti, D. Novel angiogenesis inhibitors: Addressing the issue of redundancy in the angiogenic signaling pathway. *Cancer Treat. Rev.* **2011**, *37*, 344-352.

158. Stein, M. N.; Flaherty, K. T. CCR drug updates: Sorafenib and sunitinib in renal cell carcinoma. *Clin. Cancer Res.* **2007**, *13*, 3765-3770.

159. Ma, J.; Waxman, D. J. Combination of antiangiogenesis with chemotherapy for more effective cancer treatment. *Mol. Cancer Ther.* **2008**, *7*, 3670-3684.

160. Zaki, K. A. B., B.; Corrie, P. The role of angiogenesis inhibitors in the management of melanoma. *Curr. Top. Med. Chem.* **2012**, *12*, 32-49.

161. O'Boyle, N. M.; Meegan, M. J. Designed multiple ligands for cancer therapy. *Curr. Med. Chem.* **2011**, *18*, 4722-4737.

162. Zhan, P.; Liu, X. Designed multiple ligands: An emerging anti-HIV drug discovery paradigm. *Curr. Pharm. Des.* **2009**, *15*, 1893-1917.

163. Pasquier, E.; Kavallaris, M.; Andre, N. Metronomic chemotherapy: New rationale for new directions. *Nat. Rev. Clin. Oncol.* **2010**, *7*, 455-465.

164. Murray, A. L., S. J.; Stanley, P.; Maraveyas, A.; Cawkwell, L. Sorafenib enhances the in vitro anti-endothelial effects of low dose (metronomic) chemotherapy. *Oncol. Rep.* **2010**, *24*, 1049-1058.

165. Blansfield, J. A.; Caragacianu, D.; Alexander, H. R.; Tangrea, M. A.; Morita, S. Y.; Lorang, D.; Schafer, P.; Muller, G.; Stirling, D.; Royal, R. E.; Libutti, S. K. Combining agents that target the tumor microenvironment improves the efficacy of anticancer therapy. *Clin. Cancer Res.* **2008**, *14*, 270-280.

166. Naganuma, Y.; Choijamts, B.; Shirota, K.; Nakajima, K.; Ogata, S.; Miyamoto, S.; Kawarabayashi, T.; Emoto, M. Metronomic doxifluridine chemotherapy combined with the anti-angiogenic agent TNP-470 inhibits the growth of human uterine carcinosarcoma xenografts. *Cancer Sci.* **2011**, *102*, 1545-1552.

167. Zhou, F.; Hu, J.; Shao, J.-H.; Zou, S.-B.; Shen, S.-L.; Luo, Z.-Q. Metronomic chemotherapy in combination with antiangiogenic treatment induces mosaic vascular reduction and tumor growth inhibition in hepatocellular carcinoma xenografts. *J. Cancer Res. Clin. Oncol.* **2012**, *138*, 1879-1890.

168. Ismael, G. F. V.; Rosa, D. D.; Mano, M. S.; Awada, A. Novel cytotoxic drugs: Old challenges, new solutions. *Cancer Treat. Rev.* **2008**, *34*, 81-91.

169. Ulahannan, S. V.; Brahmer, J. R. Antiangiogenic agents in combination with chemotherapy in patients with advanced non-small cell lung cancer. *Cancer Invest.* **2011**, *29*, 325-337.

170. Bar, J.; Onn, A. Combined anti-proliferative and anti-angiogenic strategies for cancer. *Expert Opin. Pharmacother.* **2008**, *9*, 701-715.

171. Tripathy, D. Capecitabine in combination with novel targeted agents in the management of metastatic breast cancer: Underlying rationale and results of clinical trials. *Oncologist* **2007**, *12*, 375-389.

172. Heist, R. S.; Wang, X.; Hodgson, L.; Otterson, G. A.; Stinchcombe, T. E.; Gandhi, L.; Villalona-Calero, M. A.; Watson, P.; Vokes, E. E.; Socinski, M. A. A randomized phase II study to assess the efficacy of pemetrexed or sunitinib or pemetrexed plus sunitinib in the second-line treatment of advanced non–small-cell lung cancer. *J. Thorac. Oncol.* **2014**, *9*, 214-221.

173. Gangjee, A.; Zaware, N. Unpublished results.

174. Gangjee, A.; Zhang, X.; Namjoshi, O.; Devambatla, R. K. V.; Hamel, E.; Mooberry, S. L. Design, synthesis and biological evaluation of substituted furo[2,3-*d*]pyrimidines as potent microtubule targeting antitumor agents that circumvent Pgp and βIII-tubulin mediated resistance [abstract]. In: Proceedings of the 102nd Annual Meeting of the American Association for Cancer Research; 2011 April 2–6; Orlando, FL. Philadelphia (PA): AACR; 2011. Abstract nr 3244.

175. Gangjee, A.; Namjoshi, O. Unpublished results.

176. McTigue, M.; Wickersham, J.; Marrone, T. La Jolla Laboratories, Pfizer Worldwide Research and Development, San Diego, CA. Discovery of the selective Vegfr inhibitor Pf-00337210 (http://www.pdb.org/pdb/explore/explore.do?structureId=2xir, accessed on 09/10/2014), **2011**.

177. Huang, D.; Zhou, T.; Lafleur, K.; Nevado, C.; Caflisch, A. Kinase selectivity potential for inhibitors targeting the ATP binding site: a network analysis. *Bioinformatics* **2010**, *26*, 198-204.

178. Gangjee, A.; Zaware, N.; Devambatla, R. K. V.; Raghavan, S.; Westbrook, C. D.; Dybdal-Hargreaves, N. F.; Hamel, E.; Mooberry, S. L. Synthesis of N^4-(substituted phenyl)-N^4-alkyl/desalkyl-9*H*-pyrimido[4,5-*b*]indole-2,4-diamines and identification of new microtubule disrupting compounds that are effective against multidrug resistant cells. *Bioorg. Med. Chem.* **2013**, *21*, 891-902.

179. Wang, Z.; Sun, Y. Targeting p53 for novel anticancer therapy. *Transl. Oncol.* **2010**, *3*, 1-12.

180. O'Connor, P. M.; Jackman, J.; Bae, I.; Myers, T. G.; Fan, S.; Mutoh, M.; Scudiero, D. A.; Monks, A.; Sausville, E. A.; Weinstein, J. N.; Friend, S.; Fornace, A. J.; Kohn, K. W. Characterization of the p53 tumor suppressor pathway in cell lines of the National Cancer Institute anticancer drug screen and correlations with the growth-inhibitory potency of 123 anticancer agents. *Cancer Res.* **1997**, *57*, 4285-4300.

181. Perez, E. A. Microtubule inhibitors: Differentiating tubulin-inhibiting agents based on mechanisms of action, clinical activity, and resistance. *Mol. Cancer Ther.* **2009**, *8*, 2086-2095.

182. Gangjee, A.; Zaware, N.; Devambatla, R. K. V.; Mooberry, S. L.; Hamel, E. *Abstracts of Papers*, 242nd National Meeting of the American Chemical Society, Denver, CO, Aug 28–Sep 1, 2011; American Chemical Society: Washington, DC, 2011; MEDI 53.

183. Ravelli, R. B. G.; Gigant, B.; Curmi, P. A.; Jourdain, I.; Lachkar, S.; Sobel, A.; Knossow, M. Insight into tubulin regulation from a complex with colchicine and a stathmin-like domain. *Nature (London, United Kingdom)* **2004**, *428*, 198-202.

184. Chemical Computing Group, Inc. Molecular Operating Environment (MOE 2013.08). http://www.chemcomp.com (accessed August 24, 2014).

185. Gangjee, A.; Zhao, Y.; Raghavan, S.; Rohena, C. C.; Mooberry, S. L.; Hamel, E. Structure-activity relationship and in vitro and in vivo evaluation of the potent cytotoxic anti-microtubule agent *N*-(4-methoxyphenyl)-*N*,2,6-trimethyl-6,7-dihydro-5*H*-cyclo-penta[*d*]pyrimidin-4-aminium chloride and its analogues as antitumor agents. *J. Med. Chem.* **2013**, *56*, 6829-6844.

186. Gangjee, A.; Zhang, X. Unpublished results.

187. Kaplan, J. E.; Benson, C.; Holmes, K. K.; Brooks, J. T.; Pau, A.; Masur, H. Guidelines for Prevention and Treatment of Opportunistic Infections in HIV-Infected Adults and Adolescents. Recommendations from CDC, The National Institutes of Health and the HIV Medicine Association of the Infectious Diseases Society of America. CDC, *MMWR*, April 10, **2009**, Vol *58*, NoRR-4.

188. Katlama, C.; De Wit, S.; O'Doherty, E.; Van Glabeke, M.; Clumeck, N; European Network for Treatment of AIDS Toxoplasmosis Study Group. Pyrimethamine-Clindamycin vs. Pyrimethamine-Sulfadiazine as acute and long-term therapy for toxoplasmic encephalitis in patients with AIDS. *Clin. Infect. Dis.* **1996**, *22*, 268-275.

189. Dedicoat, M.; Livesley, N. Management of toxoplasmic encephalitis in HIV-infected adults (with an emphasis on resource-poor settings). *Cochrane Database Syst. Rev.* **2006**, Issue 3. Art. No.: CD005420. DOI: 10.1002/14651858.CD005420.pub2.

190. Haruki, H.; Pedersen, M. G.; Gorska, K. I.; Pojer, F.; Johnsson, K. Tetrahydrobiopterin biosynthesis as an off-target of sulfa drugs. *Science* **2013**, *340*, 987-991.

191. Aspinall, T. V.; Joynson, D. H. M.; Guy, E.; Hyde, J. E.; Sims, P. F. G. The molecular basis of sulfonamide resistance in *Toxoplasma gondii* and implications for the clinical management of toxoplasmosis. *J. Infect. Dis.* **2002**, *185*, 1637-1643.

192. Gangjee, A.; Zaware, N.; Yang, J.; Devambatla, R. K. V.; Kisluik, R. L. *Abstracts of Papers*, 238th National Meeting of the American Chemical Society, Washington, DC, Aug 16–20, 2009; American Chemical Society: Washington, DC, 2009; MEDI 117.

193. Zaware, N.; Sharma, H.; Yang, J.; Devambatla, R. K. V.; Queener, S. F.; Anderson, K. S.; Gangjee, A. Discovery of potent and selective inhibitors of *Toxoplasma gondii* thymidylate synthase for opportunistic infections. *ACS Med. Chem. Lett.* **2013**, *4*, 1148-1151.

194. LeadIT2.1, St. Augustin, Germany.

195. Henderson, E. A.; Bavetsias, V.; Theti, D. S.; Wilson, S. C.; Clauss, R.; Jackman, A. L. Targeting the α-folate receptor with cyclopenta[*g*]quinazoline-based inhibitors of thymidylate synthase. *Bioorg. Med. Chem.* **2006**, *14*, 5020-5042.

196. Itoh, T.; Mase, T. A general palladium-catalyzed coupling of aryl bromides/triflates and thiols. *Org. Lett.* **2004**, *6*, 4587-4590.

197. Beletskaya, I. P.; Cheprakov, A. V. Copper in cross-coupling reactions: The post-Ullmann chemistry. *Coord. Chem. Rev.* **2004**, *248*, 2337-2364.

198. Zhang, L.; Fan, J.; Vu, K.; Hong, K.; Le Brazidec, J.-Y.; Shi, J.; Biamonte, M.; Busch, D. J.; Lough, R. E.; Grecko, R.; Ran, Y.; Sensintaffar, J. L.; Kamal, A.; Lundgren, K.; Burrows, F. J.; Mansfield, R.; Timony, G. A.; Ulm, E. H.; Kasibhatla, S. R.; Boehm, M. F. 7'-Substituted Benzothiazolothio- and Pyridinothiazolothio-Purines as Potent Heat Shock Protein 90 Inhibitors. *J. Med. Chem.* **2006**, *49*, 5352-5362.

199. Zhao, X.; Li, F.; Zhuang, W.; Xue, X.; Lian, Y.; Fan, J.; Fang, D. A new method for synthesis of Nolatrexed dihydrochloride. *Org. Process Res. Develop.* **2010**, *14*, 346-350.

200. Monnier, F.; Taillefer, M. Catalytic C-C, C-N, and C-O Ullmann-type coupling reactions. *Angew. Chem. Int. Ed.* **2009**, *48*, 6954-6971.

201. Guo, X.; Rao, H.; Fu, H.; Jiang, Y.; Zhao, Y. An inexpensive and efficient copper catalyst for *N*-arylation of amines, amides and nitrogen-containing heterocycles. *Adv. Synth. Catal.* **2006**, *348*, 2197-2202.

202. Shen, H.; Vollhardt, K. P. C. Remarkable switch in the regiochemistry of the iodination of anilines by *N*-iodosuccinimide: Synthesis of 1,2-dichloro-3,4-diiodobenzene. *Synlett* **2012**, 208-214.

203. Gangjee, A.; Zaware, N.; Raghavan, S.; Disch, B. C.; Thorpe, J. E.; Bastian, A.; Ihnat, M. A. Synthesis and biological activity of 5-chloro-N^4-substituted phenyl-9*H*-pyrimido[4,5-*b*]indole-2,4-diamines as vascular endothelial growth factor receptor-2 inhibitors and antiangiogenic agents. *Bioorg. Med. Chem.* **2013**, *21*, 1857-1864.

204. Gangjee, A.; Patel, J.; Kisliuk, R. L.; Gaumont, Y. 5,10-Methylenetetrahydro-5-deazafolic acid and analogs: Synthesis and biological activities. *J. Med. Chem.* **1992**, *35*, 3678-3685.

205. Lubinu, M. C.; De Luca, L.; Giacomelli, G.; Porcheddu, A. Microwave-promoted selective mono-N-alkylation of anilines with tertiary amines by heterogeneous catalysis. *Chem. Eur. J.* **2011**, *17*, 82-85.

206. Abdel-Magid, A. F.; Carson, K. G.; Harris, B. D.; Maryanoff, C. A.; Shah, R. D. Reductive amination of aldehydes and ketones with sodium triacetoxyborohydride. Studies on direct and indirect reductive amination procedures. *J. Org. Chem.* **1996**, *61*, 3849-3862.

207. Taylor, E. C.; Cocuzza, A. J. Synthesis and properties of 7-azaxanthopterin. *J. Org. Chem.* **1979**, *44*, 1125-1128.

208. Kobayashi, K.; Komatsu, T.; Yokoi, Y.; Konishi, H. Synthesis of 2-aminoindole-3-carboxylic acid derivatives by the copper(I) iodide catalyzed reaction of *N*-(2-iodophenyl)formamides with malononitrile or cyanoacetates. *Synthesis* **2011**, 764-768.

209. Zaware, N. Synthesis of pyrrolo[2,3-*d*]pyrimidines and pyrimido[4,5-*b*]indoles as inhibitors of multiple tyrosine kinases, folate metabolizing enzymes and tubulin. Ph.D. Dissertation, Duquesne University, Pittsburgh, PA, October 2009.

210. Risinger, A. L.; Jackson, E. M.; Polin, L. A.; Helms, G. L.; LeBoeuf, D. A.; Joe, P. A.; Hopper-Borge, E.; Luduena, R. F.; Kruh, G. D.; Mooberry, S. L. The taccalonolides: Microtubule stabilizers that circumvent clinically relevant taxane resistance mechanisms. *Cancer Res.* **2008**, *68*, 8881-8888.

211. We thank the NCI for providing the data for hollow fiber assay and in vivo toxicity study.

212. Gangjee, A.; Zhao, Y.; Hamel, E.; Westbrook, C.; Mooberry, S. L. Synthesis and biological activities of (*R*)- and (*S*)-*N*-(4-methoxyphenyl)-*N*,2,6-trimethyl-6,7-dihydro-5*H*-cyclopenta[*d*]pyrimidin-4-aminium chloride as potent cytotoxic antitubulin agents. *J. Med. Chem.* **2011**, *54*, 6151-6155.

213. Hamel, E.; Lin, C. M. Separation of active tubulin and microtubule-associated proteins by ultracentrifugation and isolation of a component causing the formation of microtubule bundles. *Biochemistry* **1984**, *23*, 4173-84.

214. Verdier-Pinard, P.; Lai, J.-Y.; Yoo, H.-D.; Yu, J.; Marquez, B.; Nagle, D. G.; Nambu, M.; White, J. D.; Falck, J. R.; Gerwick, W. H.; Day, B. W.; Hamel, E. Structure-activity analysis of the interaction of curacin A, the potent colchicine site antimitotic agent, with tubulin and effects of analogs on the growth of MCF-7 breast cancer cells. *Mol. Pharmacol.* **1998**, *53*, 62-76.

215. Stockwell, B. R.; Haggarty, S. J.; Schreiber, S. L. High-throughput screening of small molecules in miniaturized mammalian cell-based assays involving post-translational modifications. *Chem. Biol.* **1999**, *6*, 71-83.

216. Marks, M. G.; Shi, J.; Fry, M. O.; Xiao, Z.; Trzyna, M.; Pokala, V.; Ihnat, M. A.; Li, P.-K. Effects of putative hydroxylated thalidomide metabolites on blood vessel density in the chorioallantoic membrance (CAM) assay and on tumor and endothelial cell proliferation. *Biol. Pharm. Bull.* **2002**, *25*, 597-604.

217. Johnson, E. F.; Hinz, W.; Atreya, C. E.; Maley, F.; Anderson, K. S. Mechanistic characterization of *Toxoplasma gondii* thymidylate synthase (TS-DHFR)-

dihydrofolate reductase: Evidence for a TS intermediate and ts half-sites reactivity. *J. Biol. chem.* **2002**, *277*, 43126-43136.

218. Otwinowski, Z. M., W. Processing of X-ray Diffraction Data Collected in Oscillation Mode. *Methods Enzymol. Macromol. Crystallogr.* **1997**, *276*, 307-326.
219. Collaborative Computational Project, Number 4. The CCP4 Suite: Programs for Protein Crystallography. *Acta Crystallogr. D Biol. Crystallogr.* **1994**, *50*, 760-763.
220. Storoni, L. C.; McCoy, A. J.; Read, R. J. Likelihood-enhanced fast rotation functions. *Acta Crystallogr. D Biol. Crystallogr.* **2004**, *60*, 432-438.
221. Schüttelkopf, A. W.; van Aalten, D. M. F. PRODRG - a tool for high-throughput crystallography of protein-ligand complexes. *Acta Crystallogr. D Biol. Crystallogr.* **2004**, *60*, 1355-1363.
222. Emsley, P.; Cowtan, K. Coot: Model-building tools for molecular graphics. *Acta Crystallogr. D Biol. Crystallogr.* **2004**, *60*, 2126-2132.
223. DeLano, W. L. *The PyMol Molecular Graphics System*; DeLano Scientific: San Carlos, CA, 2002.

VIII. APPENDIX

A. Biological evaluations

The biological evaluations of the compounds were performed by Dr. Susan Mooberry (tumor cell inhibitory assays, microtubule depolymerization assay and in vivo xenograft studies; Department of Pharmacology, University of Texas Health Science Center at San Antonio, San Antonio, TX 78229); Dr. Ernest Hamel (colchicine binding and bovine brain tubulin polymerization assays; Screening Technologies Branch, Developmental Therapeutics Program, Division of Cancer Treatment and Diagnosis, Frederick National Laboratory for Cancer Research, National Cancer Institute, Frederick, MD 21702); Dr. Michael Ihnat (RTK inhibitory assay, tumor cell inhibitory assays, CAM assay, in vivo xenograft and allograft studies; Department of Pharmaceutical Sciences, University of Oklahoma College of Pharmacy, Oklahoma City, OK 73117); Dr. Karen Anderson (tgTS inhibitory assay and X-ray crystallography studies; Department of Pharmacology, Yale University School of Medicine, New Haven, CT 06511); Dr. Sherry F. Queener (DHFR inhibitory and *T. gondii* cell culture studies; Department of Pharmacology and Toxicology, Indiana University School of Medicine, Indianapolis, IN 46202); and National Cancer Institute (60 cell tumor cell line screening assay and in vivo toxicity study; NCI, Developmental Therapeutics Program).

A.1 Biological data of 2,4-diamino-5-arylthio-9*H*-pyrimido[4,5-*b*]indoles

Table 7 shows inhibitory data for target compounds **1a**–**7a** against EGFR, VEGFR-2 and PDGFR-β kinases. Kinase inhibition was performed in cell-based assays and therefore, it should be noted that cellular permeability might play a role in the activities

of these compounds. Whole cell assays were used for measuring RTK inhibition as these assays afford more meaningful results for translation to *in vivo* studies.

Table 7. Inhibition of RTKs by target compounds **1a**–**7a** [Data kindly provided by Dr. Michael Ihnat, Department of Pharmaceutical Sciences, University of Oklahoma College of Pharmacy, OK 73117]

Compd	Inhibition of			
	hTS (μM)	**EGFR (nM)**	**VEGFR-2 (nM)**	**PDGFR-β (nM)**
1 (lead)	0.54	15.1 ± 2.5	22.6 ± 2.7	2.8 ± 0.3
2 (lead)	0.39	10.41 ± 1.9	56.3 ± 8.2	40.3 ± 6.7
1a	n.d.[a]	26.9 ± 5.2	38.6 ± 5.2	76.9 ± 9.4
2a	n.d.[a]	11.3 ± 1.7	22.0 ± 3.7	50.0 ± 6.5
3a	n.d.[a]	27.0 ± 4.2	38.2 ± 7.0	86.1 ± 10.7
4a	n.d.[a]	23.6 ± 3.8	35.1 ± 6.6	73.1 ± 8.8
5a	n.d.[a]	12.6 ± 2.0	17.8 ± 1.9	55.8 ± 7.2
6a	n.d.[a]	24.2 ± 3.8	42.5 ± 6.9	70.1 ± 8.5
7a	n.d.[a]	n.d.[a]	n.d.[a]	n.d.[a]
Raltitrexed	0.38			
Sunitinib		172.1 ± 19.4	18.9 ± 2.7	83.1 ± 10.1
Erlotinib		1.2 ± 0.2	124.7 ± 18.2	

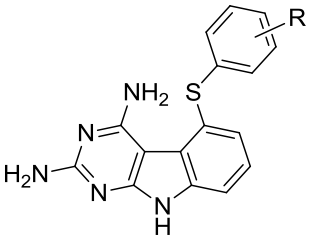

1a R = 4'-F
2a R = 4'-CF_3
3a R = 3'-Me
4a R = 2'-Me
5a R = 3',4'-diMe
6a R = 3'-OMe
7a R = 2'-OMe

[a]n.d. not determined.

The 4'-CF_3 analog **2a** and 3',4'-dimethyl analog **5a** were the most potent inhibitors against EGFR and VEGFR-2 kinases with activities comparable to the lead compound **1** where as **1a**, **3a**, **4a** and **6a** had 1.5-fold lower inhibition than **1** (Table 7). Compounds **3a** and **4a** with 3'- and 2'-methyl groups, respectively, displayed lower EGFR and VEGFR-2 kinase inhibition than the 4'-Me analog **2**, thus indicating the importance of the methyl group at *para*-position for activity. The 4'-CF_3 analog **2a** had a 2-fold increased VEGFR-

2 inhibition than the 4'-Me analog **2** and had activity comparable to the 4'-Cl analog **181**. In this series of compounds, incorporation of strong electron-withdrawing groups at *para*-position of the thioaryl moiety gave higher VEGFR-2 potency while retaining EGFR inhibition. However, this improvement in activity cannot be entirely due to electron-withdrawing effect because the 4'-F analog **1a** was less active than the 4'-H analog **1**. The 3',4'-dimethyl analog **5a** showed 3-fold higher anti-VEGFR-2 activity than the 4-Me analog **2**. In the PDGFR-β inhibition assay, target compounds **1a–6a** were 25–40-fold less active than the lead compound **1** (Table 7). The data indicates that substitution on the thioaryl ring can be detrimental to PDGFR-β kinase inhibition.

Lead compounds **1** and **2** were evaluated in MDA-MB-435 and 4T1 orthotopic breast cancer models.

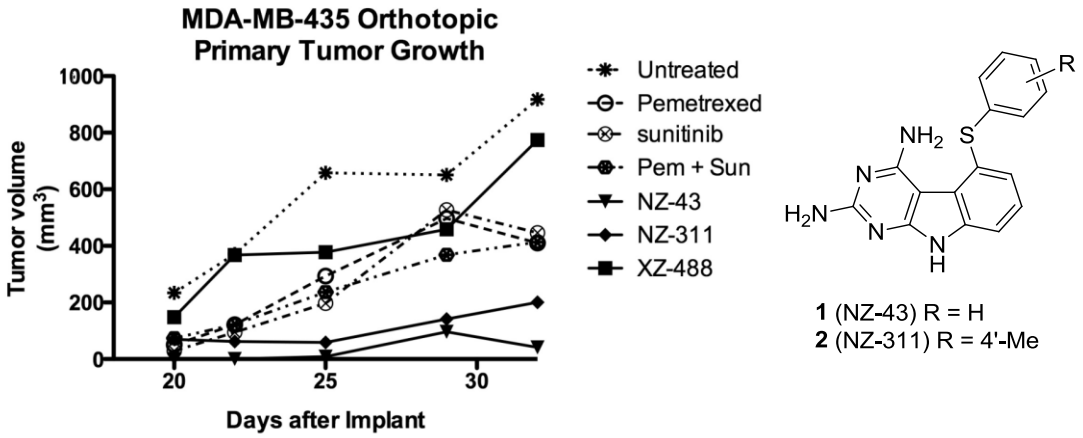

Figure 44. Compounds **1** (NZ-43) and **2** (NZ-311) significantly decreased primary tumor growth and tumor vascular density in the MDA-MB-435 flank xenograft model. Human BLBCs, MDA-MB-435, were implanted into the lateral flank of NCr athymic nu/nu nude mice at 500,000 cells, and the mice were treated with carrier, pemetrexed, sunitinib, pemetrexed + sunitinib or **1** (25 mg/kg) or **2** (35 mg/kg) twice weekly until the end of the experiment. Tumor size was assessed by measuring tumor length, width, and depth twice

weekly using Vernier calipers. Tumor volume was calculated with the ellipsoid formula: volume = 0.52 (length × width × depth) and graphically represented as days after implantation. Statistics on these graphs were two way ANOVA with repeated measures post-test. [Data kindly provided by Dr. Michael Ihnat, Department of Pharmaceutical Sciences, University of Oklahoma College of Pharmacy, OK 73117]

In the MDA-MB-435 orthotopic xenograft model, compounds **1** (25 mg/kg) and **2** (35 mg/kg) significantly decreased tumor volume better than the combination of pemetrexed (30 mg/kg) and sunitinib (30 mg/kg) (Figure 44). Based on the remarkable potency compared to the combination of pemetrexed and sunitinib, compounds **1** and **2** are undergoing further preclinical evaluation.

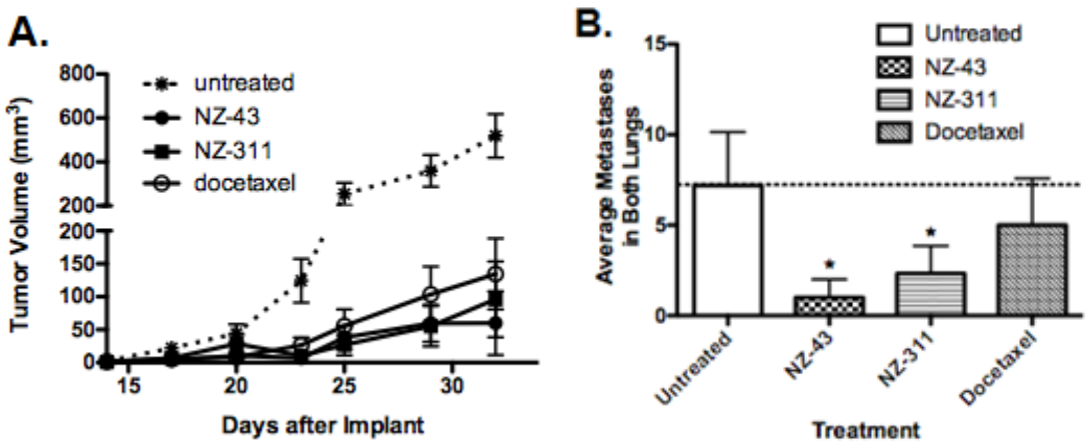

Figure 45. Compounds **1** (NZ-43) and **2** (NZ-311) decreased primary tumor growth and lung metastases in the 4T1 orthotopic breast model. *, $P < 0.05$ by one way ANOVA with a Neuman−Keuls post-test. 4T1-Lucerase/GFP tagged cells were implanted orthotopically into BALB/c mice at 7500 cells, and the mice were treated with carrier, docetaxel, or **1** or **2** at their MTDs twice weekly until the end of the experiment. (A) Tumor volume was calculated with the ellipsoid formula: volume = 0.52 (length × width × depth). (B) After 32 days, animals were euthanized and lungs were excised and

immediately imaged at 25× using the LumaScope fluorescent imaging system. The number of metastases in both lungs was counted visually and represented graphically. [Data kindly provided by Dr. Michael Ihnat, Department of Pharmaceutical Sciences, University of Oklahoma College of Pharmacy, OK 73117]

Compounds **1** (25 mg/kg) and **2** (35 mg/kg) decreased tumor volume better than or equal to docetaxel (35 mg/kg) in the 4T1 triple negative orthotopic allograft model (Figure 45A). Also, compounds **1** and **2** significantly reduced tumor metastases compared to docetaxel (Figure 45B). Reduction of tumor metastases is important because many cancer patients die of metastatic disease.

A.2 Biological data of 4-substituted 5-methyl-furo[2,3-*d*]pyrimidines

Compounds **1b**–**4b** and **1c**–**5c** were first evaluated for their ability to depolymerize microtubules (Table 8). These compounds were also tested for their antiproliferative effects against MDA-MB-435 cell lines using the sulforhodamine B (SRB) assay. Compounds **1b**–**4b** with different alkyl groups at the N^4-position had decreased microtubule depolymerizing activity and IC_{50} values compared to the lead N^4-methyl analog **182**. The activity decreased with increased homologation and the N^4-*i*Pr analog **2b** was 60-fold less active (IC_{50}) than the N^4-Et **1b**.

The N^4-Me analogs **1c**–**5c** with variations at the 4'-position were less active as microtubule depolymerizers than the lead **182**. The 4'-ethyl analog **1c** had 30-fold decreased activity than the 4'-methoxy **182**, indicating the importance of a hydrogen bond acceptor at 4'-position. The 4'-SMe analog **2c**, 4'-NHMe analog **3c** and 4'-NMe_2 analog **4c**, respectively, had 2-, 10- and 6-fold decreased microtubule depolymerizing activity than the 4'-OMe analog **182**. In addition, compounds **2c**–**4c** had 3–18-fold lesser activity

in the MDA-MB-435 cell line. This data indicates that bioisosteric replacement of 4'-OMe group is detrimental to tubulin inhibitory and antiproliferative activities. The 4'-NO_2 analog **5c**, as expected, had no activity in the microtubule depolymerization assay. N^4-Desmethyl intermediates **213**–**215**, **218** and **219** were also tested for microtubule depolymerization and were inactive with EC_{50} >10 μM (Table 8).

Table 8. Antiproliferative and microtubule depolymerizing effects of target compounds **1b**–**4b** and **1c**–**5c** and intermediates **213**–**215**, **218** and **219** [Data kindly provided by Dr. Susan Mooberry, Department of Pharmacology, University of Texas Health Science Center at San Antonio, TX 78229]

Compd	**IC_{50} ± SD (nM) (MDA-MB-435)**	**EC_{50} (nM) for microtubule depolymerization**
182 (lead)	4.3 ± 0.3	23.9 ± 5.6
1b	8.1 ± 0.47	53
2b	504 ± 28	EC_{50} >10 μM
3b	27.3 ± 4.5	310
4b	100.3 ± 6.5	340
1c	183.1 ± 12.7	750
2c	12.3 ± 0.9	45
3c	73.7 ± 2.7	240
4c	43.8 ± 4.2	140
5c	n.d.	EC_{50} >10 μM
213	n.d.	EC_{50} >10 μM
214	n.d.	EC_{50} >10 μM
215	n.d.	EC_{50} >10 μM
218	n.d.	EC_{50} >10 μM
219	n.d.	EC_{50} >10 μM
CA4	4.4 ± 0.46	9.8

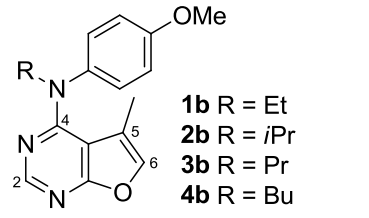

1b R = Et
2b R = *i*Pr
3b R = Pr
4b R = Bu

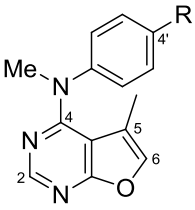

1c R = Et
2c R = SMe
3c R = NHMe
4c R = NMe_2
5c R = NO_2

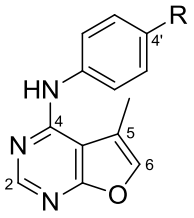

213 R = Et
214 R = SMe
215 R = NHMe
218 R = NMe_2
219 R = NO_2

[a]n.d. not determined.

Table 9. Effects of **1b**–**4b** and **2c** on tubulin assembly and colchicine binding [Data kindly provided by Dr. Ernest Hamel, Division of Cancer Treatment and Diagnosis, Frederick National Laboratory for Cancer Research, National Cancer Institute, MD 21702]

Compd	**Inhibition of tubulin assembly (IC_{50} ± SD (μM))**	**Inhibition of colchicine binding (% inhibition ± SD)**	
		1 μM	**5 μM**
182 (lead)	3.3 ± 0.5	71 ± 6	96 ± 2
1b	0.97 ± 0.09	84 ± 0.7	95 ± 0.5
2b	3.0 ± 0.2		47 ± 0.2
3b	1.1 ± 0.1	75 ± 1	92 ± 0.3
4b	1.3 ± 0.2	61 ± 0.4	87 ± 0.2
2c	1.2 ± 0.007	79 ± 2	94 ± 0.01
CA4	0.96 ± 0.07	90 ± 1	99 ± 0.2

Based on their microtubule depolymerizing activities, compounds **1b**–**4b**, and **2c** were tested for their direct effects on tubulin assembly and colchicine binding (Table 9). Except **2b**, all compounds, at 5 μM, inhibited [^{3}H]-colchicine binding to the protein comparable to CA4. Compounds **1b** (N^4-Et), **3b** (N^4-Pr) and **4b** (N^4-Bu) inhibited tubulin assembly about as well as CA4 and about 3-fold better than **182** (N^4-Me).

Compounds **1b**, **3b** and **4b**, at 5 μM concentration, also inhibited binding of [^{3}H]-colchicine by 87–95%, whereas the N^4-isopropyl analog **2b** showed only 47% inhibition (Table 9). The lower activity might be due to steric hindrance in the colchicine binding site. The data indicates that the N^4-alkylation is tolerated for tubulin inhibition. Compound **2c** (4'-SMe) inhibited tubulin assembly comparable to CA4 and is 3-fold better than the lead 4'-OMe analog **182**.

Table 10. RTK inhibitory activities of target compounds **1b**–**3b** and **1c**–**5c** and intermediates **214**, **215**, **218** and **219** [Data kindly provided by Dr. Michael Ihnat, Department of Pharmaceutical Sciences, University of Oklahoma College of Pharmacy, OK 73117]

Compd	**EGFR (nM)**	**VEGFR-2 (nM)**	**PDGFR-β (nM)**	**A431 Cytotoxicity (nM)**	**CAM angiogenesis inhibition (μM)**
182 (lead)	15.5 ± 2.0	9.3 ± 0.72	12.3 ± 2.0	5.1 ± 0.56	n.d.
1b	92.5 ± 9.9	67.3 ± 6.9	51.4 ± 7.2	3.4 ± 3.3	0.812 ± 0.091
2b	10.1 ± 0.91	23.4 ± 4.1	42.6 ± 5.6	4.8 ± 3.1	0.480 ± 0.078
3b	7.1 ± 0.74	12.0 ± 1.6	38.9 ± 6.6	2.3 ± 2.5	0.301 ± 0.044
1c	4.0 ± 0.39	7.8 ± 0.94	28.9 ± 4.0	1.4 ± 0.5	0.287 ± 0.040
2c	7.2 ± 0.81	13.6 ± 2.0	62.2 ± 9.6	2.9 ± 3.0	0.520 ± 0.051
3c	6.4 ± 0.97	12.7 ± 1.8	57.8 ± 9.9	2.9 ± 3.4	0.707 ± 0.082
4c	3.1 ± 0.06	15.6 ± 2.2	63.0 ± 10.7	1.0 ± 0.1	0.653 ± 0.072
5c	>200	>200	>300	432.7 ± 30.7	1.058 ± 0.124
214	>200	>200	>300		
215	>200	>200	>300		
218	>200	>200	>300		
219	>200	>200	>300		
Semaxanib		12.9			60 ± 10.1
Cisplatin				10.6	18.2 ± 2.1
Sunitinib	172.1 ± 19.4	18.9 ± 2.7	83.1 ± 10.1	n.d.	1.3 ± 0.07
Erlotinib	1.2 ± 0.2	124.7 ± 18.2	n.d.	n.d.	29.1 ± 1.9

[a]n.d. not determined.

Compounds **1b**–**3b** and **1c**–**5c** were evaluated for inhibition against EGFR, VEGFR-2 and PDGFR-β kinases using high-throughput phosphotyrosine ELISA (Table 10). Compounds **3b** and **1c**–**4c** inhibited EGFR kinase less than 5-fold compared to the standard EGFR kinase inhibitor erlotinib. The N^4-Me-4'-*N*,*N*-diMe analog **4c** is the most

potent EGFR kinase inhibitor with an IC_{50} of 3.1 nM. With the exception of compound **1b**, the EGFR kinase inhibition data correlated very well with the A431 cytotoxicity data. Compounds **1b**–**3b** and **1c**–**4c** had single-digit nanomolar IC_{50} values in EGFR-overexpressing A431 cells.

Compounds **2c**, **3c** and **1c**–**4c** showed VEGFR-2 kinase inhibition better than or equal to the standard VEGFR-2 kinase inhibitor sunitinib (Table 10). In PDGFR-β kinase assay, compounds **1b**–**3b** and **1c**–**4c** had better activity than the standard sunitinib. Antiangiogenic effects of target compounds were evaluated using chorioallantoic membrane (CAM) assay. Compounds **1b**–**3b** and **1c**–**4c** had submicromolar inhibition of angiogenesis and are more potent than multi-RTK inhibitor sunitinib. Among the target compounds, compounds **3b** and **1c** are the most potent compounds in the CAM assay, with potencies about 4-fold better than sunitinib. Compound **5c** with electron-withdrawing NO_2 group at the 4'-position showed no activity against EGFR, VEGFR-2 and PDGFR-β kinases. However, in the CAM assay, compound **5c** had potency comparable to sunitinib. N^4-Desmethyl intermediates **213**–**215**, **218** and **219** were also tested for RTK inhibition and were inactive (IC_{50} >200 nM) against VEGFR-2, PDGFR-β and EGFR kinases.

At the N^4-position, longer chain alkyl groups were favored for the inhibition of tubulin and EGFR kinase but were not tolerated for VEGFR-2 and PDGFR-β inhibition, indicating steric intolerance at the N^4-position for anti-VEGFR-2 and anti-PDGFR-β activity. At the 4'-position of furo[2,3-*d*]pyrimidines, both hydrogen-bond acceptor and hydrophobic group were required for inhibition of tubulin and EGFR kinase. However, for VEGFR-2 and PDGFR-β inhibition, hydrogen-bond acceptor at 4'-position was not

required. Compounds **1b**, **3b** and **2c**–**4c** had potent multi-RTK inhibition along with potent anti-tubulin activity, thus making them single agents with combination chemotherapy potential. Compounds **2b** (N^4-*i*Pr-4'-OMe) and **1c** (N^4-Me-4'-Et) showed potent RTK inhibition with weak microtubule depolymerizing activity. Therefore, compounds **2b** and **1c** can be used in anticancer chemotherapy either alone as RTK inhibitors or in combination chemotherapy with other cytotoxic agents.

Table 11. Target compounds **1b**, **3b**, **4b** and **1c**–**4c** circumvent Pgp and βIII-tubulin mediated resistance [Data kindly provided by Dr. Susan Mooberry, Department of Pharmacology, University of Texas Health Science Center at San Antonio, TX 78229]

Compd	**IC_{50} ± SD (nM)**			**IC_{50} ± SD (nM)**		
	SKOV3	**SKOV3-MDR1-M6/6**	**Rr**[a]	**HeLa**	**HeLa WTβIII**	**Rr**[a]
182 (lead)	7.7 ± 0.8	8.4 ± 0.4	1.1	9.5 ± 0.8	8.1 ± 0.9	0.9
1b	14.5 ± 1.0	18.3 ± 1.0	1.3	15.8 ± 1.4	14.6 ± 1.8	0.9
3b	40.3 ± 2.6	71.0 ± 19	1.8	33.8 ± 7.4	35.3 ± 9.9	1.0
4b	147.8 ± 2.9	200.0 ± 17.1	1.4	111.1 ± 19.0	115.9 ± 9.8	1.0
1c	155.8 ± 15.0	161.9 ± 21.5	1.0	120.5 ± 4.2	159.0 ± 17.6	1.3
2c	18.6 ± 0.1	32.1 ± 1.5	1.7	15.7 ± 1.2	14.9 ± 1.9	0.9
3c	73.8 ± 1.8	85.6 ± 5.0	1.2	95.0 ± 9.0	101.0 ± 22.0	1.1
4c	70.3 ± 6.1	91.2 ± 19.5	1.3	57.7 ± 5.0	59.4 ± 6.8	1
Paclitaxel	5.0 ± 0.6	1,200 ± 58	240	2.8 ± 0.36	24.0 ± 3.0	8.6
CA4	5.5 ± 0.5	7.2 ± 1.1	1.3	3.3 ± 0.4	3.3 ± 0.3	1

[a]Rr: Relative resistance

Potent microtubule depolymerizing agents **1b**, **3b**, **4b** and **1c**–**4c** were evaluated for Pgp-mediated drug resistance in an SKOV3 isogenic cell line pair (Table 11).[210] This cell line pair consists of the parental SKOV3 ovarian carcinoma cell and the Pgp-overexpressing SKOV3 MDR-1-6/6 cell line. The relative resistance value, designated

Rr, is obtained by dividing the IC_{50} values obtained in the Pgp-expressing MDR-1-6/6 cells by the IC_{50} obtained in the parental cells. A low Rr indicates that the cell lines have similar sensitivity to the compound and that the compound is able to overcome the expression of Pgp. It also suggests that the compound is a poor substrate for transport by Pgp. On the other hand, compound with a high Rr value indicates Pgp-mediated drug resistance. In this cell line pair, paclitaxel has a high Rr value of 240 (Table 11) while target compounds **1b**, **3b**, **4b** and **1c**–**4c** had low Rr values of less than 2, similar to that observed with CA-4. The data indicates that the target compounds circumvent Pgp-mediated drug resistance observed with taxanes and vinca alkaloids.

Compounds **1b**, **3b**, **4b** and **1c**–**4c** were also assessed for βIII-tubulin mediated resistance in an isogenic HeLa cell line pair (Table 11).[210] Rr value of a compound will be obtained by dividing the IC_{50} value of the compound in the βIII-tubulin expressing HeLa WTβIII cell line by the IC_{50} value in the parental HeLa cell line. Paclitaxel showed βIII-tubulin mediated resistance as it had an Rr value of 8.6. Compounds **1b**, **3b**, **4b** and **1c**–**4c** had an Rr value of ≈1.0 implying equal sensitivity to the βIII-expressing cell line. The data suggests that these compounds circumvent βIII-tubulin mediated resistance associated with taxanes and vinca alkaloids.

The NCI performed the hollow fiber assay[211] for lead compound **182**. The hollow fiber assay provides an initial *in vivo* experience for agents found to have reproducible activity in *in vitro* anticancer assays. Tumor cell lines used in the hollow fiber assay are non-small cell lung carcinoma lines NCI-H23 and NCI-H522, breast carcinoma lines MDA-MB-231 and MDA-MB-435, colon sarcoma lines SW-620 and COLO 205, melanoma lines LOX and UACC-62, ovarian carcinoma lines OVCAR-3 and OVCAR-5,

and glioma lines U251 and SF-295. Compound **182** had an intraperitoneal (ip) score of 20 out of 48, subcutaneous (sc) score of 12 out of 48 and total score of 32 of 96. Based on the hollow fiber assay data, compound **182** was selected for xenograft studies in mice.

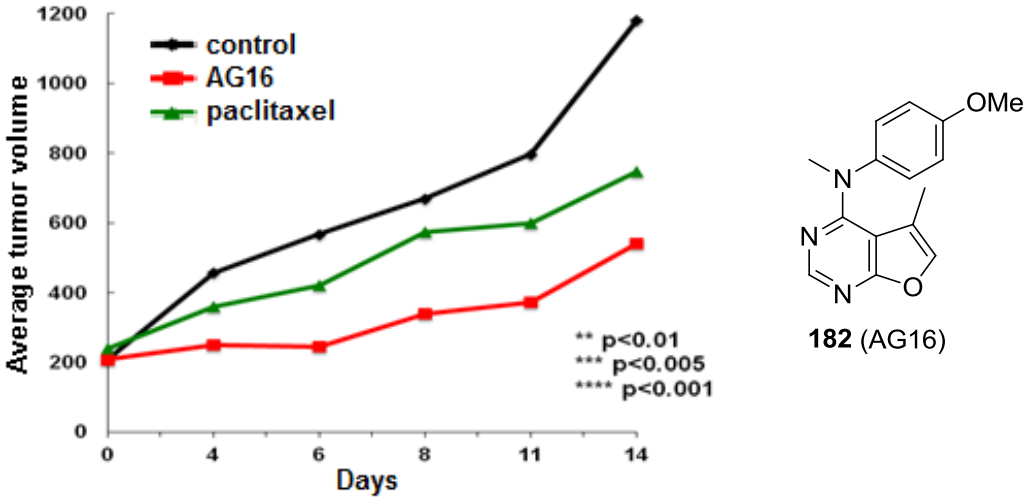

Figure 46. Compound **182** (AG16) considerably decreased tumor volume in MDA-MB-435 tumor xenografts. [Data kindly provided by Dr. Susan Mooberry, Department of Pharmacology, University of Texas Health Science Center at San Antonio, TX 78229]

Compound **182** (AG16) was tested for antitumor effects in MDA-MB-435 tumor fragments (Figure 46). MDA-MB-435 tumor fragments were injected s.c. into the flank of nude mice. Once tumors reached ~200 mm^3, mice were injected i.p. with **182** (60 mg/kg on days 1 and 3 and 50 mg/kg on day 9) or paclitaxel (20 mg/kg every other day until day 11). Three doses of **182** (60 mg/kg on days 1 and 3, and 50 mg/kg on day 9) led to highly significant inhibition of tumor growth superior to paclitaxel throughout the trial.

The NCI performed toxicity studies on **182** in the athymic nude mice.[211] Compound **182** in 100% DMSO was administered i.p. on Day 1 and the mice were observed for survival for 15 days. Mice with the compound dose of 12.5, 25 and 50 mg/kg survived for 15 days. Higher compound doses of 100, 250 and 500 mg/kg resulted in the death of

mice after 4, 1 and 1 days respectively. Based on this data, compound **182** can be considered safe at doses ≤50 mg/kg in mice.

A.3 Biological data of N^4-aryl-5-chloro-2,4-diamino-pyrimido[4,5-*b*]indoles

Compounds **1d**–**4d** and **6d** were evaluated for antiproliferative effects in MDA-MB-435 cell lines (Table 12). Compounds **1d**–**4d** had >40-fold lower activity than the 4'-OMe analog **183**. The data indicates that the methoxy group at 4'-position is important for antiproliferative activity. Compound **6d** displayed 1.5-fold higher IC_{50} than **183**, indicating that conformational restriction of the N^4-phenyl ring is not conducive to activity.

Table 12. Antiproliferative and microtubule depolymerizing effects of **1d**–**6d** [Data kindly provided by Dr. Susan Mooberry, Department of Pharmacology, University of Texas Health Science Center at San Antonio, TX 78229]

Compd	**IC_{50} ± SD (μM) (MDA-MB-435)**
183 (lead)	0.183
1d	4.19 ± 0.5
2d	3.03 ± 0.3
3d	4.22 ± 0.5
4d	6.47 ± 0.3
5d	n.d.[a]
6d	0.271 ± 0.004
CA4	3.4 ± 0.6 nM

[a]n.d. not determined.

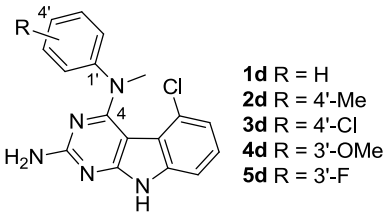

1d R = H
2d R = 4'-Me
3d R = 4'-Cl
4d R = 3'-OMe
5d R = 3'-F

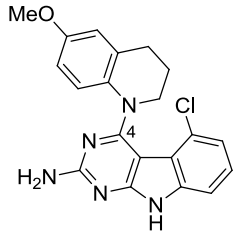

6d

Lead compound **183** was evaluated by the NCI using hollow fiber assay.[211] Compound **183** had an intraperitoneal (ip) score of 4 out of 48, subcutaneous (sc) score of

0 out of 48 and total score of 4 of 96. A compound is considered for xenograft testing if it has a combined ip + sc score of 20 or greater, a sc score of 8 or greater, or produces cell kill of any cell line at either dose level evaluated. Compound **183** (75 mg/kg) did not satisfy these criteria and hence was not selected for xenograft studies in mice.

A.4 Biological data of 2,4-substituted pyrimido[4,5-*b*]indoles

Table 13. Effects of **1e**–**3e** and **1f**–**3f** on proliferation of MDA-MB-435 cells and microtubule depolymerization in A-10 cells [Data kindly provided by Dr. Susan Mooberry, Department of Pharmacology, University of Texas Health Science Center at San Antonio, TX 78229]

Compd	**IC_{50} ± SD (nM) (MDA-MB-435)**	**EC_{50} (nM) for microtubule depolymerization**
185 (lead)	14.7 ± 1.5	105 ± 12
1e	23.5 ± 1.2	198 ± 8
2e	54.4 ± 4.0	152 ± 2.8
3e	14.4 ± 0.5	83 ± 4
1f	89.1 ± 10.2	1100
2f	33.9 ± 3.4	136
3f	130.2 ± 7.8	1200
CA4	3.4 ± 0.6	13.0

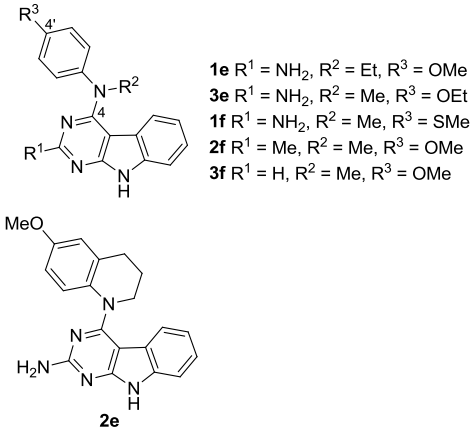

Among 2,4-substituted pyrimido[4,5-*b*]indoles **1e**–**3e** and **1f**–**3f**, compound **3e**[178] had the most antiproliferative and microtubule depolymerizing effects and was comparable or better than the lead compound **185** (Table 13). Conformationally restricted analog **2e** had 3.5-fold higher IC_{50} than **185**, thus indicating that restriction of the N^4-phenyl ring is not

tolerated. Replacement of the 4'-OMe (**185**) with 4'-SMe group (**1f**) resulted in 6-fold increase in $IC_{50.}$ The 2-methyl **2f** and the 2-H analog **3f** displayed lower activity than the 2-amino **185** in both cell proliferation and microtubule depolymerizing assays indicating the importance of 2-amino group for antitubulin activity in this series of analogs.

Table 14. Compounds **1e–3e** and **1f–3f**: Inhibition of tubulin assembly and binding of [^{3}H]-colchicine [Data kindly provided by Dr. Ernest Hamel, Division of Cancer Treatment and Diagnosis, Frederick National Laboratory for Cancer Research, National Cancer Institute, MD 21702]

Compd	**Inhibition of tubulin assembly IC_{50} ± SD (μM)**	**Inhibition of colchicine binding (% inhibition ± SD) at 5 μM**
185 (lead)	1.4 ± 0.007	84 ± 0.5
1e	1.7 ± 0.2	76 ± 3
2e	2.2 ± 0.1	71 ± 5
3e	1.7 ± 0.07	82 ± 1
1f	2.3 ± 0.3	67 ± 5
2f	1.2 ± 0.04	67 ± 5
3f	2.3 ± 0.4	62 ± 4
CA4	1.0 ± 0.09	99 ± 0.2

Target compounds **1e**, **3e** and **2f** inhibited tubulin assembly comparable to CA4 (Table 14). In this series of compounds, compound **3e**[178] was the most potent in the colchicine displacement assay, with activity comparable to the lead compound **185**.

Compounds **1e–3e** and **1f–3f** were evaluated for Pgp and βIII-tubulin mediated resistance in isogenic SKOV3 and HeLa cell line pairs, respectively (Table 15).[210] In SKOV3 cell line pair, paclitaxel has a high Rr value of 590 indicating that the cells overexpressing Pgp were resistant to paclitaxel. Target compounds **1e–3e** and **1f–3f** had

Rr values of less than 2, similar to that observed with CA-4. Compound **3e**[178] had almost 2-fold lesser activity than CA4 in both wild type and Pgp-overexpressing SKOV3 cell lines.

Table 15. Compounds **1e–3e** and **1f–3f** are effective in cell lines expressing Pgp or βIII-tubulin [Data kindly provided by Dr. Susan Mooberry, Department of Pharmacology, University of Texas Health Science Center at San Antonio, TX 78229]

Compd	**IC_{50} ± SD (nM)**			**IC_{50} ± SD (nM)**		
	SKOV3	**SKOV3 MDR-1-6/6**	**Rr**[a]	**HeLa**	**WT βIII**	**Rr**[a]
185 (lead)	27.6 ± 1.8	34.4 ± 5.9	1.2	21.3 ± 2.2	21.4 ± 3.5	1.0
1e	53.0 ± 1.9	72.0 ± 7.9	1.4	32.8 ± 0.8	45.5 ±1.0	1.4
2e	83.2 ± 5.7	134.7 ± 23.2	1.6	72.1 ± 7.9	87.0 ± 4.1	1.2
3e	23.0 ± 1.1	29.1 ± 1.7	1.3	23.1 ± 0.8	18.8 ± 0.5	0.8
1f	156.4 ± 16.0	160.1 ± 14.9	1.0	117.7 ± 13.2	78.4 ± 4.0	0.7
2f	60.5 ± 2.4	78.0 ± 8.4	1.3	50.5 ± 5.3	31.8 ± 2.5	0.6
3f	173.2 ± 8.6	223.7 ± 21.2	1.4	141.5 ± 8.1	99.5 ± 11.8	0.8
paclitaxel	4.4 ± 0.6	2596 ± 119	590	1.6 ± 0.5	9.2 ± 0.2	5.8
CA4	9.7± 0.2	11.5 ± 1.7	1.2	4.7 ± 1.1	5.2 ± 0.4	1.1

[a]Rr: Relative resistance

In the HeLa cell line pair, paclitaxel showed βIII-tubulin mediated resistance as it had an Rr value of 5.8 (Table 15) where as target compounds **1e–3e** and **1f–3f** had an Rr value of ≈1.0 implying equal sensitivity to the βIII-expressing cell line. Compound **3e**[178] displayed potency comparable to the lead compound **185** in HeLa and βIII-tubulin expressing cell lines. The data indicates that these compounds overcome Pgp and βIII-tubulin mediated resistance observed clinically with taxanes and Vinca alkaloids.

Lead compound **185** was evaluated using hollow fiber assay by the NCI.[211] Compound **185** had an intraperitoneal (ip) score of 14 out of 48, subcutaneous (sc) score

of 2 out of 48 and total score of 4 of 96. Compound **185** was not considered for xenograft studies as it had a combined ip + sc score of less than 20, a sc score of less than 8, and did not produce cell kill of any cell line at dose level (150 mg/kg) evaluated.

A.5 Biological data of 2-amino-4-oxo-5-thioaryl-9*H*-pyrimido[4,5-*b*]indoles

Table 16. Kinetic evaluation of **1g**, **2g**, **4g** and **7g** reveals species selectivity for tgTS over hTS[a]

Cmpd	IC_{50} (nM)		K_i (nM)		Selectivity
	tgTS	hTS	tgTS	hTS	(hTS K_i/ tgTS K_i)
1g	23 ± 6.6	481 ± 162	2.0 ± 0.6	55.7 ± 18.8	27.9
2g	21 ± 13	28.8 ± 21	1.8 ± 1.1	3.3 ± 2.4	1.83
4g	35.8 ± 2.9	3250 ± 184	3.1 ± 0.25	378 ± 21	121.9
7g	43.4 ± 5.2	738.7 ± 235.4	3.8 ± 0.4	85.6 ± 27.3	22.5

[a]*T. gondii* TS–DHFR (25 nM) and human TS (50 nM) were preincubated with 100 μM dUMP and inhibitor. The reaction was initiated with 100 μM methyleneTHF.

Compounds **1g**, **2g**, **4g** and **7g** exhibited single-digit nanomolar K_i values against tgTS (Table 16).[193] More importantly, compound **1g**, **4g** and **7g**, respectively, showed unprecedented 28-fold, 122-fold and 22-fold selectivity for tgTS over hTS.

To determine the structural basis for the observed activity and selectivity, X-ray co-crystal structures of **1g** and **4g** with *T. gondii* TS–DHFR was determined (Figure 47).[193] The atomic coordinates of *T.gondii* TS–DHFR/compound **1g** and **4g** described here have been deposited in the PDB (www.pdb.org) with accession codes 4KY4 and 4KYA, respectively. Upon superimposing the tgTS and hTS, almost all of the residues in the active site were found to be identical. It was surprising that a remarkable 28-fold selectivity (K_i value) was observed for **1g** despite almost identical architectures of the active sites of tgTS and hTS.

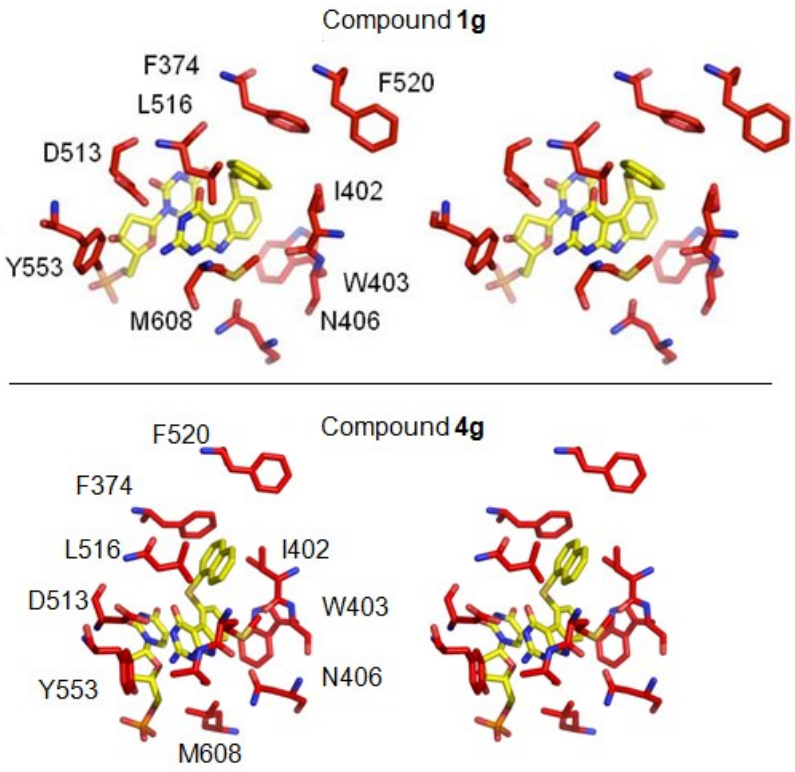

Figure 47. Inhibitors **1g** and **4g** in the active site of *T. gondii* TS. The key residues are highlighted in red. The inhibitors **1g** and **4g** and the substrate dUMP are colored yellow.[193]

As shown in Figure 47, the crystal structure of the tgTS–DHFR with **1g** and **4g** revealed extensive base stacking interactions between the inhibitor and the nucleotide dUMP as expected. The phenyl ring of **1g** or the 1'-naphthyl ring of **4g** are oriented almost at a right angle to the tricyclic scaffold and interacts with Ile402, Leu516, Phe520 and Met608. The scaffold is also stabilized by hydrophobic interactions of the C-ring with Trp403. Using X-ray co-crystal structure of **1g** with tgTS–DHFR, ligand interactions were generated using MOE 2013.08[184] (Figure 48).

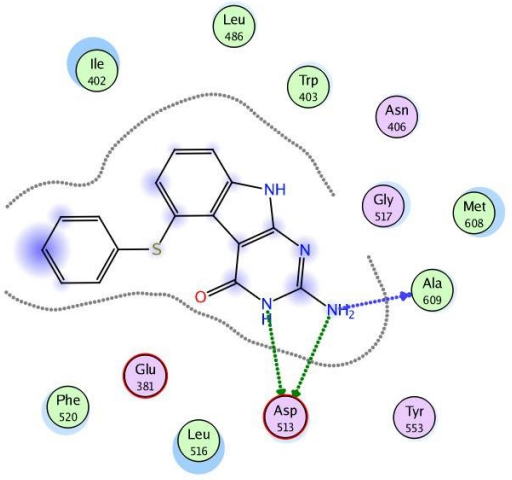

Figure 48. Interactions between **1g** and residues in the active site of tgTS.

Compound **1g** is bound to the active site by aromatic stacking of the pyrimido[4,5-*b*]indole scaffold and the dUMP pyrimidine ring. Additionally, hydrogen bonds are formed between the N9 of **1g** and carboxyl of Asn406, the N3 and the 2-NH_2 group with the –COOH of Asp513 (Figure 48). The 2-NH_2 group forms additional hydrogen bond with the backbone oxygen of Ala609.

Table 17. *Toxoplasma* cell culture study of **1g**, **2g** and **4g**

Condition	***T. gondii* in media at Day 4**	***T. gondii* in cells at Day 4**	**Estimated IC_{50} value, μM[a]**
No drug	3710000	1140000	
1g (5 μM)	100000	140000	3.7
2g (5 μM)	2350000	340000	2.6
4g (5 μM)	<25000	<2500	0.6
pyrimethamine (3 μM)	<25000	<2500	0.57

[a]Dose response curves using data from the three concentrations of test compounds gave estimates of IC_{50} values.

Compounds **1g**, **2g** and **4g** have also been evaluated against *T. gondii* cells in culture (Table 17).[193] The culture model requires that the experimental compounds rapidly kill exposed tachyzoites as they are released from cells and/or that the experimental compounds penetrate the cell and the vacuole containing tachyzoites where the compounds may kill the organism or prevent its replication. Compound **4g**, at 5 μM, was found to be equivalent to pyrimethamine at 3 μM indicating a significant effect on *T. gondii* in culture comparable to a clinically used agent PM. Both compounds **1g** and **2g**, at 5 μM, were 4–6 times less active than pyrimethamine at 3 μM.

Methods for biological evaluation

Effects of compounds on cellular microtubules. A-10 cells were used to evaluate the effects of the compounds on cellular microtubules using indirect immunofluorescence techniques.[212] Cells were treated for 18 h with compounds and microtubules were visualized with an antibody towards β-tubulin (Sigma–Aldrich Co.). EC_{50} values were calculated from an average of a minimum of three independent experiments.

Sulforhodamine B (SRB) assay. The SRB assay was used to evaluate the antiproliferative and cytotoxic effects of the compounds against cancer cells.[210] MDA-MB-435, SK-OV-3 and HeLa cells were purchased from the American Type Culture Collection (Manassas, VA). The IC_{50} values (concentration required to cause 50% inhibition of proliferation) represent an average of 3 independent experiments using triplicate points in each experiment.

In vitro tubulin polymerization. The effect of the compounds on tubulin polymerization was measured using purified porcine brain tubulin (Cytoskeleton Inc.).[55] Briefly, 2.2 mg/mL of purified porcine brain tubulin was incubated with tubulin polymerization buffer (80 mM Na-PIPES, pH 6.9, 1 mM EGTA, 1 mM $MgCl_2$, 10 mM GTP and 10% glycerol) and 10 μM of each corresponding drug. The polymerization of tubulin was monitored turbidimetrically by measuring the absorbance at 340 nm at 37 °C in a SpectraMax 96-well plate spectrophotometer.

Quantitative tubulin studies. Bovine brain tubulin was purified as described previously.[213] Briefly, 1.0 mg/mL of tubulin (10 μM) was incubated for 15 min with 0.8M monosodium glutamate (pH of 2M stock solution adjusted to 6.6 with HCl), varying compound concentrations and 4% (v/v) dimethyl sulfoxide (DMSO) as solvent. After preincubation, 0.4 mM GTP was added. The reaction mixtures were transferred to the cuvettes at 0 °C and were placed in a recording spectrophotometer equipped with an electronic temperature controller. After baselines were established, the temperature was jumped over about 30 s to 30 °C, and changes in turbidity were monitored for 20 min. The compound concentration that caused a 50% reduction in increase in turbidity, interpolated from the values obtained with defined compound concentrations, was defined as the IC_{50} value. The assay to measure inhibition of [^{3}H]colchicine binding was described in detail previously.[214] Briefly, 0.1 mg/mL (1.0 μM) tubulin was incubated, at 37 °C, 5.0 μM [^{3}H]colchicine, and potential inhibitors at 1.0 or 5.0 μM, as indicated. Incubation was for 10 min at which point the reaction has reached 40-60% of the maximum colchicine that can be bound in reaction mixtures without inhibitor. The

[^{3}H]colchicine was a product of Perkin–Elmer. CA4 was a generous gift of Dr. G. R. Pettit, Arizona State University.

Antibodies. The PY-HRP antibody was obtained from BD Transduction Laboratories (Franklin Lakes, NJ). Antibodies against EGFR, VEGFR-2, and PDGFR-β were purchased from Cell Signaling Technology (Danvers, MA).

Phosphotyrosine enzyme–linked immunosorbent assay (ELISA). A high-throughput phosphotyrosine ELISA was developed for evaluating the effect of compounds on RTKs.[215] Cells used for these experiments have been shown to overexpress particular RTKs; specifically A431 for EGFR, U251 for VEGFR-2, and SH-SY5Y for PDGFR-β**.** Briefly, cells at 60–75% confluence are placed in serum-free medium for 18 h to reduce the background of phosphorylation. Cells were always >98% viable by Trypan blue exclusion. Cells were then pretreated for 60 min with a dose-response relation of 100-1.4 μM compound followed in ⅓ Log increments by 100 ng/mL of purified growth factor (EGF, VEGF, or PDGF-BB) for 10 min. The reaction was stopped, and the cells were permeabilized by quickly removing the media from the cells and adding ice-cold tris-buffered saline (TBS) containing 0.05% Triton X-100, protease inhibitor cocktail, and tyrosine phosphatase inhibitor cocktail (Sigma–Aldrich Co.). The TBS solution was then removed, and cells fixed to the plate for 30 min at 60 °C and further incubation in 70% ethanol for an additional 30 min. Cells were further exposed to block (TBS with 1% BSA) for 1 h, washed, and then a horseradish peroxidase (HRP)-conjugated phosphotyrosine (PY) antibody was added overnight. The antibody was removed, cells were washed again in TBS, exposed to an enhanced luminol ELISA substrate, (Pierce Chemical EMD, Rockford, IL) and light emission was measured using a plate reader. The

known RTK-specific inhibitors (semaxanib, sunitinib, erlotinib) were used as positive controls for kinase inhibition. Data were graphed as a percent of cells receiving growth factor alone, and IC_{50} values were calculated from two to three separate experiments (n = 8–24) using sigmoidal dose-response relations in Prism 3.0 software (GraphPad).

Chorioallantoic membrane (CAM) assay. The CAM assay is a standard assay for testing antiangiogenic agents and was performed as previously[216] described. Briefly, fertile leghorn chicken eggs (CBT Farms, Chestertown, MD) were allowed to grow until 10 days of incubation. The pro-angiogenic factors, human VEGF-165 and basic fibroblast growth factor (bFGF) (100 ng each) were then added at saturation to a 6 mm microbial testing disk (BBL, Cockeysville, MD) and placed onto the CAM by breaking a small hole in the superior surface of the egg. To the same microbial disk, antiangiogenic compounds were then added 8 h after the VEGF/bFGF at saturation and embryos were allowed to incubate for an additional 40 h. After 48 h, CAMs were perfused with 2% paraformaldehyde/3% glutaraldehyde containing 0.025% Triton X-100 for 20 sec, excised around the area of treatment, fixed again in 2% paraformaldehyde/3% glutaraldehyde for 30 min, placed on Petri dishes, and a digitized image taken using a dissecting microscope (Wild M400; Bannockburn, IL) at 7.5× and SPOT enhanced digital imaging system (Diagnostic Instruments, Sterling Heights, MI). A grid was then added to the digital CAM images and the average number of vessels within 5–7 grids were counted as a measure of vascularity. Sunitinib and semaxanib were used as positive controls for antiangiogenic activity. Data were graphed as a percent of CAMs receiving bFGF/VEGF only and IC_{50} values calculated from two to three separate experiments (n = 5–11) using non-linear regression dose-response relation analysis.

MDA-MB-435 flank tumor model. Human MDA-MB-435 basal-like breast cancer cells (500,000) in media were implanted into the lateral flank of 8 week old female NCr athymic nu/nu nude mice (Charles River, Wilmington, DE). Tumor sizes (length, width, depth) were measured twice weekly. When volumes reached 75–100 mm^3 (day 7 after implantation), the tumors were treated with drugs at their maximum tolerated dose (MTD) and tumor volumes were measured twice weekly. The MTD of docetaxel was found to be 35 mg/kg, sunitinib 30 mg/kg, pemetrexed 30 mg/kg, **1** 25 mg/kg and **2** 35 mg/kg.

4T1 triple negative breast orthotopic allograft model. 4T1-Luc2GFP dual luciferase/GFP tagged cells were purchased from Caliper Life Sciences (Hopkinton, MA) and maintained in Dulbecco's modification of minimal essential media (DMEM) containing 10% Cosmic Calf Serum (Hyclone, Logan, UT). 750 cells [verified by fluorescence imaging to be >98% GFP positive and counted three times on a TC10 automated cell counter (BioRad, Hercules, CA)] in 100 μL PBS with 1 mM EDTA were implanted subcutaneously into the left fat pad #4 of 8 week old female BALBc/J mice using a tuberculin syringe. The MTD of drugs were delivered to animals twice weekly starting three days after implantation. Tumor sizes (length, width, depth) were measured three times weekly. At day 33 post implantation, animals were humanely euthanized using the AALAC approved method of carbon dioxide asphyxiation. Tumors and lungs were removed and fresh lungs imaged using a LumaScope fluorescent imaging system (Bulldog Bio, Portsmouth, NH) at 25× magnification with the number of metastases per lung counted by hand from captured images.

Expression, Purification, and crystallization of *T. gondii* TS-DHFR. Wild-type *T. gondii* TS–DHFR was expressed and purified as described previously.[217] The loop truncated form of TS–DHFR enzyme was purified as described before for structure determination. Wildtype TS–DHFR was used for kinetic assays. Briefly, the TS–DHFR was overexpressed in *E. coli* BL21 cells after induction with IPTG. In the final step, the protein was stored in buffer containing 25 mM Tris pH 7.3 and 10 mM DTT. The ligands NADPH, methotrexate, dUMP and the inhibitor were added to a final concentration of 500 μM. Crystallization was achieved at a concentration of 10 mg/mL with a 1:1 ratio of the enzyme and the well solution containing PEG 3350 and potassium phosphate. The crystals were cryoprotected in mother liquor containing ethylene glycol and frozen in stepwise transfers into liquid nitrogen. Data were collected at beamlines X25 and X29 at Brookhaven National Laboratory.

X-Ray structure determination. Initial processing of X-ray data was accomplished by using HKL2000.[218] The loop truncated model (PDB accession code: 4EIL) was used as the search model for molecular replacement by using PHASER.[219] Refinement of the structure was carried out by REFMAC.[220] The ligand and its topology file was generated by the PRODRG server,[221] and manual adjustments to the model and the ligand were made in COOT.[222] Figure was generated using PYMOL.[223]

IC_{50} and K_i values of *T. gondii* TS–DHFR. Separately, the *T. gondii* TS–DHFR (25 nM) and human TS (50 nM) were incubated with dUMP and inhibitor both at 100 μM, and the reaction was initiated with methylene tetrahydrofolate (100 μM).[193] The change in absorbance was monitored by TECAN plate reader at 340 nm. The data was plotted using KALEIDAGRAPH. The IC_{50} values were then determined, from which K_i was

determined. The nucleotide dUMP, the cofactor NADPH and methylene tetrahydrofolate were purchased from Sigma–Aldrich Co.

***T. gondii* cell culture study.** *T. gondii* strain PHΔHX was grown in culture on an immortalized human cell line (human telomerase reverse transcriptase (H-tert)) both to prepare innoculum and for the experimental drug tests.[193] Freshly lysed parasites were removed from culture, resuspended in sterile phosphate buffered saline, counted, and diluted in medium to allow addition of 1300 *T. gondii* tachyzoites to each well of 24-well culture plates containing monolayers of H-tert cells. After incubation for 4 h at 37 ºC, each well received either 500 μL of media (DMEM, 1% fetal calf serum), or media including various concentrations (5, 0.5, 0.05 μM) of experimental drug. Wells were evaluated visually and one set of wells was harvested daily for four days. Media (10 μL) from harvested wells was spread over a 1 cm square area on a microscope slide; cells in harvested wells were scraped and resuspended in 100 μL of fresh medium and 10 μL was spread over a 1 cm square area on a microscope slide. After air-drying, each slide was fixed in methanol and stained with Giemsa Plus. Organisms and cells/1000× field were counted as an indication of growth of *T. gondii* in the presence or absence of test compounds or pyrimethamine, which served as the positive control. By day 2 of growth, *T. gondii* tachyzoites began to be detected in the sampled control cell monolayers. By day 4, untreated monolayers were mostly lysed with numerous tachyzoites in both media samples and cell samples.

B. Bulk synthesis of lead compounds 182, 183, 185 and target compound 4g

N^4-Methylation of **181** using dimethyl sulfate furnished **182** in 70% yield (Scheme 48).[174] This scheme was used to synthesize 2 g of **182** required for preclinical evaluation.

Scheme 48. Synthesis of **182**

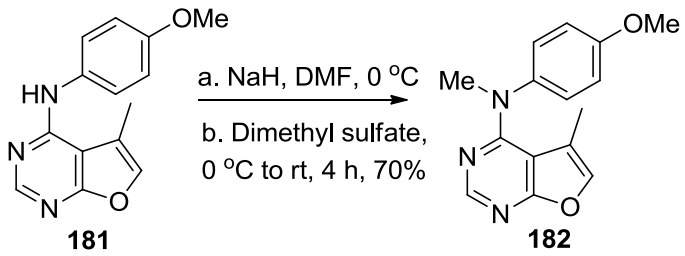

Scheme 49. Synthesis of **183**

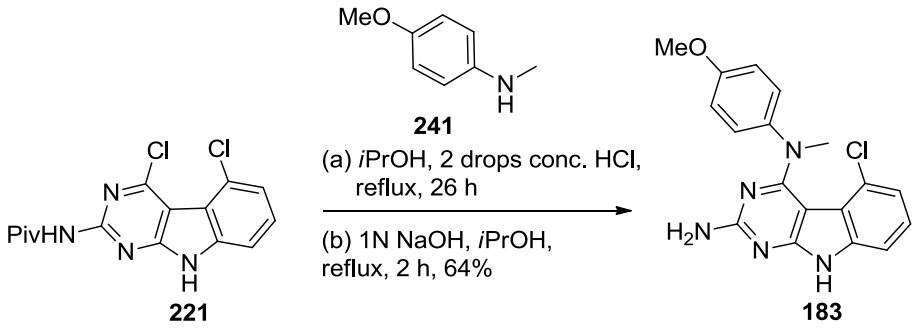

Nucleophilic displacement of the 4-chloro of **221** with *N*-methyl-4-methoxyaniline **241** followed by deprotection of the 2-amino group provided **183** in 60% yield (Scheme 49).[182] This procedure was utilized to synthesize 250 mg of **183** required for hollow fiber assay.

Scheme 50. Synthesis of **185**

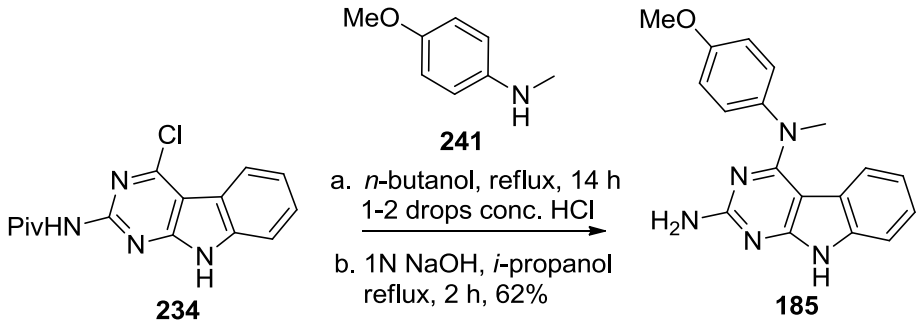

Compound **234** was reacted with *N*-methyl-4-methoxyaniline **241** in *n*-butanol at reflux followed by base-mediated deprotection of the 2-amino group to afford **185** in 62% yield (Scheme 50). This procedure was employed to synthesize 500 mg of **185** in improved yield (62%) over the reported[178] procedure (42%) in which the displacement was carried out in isopropanol at reflux for 72 h.

Scheme 51. Synthesis of **4g**

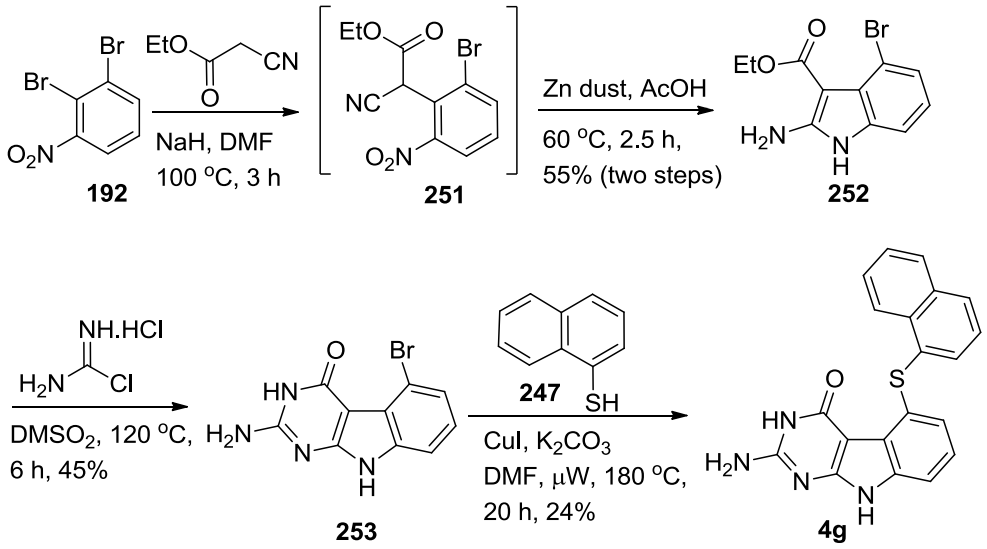

Displacement of the 2-bromo of **192** with ethyl cyanoacetate furnished **251** (Scheme 51).[173] Zinc-catalyzed reduction of the 2-nitro of **251** followed by cyclization provided the substituted indole **252**. Cyclocondensation of **252** with carbamimidic chloride hydrochloride[195] afforded 2-amino-4-oxo-5-bromo-pyrimido[4,5-*b*]indole **253**. Reaction temperature should be maintained between 120–125 °C to prevent the formation of side products. Ullmann coupling of **253** and 1-naphthylthiol **247** furnished target compound **4g** in 24% yield.[193] Column chromatography of **4g** should not be carried out using a CombiFlash® Rf system because **4g** sticks to the silica gel and does not elute out.

Experimental section for Schemes 48–51.

***N*-(4-Methoxyphenyl)-*N*,5-dimethylfuro[2,3-*d*]pyrimidin-4-amine (182).**

To a 25 mL round bottom flask was weighed **181** (510 mg, 2 mmol) and was added DMF (10 mL) to afford a solution. The flask was purged with argon for 5 min followed by cooling down to 0 ºC using ice bath. Sodium hydride (144 mg, 6 mmol) was added to the solution at 0 ºC. The solution was stirred for 30 min at 0 ºC under argon atmosphere. Dimethyl sulfate (757 mg, 6 mmol) was injected to the reaction mixture and the flask was warmed to room temperature. The mixture was stirred at room temperature for another 3 h at the end of which 1N HCl (5 mL) was added carefully to quench the reaction followed by water (10 mL) to afford a precipitate. The product was extracted with ethyl acetate (10 mL × 3). The combined organic extracts were washed with brine (10 mL), dried (anhydrous sodium sulfate) and concentrated under reduced pressure. Silica gel (2 g) was added and the solvent evaporated to obtain a plug. Column chromatography by elution with hexanes and ethyl acetate (5:1) afforded **182** (416 mg, 70%) as an off-white solid. TLC R_f = 0.87 ($CHCl_3$/MeOH, 10:1); mp 87.0–87.8 ºC (lit.[174] 84.8–85.6 ºC); ^{1}H NMR (400 MHz, DMSO-d_6): δ = 1.05 (s, 3H, CH_3), 3.44 (s, 3H, OCH_3), 3.77 (s, 3H, NCH_3), 6.96–6.98 (d, 2H, Ar, J = 9.0 Hz), 7.19–7.22 (d, 2H, Ar, J = 9.0 Hz), 7.52 (s, 1H, C_6-CH), 8.45 (s, 1H, C_2-CH). Elemental analysis calculated (%) for $C_{15}H_{15}N_3O_2$: C, 66.90; H, 5.61; N, 15.60. Found: C, 66.92; H, 5.66; N, 15.65.

5-Chloro-N^4-(4-methoxyphenyl)-N^4-methyl-9*H*-pyrimido[4,5-*b*]indole-2,4-diamine (183).

Compound **221** (60 mg, 0.178 mmol) was treated with *N*-methyl-4-methoxyaniline **241** (73 mg, 0.533 mmol), 20 mL of isopropanol, and 2 drops of conc. HCl in a 100 mL round bottom flask. The reaction mixture was heated to reflux for 20 hours. The solvent was evaporated and neutralized with 4 mL of ammonia (7N) in methanol. To the solution was added silica gel, four times the weight of the reaction mixture, and the solvent was removed under reduced pressure to provide a plug. The plug was transferred on top of a column packed with silica gel, twenty times the weight of plug, eluted with 1% methanol in chloroform. Fractions containing the product (TLC) were pooled and evaporated to give a solid which was further deprotected using 4 mL 1N NaOH solution in 30 mL isopropanol upon reflux for 4 hours. The solvent was evaporated to obtain a brown colored solid. The resulting precipitate was then dissolved in methanol. To the solution was added silica gel, four times the weight of the reaction mixture, and the solvent was removed under reduced pressure to provide a plug. The plug was transferred on top of a column packed with silica gel, twenty times the weight of plug, eluted with 0.5% methanol in chloroform. Fractions containing the product (TLC) were pooled and evaporated to provide **183** in 60% yield. TLC R_f = 0.42 ($CHCl_3$/MeOH, 10:1); mp 180.1–180.6 °C (lit.[182] 179.0–180.0 °C). ^{1}H NMR (DMSO-d_6): δ = 3.30 (s, 3H, OCH_3), 3.66 (s, 3H, N-CH_3), 6.55 (s, 2H, NH_2, exch), 6.76–7.25 (m, 7H, Ar), 11.65 (s, 1H, 9-NH, exch). Elemental analysis calculated (%) for $C_{18}H_{16}ClN_5O$: C, 61.10; H, 4.56; N, 19.79; Cl, 10.02. Found: C, 60.91; H, 4.63; N, 19.74; Cl, 10.19.

N^4-(4-Methoxyphenyl)-N^4-methyl-9*H*-pyrimido[4,5-*b*]indole-2,4-diamine (185).

Compound **234** (60 mg, 0.178 mmol) was treated with *N*-methyl-4-methoxyaniline **241** (73 mg, 0.533 mmol), 20 mL of *n*-butanol, and 2 drops of conc. HCl in a 100 mL round bottom flask. The reaction mixture was heated to reflux for 76 hours. The solvent was evaporated and neutralized with 4 mL of ammonia (7N) in methanol. To the solution was added silica gel, four times the weight of the reaction mixture, and the solvent was removed under reduced pressure to provide a plug. The plug was transferred on top of a column packed with silica gel, twenty times the weight of plug, eluted with 1% methanol in chloroform. Fractions containing the product (TLC) were pooled and evaporated to give a solid which was further deprotected using 4 mL 1N NaOH solution in 10 mL isopropanol upon reflux for 2 hours. The solvent was evaporated to obtain a brown colored solid. The resulting precipitate was then dissolved in methanol. To the solution was added silica gel, four times the weight of the reaction mixture, and the solvent was removed under reduced pressure to provide a plug. The plug was transferred on top of a column packed with silica gel, twenty times the weight of plug, eluted with 0.5% methanol in chloroform. Fractions containing the product (TLC) were pooled and evaporated to provide **185** in 62% yield. TLC R_f = 0.70 ($CHCl_3$/MeOH, 5:1); mp 246.8–247.2 °C (lit.[178] 245.3–245.7 °C). ^{1}H NMR (DMSO-d_6): δ = 3.34 (s, 3H, OCH_3), 3.73 (s, 3H, N-CH_3), 5.77–5.79 (m, 1H, Ar), 6.21 (s, 2H, NH_2, exch), 6.53–6.57 (m, 1H, Ar), 6.90–6.99 (m, 3H, Ar), 7.14–7.17 (m, 3H, Ar), 11.24 (s, 1H, 9-NH, exch). Elemental analysis calculated (%) for $C_{18}H_{17}N_5O \cdot 0.20CH_3OH$: C, 67.05; H, 5.52; N, 21.46. Found: C, 66.97; H, 5.47; N, 21.55.

Ethyl 2-amino-4-bromo-1*H*-indole-3-carboxylate (252).

To an ice-cold solution of ethyl cyanoacetate (5.41 g, 57.8 mmol) in anhydrous DMF (170 mL) under argon atmosphere was added sodium hydride (1.15 g, 47.8 mmol). Thus formed white suspension was stirred for 15 min and then treated with 1,2-dibromo-3-nitrobenzene **192** (4 g , 14.2 mmol). The suspension was heated at 100 °C for 3 h. After cooling the reaction micture to rom temperature, 50 mL H_2O was added and the resulting mixture was acidified to pH 2.0 with conc. HCl. The mixture was extracted with ether (3x) and then the combined organic phases were dried using anhydrous sodium sulfate and concentrated to give ethyl (2-bromo-6-nitrophenyl)(cyano)acetate **251** as a yellow oil. The material was used directly for the next step.

A solution of **251** (3.42 g, 11 mmol) in glacial AcOH (150 mL) was treated with a single charge of zinc dust (10.26 g, 156 mmol). The mixture was heated at 60 °C for 45 min and then recharged with Zn dust (3.42 g, 52 mmol). After heating for another 105 min, the mixture was cooled to room temperature and then filtered through a pad of Celite. The pad was washed well with AcOH, the filtrate was concentrated and then neutralized with 5% aq. $NaHCO_3$. The precipitate was collected and then dissolved in methanol. Silica gel (5 g) was added to make the plug and was then purified by column chromatography, eluting sequentially with 0% and 1% MeOH in $CHCl_3$. The fractions containing the pure product (TLC) were pooled and evaporated to give **252** (55% from **192**) as a brown solid. TLC R_f = 0.30 ($CHCl_3$/MeOH, 10:1 with 2 drops of conc. NH_4OH); mp 136.1–137.0 ºC. ^{1}H NMR (400 MHz, DMSO-d_6): δ = 1.27–1.31 (t, 3H, CH_3); 4.17–4.22 (q, 2H, CH_2); 6.75–6.79 (m, 1H, Ar); 6.82 (bs, 2H, NH_2, exch); 7.11–7.14 (m, 2H, Ar); 10.93 (s, 1H, NH, exch). ^{1}H NMR agreed well with the literature reported[209] values.

2-Amino-5-bromo-3,9-dihydro-4*H*-pyrimido[4,5-*b*]indol-4-one (253).

A mixture of ethyl 4-bromo-2-amino-1*H*-indole-3-carboxylate **252** (400mg, 1.41 mmol), carbamimidic chloride hydrochloride (325 mg, 2.82 mmol) and methyl sulfone (3 g) was stirred at 120 °C for 14 h. The reaction mixture was neutralized by ammonia in methanol (2–3 mL) and then 40 mL methanol and 3 g silica gel were added. Thus obtained plug was purified by column chromatography on silica gel sequentially eluting with 1%, 5% and 10% MeOH in $CHCl_3$ to afford **253** (45%) as a brown solid. TLC R_f = 0.43 ($CHCl_3$/MeOH, 5:1 with 2 drops of conc. NH_4OH); mp >250 °C; ^{1}H NMR (400 MHz, DMSO-d_6) δ = 6.59 (bs, 2H, NH_2, exch); 6.97–7.01 (m, 1H, Ar); 7.23–7.25 (m, 2H, Ar); 10.38 (s, 1H, NH, exch); 11.66 (s, 1H, NH, exch). ^{1}H NMR agreed well with the literature reported[209] values.

2-Amino-5-(1-naphthylsulfanyl)-3,9-dihydro-4*H*-pyrimido[4,5-*b*]indol-4-one (4g).

Compound **253** (100 mg, 0.36 mmol), 1-naphthylthiol **247** (230 mg, 1.43 mmol), copper iodide (272 mg, 1.43 mmol) and potassium carbonate (396 mg, 2.86 mmol) were added to a Biotage® microwave vial. Around 10 mL DMF was added as solvent and the tube was sealed and purged with argon for 5 min. The reaction was run in a microwave at 180 °C for 20 h. After cooling to room temperature, the DMF was removed under reduced pressure and the crude product was purified by column chromatography, sequentially eluting with 0%, 5% and 8% methanol in chloroform. Fractions containing the product (TLC) were pooled and evaporated to afford the desired product **4g** as a white solid: yield 24%. TLC R_f = 0.46 ($CHCl_3$/MeOH, 5:1 with two drops conc. NH_4OH); mp >300 °C (lit.[193] >250 °C); ^{1}H NMR (400 MHz, DMSO-d_6): δ = 6.04 (d, 1H, J = 8.0 Hz, C7-CH),

6.54 (bs, 2H, NH_2, exch), 6.75 (t, 1H, J = 7.6 Hz, C6-CH), 6.97 (d, 1H, J = 8.0 Hz, C8-CH), 7.48–7.57 (m, 3H, Ar), 7.73–7.75 (m, 1H, Ar), 7.99–8.02 (m, 2H, Ar), 8.19–8.21 (m, 1H, Ar), 10.40 (s, 1H, 3-NH, exch), 11.53 (s, 1H, 9-NH, exch). HRMS (ESI): *m/z* calculated for $C_{20}H_{14}N_4OS + H^+$ [$M+H^+$]: 359.0967. Found: 359.0981. Elemental analysis calculated (%) for $C_{20}H_{14}N_4OS \cdot 0.14CHCl_3$: C, 64.48; H, 3.80; N, 14.94; S, 8.55. Found: C, 64.27; H, 3.69; N, 14.94; S, 8.79. ^{1}H NMR agreed well with the literature reported[193] values.